MOLECULAR GENETICS AND MOLECULAR BIOLOGY OF CATARACT

ALPANA DAVE, M.Biotech

Department of Ophthalmology, School of Medicine

Faculty of Medicine, Nursing and Health Sciences

Flinders University, Adelaide

May 2015

For my parents

Table of Contents

Thesis summary

Cataract is an opacification of the ocular lens and is classified as congenital cataract (CC) or as age-related cataract (ARC) depending on the age-of-onset. Causative mutations and SNPs in *EPHA2* have been implicated in congenital and age-related cataract, respectively. *EPHA2* encodes a tyrosine kinase receptor which is expressed in lens cells and plays an important role in lens development. The main objective of this project was to investigate the role of *EPHA2* in congenital and age-related cataract development.

CC causing mutations in *EPHA2* were previously reported through linkage and candidate-gene analysis including a mutation reported in an Australian family. However, the genetic contribution of mutations in *EPHA2* to CC cases in Australia is unknown. To determine this, *EPHA2* gene was screened for mutations in a South-Eastern Australian cohort of CC cases. We found two families, each with a novel mutation and two new families with a previously reported causative mutation in *EPHA2*. The mutations in *EPHA2* accounted for 4.7% of CC cases in South-Eastern Australia.

Further, we investigated the effect of two previously reported and three mutations found in this study on EPHA2 localisation. EPHA2 is highly expressed in epithelial cells and interacts with cell-junction proteins. Therefore we analysed the effect of these mutations in epithelial cell lines. Two mutant proteins localised in the perinuclear region and co-localised with a cis-golgi marker. These mutations possibly delay recruitment of mutant

EPHA2 to the cell membrane affecting its function. The other three mutations localised to the cell periphery as the wild-type protein.

Environmental factors namely, age, gender and ultraviolet-B (UV-B) radiation are associated with increased risk of ARC development and also affect *EPHA2* expression. We investigated if these environmental factors interact with *EPHA2* and consequently affect ARC development using an *Epha2*$^{-/-}$ mice. These mice, on FVB/NJ background, were reported to develop ARC between 5-8 months of age while *Epha2*$^{+/-}$ mice had clear lenses until 14 months of age. However, we found that *Epha2*$^{-/-}$ and *Epha2*$^{+/-}$ mice on C57BL/6J background developed cataract by 4 months and 8 months of age, respectively, likely attributable to differences in the background strain compared to the previous report. Consistent with previous reports, diffused localisation of cell-junction proteins in *Epha2* knockout lenses suggested that lack of Epha2 may affect lens cellular junctions. Accumulation of a partial Epha2 fusion protein, generated as a result of the knockout, may contribute to the difference in phenotype observed in *Epha2* knockout mouse strains. Additionally, gender had a small effect on cataract progression in *Epha2* knockout mice. UV-B exposure of *Epha2*$^{+/-}$ and *Epha2*$^{+/+}$ mice demonstrated a dose-dependent difference in cataract development in both the genotypes and no difference in UV-B-induced cataract between the two genotypes.

Overall, mutations in *EPHA2* contribute to a significant proportion of CC in South-Eastern Australia. Analysis of causative mutations and studies in *Epha2*$^{-/-}$ mouse suggest a role of *Epha2* at cell-junctions in the lens, disruption of which results in cataract. Additionally, this study demonstrates an effect of age and gender on *Epha2* mediated ARC development.

Declaration

I certify that this thesis does not incorporate without acknowledgement any material previously submitted for a degree or diploma in any university; and that to the best of my knowledge and belief it does not contain any material previously published or written by another person except where due reference is made in the text.

Alpana Dave

Acknowledgements

First and foremost, I would like to thank Shiwani Sharma for her guidance and support all through these years. I am grateful for her untiring efforts and patience all these years. I am thankful to Jamie Craig for his feedback on the different aspects of my work and for taking time out to examine the mice used in this study; without his help the animal work presented in this thesis would not have been possible. I would also like to thank Kathryn Burdon, for her guidance and feedback on my work.

I am thankful to Kate Laurie, Emmanuelle Souzeau, Sandra Staffieri and David Mackey for their help with the mutation screening of *EPHA2* in congenital cataract patients. I am grateful to Raman Kumar and Sarah Martin for their help in generating the wild-type EPHA2-Myc construct used in the present study. I would also like to thank Angela Chappell for helping us set-up a system for photographing the mice used in this study. A special thank you to Rebecca Hamilton and Karina Skrzypiec, for their help with eye examinations and UV-B treatment of the mice. I am grateful to Robb de Iongh for teaching me tissue sectioning and labelling; to Miriam Keane for her help with the statistical analysis performed in the present study. I am thankful to the Flinders Animal facility for their help with animal breeding and maintenance; Department of Biomedical Engineering for building the UV-B treatment station used in the present work.

I would like to thank my friends Divi, Meru, Nisha, Siddharth and Sudha (to name a few) for their constant encouragement through these years. I am thankful to my friend and husband, Shresth for instilling the faith in me that the end is in sight; to Shresth's family for their support; to my sister, Shilpa, for her constant motivation and support. And last but not the least, my parents for believing in me and for encouraging me in all my endeavours; for all the sacrifices they have made over the years to pave a path for my career. As a small gesture of my appreciation, I dedicate this thesis to my parents.

Publications arising from this thesis

1. Dave A, Laurie K, Staffieri SE, Taranath D, Mackey DA, Mitchell P, Jie Jin Wang, Jamie E Craig, Kathryn P Burdon, Shiwani Sharma. Mutations in the EPHA2 gene are a major contributor to inherited cataracts in South-Eastern Australia. PLoS One 2013;8(8):e72518.

List of Abbreviations

α	Alpha
αTN4	Mouse lens epithelial cell line
AD	Autosomal Dominant
AGRF	Australian Genomics Research Facility
AJ	Adherens junctions
AR	Autosomal Recessive
ARC	Age-related cataract
ACG	Average Cataract Grade
β	Beta
BCA	Bicinchoninic acid
Bfsp2	Beaded filament structural protein 2
β-geo	Beta-galactosidase and neomycin phosphotransferase
BMES	Blue Mountains Eye Study
bp	Base pairs
Caco2	Human Adenocarcinoma cell line

cDNA	Complimentary deoxyribonucleic acid
CMV	Cytomegalovirus
CRYAA	Crystallin alpha A
dH_2O	Deionised water
DMEM	Dulbecco's Modified Eagle's medium
DNA	Deoxy ribonucleic acid
dNTP	Deoxyribonucleotide triphosphate
E9, E10, E11	Embryonic day 9, 10 or 11
EDTA	Ethylenediaminetetraacetic acid
EGFP	Enhanced Green Fluorescent Protein
EGFR	Epithelial Growth Factor Receptor
EPHA2	EPH Receptor A2
ER	Endoplasmic Reticulum
FGF	Fibroblast Growth Factor
GALT	Galactose-1 phosphate uridyltransferase
gDNA	Genomic DNA
GFP	Green Fluorescent Protein

GJA3 or A8	Gap junction Alpha 3 or alpha 8
GPI	Glycosylphosphatidylinositol
GSH	Glutathione
HEK 293A	Human Embryonic Kidney 293A
HET	Heterozygous
HOMO	Homozygous
HRP	Horse-radish peroxidase
HRT	Hormone replacement therapy
HSF4	Heat Shock Factor protein 4
IRES	Internal Ribosomal Entry Site
kDa	Kilo daltons
LB Agar/Media	Luria Broth Agar/Media
LIM2	Lens Intrinsic membrane Protein 2
MDCK	Madin Darby Canine Kidney
MEF	Mouse Embryonic Fibroblast
mg	Milligrams
ml	Millilitre

µl	Microlitre
µg	Micrograms
MSY	Maryland Sun Years
NBF	Neutral Buffered Formalin
ng	Nanograms
NHS	Nance Horan Syndrome
NSA	Normal South Australian
PAGE	Polyacrylamide Gel electrophoresis
PBS	Phosphate Buffered Saline
PCR	Polymerase chain reaction
PDZ	PSD-95, DLG, ZO-1
PGK	Phosphoglycerate kinase
PLAP	Placental Alkaline Phosphatase
PolyPhen	Polymorphism Phenotyping
PVDF-LF	Polyvinyidine fluoride-low fluorescence
RE	Restriction Enzyme
RIPA	Radio-immunoprecipitation assay

RVEEH	Royal Victorian Eye and Ear Hospital
SA	Streptavidin
SAM	Sterile Alpha Motif
SAP	Shrimp Alkaline Phosphatase
SDS	Sodium Dodcecyl Sulphate
SIFT	Sorting Intolerant from Tolerant
SNP	Single Nucleotide Polymorphism
SRA01/04	Human Lens epithelial cell line
TBE	Tris Borate-EDTA
TBST	Tris Buffered Saline and Tween 20
TJ	Tight Junctions
UV	Ultraviolet
U	Unit
WT	Wild-type

1. Introduction

1.1 The Eye

The eye is an organ responsible for vision (1). Figure 1.1(a) shows anatomy of the human eye (2). It consists of two segments; the anterior segment comprising the cornea, iris, ciliary body and the lens and posterior segment comprising the choroid, retina, optic nerve and the sclera. The lens is a crystalline structure responsible for refraction and focusing light on the retina. It is held in its place by suspensory ligaments and accommodates, with the help of the ciliary body. The anterior chamber between the cornea and the lens is filled with a viscous fluid, aqueous humor, which provides nutrients to the lens and maintains the pressure in the eye. The gel-like vitreous humor in the posterior chamber between the lens and the retina help maintain the shape of the eye.

The work in this thesis is related to the ocular lens which plays an essential role in maintaining clear vision.

1.2 The Lens

1.2.1 Lens structure

The ocular lens is made up of an outer capsule, a layer of anterior epithelial cells and lens fiber cells (3). Figure 1.1(b) shows the structure of the human lens. The lens capsule, an elastic fibrillar structure, is a thickened basement membrane secreted by the lens epithelial cells (3). A highly regulated proliferation of lens epithelial cells gives rise to fiber cells which make the bulk of the lens. The fiber cells form concentric zones of varying refractive index and appear hexagonal in cross-section.

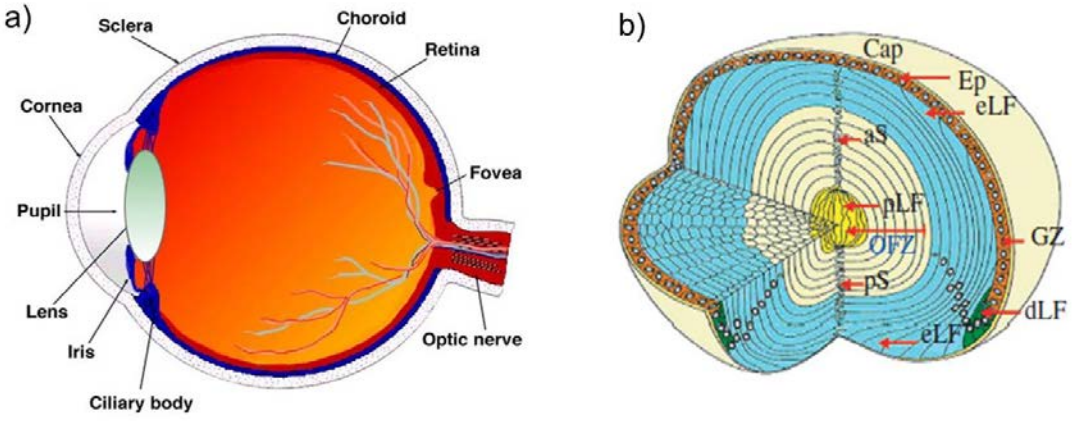

Figure 1.1: Gross anatomy of the eye and the lens.

a) A schematic diagram of the human eye. The figure shows outer fibrous (white), middle choroid (blue) and inner neural (red) layers of the eye with different parts marked. Taken from Kolb H., Gross Anatomy of the eye, 2005 (2). b) A schematic diagram of the lens anatomy. The lens is encapsulated by the outer lens capsule (Cap). The anterior surface of the lens has a layer of epithelial cells (Ep). These cells divide at the lens equator at the germinative zone (GZ) to give rise to differentiating (dLF) and elongating (eLF) lens fiber cells. The elongating cells lose their organelles to form the organelle free zone (OFZ). The fiber cells migrate to form the anterior (aS) and posterior (pS) suture. The centre of the lens comprises of the primary (pLF) lens fiber cells. Taken from: Bassnett et al., Phil Trans R Soc B, 2011, 366. (7).

The lens is an avascular tissue with no neural innervation that derives its nutrients from the aqueous and vitreous humors (4). It is primarily made up of highly soluble proteins which maintain lens clarity. Lens proteins account for 33% of its net weight and are primarily composed of alpha (α), beta (β) and gamma (γ) crystallins (5, 6). The α and β crystallin molecules oligomerise to form water soluble high molecular weight aggregates (6).

Additionally, orderly arrangement of denucleated fiber cells, narrow inter-fiber spaces, absence of vacuoles and an efficient cell-cell communication in the lens plays an important role in maintaining its transparency and hence clear vision (5, 7).

1.2.2 Lens morphogenesis and development

The lens develops from a specialized surface ectoderm known as lens ectoderm, which overlays the optic vesicle (8). Studies conducted in developing mouse lens show that by embryonic day 9 (E9) the optic vesicle extends towards the lens ectoderm (Figure 1.2a) (9). Thickening of the lens ectoderm by middle of E9 leads to formation of the lens placode (Figure 1.2b). The lens placode invaginates along with the optic vesicle to form the lens pit in the optic cup by middle of E10 (Figure 1.2c). Distinct layers of the retina also begin to be formed by this stage. The lens pit then detaches itself from the surface ectoderm to form the lens vesicle by middle of E11 (Figure 1.2d and Figure 1.3a) (10).

Lens progenitor cells from the posterior pole of the vesicle exit the cell cycle and differentiate to form primary fiber cells. These cells elongate into the lumen of the lens vesicle towards the anterior and form the embryonal lens nucleus (Figure 1.3b and c). The cells in the anterior of the lens vesicle form the anterior lens epithelium. The lens epithelial

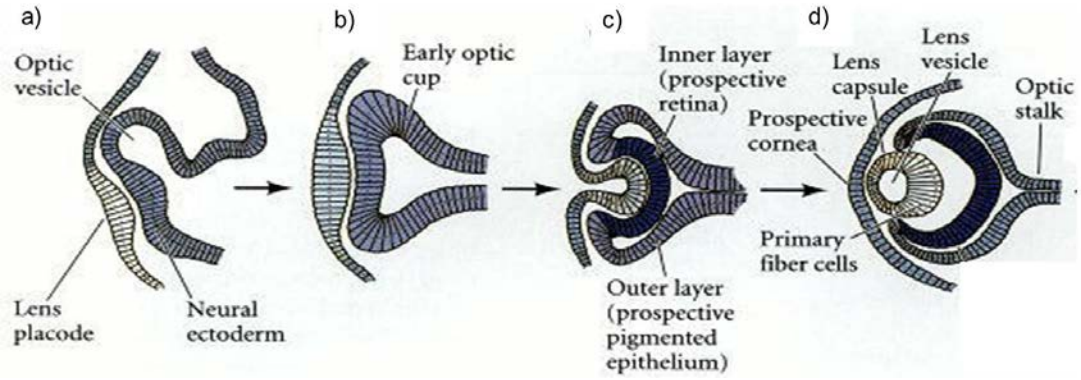

Figure 1.2: Schematic representation of lens morphogenesis

a) The surface ectoderm is laid on the neural ectoderm. The central region of surface ectoderm thickens near the optic vesicle forming the lens placode b) The lens placode enlarges and the optic vesicle forms the early optic cup. c) The lens placode then invaginates with the neural ectoderm forming the lens pit. A distinct neural layers also begins to develop by this stage. d) The lens pit then detaches from the optic vesicle forming the lens vesicle. Taken from Gilbert SF. Induction and Competence. In: Developmental Biology (9).

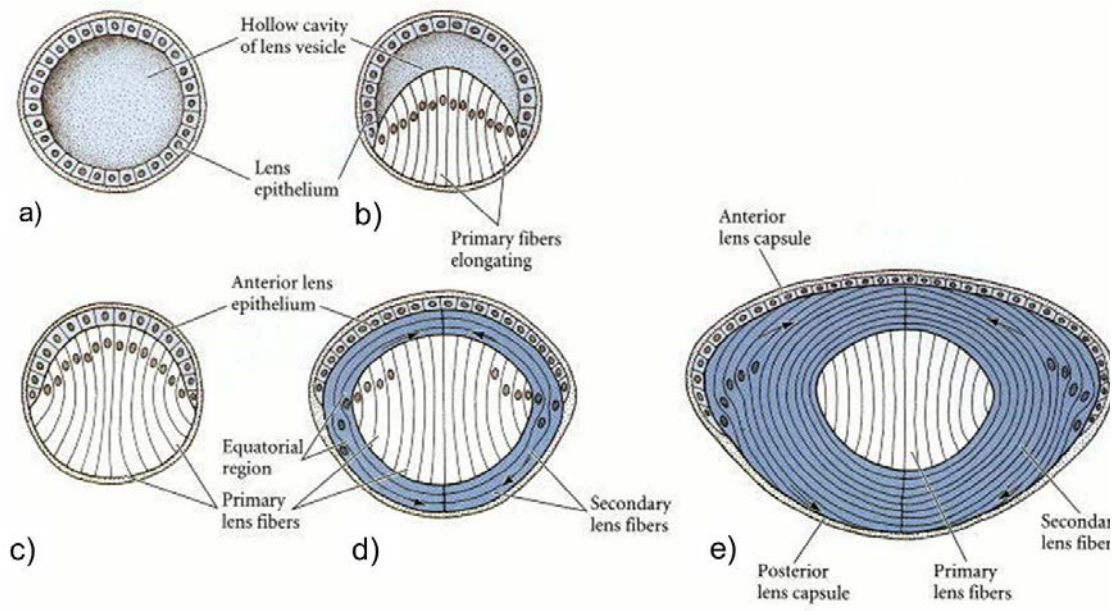

Figure 1.3: Schematic representation of stages of mouse lens differentiation

a) Shows lens vesicle formed by the lens epithelial cells. b) and c) show the elongation of primary fiber cells in the posterior of the lens giving it a distinct polarity. d) illustrates cell division at the lens equator leading to formation of differentiated secondary fiber cells. e) shows an adult lens with continuous cell division at the lens equator and migration of cells to the lens cortex indicated by arrows. Taken from Gilbert SF. Development of the vertebrate Eye. In: Developmental Biology (10).

cells, in the anterior and primary fiber cells, in the posterior, lead to establishment of a distinct polarity in the lens. The anterior and posterior surfaces of the lens merge at the lens equator. Lens epithelial cells divide at the lens equator generating newly formed cells which further differentiate to form secondary fiber cells. These cells then migrate to the region around the lens nucleus, forming the lens cortex (Figure 1.3d). Fiber cells elongate and lose their organelles after differentiation and become metabolically inactive forming an organelle free zone (11, 12). As the lens develops, lens sutures are formed as a result of terminal ends of the secondary lens fibers ending against each other (Figure 1.3e).

Cells in the central region of the lens epithelium are believed to be stem-cell like and do not divide, however they retain the ability to divide in response to an injury. Cells around the central lens epithelium and in the equatorial region proliferate and help in normal lens maintenance (13). The lens grows in size throughout life as the newly generated fiber cells are added to the lens cortex and the older fiber cells move towards the centre (14). As shown in Figure 1.4, the Oxford system of grading divides the cortical region of the lens into different zones from C1-C4, where C1 is under the capsule and C4 is perinuclear (15). The zone C1 comprises of two zones namely, C1 α and C1 β. These cortical zones form regions of high, zone C1 and C3, and low, zone C2 and C4, light scattering. The continuous growth of the lens leads to a constant increase in thickness of zone C2 (16).

Lens induction and development occurs under the influence of various molecules and a synergy of signalling pathways. A gradient of fibroblast growth factor (FGF) in the antero-posterior direction in the eye induces proliferation of lens epithelial cells in low levels of FGF and facilitates epithelial cell migration and fiber cell differentiation in high levels of FGF (17, 18). Apart from FGF, Wnt-Frizzle signalling has been identified to contribute in

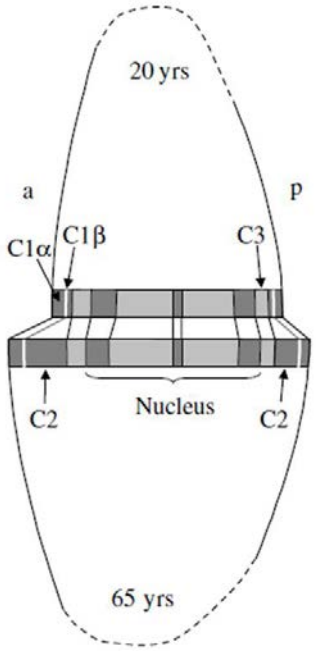

Figure 1.4: Schematic representation of cortical zones in a young and aged lens

The figure represents the cortical zones defined according to the Oxford System in a cross-section of a young (top half) and aged (bottom half) lens. The cortical region of the lens can be further divided into zones C1-C4. Due to difficulty in distinguishing zone C4 from the nuclear layer, only layers C1-C3 are shown in the figure. The region behind the anterior capsule and in front of the posterior capsule is zone C1, which is further divided into C1 α and C1 β. An increase in zone C2 is observed with age. a: Anterior; p: posterior. Taken from Dubbelman et al., 2003, Vis Res, 43 (16)

lens epithelial cell differentiation (19, 20). Further, a host of growth factors lead to induction of various signalling pathways regulating lens cell proliferation and differentiation (21-31).

1.2.3 Lens function and physiology

In addition to its function as a refractive tissue, the lens affects growth of the eye and development of other ocular tissues. The absence of the lens leads to development of only a scleral-like tissue instead of the cornea (32). Lens development also affects the position of the retina in the eye (33). The presence of live lens cells also facilitates accumulation of vitreous volume which in turn helps in developing normal sized eye (34).

Formation of organelle free zone, credited to the orderly removal of cell organelles, plays a critical role in lens transparency (35). All the fiber cells within the organelle free zone are suggested to have fused membranes to ease transport of molecules (36). In contrast, in the lens cortex, fiber cells only in a single layer of the cortex have fused membranes to facilitate the transfer of molecules (37). Ionic balance in the lens is preserved through ionic pumps such as Na^+/K^+ and Ca^+ ATPase (5). Its osmotic balance is maintained through presence of gap junctions and aquaporin channels, which assist in transfer of water and other small molecules across the membranes. The lens is exposed to oxidative stress and xenobiotics throughout life despite which it continues to remain transparent. This suggests an important role of free radical scavenging molecules in combating the oxidative stress. Glutathione (GSH) is the most abundant antioxidant molecule in the lens (38). The GSH and reduced nicotinamide adenine dinucleotide phosphate (NADPH) dependent enzyme

systems facilitate removal of reactive oxygen species and presence of mechanisms for DNA repair and removal of damaged proteins assist in elimination of by-products of oxidative stress (39-41).

Together these unique qualities of the ocular lens contribute to its clarity. Disruption of processes involved in lens induction and development or alteration of its structural properties result in loss of lens transparency. Cataract is an opacification of the ocular lens that impairs vision and is the focus of this thesis.

1.3 Cataract

Cataract causes obstruction in the light path leading to blurred vision and is the major cause of blindness worldwide (42). Cataract development is usually associated with breakdown of lens microarchitecture or abnormal protein aggregation. It commonly occurs as a result of aging processes (age-related cataract). Rarely, it can be present from birth or develop during childhood or early in life (early-onset cataract).

Cataract is treated surgically by phacoemulsification. This involves breaking up the affected lens using an ultrasonic probe and aspirating its contents. The lens is then replaced by an artificial intraocular lens.

Early-onset cataract is the most common cause of treatable visual impairment in children and accounts for half of the cases of childhood blindness in the world (43, 44).

1.3.1 Early-onset cataract

Early-onset cataract is classified as congenital if it is present from birth and as pediatric or juvenile, respectively, if it develops during early childhood or in adolescence (45). All three forms of early-onset cataract are referred to as congenital cataract in this thesis. Congenital cataract occurs at a rate of 1-6 per 10,000 births in developed countries and 5-15 per 10,000 births in developing countries (43). In the absence of a timely referral to an ophthalmologist, cataract can interfere with normal visual development in children resulting in amblyopia (or lazy eye; due to lack of stimulation of the nerve pathways from an eye to the brain) or nystagmus (involuntary eye movements) (46). Post-operative complications of cataract surgery such as glaucoma (damage to the retina and optic nerve), develop in a proportion of cases and may potentially lead to blindness (47). The age at presentation and surgery with other factors might be critical in determining the probability of developing secondary glaucoma (48, 49). Along with treatment costs, long-term rehabilitation and visual assistance are required for patients (50).

The phenotype of congenital cataract is determined by the position and appearance of the lens opacity (51). Nuclear cataract, which is opacity in the lens nucleus, indicates deregulation of early processes in lens development whereas opacity in the cortex of the lens affecting the newly formed secondary fiber cells, referred to as cortical cataract, indicates deregulation of a later event in lens development. Total cataract is the complete opacity of the nucleus and cortex of the lens. Opacification of the discrete lamellae formed as a result of concentric deposition of secondary fiber cells, are referred to as lamellar cataract, and may be pulverulent or dot-like in appearance. Sutural opacities occur due to opacification of the anterior and/or posterior sutures. Posterior polar cataract as the name

suggests affects the posterior pole of the lens and is thought to develop due to degeneration of fiber cells or necrosis of migrating cells (52). On the other hand, abnormal detachment of lens vesicle from the surface ectoderm during lens development may result in opacity at the anterior pole of the lens referred to as anterior polar cataract (53).

Congenital cataract can occur due to a metabolic disorder, intrauterine infection, exposure to toxins, trauma during development or genetic abnormality (44). The underlying cause of a proportion of congenital cataracts is still unknown leading to difficulty in management of such cases. Vitamin A deficiency and intrauterine infections such as rubella, cytomegalovirus and toxoplasmosis contribute to avoidable causes of congenital cataract especially in developing countries (54, 55). Vitamin A supplementation and immunization programs have been instrumental in lowering the incidence of such cataracts. Up to a quarter of congenital cataracts are caused due to genetic mutations (56) and are referred to as inherited congenital cataracts.

1.3.1.1 Inherited congenital cataracts

Inherited congenital cataracts are genetically and phenotypically heterogeneous (57). They may have autosomal dominant, autosomal recessive or X-linked modes of inheritance (58). These can occur as part of a syndrome or in isolation.

In syndromic congenital cataract, cataract may be associated with other systemic or ocular abnormalities (59, 60). However, it may not be clearly distinguishable from isolated cataract when first diagnosed due to the progressive development of the anomalies. To

date, causative mutations in at least 150 genes have been reported and genes for at least eight congenital cataract causing syndromes are still unknown (58).

1.3.1.1.1 Isolated congenital cataract

Mutations in genes can also lead to isolated cataract. The same mutation can lead to different cataract phenotypes in different families or within the same family (45). At least 24 known genes with mostly missense or frameshift causative mutations have been reported so far (58). In addition, linkage to at least nine loci with an unknown causative gene is known to date (58). Most of the inherited isolated cataracts follow an autosomal dominant mode of inheritance. Nearly 50% of the isolated congenital cataract causing mutations have been reported in at least 11 different crystallin genes (58). These mutations typically result in nuclear or lamellar opacities. A quarter of the known causative mutations are in genes encoding for membrane proteins and gap junction proteins (45). Genes encoding membrane associated proteins, cytoskeletal proteins, transcription factors and cytoplasmic proteins are also known to harbor congenital cataract causing mutations. All these causative genes have been predominantly identified through linkage analysis and candidate gene analysis. Lately, whole exome sequencing has emerged as a novel tool to identify causative mutations in affected families especially with limited family history and accessible genetic material (61-63). Appendix 1.1 lists all the genes, mutations in which have been reported to cause isolated congenital cataracts. *EPH receptor A2* (*EPHA2)* gene is the most recently identified congenital cataract causing gene (64-69).

1.3.1.2 Molecular effects of causative mutations

Mutation in a gene may result in a gain or a loss of function of the mutant protein and suggest a role of the causative gene in lens development. Lens development involves a well regulated orderly expression of different genes at various stages of lens morphogenesis which may relate to the diverse congenital cataract phenotypes (70).

Studies both *in vitro,* by over-expressing the mutant gene in cultured cells or *in vivo,* by generating transgenic or knockout animal models have assisted in determining the functional effects of causative mutations in a gene. For example, analysis of the R116H mutation in the *CRYAA* gene revealed modification of secondary structure, chaperone activity and aggregation state of the mutant protein in a cell culture system (71). These results suggested that increased self-aggregation of the mutant protein and co-aggregation with target proteins was probably the underlying cause of cataract development. Similarly analysis of lenses from a knock-in mouse model of R49C mutation in the *CRYAA* gene revealed decreased solubility of some crystallin proteins and increased cell death in the lens due to the presence of the mutation (72). These results again suggest that causative mutations in the *CRYAA* gene promote insoluble protein aggregation perhaps leading to cell apoptosis. Such studies also enable identification of key role of the wild-type protein in lens induction, development and/or maintenance of lens transparency and its role in cataractogenesis (70).

1.3.2 Age-related cataract

Age-related cataract (ARC) begins to develop in people over ~ 45 years of age due to progressive damage to the lens over time (73). Phenotypically it is classified as cortical, nuclear or posterior subcapsular cataract. Cortical and nuclear opacifications have been described above (Section 1.3.1). Subcapsular cataract refers to opacification of the posterior pole of the cortex close to the posterior capsule. ARC accounts for approximately 48% of blindness in the world. (74). In the United States alone, people affected with cataract are estimated to be 30.1 million by 2020 (75). Due to lack of awareness and access to surgeries the disease burden is significantly more in developing countries (76, 77). Although usually successful, cataract surgery in older patients may lead to post-surgical complication such as posterior subcapsular cataract (78). With an increasing aging world population, visual impairment due to age-related cataract imposes a social, physical and medical burden on societies (74).

1.3.2.1 Changes in lens with age and Age-related cataract

The ocular lens grows throughout life without shedding damaged cells. Therefore it is important that mechanisms to recoup the damage due to various environmental insults are in place, failure of these can lead to lens opacity.

There is an exponential increase in light scattering by ocular lens with age (79). Older lenses have a stiffer nucleus possibly due to high proportion of cholesterol, reduced water content and altered lipid content in the cell membranes (80-82). The increased rigidity of the membranes might affect function of various membrane bound or membrane interacting

proteins. Reduced elasticity of the lens nucleus with age leads to decline in lens accommodation and hence presbyopia or age-related long sightedness (83). The age-related discolouration of lens nucleus is attributed to changes in lens proteins or perhaps generation of chromophores contributing to age-related nuclear cataract (84). Additionally, there is a significant decrease with age in antioxidant compound GSH levels in the lens nucleus (85) which may lead to accumulation of damage due to oxidative stress over time. This is also supported by the observations that proteins from older lenses have more post-translational modifications including oxidation as compared to younger lenses (86, 87). The formation of a barrier in the lens around middle age restricts the transport of small molecules such as antioxidants and scavenging molecules from the cortex to the lens nucleus rendering the lens nucleus susceptible to age-related changes and environmental insults.(88).

Unlike the deeper cortex, the superficial cortex of the lens has adequate supply of nutrients and antioxidant molecules (5). Cortical opacities are generally not uniform indicating variability in the nature of damage to the fiber cells. It has been suggested that stiffness of the lens causes mechanical stress at the nuclear-cortical interface during accommodation, thus leading to breakdown of cortical fiber cell arrangement and hence cortical cataract (5). The opaque fiber cells have increased amounts of free Ca^{++} which could possibly lead to increased protein aggregation (89). However, due to lack of enough evidence it is difficult to predict if these theories explain the cause or effect of cortical cataract development and need further investigation.

Cataract, once developed is irreversible. Even though the mechanism of ARC development is unclear, increased oxidative stress is known to play a role in the process (90, 91). Due to

the economic burden and social impact of cataract surgery, recent focus has been on preventing development or delaying progression of cataract by the use of various pharmacologically active compounds such as Vitamin C and E, several plant derived compounds and other compounds with antioxidant properties (92-110). However, none of these compounds have convincingly demonstrated an effect on human cataract development or progression.

Epidemiological studies provide insight into factors involved in ARC development. Several studies have reported inter-racial differences in the prevalence of ARC phenotypes. In Icelandic, Japanese, Chinese, African-Americans and African-Caribbean populations cortical cataract is more prevalent than nuclear cataract while in Caucasian Americans nuclear cataract is more common (111-115). In the Singaporean-Malay population incidence of both cortical and nuclear cataracts were comparable and they were at a higher overall risk of developing ARC as compared to Asian and Caucasian populations (111, 114). In an Indian population, the total incidence of cataract was approximately 73% with a higher prevalence of nuclear cataract (116). The differences in prevalence among populations are believed to be due to differences in lifestyle, environment and genetic backgrounds.

1.3.2.2 Environmental risk factors

Epidemiological studies suggest an important role of environmental modifiers in the likelihood of developing ARC. A complex gene-environment interaction contributes to

ARC thus necessitating an understanding of the modifiable risk factors, some of which are discussed below.

Ultraviolet light (UV) exposure is a known risk factor for developing cortical cataract (117). It is difficult to quantify long-term UV exposure over years due to differences in length of exposure and protection used by individuals. Nonetheless, UV exposure over a period of time causes most damage in the nasal quadrant in the anterior cortex of the lens (118), thought to be due to oxidative stress following the exposure (115). Reduction in the amount and stability of the UV filters in the lens with age leads to an increased susceptibility to UV-induced ARC (119-124). It has been reported to contribute an attributable risk of 10% in an Australian population (125).

Diabetes increases the risk of developing cortical and posterior subcapsular or mixed cataracts (126-128). The risk of cataract development is associated with both, the duration of diabetes and levels of glycated hemoglobin (129). Increased accumulation of glycated end products, altered gene regulation, oxidative nitrosative stress and increased osmotic stress in the lens are some of the suggested mechanisms of cataract development related to diabetes (130-134). Association of 15 loci with diabetic cataract in a Taiwanese population demonstrates genetic susceptibility to this form of cataract (135). The association of diabetes with cataract also exhibits vulnerability of the lens to metabolic stresses.

Smoking is associated with development of nuclear and subcapsular cataract (136-138). Approximately 20% of cataracts in the U.S. are attributed to smoking (139). The oxidative stress induced by smoking or the tobacco by-products may lead to the increased risk of ARC (140). Epidemiological studies show a dose-response association of smoking with

cataractogenesis and reduced risk of cataract development on cessation of smoking (141, 142). These observations suggest that changes to the lens due to smoking are reversible and perhaps can be avoided.

Multiple epidemiological studies have reported a greater risk of ARC development in women (116, 143-146) and a protective effect of hormone replacement therapy (HRT) in cataractogenesis (117, 147). Conversely, some studies report either no or increased association between HRT and cataract development (148-150). This discrepancy in associations could either be due to a small protective effect of HRT or due to differences in the study designs. However a meta-analysis of the existing studies suggests that there is a protective effect of HRT in nuclear cataract (151).

Apart from the well-established risk factors, there are emerging factors associated with the risk of cataract development. Myopia or shortsightedness is associated with an increased risk of developing nuclear and subcapsular cataract in multiple populations (152-154). Epigenetic regulation of *CRYAA* in myopic patients may contribute to their increased susceptibility to cataractogenesis (155). Interestingly, Pseudoexfoliation Syndrome, another ocular condition which is characterized by accumulation of fibrillar deposits on the anterior surface of the lens, is also associated with increased risk of developing nuclear cataract in multiple populations (156-159). Use of corticosteroids for treatment of glaucoma, along with drugs used for treatment of hypertension and diabetes, also lead to an elevated risk of usually nuclear cataract (160-162). However, it is not entirely clear if the presence of the disease or administration of drugs is associated with the increased risk. In addition to other ocular and systemic diseases, various lifestyle factors are associated with increased risk of developing cataract. A high socio-economic status is associated with

lower risk of developing cataract probably due to better nutrition linked to the affluent lifestyle (137, 147, 163). Interestingly, moderate alcohol consumption is associated with a lower risk of developing cataract as compared to high or no consumption of alcohol (164). A case-control study in a Greek population and another study in American women demonstrated predisposition to cataract development due to a high fat diet (165, 166). The understanding of these associations is still evolving and requires further studies.

1.3.2.3 Genetic risk factors

Apart from the above mentioned environmental modifiers, genetic predisposition places some individuals at an increased risk of development of ARC. In twin studies heritability of age-related cortical cataract was reported to be 53%-58% and that of nuclear cataract to be 14%-48% (167). In addition, familial aggregation of cortical and nuclear cataracts suggests involvement of genetic factors (168, 169). Variants in genes involved in isolated or syndromic congenital cataract, such as *GALT* (9p13), *Solute carrier family 16 member 12* (*SLC16A12*; 10q23), *HSF4* (16q21), *CRYAA* (21q22) and mutations in *GJA3 (*6q21*), GJA8 (*1q21*)* and *LIM2 (19q13)* have been associated, in different populations, with ARC (170-175). In addition, other functionally important genes in the lens such as antioxidant genes, *Superoxide dismutase 1* (*SOD1;* 21q22), *Glutathione peroxidase* (*GPX*, 3p21), *Catalase* (*CAT*, 11p13) and *Idoleamine 2,3 dioxygenase* (*IDO;* 8p12) or genes known to play a role in protein processing such as *5,10-methylenetetrahydrofolate reductase* (*MTHFR;* 1p36) have been associated with ARC through case-control studies (176-178). However, these associations also have not been replicated. Variants in another free-radical scavenging gene *Glutathione S-transferase mu-1* (*GSTM1*, 1p13.3) have been reported to

contribute to development of ARC in multiple studies (179-181). Similarly *N-acetyltransferase type 2* (*NAT2*, 8p22), which removes free radicals by acetylation and genes encoding for DNA repair enzymes such as *Xeroderma pigmentosum complementation group D* (*XPD*; 19q13) and *X-ray repair complementing defective in chinese hamster 1* (*XRCC;* 19q13) have each been associated with ARC in at least two case-control studies (182-185). Association of obesity associated gene, *Fat-mass and obesity associated (FTO*; 16q12) with ARC again demonstrates a gene-environment interaction in ARC development (186, 187). Association of microRNAs (miRNA), which are small non-coding RNA molecules, such as *Let7a* with ARC has also been reported in a Japanese population (188). Downregulation of *CRYAA* expression due to methylation of its promoter in nuclear cataracts, provide evidence of epigenetics regulation in cataract development (174). These associations indicate the varied processes involved in age-related cataract development.

A genome-wide linkage study in affected families identified a locus on chromosome 1p linked to age-related cortical cataract (189). A subsequent study reported mutations in the *EPHA2* gene to cause congenital cataract and association of the common variants in the gene to be associated with age-related cortical cataract (68). Association of *EPHA2* with ARC has been independently replicated in Chinese, Indian, American, British and Australian populations (190-192). In the present work, the effect of environmental factors on *EPHA2* mediated cataractogenesis was investigated.

1.3.2.4 Understanding interaction of multiple factors in ARC development

The complex gene-environment or gene-gene interactions which determine an individual's risk of development of ARC can be further understood using animal models of ARC. The influence of environmental modifiers such as UV exposure and diabetes on cataract development has been demonstrated in several rodent models of cataract (193-195). The damage caused due to UV exposure and the repair mechanisms in the ocular lens have been investigated in multiple studies (196-199). In addition to providing proof of association of diabetes with increased susceptibility to cataract development, studies in diabetic rodent models facilitate investigation of common molecular pathways affected by both the diseases (131, 200, 201).

Various mouse mutants have been generated for studying age-related progression of cataract. Some of the most studied models of ARC include Emory mouse and Senescence Accelerated Mouse. Emory mouse is a well characterized model for ARC (202). This mouse develops spontaneous autosomal dominant anterior cortical cataract at 5-6 months of age progressively developing to complete opacity. Emory mouse has been used to demonstrate gender-related differences and effect of UV-B exposure on cataract development and progression (203, 204). Senescence Accelerated Mouse provides a model for accelerated aging. Two strains of Senescence Accelerated Mouse develop cataract due to degeneration of the lens cortex leading to mature cataract with age (205, 206). However, the underlying genetic abnormality in both these mouse models is unknown.

Some mice with a known genetic defect develop ARC. For example, mouse lacking antioxidant gene *glutathione peroxidase-1* (*Gpx*) or transcription factor *Clock* gene develop ARC (207, 208). These two mouse mutants demonstrate the effect of oxidative stress and

circadian clock, respectively, on cataract development. Mouse lacking DNA repair enzymes such as mice with mutated ataxia telangiectasia (*Atm)* are rendered more sensitive to developing cataracts upon irradiation (209). Recently, mouse carrying mutation in the crystallin gene *Cryba2*, mutations in which cause congenital cataract in humans, was reported to develop ARC (210). Likewise, LEGSKO mouse characterized by lack of GSH synthesis begins to develop nuclear cataract from 4 months of age (211).

Multiple strains of the *Epha2* knockout mouse are available and exhibit different lens phenotypes (191, 212-214). At least three of these strains develop progressive cataract demonstrating the effect of lack of *Epha2* in the lens. To further understand the mechanisms of cataractogenesis, the work in this thesis focuses on role of *EPHA2* in cataract development.

1.4 The *EPHA2* gene and Cataract

The *EPHA2* gene located on 1p36, is the only gene that has been reproducibly implicated in both congenital and age-related forms of cataract. Congenital cataract causing mutations in the gene, with both autosomal dominant or recessive mode of inheritance, have been identified in families from different ethnicities (64-69). These include both missense and frameshift mutations that lead to either posterior polar, nuclear, progressive posterior, zonular or total cataract. A congenital cataract causing mutation in the gene was reported in an Australian family by our group (65). Additionally, at least four of these causative mutations led to destabilization and aggregation of mutant EPHA2 protein and impaired cell migration (215). *EPHA2* has also been associated with an increased risk of age-related

cortical or posterior subcapsular cataract development in multiple populations including in an Australian cohort (68, 190-192). The associated single nucleotide polymorphisms (SNPs) are present in the exons, introns and in the untranscribed region (UTR) of the gene. Whether involvement of *EPHA2* in both forms of cataract could provide understanding of a link between congenital and age-related cataract remains to be investigated. The *Epha2*$^{-/-}$ mice also develop cataract (191, 213) or exhibit altered lens shape, lens cell migration and refractive properties (212); further demonstrating importance of Eph signalling in lens development and lens homeostasis.

At the commencement of this study the function of *EPHA2* in the lens and its role in cataract development is not well understood. We wanted to further examine how defects in the gene lead to both congenital and age-related cataract.

1.5 Eph-ephrin molecules

EPHA2 belongs to the Eph family of receptor tyrosine kinases. Eph receptors are the largest family of receptor tyrosine kinases (216). These are of two types- EphA and EphB receptors. Nine EphA (EphA1-8 and EphA10) and 5 EphB receptors are known to date (216). An Eph receptor typically consists of an extracellular region containing a globular ligand binding, a cysteine-rich and three fibronectin-rich domains followed by a transmembrane segment and an intracellular region containing, a tyrosine kinase, sterile alpha motif (SAM) and a PSD-95, DLG, ZO-1 (PDZ) domain (Figure 1.5a) (216, 217). Eph receptors interact with either a glycosylphosphatidylinositol (GPI) anchored Ephrin-A or transmembrane Ephrin-B ligand (Figure 1.5a). Five Ephrin-A and 3 Ephrin-B ligands

are known to date. Usually an EphA or EphB receptor expressed on a cell respectively interacts with an Ephrin-A or Ephrin-B ligand expressed on a neighbouring cell. Exceptions to this are EphA4 and EphB2 receptors which respectively interact with Ephrin-B1 and Ephrin-A5 ligands (218, 219). EphA2 is known to interact with Ephrin-A1 and Ephrin-A5 (220). Several Eph receptors and their Ephrin ligands are known to be expressed in the ocular lens; Ephrin-A1, A3-4 and B1-3 ligands and EphB2-3 receptors are only expressed in lens epithelial cells while EphA2-4, B4, B6 receptors and Ephrin-A5 ligand are expressed in both lens epithelial and fiber cells (213, 221). The function of these receptors and ligands in the lens is not clearly understood.

1.5.1 Eph-Ephrin signalling and its roles

The Eph-Ephrin interaction leads to bidirectional signalling, forward signalling in the receptor bearing cell and reverse signalling in the ligand bearing cell (Figure 1.5b) (217). The receptor-ligand interaction leads to dimerization and oligomerisation of the receptor-ligand complex leading to formation of a signalling cluster (Figure 1.5d). This leads to activation of numerous signalling cascades (Figure 1.6). The signalling is terminated by internalization and degradation of the receptor-ligand complex in the receptor bearing cell or by cleavage of the extracellular domain of either the receptor or ligand by metalloproteases (Figure 1.5c). Occasionally, the receptor and ligand on the same cell interact with each other leading to downregulation of Eph-ephrin signalling (222).

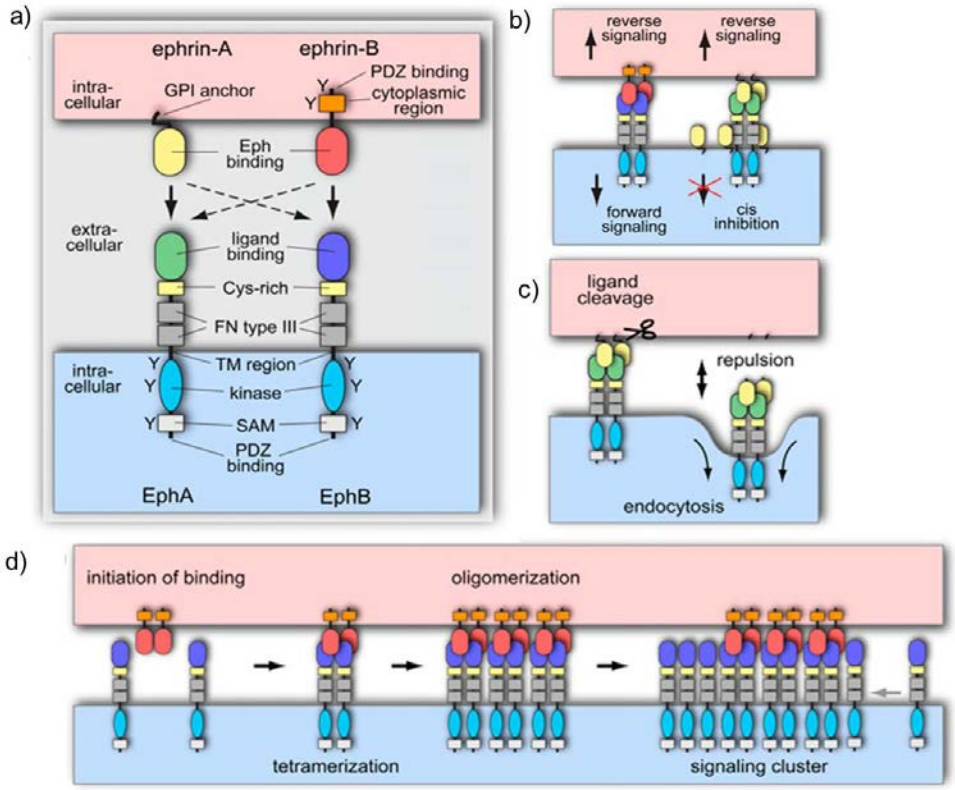

Figure 1.5: Structural domains and signalling through Eph-ephrin molecules

a) Shows the structural domains of Eph receptors and their Ephrin ligands. The receptor comprises of ligand-binding (green or violet), cysteine-rich (yellow), fibronectin-rich type III domains (grey), a transmembrane region (TM region) followed by the kinase (blue), SAM (white) and PDZ domain. Ephrin-A ligands are GPI-anchored and consist of a receptor binding domain (yellow). Ephrin-B ligands comprise of a receptor binding domain (red), transmembrane segment, cytoplasmic region (orange) and a PDZ domain. The dashed arrows indicate interaction of EphA receptors with Ephrin-B ligands and of EphB receptors with Ephrin-A ligands b) shows the interaction of Eph receptor with its Ephrin ligand on the neighbouring cell. This interaction leads to forward signalling in the receptor bearing cell and reverse signalling in the ligand bearing cell. Interaction of the receptor and ligand in the same cell leads to cis-inhibition. c) shows termination of signalling that occurs by enzymatic cleavage of the extracellular domain and endocytosis of the receptor-ligand complex by receptor bearing cell leading to repulsion of neighbouring cells that plays an important role in cell sorting and cell migration. d) shows the receptor-ligand interaction leading to dimerization and oligomerisation of the receptor-ligand complex, and finally formation of a signalling cluster. This signalling cluster activates several signalling cascades. Adapted from Pitulescu and Adams, 2010, Genes Dev, 24. (216)

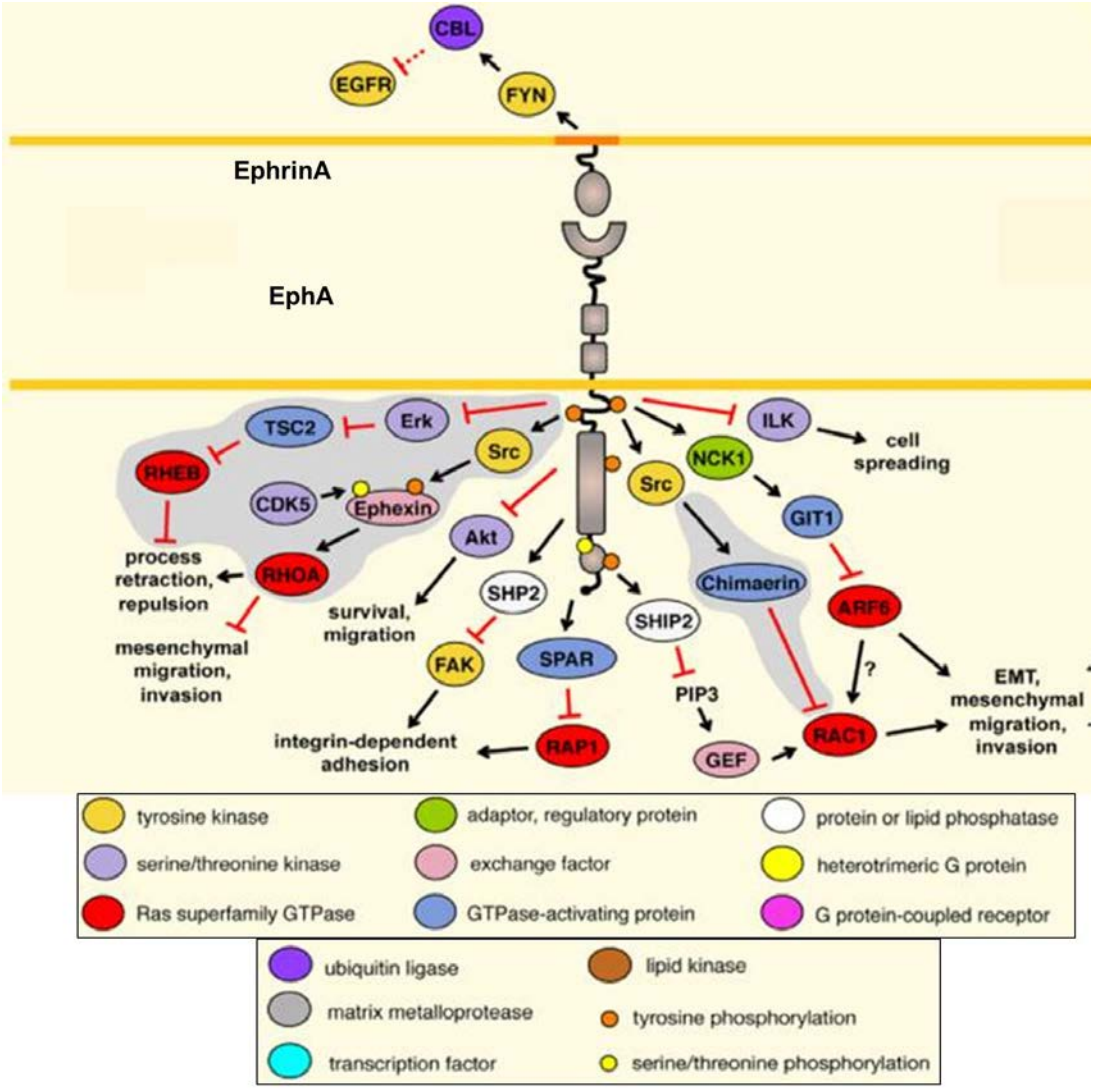

Figure 1.6: EphA-ephrin-A signalling pathways

EphA receptors interact with their respective Ephrin ligands to bring about cell signalling. Signalling in the receptor bearing cell is called forward signalling and in the ligand bearing cell is called reverse signalling. The figure illustrates various downstream effectors involved in cell signalling mediated through EphA-ephrin-A molecules. The different types of effector molecules are indicated in the receptor bearing cell. This signalling plays a critical role in cell adhesion and repulsion, migration, survival and epithelial to mesenchymal transformation. Taken from Pasquale, 2010, Nat Rev Cancer, 10. (215)

Alternatively, the receptor can act independently of the ligand by interacting with other signalling pathways. For example, Epha2 interacts with Src-kinase pathway and Epidermal Growth Factor Receptor (EGFR) pathway (223, 224). Reverse signalling via the Ephrin ligand generally acts through the Src kinase pathway (225). There are only a few studies reporting effect of EphrinA reverse signalling (226). Ephrin B reverse signalling is known to contribute to tumour invasion by altering gene transcription, promoting cell migration and slowing down cell-junction formation (227-230).

The Eph-ephrin signalling is known to play a vital role in numerous developmental, physiological and pathological processes by mainly modulating epithelial cell adhesion and repulsion. This signalling has an important role during development in defining tissue boundaries through cell sorting by careful regulation of the adhesive and repulsive forces between cells (231). Additionally, through modulation of cell cytoskeleton, cell-cell and cell-substrate adhesion/repulsion and cell protusion dynamics this signalling plays a critical role in various cellular processes (225). Studies suggest the importance of this signalling in cell migration, cell spreading and survival, regulating immune response, repair after injuries and cell homeostasis (232-239). Eph-ephrin signalling also regulates epithelial-to-mesenchymal transition and therefore has a key role in diseases such as cancer (216).

1.5.2 *EPHA2* signalling and its function

The EPHA2 protein, formerly known as epithelial cell kinase (eck), is a 130 kDa transmembrane receptor which is known to interact with its Ephrin-A ligands. The *EPHA2* gene is highly expressed during gastrulation, in rhombomeres of the hindbrain during

development, embryonic stem cells, embryonic spinal cord and retina (240). Its expression is more restricted to proliferating epithelial cells during development and in adult tissues (241). Adult epithelial cells in the ovary, kidney, lung and colon express low levels of *EPHA2* (242-246).

EPHA2 signalling is involved in several biological processes. Upregulation of *EPHA2* receptor expression was identified in a screen of human cancer cells (247). The gene is frequently overexpressed in breast, ovarian, esophageal, lung, glioblastoma, colorectal and prostate cancers and the expression correlates with the metastatic potential and poor survival. Therefore *EPHA2* serves as a potential drug target for cancer treatment (248-254). Its expression in tumors also promotes angiogenesis (252, 255, 256). Exogenous overexpression of the protein in non-metastatic cells results in their oncogenic transformation (257). Activated EPHA2 upregulates expression of extracellular matrix protein, fibronectin, thereby increasing cell-matrix adhesion and promoting malignancy (258). Crosstalk with other oncogenic pathways like EGFR or Src-kinase pathways is thought to lead to its metastatic potential (223, 224). Expression of the unphosphorylated protein in cancer cells indicates silencing of EphA2 forward signalling that contributes to its tumorigenic potential (256, 259, 260). The chromosomal region 1p36, where the *EPHA2* gene is located, is frequently deleted in a number of cancerous cells resulting in loss of EPHA2 function (261). Therefore *EPHA2* potentially acts as an oncogene and a tumor suppressor depending on the stage of cancer.

Similar to other Eph-ephrin molecules, *EPHA2* is essential for neural development. Its interaction with a guanine-exchange factor, Tiam1, leads to neurite outgrowth in cultured cells (262). The signalling regulates insulin secretion thereby playing an important role in

glucose homeostasis (234). Due to its involvement in cell communication, this signalling is vital for bone homeostasis (263). EPHA2 signalling is essential in cell migration and adhesion and thus has an important role in maintaining epithelial cell homeostasis and cell-junctions (264-267). Oxidation of EPHA2 due to oxidative stress in old heart progenitor cells affects internalization of the receptor-ligand complex impairing cell migration (268).

Epha2 expression is conserved between human and mouse lens (191). In the mouse lens it is expressed in lens epithelial cells and superficial fiber cells with limited expression in mature fiber cells (212). *Epha2*$^{-/-}$ mouse have lens opacification (191, 213, 214) and/or disrupted lens architecture resulting in altered suture formation and smaller lenses (212). These results demonstrate the importance of Epha2 in lens development and in maintaining lens homeostasis.

1.6 Hypothesis and aims of the project

The genetic link between *EPHA2* with cataract is well-established but the mechanism of cataract development is not well understood. The main objective of the work presented in this thesis was to elucidate the role of *EPHA2* in congenital and ARC development. This was investigated by adopting three approaches, that is, human genetic study, examining effects of causative mutations in a cell culture system and analyzing effects of environmental modifiers in a knockout mouse model. The human lens grows throughout life; cell migration, homeostasis and effective cell-cell communication play a critical role in maintaining lens transparency. Disruption of *EPHA2* function in the lens may affect these cellular processes, hence leading to cataract development.

At the initiation of this work, a few families from different ethnic backgrounds were known to have congenital cataract causing mutations in the gene. This included an Australian family, mutations in which were reported by our group. However, the overall genetic burden of mutations in *EPHA2* to congenital cataract was unknown. Therefore we investigated the genetic contribution of *EPHA2* to congenital cataract in an Australian cohort. Moreover, recently, the effect of four causative mutations in *EPHA2* has been analysed in cell lines which do not form established cell-junctions (215). As EPHA2 is expressed in a variety of epithelial cells, we performed localisation analysis of mutant EPHA2 proteins in epithelial cell lines to examine the potential effect of the causative mutations on protein function.

Apart from genetic association of SNPs in *EPHA2* with age-related cortical cataract, *EPHA2* and ARC are associated with a common set of environmental risk factors. Previous work in cultured cells and mouse lens has been instrumental in demonstrating that age, estrogen (female hormone) and UV exposure affect Epha2 expression (191, 269, 270). Interestingly, these three environmental modifiers are also known risk factors for developing ARC (74). Therefore we investigated if an interaction of these environmental factors with Epha2 affects ARC development. For this we analysed the effect of inevitable and modifiable risk factors namely age, gender and UV exposure on *Epha2* mediated cataract development using an *Epha2* knockout mouse model.

The following chapters describe the results of each of these studies.

2. Genetic contribution of mutations in the *EPHA2* gene to inherited cataracts in South-Eastern Australia

Please note that the work presented in this chapter has been published.

2.1.Introduction

Inherited congenital cataract causing genes are mapped/identified either through linkage analysis in large families or by candidate gene analysis (58). One of the most recently identified causative genes is the *EPHA2* gene, mutations in which have only been reported in the last six years. As described in Chapter 1, section 1.5, the gene encodes a transmembrane tyrosine kinase receptor comprising a ligand binding, a cysteine-rich and three fibronectin-rich domains followed by a transmembrane segment, the juxtamembrane region, a tyrosine kinase, SAM and a PDZ domain (216). Causative mutation in the *EPHA2* gene was first identified through linkage analysis in a European-American family with autosomal dominant posterior polar congenital cataract (68). This family was found to carry a missense change, c.2842G>T (p.G948W), in the SAM domain of the protein. Following this initial report, mutations in *EPHA2* have been reported to cause congenital cataract in multiple families and lead to diverse cataract phenotypes. A missense mutation, c.2819C>T (p.T940I), in a Chinese family and a frameshift mutation, c.2915_2916delTG (p.V972GfsX39), in a British family both lead to autosomal dominant posterior polar cataract (65) while another missense mutation, c.2668C>T (p.R890C), also in a Chinese family leads to autosomal dominant progressive posterior cataract (67). An Australian family with autosomal dominant total cataract was found to carry a splicing mutation c.2826-9G>A (p.D942fsXC71) in *EPHA2* by our group (65). This family was from our South-Eastern Australian cohort of congenital cataract cases and the causative gene in the family was previously mapped to chromosome 1p through linkage analysis (271).

Recently, a duplication mutation c.2925dupC (p.I976HfsX37) leading to C-terminal extension of the protein was reported in another Caucasian family from Unites States (69) .

Autosomal recessive mode of inheritance of mutations in *EPHA2* has also been reported in two families. These include a Pakistani family with nuclear cataract carrying a missense mutation c.2353 G>A (p.A785T) (66) and a Saudi Arabian family with unknown cataract phenotype carrying a missense mutation c.1405T>C (p.Y469H) (64).

A few studies have examined the genetic burden of mutations in a causative gene on congenital cataract in different cohorts. Screening of crystallin genes, mutations in which are a significant contributor to congenital cataract, in an Australian and Indian cohort of cases revealed a mutation frequency of 5.2% and 16.6%, respectively (272, 273). With the advent of exome sequencing, similar studies examining the frequency of causative genes have been performed in cohorts from other countries (62, 64, 274). However, these mutations only account for a small proportion of congenital cataract cases. As is evident, mutations in the *EPHA2* gene have been found in families from different ethnic backgrounds however, no studies have examined the overall genetic burden of mutations in *EPHA2* to congenital cataract. We wanted to analyse the frequency of mutations in *EPHA2* in congenital cataract cases in Australia. For this, we screened a South-Eastern Australian cohort of inherited cataract cases for causative mutations in the gene.

2.2. Materials and Methods

2.2.1. Patient recruitment

Ethics approval for the study was obtained from the Southern Adelaide Clinical Human Research Ethics Committee and the Royal Victorian Eye and Ear Hospital (RVEEH) Human Research Ethics Committee. Probands with familial cataract and their family members were recruited from the Flinders Medical Centre (Adelaide), Women's and Children's Hospital (Adelaide), Royal Children's Hospital (Melbourne) and RVEEH (Melbourne) over the past 14 years. RVEEH also served as a tertiary referral center for patients from Tasmania. Family history of the disease in all the families was available through previous clinical records. All participants gave written informed consent to be included in the study.

2.2.2. Control cohorts

Normal South Australian (NSA) controls were healthy individuals above the age of 50 years recruited from around Adelaide, Australia, with no record of congenital cataract surgery. Out of the 270 controls screened, 64 individuals had age-related cataract.

Blue Mountains Eye Study (BMES) is an Australian population-based study (275). The participants were recruited since 1996 from the Blue Mountains region west of Sydney, Australia. A survey of vision and common eye diseases was conducted for all the participants with a follow-up after 10 years. This study comprised of both age-related cataract cases and controls. In the present study DNA samples from the BMES cohort were

used for screening the rare variant found in Exon 17 of *EPHA2* gene. All cases with diabetes were excluded from the study. Age-related cataract cases above the age of 50 years with cortical cataract in ≥25% in either eye were used as cases. Individuals above the age of 65 years with no cataract of any phenotype were used as controls.

2.2.3. DNA extraction

Genomic DNA (gDNA) of recruited individuals was extracted from either whole blood using QIAamp DNA blood maxi kit (QIAGEN Pty Ltd, VIC, Australia) or saliva using Oragene collection kit (DNA Genotek, ON, Canada) or buccal swab using Gentra PureGene Reagent (QIAGEN Pty Ltd, VIC, Australia).

DNA samples with sub-optimal quantity were amplified using illustra™ GenomiPhi™ DNA amplification kit (GE Healthcare, NSW, Australia). One to five microliters of gDNA was mixed with sample buffer to make up a volume of 10 µl and denatured at 95°C for 3 minutes. The master mix with 9 µl reaction buffer and 1 µl Phi29 DNA polymerase enzyme was added to this mixture and the mixture was amplified at 30°C for 90 minutes. The enzyme was deactivated at 65°C for 10 minutes.

The suitability of the old and pre-amplified gDNA samples to be used for sequencing was determined by polymerase chain reaction (PCR) amplification of Exon 6 of the *EPHA2* gene. In-house *EPHA2* primers were used for the amplification reaction (Refer to Appendix 2.1). Forty nanograms of old gDNA or 2 µl of one-tenth dilution of pre-amplified gDNA was amplified using 0.25 units (U) of HotStar Taq *Plus* DNA polymerase (QIAGEN Pty Ltd, VIC, Australia) in the presence of 1 × reaction buffer (QIAGEN Pty

Ltd, VIC, Australia), 0.1 mM dNTP mix (QIAGEN Pty Ltd, VIC, Australia) and 0.5 µM of each primer (Geneworks Pty. Ltd., Adelaide, Australia) in a total 20 µl volume. HotStar Taq *Plus* DNA polymerase was activated at 95°C for 5 minutes, followed by denaturation at 95°C for 30 seconds, annealing at 57°C for 30 seconds and extension at 72°C at 30 seconds for 30 cycles. This was followed by post-extension at 72°C for 10 minutes and incubation at 4°C for 5 minutes. PCR products were visualized on a 1% agarose gel prepared by dissolving 1 g agarose (Promega, VIC, Australia) in 100 ml Tris-Borate-Ethylenediaminetetraacetic acid (EDTA); (TBE) buffer (See Appendix 3.1). The concentration of pre-amplified DNA was estimated by the intensity of PCR product on the agarose gel while the concentration of gDNA samples was spectrophotometrically determined using SmartSpec™ Plus (BioRad Laboratories Pty Ltd, NSW, Australia).

2.2.4. Mutation screening

Eighty four probands with inherited cataract were included in this study. All 17 exons including the intron-exon boundaries of the *EPHA2* gene (GenBank accession NM_004431.3) were amplified by PCR and sequenced at the Australian Genomics Research Facility (AGRF; QLD, Australia; 68 cases) or in-house (16 cases) by direct sequencing using BigDye Terminators (Applied Biosystems, VIC, Australia). One microgram gDNA or one-tenth dilution of the pre-amplified gDNA from cases, in a total volume of 100 µl each was sent to the AGRF for sequencing. The sequencing of 16 index cases using in-house primers was performed by Ms Kate Laurie, Flinders University, Adelaide, Australia. Sequences of the primers used for sequencing in-house and at AGRF

are listed in Appendix 2.1 and 2.2, respectively. Forty nanograms of gDNA was used for amplification.

All samples that failed to produce a sequence using automated systems at AGRF were sequenced using in-house primers. Exons 1 to17 were amplified by PCR as described previously in section 2.2.3. The amplification of Exon17 was performed for 35 cycles. The PCR products were visualized on a 1% agarose gel. The PCR products were prepared for sequencing by removing excess primers and unused dNTPs by treatment with 10 U Exonuclease I (New England Biolabs, Genesearch Pty Ltd, QLD, Australia) and 2 U of Shrimp Alkaline Phosphatase (SAP) (USB®, Millennium Science Pty. Ltd., VIC, Australia) at 37°C for 1 hour followed by enzyme deactivation at 65°C for 15 minutes.

2.2.5. Sequencing analysis

Sequence of exons of the *EPHA2* gene in the probands was compared with the reference sequence NM_004431.3 using Sequencher 4.1.0 (Gene Codes Corporation, MI, USA). All non-synonymous changes were examined for their presence in dbSNP build 132 (276). Any novel or potentially disease causing variants in an individual were further assessed for segregation with the disease in other available affected and unaffected family members by direct sequencing as described above. The segregating mutations were assessed in controls using Custom Taqman® or SNaPshot assay.

2.2.6. Custom Taqman assay

The variant c.1751C>T in Exon 10 was screened in NSA controls using a custom Taqman® assay (Applied Biosystems, VIC, Australia). The forward and reverse primers along with allele specific probes were designed using Custom Taqman® assay design tool (Refer to Appendix 2.3 for sequence of the probes). The 40 × SNP assay was diluted with an equal volume of 1 M Tris-EDTA (TE) buffer to obtain a 20 × concentration of the assay. Forty nanograms DNA was amplified using 5 µl of 2 × Taqman genotyping mix (Applied Biosystems, VIC, Australia) and 0.5 µl of 20 × SNP genotyping assay in a total 10 µl volume. AmpliTaq Gold Enzyme was activated at 95ºC for 10 minutes, followed by 40 cycles of denaturation for 15 seconds at 92ºC and annealing/extension for 1 minute at 60ºC. The assay was performed on a StepOne Plus RealTime PCR System (Applied Biosystems, VIC, Australia) and results were analysed using StepOne software v2.1 (Applied Biosystems, VIC, Australia).

2.2.7. SNaPshot assay

The variant c.2875G>A in Exon 17 was screened in 217 NSA controls and in additional 150 BMES age-related cataract cases and 271 BMES controls using SNaPshot assay (Applied Biosystems, VIC, Australia). The region around the variant was amplified using the same primers as used for in-house sequencing. The PCR products were prepared for SNaPshot reaction by removing excess primers and unused dNTPs by treatment with Exonuclease and SAP as described previously in section 2.2.4. The SNaPshot reaction was performed under the following conditions using a probe with sequence- 5'-TCC TTG AGT CCC AGC AGG CTG TAG G 3'; Assay conditions used were as follows: 25 cycles of

denaturation at 96°C for 10 seconds, annealing at 50°C for 5 seconds and extension at 60°C for 30 seconds. The excess primers and nucleotides were removed by treatment with Exonuclease and SAP as described previously. These amplified fragments were then electrophoresed on a ABI PRISM 3100 Genetic Analyzer (Applied Biosystems, VIC, Australia) with GS120 LIZ™ size standards and results analysed using Peak Scanner software v1.0 (Applied Biosystems, VIC, Australia).

2.2.8. Haplotype analysis

Haplotype analysis was performed, in the family previously reported to carry the splice mutation c.2826-9G>A (Family 16) and two new families (Family 42 and Family 83) found to carry the same mutation in this study, to determine if the mutation was inherited from a common ancestor in these families (65). DNA from all available affected and unaffected family members was used for the analysis. Four microsatellite markers namely D1S228, D1S507, D1S436 and D1S2644 in the chromosome region 1p36 were typed (271). Primers for D1S228, D1S507 and D1S2644 markers were fluorescently labelled with FAM fluorophore and for D1S436 marker with HEX fluorophore (Geneworks Pty. Ltd., Adelaide, Australia). Forty nanograms or 4 µl of one-tenth dilution of the pre-amplified gDNA was used as template to amplify the microsatellite markers of interest using PCR. The reaction was set-up as mentioned in section 2.2.3 and amplified by denaturation at 95°C for 30 seconds, annealing at 57°C for 30 seconds and extension at 72°C for 30 seconds for 35 cycles (D1S436) or 30 cycles (D1S228, D1S507, D1S2644) (277). The amplified fragments were pooled for analysis by mixing 1 in 15 dilution of PCR

product carrying D1S507 marker and 1 in 7.5 dilution of fragments carrying D1S436 in one pool; 1 in 15 dilution of each PCR products carrying D1S228 and D1S2644 marker in the second pool. The samples were electrophoresed on an ABI PRISM3100 Genetic Analyser (Applied Biosystems, CA, USA) and results analysed using Peak Scanner software v1.0 with ROX labelled GS500 size standards.

2.2.9. Bioinformatics analysis

CLUSTALW was used to perform multiple sequence alignment of EPHA2 protein sequence from human (GenPept accession NP_004422.2), mouse (GenPept accession NP_034269.2), aquatic frog (GenPept accession AAH75556.1), rhesus monkey (GenPept accession NP_001035768.1), chicken (GenPept accession XP_001234814.2) and zebrafish (GenPept accession NP_571490.1) (278). Pathogenicity of the novel mutations or variants was predicted using Sorting Intolerant from Tolerant (SIFT) and Polymorphism Phenotyping v2 (PolyPhen2) softwares (279, 280).

2.3.Results

Our cohort of congenital cataract cases comprised of both sporadic cases and familial congenital cataract cases with autosomal dominant or recessive mode of inheritance. All cases were recruited from the South-Eastern Australian states of South Australia, Victoria and Tasmania. As majority of the reported causative mutations in the gene show an autosomal dominant inheritance, for the purpose of this study, only familial cases with autosomal dominant inheritance were selected. Eighty four index cases were screened for

mutations in all exons of the *EPHA2* gene. We found non-synonymous variants c.493G>A in Exon 3 (rs150790360) in probands from family 41 and family 75 and c.2837G>A in Exon 17 (rs149692543) in proband from family 111. These variants did not segregate with the disease in the respective families and hence were not causative. These variants were subsequently identified in a large-scale exome sequencing project which genotyped controls and patients with heart, lung and blood disorder (281). We also found commonly occurring SNPs rs116039767, rs2230597, rs5643737, rs10907223, rs2291805 and rs3503325 in our cohort of cases. Additionally, we found three causative mutations in the *EPHA2* gene in four families in this cohort.

2.3.1. Family 115

The proband from family 115 (Figure 2.1a) presented with nuclear cataract. The sequence analysis of the proband 115-1 revealed a novel missense mutation c.1751C>T in Exon 10 of the *EPHA2* gene shown in Figure 2.1b). Another affected individual 115-2 was also found to carry the same mutation. This mutation was absent in 270 NSA controls. This substitution leads to a missense change p.P594L, of a highly conserved proline residue in the juxtamembrane domain of the protein (Figure 2.1c). The change was predicted as "probably damaging" by Polyphen2 with a score of 0.997 (sensitivity: 0.41; specificity: 0.98) and "not tolerated" by SIFT. Although both proline and leucine are non-polar amino acids, the hydrocarbon side chain of both the residues is structurally distinct. Thus this mutation is likely to have functional effects on the EPHA2 protein.

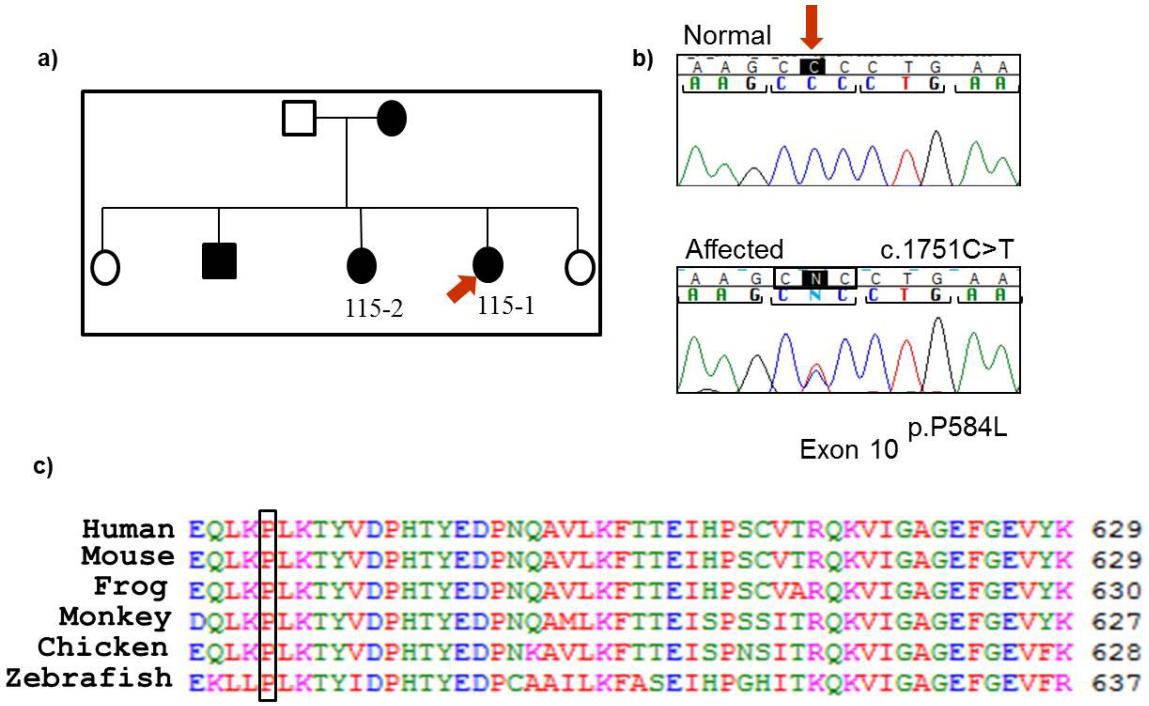

Figure 2.1: Causative mutation in *EPHA2* in Family 115

a) Pedigree of the Family 115. Solid boxes and circles indicate affected individuals. The individuals from whom DNA was available have been given a number. The proband is marked with a red arrow. b) Sequence chromatogram showing the normal (top panel) and mutated (bottom panel) *EPHA2* sequence. c.1751C>T mutation is marked with an arrow. The mutation leads to change in a codon, marked by a box, substituting a proline by a leucine at position 584 in the protein. The translation reading frame is marked with brackets in the normal and mutated sequence. c) ClustalW alignment of the region of the human EPHA2 protein including residue 584 and orthologous region in other species showing conservation of the mutated residue across species.

2.3.2. Family 42 and 83

The proband from family 42 (Figure 2.2a), 42-1, presented with nuclear cataract. Recently, another affected individual from this family, 42-12, also presented with nuclear cataract (Figure 2.2b). There wasn't any information available about phenotype of cataract in the proband from family 83, 83-9. But another affected individual from the family, 83-1, presented with nuclear cataract. On sequencing the *EPHA2* gene we found a splice mutation, c.2826-9G>A, in intron 16 in probands from both the families which also segregated with the disease in these families. This splice mutation leads to a 7 bp insertion in the transcript leading to a frameshift in the EPHA2 protein. This results in the addition of 71 amino acids at the C-terminal of the EPHA2 protein. The same splice mutation was previously reported by our research group in an Australian family, Family 16, from this cohort (65). This mutation has been suggested to affect protein function by altering protein stability and affecting cell migration (215).

As the three families (previously reported family 16 and family 42 and 83 from this study) were from the same cohort we hypothesized that they could be related to each other. To investigate this, microsatellite analysis was performed. Microsatellite markers are variable repeat regions in the genome which are inherited in families in a Mendelian fashion (282). Four microsatellite markers spanning a 5 Mbp region in and around *EPHA2* were typed in the affected and unaffected individuals from the three families (Figure 2.3). We found that the disease haplotype in the three families was different suggesting that these are three independent families. These results suggest that the mutation, c.2826-9G>A, has occurred multiple times in the population.

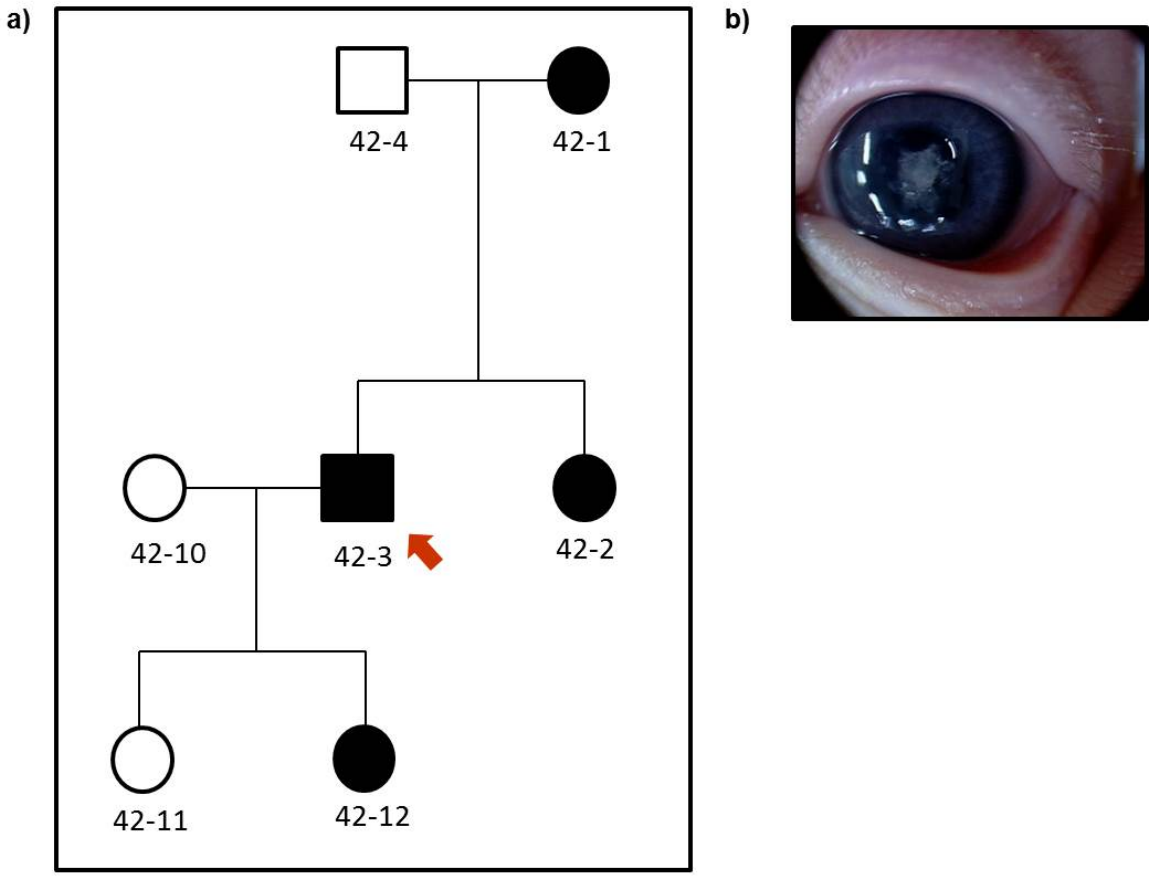

Figure 2.2: Congenital cataract in Family 42

a) Pedigree of the Family 42. Solid boxes and circles indicate affected individuals. The individuals from whom DNA was available have been given a number. The proband is marked with a red arrow. b) Cataract phenotype of 42-12 showing nuclear cataract.

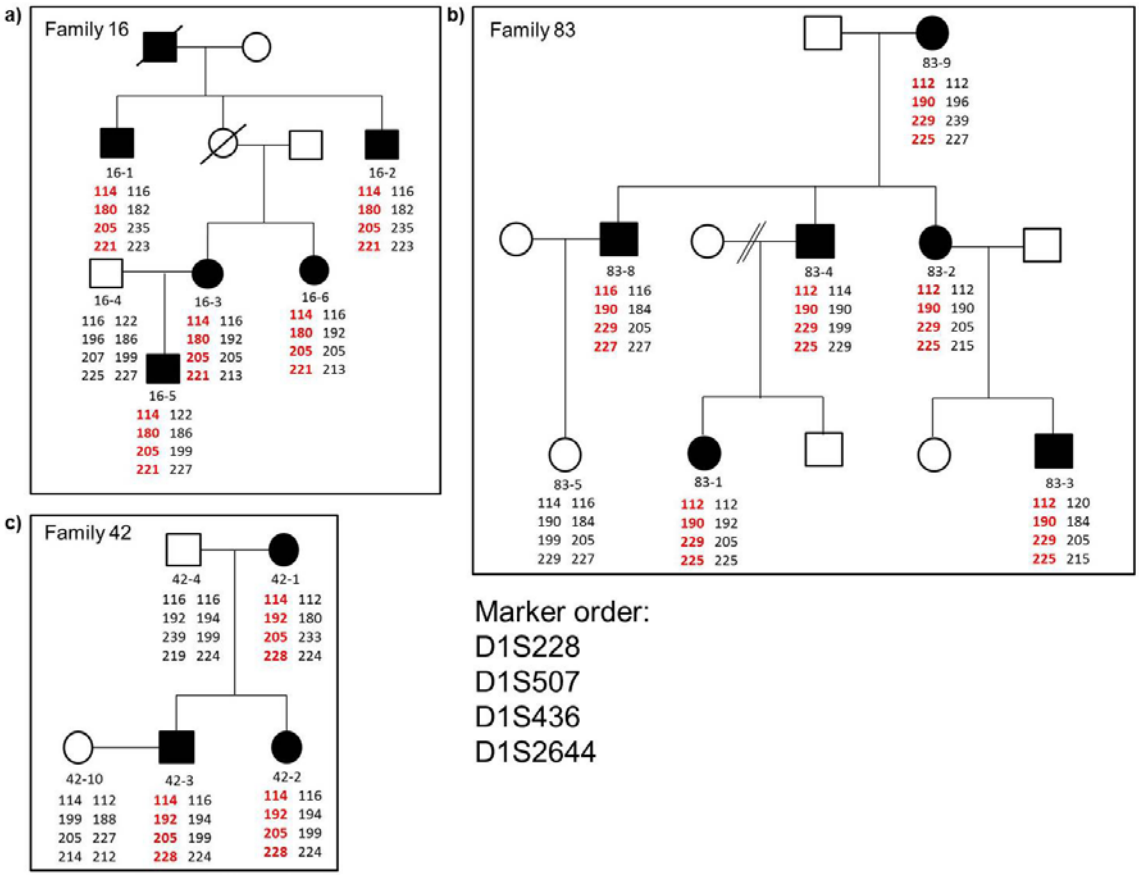

Figure 2.3: Haplotype analysis in Families 16, 83 and 42

Pedigree of the Family a) 16 b) 83 and c) 42. Solid boxes and circles represent affected family members. The individuals from whom DNA was available were given a number. Family 83 and 42, from the present study, carry the same splice mutation c.2826-9G>A as was previously reported in Family 16. The numbers represent the length of microsatellite repeat in each individual and the sequence of the numbers shows the haplotype of each family; red represents the diseased allele and black represents the normal allele. Haplotypes of members of each family at microsatellite markers D1S228, D1S507, D1S436 and D1S2644 are shown. The haplotype carrying the segregating disease allele is different in the three families.

2.3.3. Family 74

The proband 74-2 (Figure 2.4a) presented with subcapsular and cortical opacities at 17 years of age. Another affected family member, 74-1, presented with bilateral posterior subcapsular cataract at 20 years of age. A substitution, c.2875G>A, was found in exon 17 of the gene in both the affected family members (Figure 2.4b). This change alters a highly conserved alanine, a non-polar amino acid, residue to a threonine, a polar amino acid, residue (p.A959T) in the SAM domain of the protein (Figure 2.4c). The variant was found to be "probably damaging" by PolyPhen2 with a score of 0.995 (sensitivity: 0.68; specificity: 0.97) and "not tolerated" by SIFT. This change was found in two NSA controls which were also found to have age-related cataract. This variant is located one base-pair upstream to a synonymous SNP, rs3754334, which is associated with age-related cataract in multiple populations (68, 191, 283). Therefore to further explore if the associated SNP, rs3754334, was tagging the rare variant rs139787163 found in Family 74, additional age-related cataract cases and controls from the BMES cohort were screened for the presence of the variant. However, the variant was absent in all the BMES age-related cortical cataract cases and controls screened. Moreover, this variant (rs139787163) was found only in 3 out of 10,000 European American and African American participants screened in a large-scale Exome sequencing project (281). The participants in the Exome sequencing project were not screened for presence of cataract and it is possible that the three individuals carrying the variant were also affected with cataract. These findings suggest that rs139787163 is present at a low frequency in the normal population and perhaps its presence predisposes the individual to cataract development.

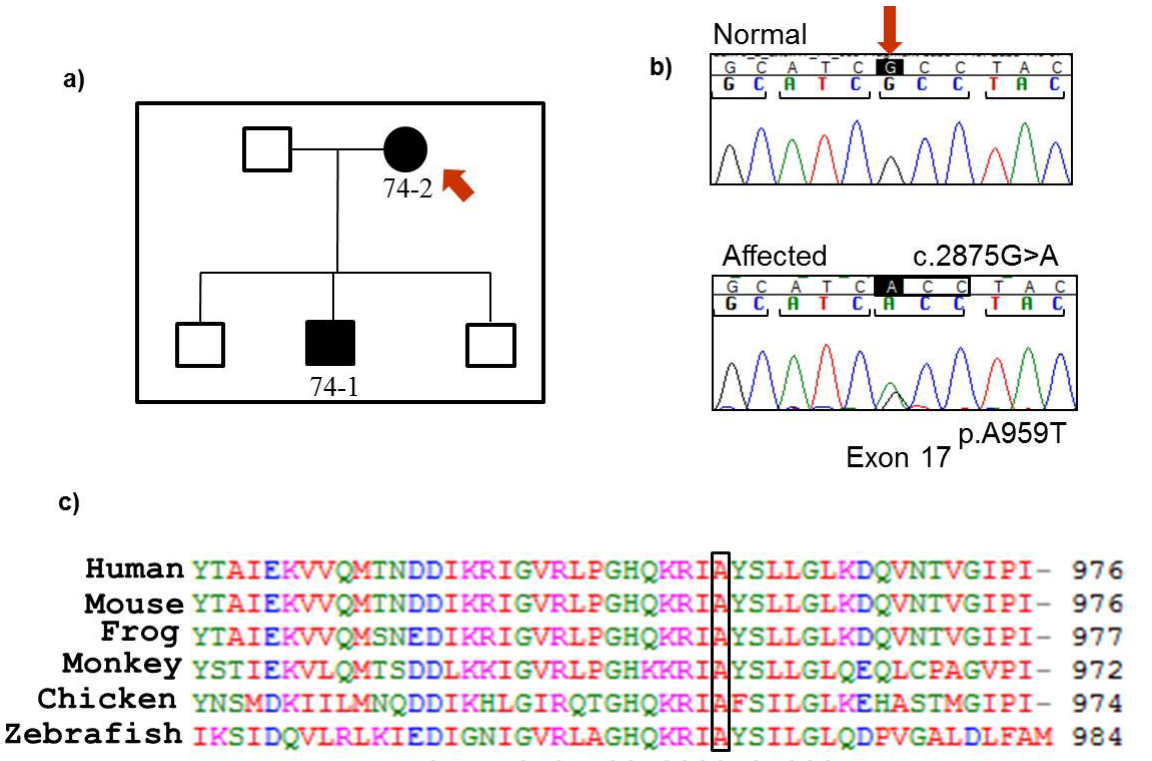

Figure 2.4: Causative mutation in *EPHA2* in Family 74

a) Pedigree of the Family 74. Solid boxes and circles indicate affected individuals. The individuals from whom DNA was available have been given a number. The proband is marked with a red arrow. b) Sequence chromatogram showing the normal (top panel) and mutated (bottom panel) *EPHA2* sequence. The variant c.2875G>A is marked by an arrow. The variant leads to change in a codon, marked by a box, substituting an alanine residue by a threonine in the protein at position 959. The translation reading frame is marked with brackets in the normal and mutated sequence. c) ClustalW alignment of the region of human EPHA2 including residue 959 showing conservation of the alanine residue across species.

Overall, we found that mutations in the *EPHA2* gene lead to 4.7% of inherited cataracts in this South-Eastern Australian cohort. Table 2.1 summarizes all the known mutations in the *EPHA2* gene, including the ones identified in the present study.

2.4.Discussion

We investigated the contribution of mutations in the *EPHA2* gene to congenital cataract in an Australian cohort. Most of the autosomal dominant congenital cataract causing mutations identified to date, affect the SAM and/or PDZ domain of the protein. These mutations affect protein stability, mutant protein localisation on ligand stimulation and cell migration (215). Two mutations with autosomal recessive inheritance affect the fibronectin-rich domain or the tyrosine kinase domain of the protein but no study, demonstrating the functional effect of these mutations, has been reported so far (64, 66).

In this study we found the first autosomal dominant mutation c.1751C>T (p.P594L) in Exon 10 of the gene affecting the juxtamembrane region of the protein. Autophosphorylation of tyrosine residues in the juxtamembrane domain of EphB receptor, regulates its activity (284). Similarly, tyrosine residues closest to the altered proline residue, at positions 588 and 594 of human EPHA2 are phosphorylated (285). Targeted mutants of murine EphA2 at these tyrosine residues affect receptor interaction with downstream signalling molecules like Vav guanidine exchange factors (286). The presence of this novel mutation could alter the phosphorylation profiles of neighbouring tyrosine residues which may affect protein activation and downstream signalling leading to cataract

Table 2.1: Summary of the reported congenital cataract causing mutations in the *EPHA2* gene

DNA change	Protein change	Location in protein domain	Inheritance	Phenotype	Reference
c.1405C>T	p.Y469H	Fibronectin rich III	Recessive	N/A	(64)
c.1751C>T	p.P584L	Juxtamembrane	Dominant	Nuclear	Dave et al.
c.2353G>A	p.A785T	Tyrosine kinase	Recessive	Nuclear	(66)
c.2668C>T	p. R890C	Between tyrosine kinase and SAM domain	Dominant	Posterior polar	(67)
c.2819C>T	p.T940I	SAM	Dominant	Posterior polar	(65)
c.2826-9G>A	p.D942fsXC71	SAM	Dominant	Total	(65)
c.2842G>T	p.G948W	SAM	Dominant	Posterior polar	(68) and Dave et al.
c.2875G>A	p.A959T	SAM	Dominant	Subcapsular and Cortical	Dave et al.
c.2915_2916delTG	p.V972GfsX39	SAM	Dominant	Posterior polar	(65)
c.2925dupC	p.I976HfsX37	PDZ	Dominant	Zonular	(69)

in the family. Additionally, alteration of the proline residue may affect protein conformation (287).

Interestingly, we found two new families carrying the same splice mutation which was previously reported in an Australian family (65). Haplotype analysis of the families demonstrated that the mutation was an independent event in the three families. The affected individual 83-8 from Family 83 has a different haplotype at the centromeric marker D1S228 and telomeric markers D1S2644 but still carries the segregating alleles at the two markers closest to *EPHA2*. A mutational event at the distal markers could explain this discrepancy (288). Also, individual 16-6, from Family 16, was reported as unaffected in the previous study (271). However, it was found to carry the same disease haplotype as the affected individuals from the family. The presence of the mutation in this individual was confirmed by direct sequencing of the *EPHA2* gene. The mutation may have incomplete penetrance in the individual 16-6.

Lastly, we found a rare non-synonymous variant rs139787163 in the gene in family 74. This variant was also found in two NSA controls. One of them had age-related anterior cortical cataract and the other had mild congenital and age-related cataract. The individual with congenital cataract underwent cataract surgery at 70 years of the age indicating that the cataract did not cause any vision impairment early in life. This variant was not present in any of the BMES cases and controls screened. The affected individuals in Family 74 were diagnosed in their teenage years suggesting that the variant led to late-onset congenital cataract in the family. A Chinese family first diagnosed at 10 years of age with progressive posterior cataract was found to carry a missense mutation, p.R890C in the

SAM domain of EPHA2 (67). This suggests that alteration of some residues in the gene may be susceptible to other genetic factors, which determine the onset of cataract in the affected individuals. Additionally, it is worth noting that the variant rs139787163 was found only in cataract affected individuals indicating that it may be altering susceptibility to cataract development depending on the presence of other environmental and/or genetic risk factors. A previously reported non-synonymous variant, R721Q, which alters a residue in the kinase domain of the protein, is associated with age-related cataract and leads to aggregation of the mutant protein (191). Similarly rs139787163 may have functional effects on the EPHA2 protein by affecting phosphorylation states of a tyrosine residue located downstream of this variant at amino acid position 960 altering downstream signalling through EPHA2. As the variant rs139787163 is present in both congenital and age-related cataract cases it also provides a link between congenital and age-related cataract making it an interesting candidate for further studies.

2.5. Conclusions

In conclusion, the results from the present study reveal that mutations in *EPHA2* account for a significant proportion of inherited cataract cases in South-Eastern Australia. In comparison to a previous study which reported frequency of mutations in crystallin genes in a subset of the same cohort (272), this study demonstrates that the frequency of mutations in *EPHA2* is comparable to the group of crystallin genes taken together in this population. These results also suggest that although mutations in the crystallin genes are thought to be the highest contributors to congenital cataract, mutations in other relatively novel causative genes such as *EPHA2* might account for a significant proportion of

congenital cataracts. It would be interesting to analyse the contribution of mutations in this gene in congenital cataract cohorts from other ethnicities. These frequencies will be a better indicator of contribution of mutations in *EPHA2* to congenital cataract in the global population. Further analysis of how these causative mutations lead to congenital cataract will help in understanding mechanisms for cataract development and role of EPHA2 in lens development and homeostasis.

3. Effect of congenital cataract causing mutations on subcellular localisation of the EPHA2 protein

3.1. Introduction

EPHA2 is a transmembrane tyrosine kinase receptor expressed in a variety of epithelial cells where it localizes to the cell periphery (246, 289). It interacts with cell-junction proteins and plays an important role in development and maintenance of epithelia (290-293).

Epithelial cells communicate with neighbouring cells through three types of cell-cell junctions from the apical to lateral membranes. These include tight junctions (TJ), which define epithelial cell polarity and regulate paracellular permeability; adherens junctions (AJ), which are responsible for cell-cell adhesion and maintaining integrity of TJs and desmosomes which provide anchoring sites for intermediate filaments (294). TJs are composed of transmembrane proteins occludin, claudins and junction adhesion molecules while AJs are composed of cadherin and nectin-based adhesion complexes. Interaction of EPHA2 with the TJ protein, Claudin-4, in fibroblast and epithelial cell lines increases paracellular permeability by delaying recruitment of Claudin-4 to TJs (295). An AJ protein, E-cadherin, regulates EPHA2 activation and localisation in epithelial cells (259, 296). Additionally, over-expression of EPHA2 destabilizes E-cadherin-based junctions promoting malignancy in epithelial cells (297). Activation of Ezrin, a protein involved in regulation of actin cytoskeleton, is also regulated by EPHA2 signalling and in turn affects epithelial cell polarity (298). These reports provide evidence for the role of EPHA2 in regulating cellular junctions.

The integrity of cellular junctions plays a critical role in maintaining cell-cell communication and homeostasis in the lens (7). As mentioned in Chapter 1, section 1.2.2, ocular lens comprises of a monolayer of lens epithelial cells and bulk of the lens consists of differentiated fiber cells (8). The fiber cells are metabolically inactive and therefore rely on cellular contacts for transport of organic and inorganic molecules across cells. Epha2 plays an important role in lens cell-cell junctions as lack of the protein in *Epha2*$^{-/-}$ mice results in altered localisation of E-cadherin and an AJ-associated protein, beta(β)-catenin, in lens epithelial cells (214); N-cadherin, an AJ protein homologous to E-cadherin expressed in lens fiber cells, has diffused localisation in *Epha2*$^{-/-}$ mice (191).

EPHA2 harbors congenital cataract causing mutations including mutations found in the genetic study in Chapter 2 (64-68). The causative mutations in *EPHA2* may affect the formation and integrity of cellular contacts in the lens. Functional effects of four causative mutations namely, c.2842G>T, c. 2819C>T, c.2915_2916delTG and c.2826-9G>A in the SAM domain of EPHA2 have been previously reported (215). These mutations lead to destabilization of the mutant protein and impair cell migration in transfected human fibroblast and/or mouse lens epithelial cells. They were found to have no effect on receptor activation but led to reduced phosphorylation of Akt, a downstream effector molecule in EPHA2 signalling. Additionally, unlike the ectopically expressed wild-type protein which localised in the cytoplasm, the mutant proteins were found to form aggregates in *Epha2*$^{-/-}$ mouse embryonic fibroblast (MEF) cells. EPHA2 localises to the cell periphery in lens fiber and epithelial cells *in vivo* (191, 212, 214). Since the wild-type EPHA2 protein localised in the cytoplasm in the MEF cells, altered localisation of mutant EPHA2 proteins

in these cells may not be an accurate representation of potential effects of the causative mutations.

In the present study, we further investigated the effect of congenital cataract causing mutations on subcellular localisation of EPHA2. EPHA2 has been reported to localise in the cytoplasm in cultured human (SRA01/04) and mouse (TN4) lens epithelial cells (299). In contrast, it localises to the cell periphery in cultured cells with established cell-junctions such as Madin Darby Canine Kidney (MDCK) cells and human adenocarcinoma (Caco2) cells (290, 299, 300).which is similar to its localisation in the lens *in vivo*. Therefore the effect of causative mutations on protein localisation was examined in these two cultured epithelial cells which polarize and form well-established cell-junctions.

We analysed the effect of five causative mutations, including the three mutations found in our genetic study (Chapter 2) and two previously reported mutations. We found that two mutations had a severe effect on protein localisation.

3.2. Materials and Methods

3.2.1. PCR-based mutagenesis

EPHA2-Myc was cloned into pQCXIP (Clontech Laboratories Inc., CA, USA) using the cloning strategy illustrated in Figure 3.1. This construct was generated by Dr. Raman Kumar, Neurogenetics Research Program, School of Paediatrics and Reproductive Health, University of Adelaide and Dr. Sarah Martin Department of Ophthalmology, Flinders

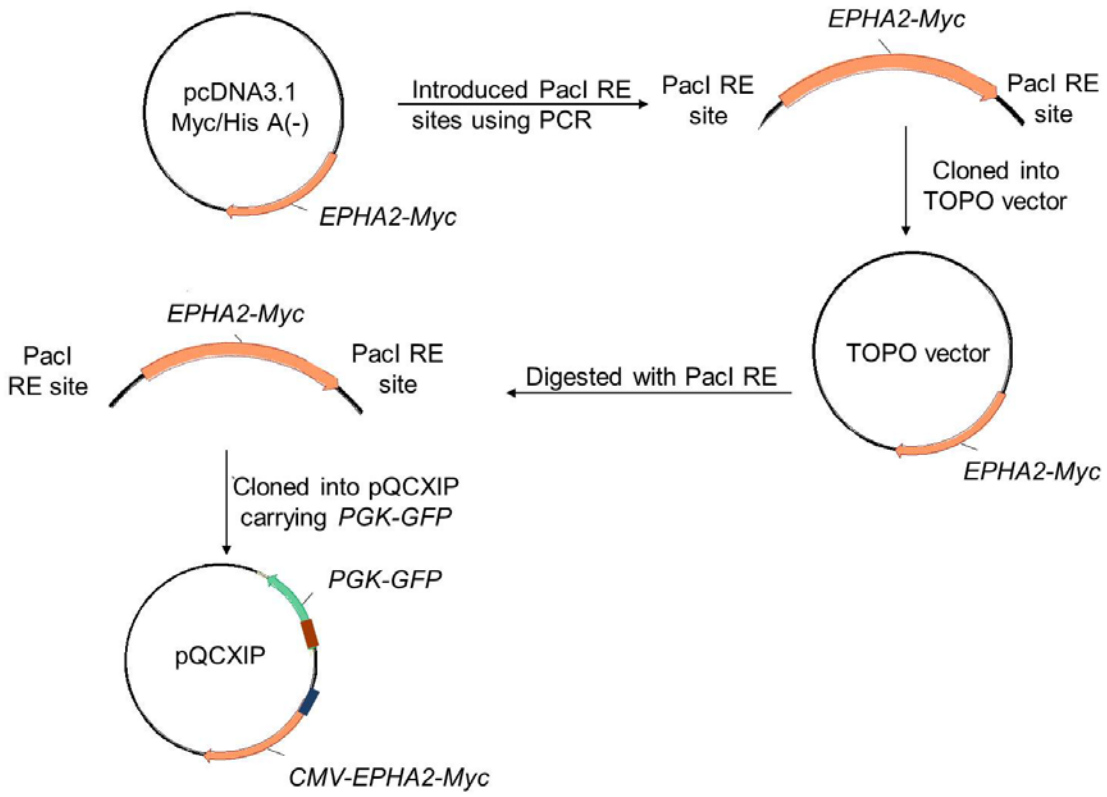

Figure 3.1: Schematic of generation of *EPHA2-Myc* in pQCXIP

EPHA2 was amplified from SRA01/04 human lens epithelial cell cDNA and cloned into pcDNA3.1 Myc/HisA(-) at XhoI and HindII sites. *EPHA2-Myc* (indicated in peach) from this construct was amplified using primers against the wild-type sequence which also introduced PacI restriction enzyme (RE) sites on either side of the cDNA fragment. This was then cloned into pTOPO® TA (Invitrogen, Life Technologies Australia Pty Ltd., VIC, Australia). pTOPO® carrying the *EPHA2-Myc* fragment was then digested with PacI RE to release *EPHA2-Myc* cDNA flanked by PacI RE sites. This fragment was then cloned in the multiple cloning site of pQCXIP carrying *PGK-EGFP* (*EGFP* indicated in green and *PGK* promoter indicated in red) at PacI RE sites. Transcription of *EPHA2-Myc* was driven by the *CMV* promoter (indicated in blue). The arrows represent the direction of transcription of *CMV-EPHA2-Myc* and *PGK-EGFP* expression cassettes. The *EGFP* and *EPHA2-Myc* genes were transcribed in opposite orientations.

University. The expression of wild-type Myc-tagged EPHA2 protein with a Myc-tag at the C-terminus was driven by the human cytomegalovirus (CMV) promoter. The construct encoded *Enhanced Green Fluorescent Protein* (*EGFP)* in a different expression cassette under the phosphoglycerate kinase (PGK) promoter. This plasmid construct is referred to as wild-type construct in this chapter.

Five mutations namely, c.1751C>T (p.P594L), c.2826-9G>A (p.D942fsXC71), c.2875G>A (p.A959T), c.2819C>T (p.T940I) and c.2915_2916delTG (p.V972GfsXC39) were separately introduced in the wild-type *EPHA2-Myc* cDNA by PCR-based mutagenesis. Figure 3.2 illustrates a schematic of the PCR-based mutagenesis method (301). To introduce each mutation, two separate PCRs were performed on wild-type *EPHA2* cDNA template to generate overlapping PCR products carrying the desired mutation. Primers used to introduce c.1751C>T or c.2819C>T mutations also created a new restriction enzyme site utilizing degeneracy of codons, which served as a diagnostic site in screening of mutant clones. The overlapping PCR products were used as template for a PCR 3 to generate mutant *EPHA2* cDNA fragments. The sequences of primers are listed in the Appendix 2.4. The primers used for the two rounds of PCR, PCR 1 and PCR 2, for generation of each mutant fragment and the respective amplification conditions are listed in Table 3.1.

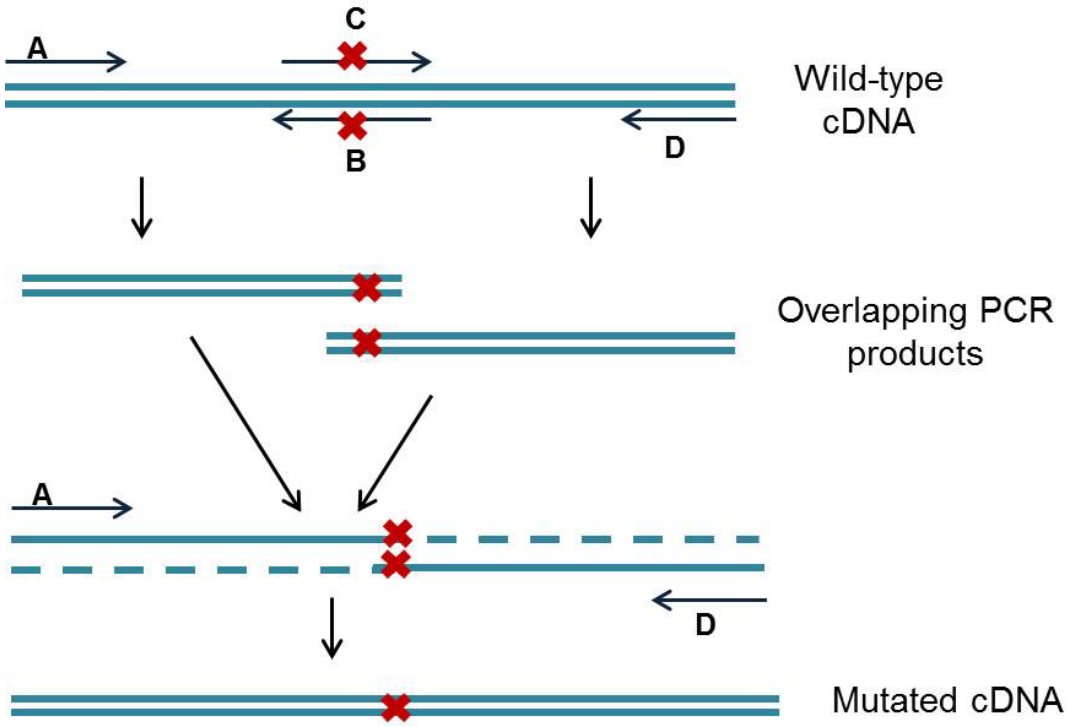

Figure 3.2: Schematic representation of PCR-based mutagenesis

Two separate first round PCRs (PCR 1 and PCR 2) were set up using forward primer A and reverse primer B or forward primer C and reverse primer D, with wild-type cDNA as a template. Forward primer C and reverse primer B, used in the two separate PCRs, carried the desired mutation. The first round PCRs gave rise to overlapping products carrying the mutation. These products were used as template for a second round of PCR using the forward primer A and reverse primer D which resulted in a PCR product carrying the desired mutation. This mutated fragment was cloned into the expression construct by replacing the corresponding wild-type fragment.

Table 3.1: Primer combinations used for generating mutant *EPHA2* cDNA fragments and the respective annealing temperatures for PCR. The expected sizes of the PCR products are indicated.

Mutation	PCR round	Forward Primer	Reverse primer	Annealing Temperature	Expected size of PCR product (bp)
c.1751C>T; (p.P594L),	PCR1	Eph Exon10Mut Fwd	Eph1751 Rev	64°C	807
	PCR2	Eph1751 Fwd	Eph exon10Mut Rev	64°C	305
	PCR3	Eph Exon10Mut Fwd	Eph exon10Mut Rev	64°C	1079
c.2819C>T; (T940I)	PCR1	Eph Mut Fwd	Eph2819 Rev	58°C	194
	PCR2	Eph2819 Fwd	Eph BglII Rev	52°C	206
	PCR3	Eph Mut Fwd	Eph BglII Rev	58°C	366
c.2826-9G>A; (D942fsXC71)	PCR1	Eph Mut Fwd	Eph2826 mod Rev	64°C	191
	PCR2	Eph2826 mod Fwd	Eph BglII Myc Rev	64°C	264
	PCR3	Eph Mut Fwd	Eph BglII Myc Rev	64°C	448
c.2875G>A; (p.A959T)	PCR1	Eph Mut Fwd	Eph2875 Rev	64°C	257
	PCR2	Eph2875 Fwd	Eph BglII Rev	60°C	139
	PCR3	Eph Mut Fwd	Eph BglII Rev	64°C	366
c.2915_2916delTG; (V972GfsXC39)	PCR1	Eph Mut Fwd	Eph2915 Rev	52°C	290
	PCR2	Eph2915 Fwd	Eph BglII Myc Rev	52°C	194
	PCR3	Eph Mut Fwd	Eph BglII Myc Rev	58°C	439

3.2.2. Primer preparation

The lyophilized primers were obtained from GeneWorks Pty Ltd, SA, Australia. They were dissolved in autoclaved Milli-Q water and incubated at 37°C for 30 minutes. The concentration of the primers was spectrophotometrically determined using SmartSpec™ Plus spectrophotometer (BioRad Laboratories Pty Ltd, NSW, Australia).

3.2.3. Polymerase chain reaction

GC-RICH PCR System (Roche Diagnostics Australia Pty Ltd, NSW, Australia) was used to perform all the PCRs. For c.1751C>T, c.2819C>T and c.2875G>A mutations wild-type construct carrying *EPHA2-Myc* was used as a template. The mutations, c.2826-9G>A and c.2915_2916delTG, lead to a frameshift resulting in the addition of 71 and 39 amino acids, respectively, in the mutant protein. As these two mutant fragments would include additional nucleotides encoding for the frameshift which were not present in the wild-type *EPHA2*, total cDNA from SRA01/04 cells was used as a template for the PCR 1 and PCR 2. This enabled amplification of cDNA fragment beyond the wild-type *EPHA2*, which included the extra nucleotides added due to the frameshift.

One-hundred-seventy nanograms of the wild-type construct or 0.5 µl cDNA from SRA01/04 cells was used as template for PCR 1 and PCR 2 in a total 25 µl volume. The desired region was amplified using 1 U of GC-Rich PCR system enzyme mix (a mixture of *Taq* DNA polymerase and *Tgo* DNA polymerase) in the presence of 1 × PCR buffer, 0.1 mM of dNTP mix and 0.5 µM of each primer. The enzyme was activated at 95°C for 3 minutes. Denaturation at 95°C for 30 seconds, followed by annealing for 30 seconds and

extension at 68°C for 30 seconds for 25 cycles. Annealing temperature employed for each primer pair is listed in Table 3.1. This was followed by a post-extension for 7 minutes at 68°C and incubation at 4°C for 5 minutes. All PCR products were analysed on a 1.2% agarose gel prepared in TBE buffer. Products of PCR 1 and PCR 2 were purified using Wizard® SV Gel and PCR Clean-Up System (Promega, VIC, Australia). Briefly, equal volume of the PCR product was mixed with the membrane binding solution; applied to the SV Minicolumn assembly and incubated at room temperature for 1 minute. It was then centrifuged at 18000 × g for 1 minute and the flow-through was discarded. Next, the minicolumn was washed with 700 µl of membrane wash solution followed by centrifugation at 18000 × g for 1 minute. After discarding the flow-through the minicolumn was washed with 500 µl of membrane wash solution and centrifuged at 18000 × g for 5 minutes. The flow-through was again discarded and the minicolumn was centrifuged briefly to remove the residual wash solution. Following this, the minicolumn was incubated with 30 µl of Milli-Q water for 1 minute and centrifuged at 18000 × g for 1 minute to elute the DNA. The DNA concentration was estimated spectrophotometrically as described in section 3.2.2.

Twenty five nanograms of the PCR 1 and PCR 2 products were used as templates for PCR 3. Using the same reaction composition and amplification conditions as PCR 1 and PCR 2, the amplification was performed for 20 cycles. The mutant *EPHA2* cDNA fragment obtained after PCR 3 was purified using Wizard® SV Gel and PCR Clean-Up System (Promega, VIC, Australia) according to manufacturer's protocol as described above and eluted in 30 µl Milli-Q water. Concentration of the eluted DNA was estimated spectrophotometrically as described in section 3.2.2 and then used for cloning. The outer

reverse primer (Eph BglII Rev and Eph BglII Myc Rev) used for PCR-based mutagenesis introduced a BglII restriction enzyme site utilizing degeneracy of codons. As a result the mutant fragments with c.2819C>T, c.2826-9G>A, c.2875G>A and c.2915_2916delTG mutations carried a BglII restriction enzyme site which was later used for cloning.

3.2.4. Recombinant DNA Cloning of mutant *EPHA2* fragments in pQCXIP

The products of PCR 3, except the mutant fragment carrying c.2875G>A, were cloned into the wild-type construct by replacing the corresponding fragment in wild-type *EPHA2-Myc* cDNA. Table 3.2 lists the restriction enzymes used for cloning each fragment. To clone *EPHA2* cDNA fragments carrying c.2819C>T, c.2826-9G>A and c.2915_2916delTG mutations, 4 µg DNA of the wild-type construct was double digested using 5 U of BstZ17I (New England Biolabs Inc, MA, USA) and 100 U of BamHI (New England Biolabs Inc, MA, USA) in a 40 µl volume, in the presence of 1 × enzyme buffer 4 (New England Biolabs Inc, MA, USA) at 37°C for one hour. To prevent incompletely digested wild-type construct from self-ligating, the 5'phosphate was removed by treatment with 1.5-2 U SAP in the presence of 1 × enzyme buffer in a total volume of 50 µl for 45 minutes at 37°C; followed by enzyme inactivation for 15 minutes at 65°C. Two-hundred nanograms of the respective mutant *EPHA2* cDNA fragments were digested using 7.5 U BstZ17I and 15 U BglII in the presence of 1 × enzyme buffer 4 in a 40 µl volume for one hour at 37°C. BamHI and BglII produce compatible cohesive ends upon digestion and therefore can be used for cloning fragments.

Plasmid DNA of the mutant *EPHA2* construct carrying c.2819C>T mutation was used as a parent vector to clone the fragment carrying c.2875G>A mutation. The vector and insert were prepared for cloning as described above.

To clone *EPHA2* carrying c.1751C>T mutation, both the wild-type construct (500 ng) and the mutant fragment (190 ng) were digested with 10 U and 5 U of BstXI, respectively, for one hour at 37°C in a 50 µl and 20 µl reaction, respectively. Similar to other mutant clones, the vector was treated with SAP before use for cloning.

Table 3.2: Restriction enzyme sites used for cloning mutated cDNA fragments

Mutation in *EPHA2* fragment	**Digested restriction sites in the insert**	**Parent vector**	**Digested restriction sites in the vector**
c.1751C>T	BstXI	Wild-type *EPHA2-Myc*	BstXI
c.2819C>T	BstX17I/BamHI	Wild-type *EPHA2-Myc*	BstX17I/BglII
c.2826-9G>A	BstX17I/BamHI	Wild-type *EPHA2-Myc*	BstX17I/BglII
c.2875G>A	BstX17I/BamHI	Mutant *EPHA2-Myc* with c.2819C>T mutation	BstX17I/BglII
c.2915_2916delTG	BstX17I/BamHI	Wild-type *EPHA2-Myc*	BstX17I/BglII

The digested mutant *EPHA2* cDNA fragments (inserts) and the digested vector were size separated on a 0.8% agarose gel prepared in TBE buffer. The specific DNA bands were excised and extracted from the agarose gel using Wizard® SV Gel and PCR Clean-Up System (Promega, VIC, Australia). The clean-up protocol was similar to the clean-up of PCR products apart from the first step, where the DNA gel slice was dissolved in membrane binding solution (10 µl of solution per 10 mg of gel slice) at 65ºC. The DNA

was eluted in 30 µl Milli-Q water. The concentration of eluted insert and vector DNA was determined spectrophotometrically as described in section 3.2.2.

Ligations were set-up on ice using the digested insert and 100 ng of the digested vector in the presence of 400 U T4 DNA ligase (New England Biolabs Inc, MA, USA) and 1 × enzyme buffer in a total 20 µl volume. The vector to insert molar ratio was maintained at 1:3. The following formula was used to calculate the amount of insert used for setting up the ligation.

Amount of Insert (ng) = (Amount of vector (ng) × size of the insert (bp) × insert: vector)/ size of the vector (bp)

The ligations were incubated overnight at 4ºC. The ligations of digested vector with and without T4 DNA ligase was used as negative controls. The following day ligated DNA was precipitated using 10% volume of 3 M sodium acetate pH 5.2, 2 µl glycogen and three volumes of 95% ethanol. The mixture was chilled at -80ºC for at least an hour and DNA was pelleted by centrifugation at 18000 × g for 10 minutes. The DNA pellet was washed thrice with 70% ethanol to remove all the salts, air dried and then resuspended in 5 µl Milli-Q water. Two microlitre of ligation was electroporated in 20 µl of ElectroMAX™ DH5α™ cells (Invitrogen, Life Technologies Australia Pty Ltd, VIC, Australia) in Gene Pulser/MicroPulser Cuvettes. The cells were electroporated at 1.8 kV using MicroPulser™ Electroporator (BioRad Laboratories Pty Ltd, NSW, Australia) followed by immediate addition of 500 µl Super Optimal Broth with Catabolite repression (SOC; Invitrogen, Life Technologies Australia Pty Ltd, VIC, Australia) medium. After incubation at 37ºC for 45 minutes, the bacteria were plated on LB agar plates (See Appendix 3.2) supplemented with 100 µg/ml ampicillin. The plates were incubated at 37ºC overnight to allow the bacteria to

form colonies. On the following day, the ratio of number of colonies on the positive agar plate, that is transformants electroporated with the ligation containing vector and insert, to the negative control, that is transformants electroporated with ligation containing only vector with T4 DNA ligase, was determined. This ratio of colonies determined the number of bacterial colonies to be cultured to screen for the mutant construct.

3.2.4.1. Screening of mutant clones

The bacterial colonies were cultured in 2 ml LB media (See Appendix 3.3) supplemented with 100 µg/ml ampicillin at 37ºC overnight to select for the recombinant clones. For extraction of plasmid DNA, the cultures were transferred to eppendorf tubes and centrifuged at 18000 × g for 2 minutes. The supernatant was discarded by vacuum suction and the bacterial pellet was resuspended in 100 µl of Buffer P1 (See Appendix 3.4) by vortexing. Then, 200 µl of P2 (See Appendix 3.5) was added, mixed by gently inverting the tube a few times and kept on ice for 5 minutes to lyse the cells. Following this 150 µl of Buffer P3 (See Appendix 3.6) was added to precipitate chromosomal DNA which was pelleted by centrifugation at 18000 × g for 10 minutes. The supernatant was transferred to a fresh tube and 95% ethanol was added to precipitate plasmid DNA. The DNA was pelleted by centrifugation at 18000 × g for 10 minutes. The DNA pellet was washed thrice with 70% ethanol, air dried and resuspended in 20 µl of Milli-Q water. The presence of mutant *EPHA2* cDNA fragment was determined by restriction enzyme digestion, as listed in Table 3.3. Two microlitre of resuspended plasmid DNA was subjected to restriction enzyme digestion with 10-50 U of the restriction enzyme in presence of 1 × enzyme reaction buffer and RNase cocktail™ enzyme mix (0.04 U RNase A and 1.6 U RNase T1;

Ambion, Life Technologies Australia Pty Ltd, VIC, Australia) in a total 10 µl volume for one hour at 37°C. For constructs carrying *EPHA2* with c.1751C>T mutation, the vector and insert prepared for cloning had symmetrical cohesive ends which could lead to ligation of the insert in either orientation. Therefore in this case the restriction enzyme digestion was also used to screen for clones with the desired orientation of the insert.

Table 3.3: Restriction enzymes used for screening of mutant *EPHA2* clones. DNA fragment sizes from mutant and wild-type constructs are indicated.

Mutation in *EPHA2*	**Restriction enzyme/s for screening**	**Expected DNA fragment size from mutant construct**	**Expected DNA fragment sizes from Wild-type construct**
c.1751C>T	BamHI	1.1 kb and 10.5 kb	60 bp and 11.6 kb
c.2819C>T	EcoRV	1.6 kb, 2.3 kb and 7.7 kb	3.9 kb and 7.7 kb
c.2826-9G>A	BamHI and EcoRI	140 bp and 11.5 kb	70 bp and 11.59 kb
c.2875G>A	EcoRV	3.9 kb and 7.7 kb	1.6 kb, 2.3 kb and 7.7 kb
c.2915_2916delTG	BamHI and EcoRI	140 bp and 11.5 kb	70 bp and 11.59 kb

.

The positive clones were cultured in 5 ml LB media supplemented with 100 µg/ml ampicillin. The plasmid DNA was extracted using QIAprep® Spin Miniprep Kit (QIAGEN Pty Ltd Australia, VIC, Australia). Briefly, bacterial cells were harvested by centrifugation at 18000 × g for 2 minutes. The bacterial cell pellet was then resuspended in 250 µl of Buffer P1 by vortexing and lysed using 250 µl of Buffer P2 followed by gentle

mixing by inverting the tube. The chromosomal DNA was pelleted by addition of Buffer N3 followed by centrifugation at 18000 × g for 10 minutes. The supernatant was applied to the QIAprep Spin column; centrifuged at 18000 × g for 1 minute and the flow-though was discarded. The column was washed with 500 µl of Buffer PB followed by centrifugation at 18000 × g for 1 minute. After discarding the flow-through the column was washed again using 750 µl of Buffer PB. The flow-through was discarded after centrifugation at 18000 × g for 1 minute. The column was centrifuged for an additional minute to remove the residual wash buffer. The DNA was then eluted in 30 µl of Milli-Q water. To confirm the presence of the mutation, the plasmid DNA was sequenced by Sanger sequencing using ABI PRISM Model 3100 Version 3.7 Genetic analyser (Applied Biosystems, VIC, Australia). The Eph Mut Fwd primer was used for sequencing all except the recombinant clones carrying the c.1751C>T mutation. These clones were sequenced using Eph Exon10 Mut Fwd primer. The plasmid DNA of the clones carrying the desired mutation was used for further study.

3.2.5. Cell culture

The human embryonic kidney 293A (HEK293A) cells and Madin Darby Canine Kidney (MDCK) epithelial cells were available in the laboratory. Human colorectal adenocarcinoma (Caco2) epithelial cells were a kind gift from Ms. Monica Dreimanis (Department of Haematology, Flinders University, Adelaide). All the cell lines were cultured in Dulbecco's Modified Eagle's medium (DMEM; GIBCO, Life Technologies Australia Pty Ltd., VIC, Australia) supplemented with 10% fetal bovine serum and penicillin/streptomycin (10,000 U/ml penicillin and 10,000 µg/ml of streptomycin; Life

Technologies Australia Pty Ltd., VIC, Australia). Cell cultures were maintained in a humidified atmosphere at 37ºC and 5% CO_2. For maintenance, the HEK293A cells were washed with phosphate buffer saline (PBS; See Appendix 3.7), dissociated using 0.05% Gibco ® Trypsin-EDTA (Life Technologies Australia Pty Ltd., VIC, Australia) twice a week and seeded at a ratio of 1:5. MDCK and Caco2 cells were dissociated using 0.25% Gibco ® Trypsin-EDTA (Life Technologies Australia Pty Ltd., VIC, Australia) once a week and seeded at a ratio of 1:10 and 1:5, respectively. MDCK and Caco2 cells were re-fed with fresh culture medium once a week.

3.2.6. Transfection of wild-type and mutant *EPHA2* constructs in cells

For protein expression studies, 4×10^5 HEK293A were seeded in six-well tissue culture plates (Corning® Costar® cell culture plates) and grown in culture media without antibiotics for 2-3 days. 70-80% confluent HEK293A cells were transfected with wild-type or mutant *EPHA2-Myc* construct using Lipofectamine® 2000 (Invitrogen, Life Technologies Australia Pty Ltd., VIC, Australia). HEK293A cells transfected with a pEGFP-c1 (Clontech Laboratories Inc., CA, USA) or wild-type *EPHA2-Myc* cloned into pcDNA3.1 Myc/HisA(-) were used as a positive control for transfection and EPHA2 protein expression, respectively.

For protein localisation studies, 4×10^5 MDCK or Caco2 cells were seeded onto glass coverslips placed in six-well tissue culture plates in culture media without antibiotics for three days. 90-95% confluent Caco2 and MDCK cells were transfected with wild-type or mutant *EPHA2-Myc* constructs using Lipofectamine® 2000.

Briefly for transfection, 4 µg of plasmid DNA and 10 µl Lipofectamine® 2000 Reagent were each diluted in Opti-MEM® (Invitrogen, Life Technologies Australia Pty Ltd., VIC, Australia) in a total volume of 250 µl each. These mixtures were incubated at room temperature for 5 minutes. Following this, the diluted DNA and Lipofectamine® 2000® Reagent were mixed and incubated at room temperature for 15-20 minutes to allow the formation of DNA-lipid complexes. These complexes were then added to the cells. The DNA-lipid complexes were removed from HEK293A cells after an hour and cells were re-fed with fresh culture media. The complexes were left on MDCK and Caco2 cells till they were used for localisation analysis.

HEK293A cells were harvested for protein extraction 24 hours and 48 hours after transfection. For this, the cells were dissociated using 0.05% Gibco Trypsin-EDTA and pelleted by centrifugation at 200 × g for 5 minutes. The supernatant was discarded by vacuum suction and the cell pellets were washed with PBS. The cells were again centrifuged at 200 × g for 5 minutes and the supernatant was discarded. The obtained cell pellets were stored at -80ºC until used for protein extraction.

3.2.7. Protein extraction and denaturing gel electrophoresis

Total cellular proteins were extracted from transfected HEK293A cells in 100 µl of radio-immunoprecipitation assay (RIPA) buffer [10 mM HEPES pH 7.5, 150 mM sodium chloride, 2 mM EDTA, 1% Triton X-100, 0.5% sodium deoxycholate, 0.1% sodium dodecyl sulfate (SDS), 25 × protease inhibitor cocktail (Roche Diagnostics Australia Pty Ltd., Castle Hill, Australia), 57 µM phenylmethylsulfonyl fluoride, 2 mM sodium

orthovanadate, 10 mM sodium pyrophosphate and 20 mM sodium fluoride]. The cells were lysed on ice for 30 minutes and then the tubes were centrifuged at 18000 × g for 10 minutes at 4ºC to pellet the cell debris. The supernatant was transferred to fresh eppendorf tubes and protein concentration estimated by Bicinchoninic acid (BCA) Protein assay (Thermo Fischer Scientific, VIC, Australia) according to manufacturer's protocol using bovine serum albumin (BSA) standards. Forty micrograms of total soluble protein was size separated on a 8% gel (See Appendix 3.10 and 3.11) by SDS–Polyacrylamide Gel Electrophoresis (PAGE). The gel was prepared according to the Laemelli method (302) using 29:1 Acrylamide:Bisacrylamide (BioRad Laboratories Pty Ltd, NSW, Australia). The gels were electrophoresed using a miniVE Integrated Vertical Electrophoresis unit (Hoefer Inc, MA, USA) in electrophoresis buffer (See Appendix 3.13) for an hour at 250 V using Powerpac™ Basic (BioRad Laboratories Pty Ltd, NSW, Australia).

3.2.8. Western blotting

For Western blotting, after SDS-PAGE the proteins were transferred on to Hybond-C Extra nitrocellulose (GE Healthcare Australia Pty Ltd., NSW, Australia) or Polyvinyidine fluoride-low fluorescence (PVDF-LF) membrane (BioRad Laboratories Pty Ltd, NSW, Australia) in Western transfer buffer (See Appendix 3.14 and 3.15) using a Trans-Blot® Turbo™ Transfer Starter System (BioRad Laboratories Pty Ltd, NSW, Australia) at 25 V, 1 A for 30 minutes.

The membrane was blocked in 5% skim milk (blocking buffer) made in 1 × Tris Buffered Saline and Tween 20 (TBST; See Appendix 3.16) for an hour and hybridised with the mouse anti-Myc (1:500, Cell Signaling Technology, Inc, MA, USA) primary antibody

diluted in blocking buffer, for 1 hour. After three washes in 1 × TBST for 10 minutes each, the blots were hybridised with the donkey anti-mouse IgG conjugated with horse-radish peroxidase (HRP) (1:500, Jackson ImmunoResearch, Laboratories, Inc PA, USA) secondary antibody diluted in blocking buffer, for 1 hour. The blots were washed three times in 1 × TBST for 10 minutes each and were developed using SuperSignal West Pico Chemiluminescent substrate (Thermo Fisher Scientific, VIC, Australia) or Amersham™ ECL™ Prime western blotting reagent (GE Healthcare Australia Pty Ltd, NSW, Australia). The signal was imaged using ImageQuant LAS 4000 Imager (GE Healthcare Australia Pty Ltd, NSW, Australia). The images were edited using Multi Gauge v3.0 software (Fujifilm Life Science, USA) and Microsoft PowerPoint (Microsoft Pty. Ltd., NSW, Australia).

3.2.9. Immunofluorescence labelling

For immunollabelling, MDCK or Caco2 cells grown on coverslips were washed twice with cold PBS and then fixed in 4% paraformaldehyde/PBS for 15 minutes at room temperature. The cells were then washed three times with PBS and permeabilised with 0.4% Triton X-100/PBS for 5 minutes. This was followed by three washes with PBS for 2 minutes each after which the cells were blocked with 5% goat or donkey serum in PBS for 10 minutes. The choice of serum used for blocking was dependent on the host animal used to generate the secondary antibody. The cells were then washed with PBS and hybridised with the primary antibody diluted in 1% goat or donkey serum/PBS for 1 hour followed by hybridisation with the secondary antibody diluted in PBS for 1 hour. The cells were washed with PBS three times for, 5 minute each, after each hybridisation. Ectopically expressed EPHA2-Myc was detected by hybridisation with a mouse anti-Myc (1:2000 for

MDCK and 1:1500 for Caco2 cells; Cell Signaling Technology, Inc, MA, USA) primary antibody and goat anti-mouse IgG conjugated with Alexa Flour 594 (1:500, Invitrogen, Life Technologies Australia Pty Ltd., VIC, Australia) or donkey anti-mouse IgG conjugated with Cy5 (1:50, Jackson ImmunoResearch, Laboratories, Inc PA, USA) secondary antibody.

For double labelling of the cells for EPHA2-Myc and the cis-golgi apparatus, the fixation, permeabilisation and blocking of cells was performed as described above. The primary antibody hybridisation was performed simultaneously with both the antibodies for 2 hours followed by sequential hybridisation with each secondary antibody for an hour each. EPHA2-Myc was labelled using a mouse anti-Myc primary antibody as described above and detected with the donkey anti-mouse IgG conjugated with Cy5 (1:50) secondary antibody. Cis-golgi apparatus was labelled using a rabbit anti-GM130 antibody (1:1000, Abcam®, MA, USA), a cis-golgi marker, and donkey anti-rabbit IgG conjugated with Alexa Flour 555 (1:1000, Invitrogen, Life Technologies Pty Ltd, VIC, Australia) secondary antibody. Transfected cells single-labelled to detect EPHA2-Myc and untransfected cells single-labelled to detect cis-golgi were used as positive controls. To ensure no cross-reactivity, the secondary antibodies used to detect the proteins were swapped. Mock transfected cells hybridised with only the secondary antibodies was used as negative controls.

After labelling the cells were mounted in Prolong Gold Antifade reagent with DAPI (Invitrogen, Life Technologies Australia Pty Ltd., VIC, Australia) and imaged on a Leica SP5 confocal microscope (Leica Microsystems Pty Ltd, NSW, Australia) using a 63 × objective. 405 nm Diode was used to excite DAPI, DPSS 561 laser for Alexa Flour 594

and Alexa Flour 555 and HeNe 633 laser to excite Cy5. The emission spectra for DAPI, Alexa Flour 594, Alexa Flour 555 and Cy5 were set at 408-488 nm, 585-700 nm, 565-620 nm and 645-730 nm, respectively. The images were captured using Leica Application Suite (LAS) microscope software (Leica Microsystems Pty Ltd, NSW, Australia).

3.3.Results

In the present study, we examined the effect of causative mutations with autosomal dominant inheritance, as in this case presence of only one mutant allele would be sufficient to analyse the functional effect of the mutation. Two missense mutations, c.2819C>T (p.T940I) and c.2842G>T (p.G948W), and a frameshift mutation, c.2915_2916delTG (p.V972GfsXC39), in the SAM domain of the protein were reported prior to the commencement of this study. Therefore to analyse the effect of two different types of mutations on protein function we chose to examine the effect of p.T940I and p.V972GfsXC39 mutation. In addition, we analysed the effect of three mutations namely, c.1751C>T (p.P594L), c.2826-9G>A (p.D942fsXC71) and c.2875G>A (p.A959T) found in the genetic study described in Chapter 2.

3.3.1. Generation of mutant *EPHA2* cDNA fragments and constructs

PCR-based mutagenesis was performed to generate mutant *EPHA2* cDNA fragments. Figure 3.2 schematically shows the process of PCR-based mutagenesis and Figure 3.3 shows representative images of PCR 1, 2and PCR 3 products for introducing c.2819C>T mutation in the wild-type EPHA2 cDNA fragment. The mutant *EPHA2* cDNA fragments

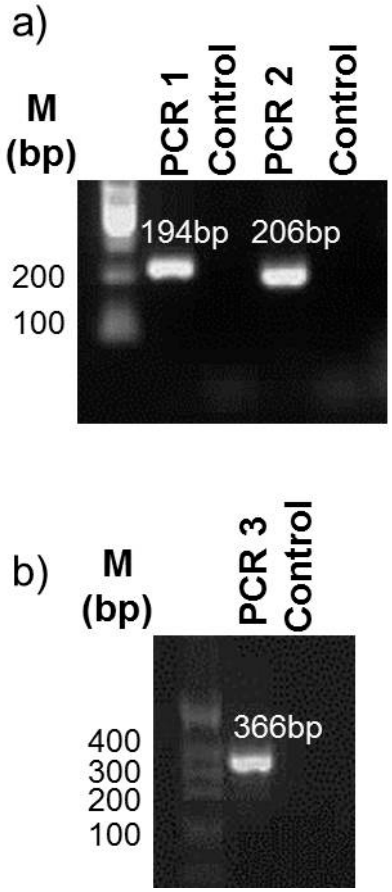

Figure 3.3: Amplification of cDNA for introducing mutations using PCR-based mutagenesis

a) Products of PCR 1 and PCR 2 generated by PCR-based mutagenesis for introducing c.2819C>T mutation. Wild-type construct carrying *EPHA2-Myc* was used as template for PCR. PCR 1 was performed using primers Eph Mut Fwd and Eph2819 Rev; PCR 2 was performed using primers Eph2819 Fwd and Eph Myc Rev. The reverse primer used for PCR 1 (Eph2819 Rev) and forward primer for PCR 2 (Eph2819 Fwd) were designed to carry the desired mutation. The primers, Eph Mut Fwd and Eph Myc Rev, were specific to the wild-type sequence. The PCR products of expected sizes of 194 bp and 206 bp were obtained by PCR 1 and PCR 2, respectively. The 194 bp sized product migrated slower than expected on the agarose gel, perhaps due to a large amount of the product loaded on the gel. b) Product of PCR 3 generated by PCR-based mutagenesis carrying c.2819C>T mutation. Equal amounts of the overlapping products of PCR 1 and PCR 2 were used as template for PCR 3. The primers Eph Mut Fwd and Eph Myc Rev were used for amplification. The expected PCR product of 366 bp was observed. PCRs without template were used as negative controls. Product sizes and DNA molecular size markers (M) are indicated in base pairs (bp).

carrying c.1751C>T, c.2826-9G>A, c.2875G>A, or c.2915_2916delTG mutation were similarly generated by PCR-based mutagenesis. These mutant fragments were then cloned into pQCXIP by replacing the corresponding wild-type fragment in the *EPHA2* cDNA. Table 3.2 lists the restriction enzyme sites used for cloning the mutated fragments. The ratio of recombinant clones transformed with the ligation of the digested vector and insert in the presence of ligase (positive) and of only digested vector with the ligase (negative control) was 700:91 for c.1751C>T, 336:90 for c.2819C>T, 298:2 for c.2826-9G>A, 92:2 for c.2875G>A, and 35:6 for c.2915_2916delTG mutation.

Twelve recombinant clones each of *EPHA2* carrying c.1751C>T, c.2819C>T, c.2826-9G>A and c.2915_2916delTG mutation and 24 clones of *EPHA2* carrying c.2875G>A mutation were screened for the presence of the mutant cDNA by diagnostic restriction digestion (Table 3.3). Based on the results from this screening, plasmid DNA of up to 8 clones of each mutation likely to carry the desired mutant construct were sequenced. Sequence chromatograms of plasmid DNA of mutant EPHA2 clones shown in Figure 3.4 illustrates the mutations inserted in wild-type cDNA. The sequencing was performed to confirm the presence of mutation in the constructs and absence of any PCR-introduced errors. Up to three positive clones of each mutation were used for protein expression analysis.

3.3.2. Protein expression analysis of mutant EPHA2 clones

Next, we wanted to determine if the mutant constructs express the desired mutant EPHA2 protein. The expression of the mutant proteins was analysed in transiently transfected

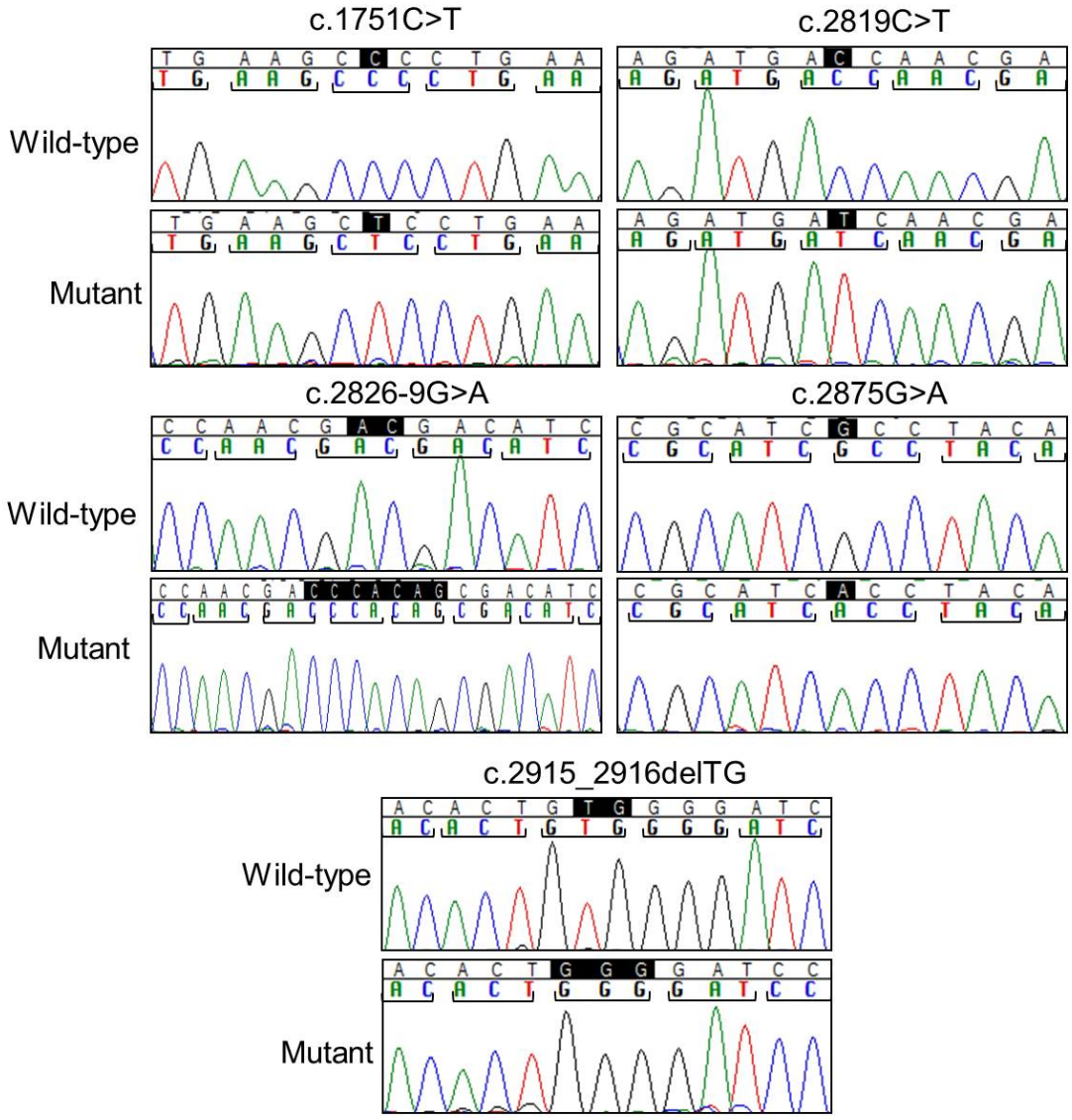

Figure 3.4: Sequence chromatograms of mutant *EPHA2* cDNA from recombinant clones carrying the desired mutation

Panels illustrate sequence chromatograms of wild-type (top) and mutated (bottom) *EPHA2-Myc* cDNA carrying c.1751C>T, c.2819C>T, c.2826-9G>A, c.2875G>A or c.2915_2916delTG mutation as indicated. The altered nucleotides introduced by PCR-based mutagenesis are boxed in black. The nucleotides boxed in the wild-type sequence chromatogram in the panel for c.2826-9G>A mutation, mark the nucleotides flanking the insertion. Similarly, the boxed nucleotides in the wild-type sequence in the panel showing c.2915_2916delTG mutation are the nucleotides which are deleted as a result of the mutation. The reading-frame in the wild-type and mutant sequence is indicated by brackets.

HEK293A cells at 24 hours and 48 hours after transfection by western blotting using an anti-Myc antibody. Three clones each of constructs carrying c.1751C>T, c.2819C>T, c.2826-9G>A or c.2915_2916delTG mutation and one clone of the construct carrying c.2875G>A mutation were analysed for protein expression. The construct expressing wild-type EPHA2-Myc was used as a positive control for EPHA2 expression; pEGFP-C1 transfected and mock transfected cells served as a negative control. All mutant constructs expressed the mutant protein band of the expected size of about 130 kDa as shown in Figure 3.5. Hybridisation of the blots with an anti-GFP antibody showed that all clones except the one carrying c.2875G>A mutation expressed varying amounts of GFP (data not shown).

3.3.3. Localisation of mutant EPHA2 protein

Next, we analysed subcellular localisation of the mutant EPHA2 proteins. Similar to the lens epithelial and fiber cells, EPHA2 plays an important role in cellular junctions in cultured epithelial cells (259, 295, 296). Therefore localisation of ectopically expressed Myc-tagged wild-type and mutant EPHA2 was analysed in two epithelial cell lines, namely MDCK and Caco2 cells. The results of immunolabelling performed at 24 hours after transfection in both the cell lines are shown in Figure 3.6 and Figure 3.7, respectively. Mock transfected cells labelled with only the secondary antibodies were used as the negative control.

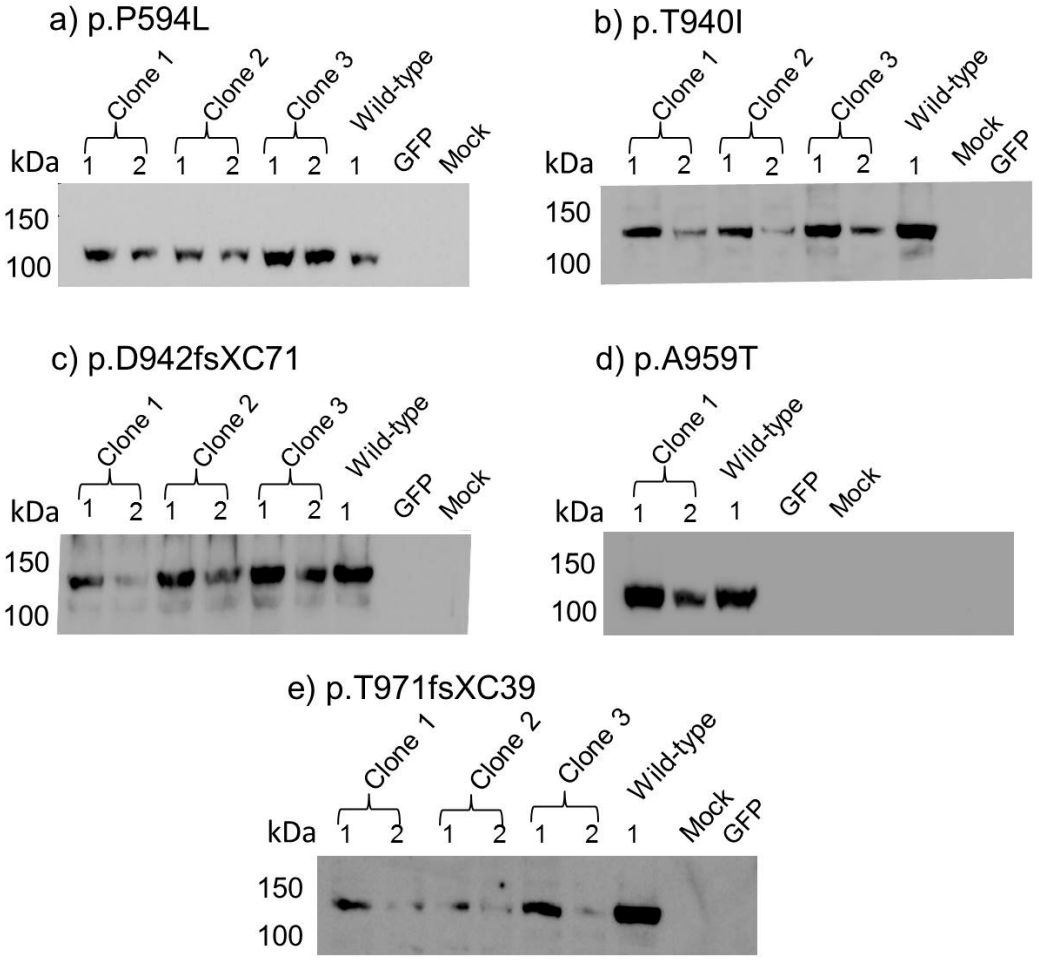

Figure 3.5: Expression of EPHA2-Myc protein from mutant constructs.

Cell lysates of HEK293A cells transiently transfected with mutant *EPHA2–Myc* constructs were analysed at 24 hours (1) and 48 hours (2) post-transfection. Equal amount of protein from each sample was loaded. The proteins were size separated by SDS-PAGE. Western blotting was performed with mouse anti-Myc primary antibody and HRP-conjugated anti-mouse IgG secondary antibody. Three clones each with EPHA2 carrying mutation p.P594L a), p.T940I b), p.D942fsXC71 c), or p.V972GfsXC39 e) and a clone carrying p.A959T d) mutation were analysed for mutant EPHA2 protein expression. Protein extracts of mock transfected cells and cells transfected with the p*EGFP-C1* construct were used as negative controls. Cells transfected with pcDNA3.1 Myc/His(-) carrying wild-type EPHA2-Myc were used as positive control. The position of protein standards are as indicated; kDa- kilo Dalton.

In MDCK cells, the wild-type EPHA2-Myc protein localised in the periphery and/or in the cytoplasmic vesicles as shown in top left panel in Figure 3.6. EPHA2 is packaged in secretory vesicles for its transport to the membrane and may be degraded in endocytic vesicles (303). Localisation of the wild-type EPHA2-Myc in the cytoplasmic vesicles may indicate its presence in either secretory or endocytic vesicles. As EPHA2 is an integral membrane protein (225), the peripheral localisation is consistent with integration of EPHA2 in the cell membrane. Likewise, cells expressing mutant EPHA2 protein with p.P594L, p.A959T or p.V972GfsX39 mutation showed presence of the mutant protein in the cell periphery and cytoplasm (Figure 3.6, asterisk in second image in the top row, second and third image in the second row). In addition, a few cells also exhibited some perinuclear localisation of the protein (Figure 3.6, triangle in second image in the top row, second and third image in the second row). This may be due to over-expression of the ectopically expressed protein. In contrast, the cells expressing mutant protein carrying p.T940I or p.D942fsXC71 mutation exhibited predominantly perinuclear localisation along with some localisation in the cytoplasm and the cell periphery (Figure 3.6,arrows in the third image in the top row and first image in the second row). Similar localisation pattern of all the mutant EPHA2 proteins was observed in Caco2 cells (Figure 3.7). We did not observe any GFP expression in either of the two cell lines perhaps due to low level expression from the *GFP* expression cassette. To determine its expression, immunolabelling using an anti-GFP primary antibody may be performed.

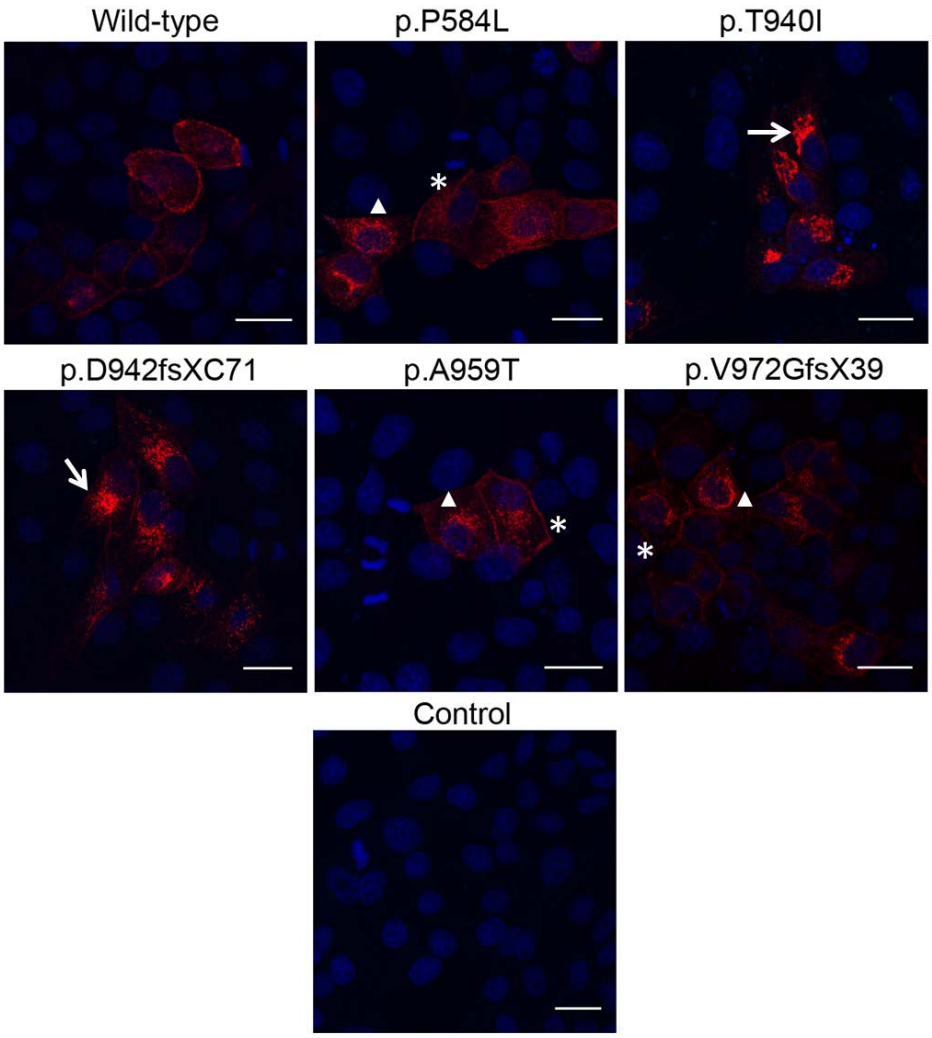

Figure 3.6: Localisation of wild-type and mutant EPHA2 protein in MDCK cells

Ectopically expressed EPHA2-Myc (red) in MDCK cells was detected using a mouse anti-Myc antibody and anti-mouse IgG conjugated with Alexa Flour 594. Nucleus (blue) was labelled with DAPI. Mock transfected cells labelled only with anti-mouse IgG conjugated with Alexa Flour 594 were used as negative control (third row). Cell expressing wild-type EPHA2-Myc served as a positive control (top left panel). p.P594L (second image in the top row), p.A959T (second image in the second row) and pV972fsX39 (third image in the second row) mutant EPHA2-Myc proteins show peripheral and cytoplasmic localisation similar to the wild-type protein (marked with asterisks). A few cells showing perinuclear localisation, possibly due to over-expression of the mutant protein, are marked by triangles. p.T940I (top right panel) and p.D942fsXC71 (first image in the second row) mutant EPHA2-Myc is seen predominantly in the perinuclear region (marked with arrows). The figure illustrates representative images from two independent experiments. Scale-bar, 20 µm

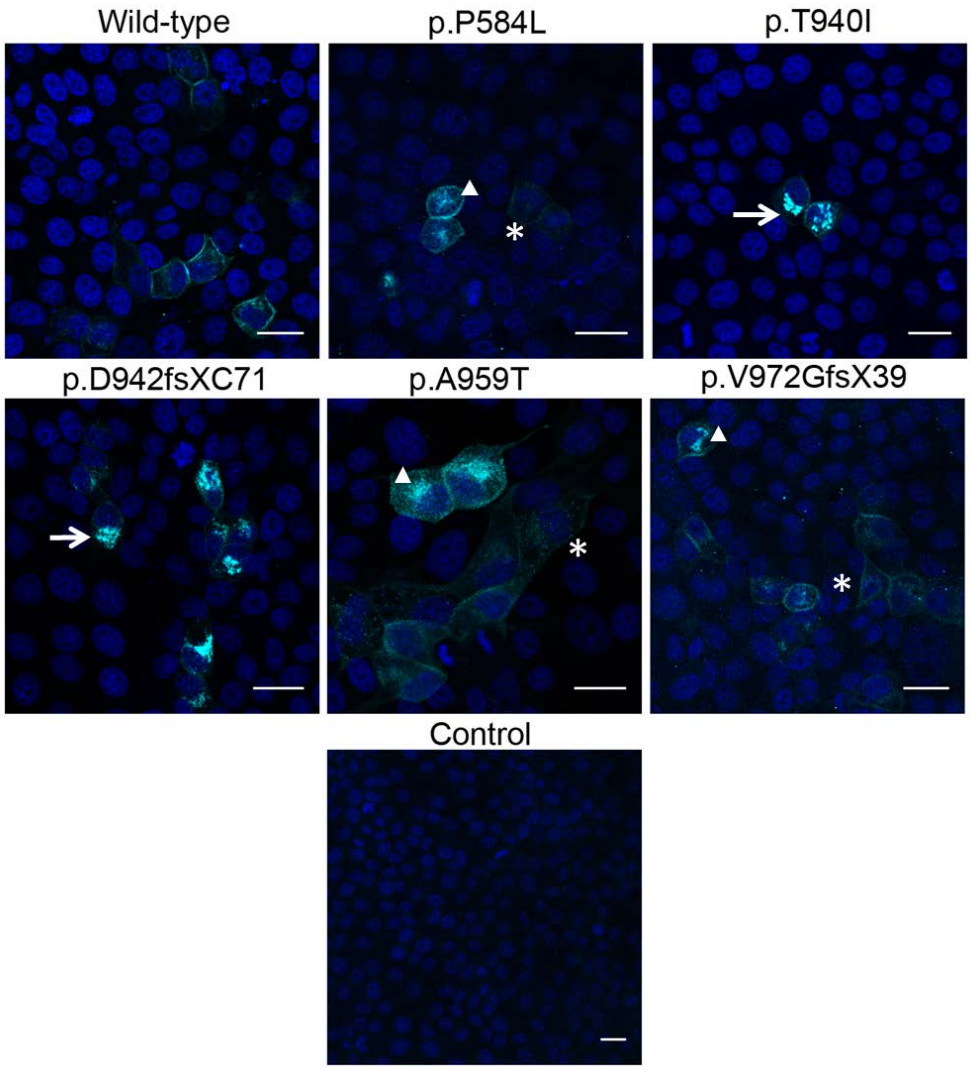

Figure 3.7: Localisation of wild-type and mutant EPHA2 protein in Caco2 cells

Ectopically expressed EPHA2-Myc (cyan) was detected in Caco2 cells using a mouse anti-Myc antibody and anti-mouse IgG conjugated with Cy5. Nucleus (blue) was labelled with DAPI. Mock transfected cells labelled only with anti-mouse IgG conjugated with Cy5 were used as negative control (third row). Cells expressing wild-type EPHA2-Myc were used as positive control (top left panel). As observed in MDCK cells, EPHA2-Myc with p.P594L (second image in the first row), p.A959T (second image in the second row) or pV972fsX39 (third image in the second row) mutation show peripheral and cytoplasmic localisation similar to the wild-type protein (marked with asterisks). A few cells showing perinuclear localisation of these mutant proteins, likely to be due to over-expression, are marked by triangles. p.T940I (top right panel) and p.D942fsXC71 (first image in the second row) mutant EPHA2-Myc is seen mostly in the perinuclear region (marked with arrows) with some mutant protein present in the cell periphery. The figure shows representative images from two independent experiments. Scale-bar, 20 µm

3.3.4. Co-localisation analysis of mutant EPHA2 proteins

The perinuclear aggregation of two mutant proteins, with p.T940I or p.D942fsXC71 mutation, suggested that the proteins were being retained in a cellular organelle near the nucleus. The pattern of localisation of the mutant proteins resembled that of the golgi apparatus (304). Therefore to determine if these mutant EPHA2 proteins are accumulated in the golgi apparatus, we performed co-localisation with a cis-golgi marker, GM130. This analysis was performed in both MDCK and Caco2 cells. Mutant and wild-type EPHA2 was labelled using an anti-Myc antibody while the cis-golgi marker was immunolabelled using an anti-GM130 antibody.

In MDCK cells, dual labelling of wild-type and mutant EPHA2 protein with the cis-golgi marker revealed no co-localisation of the cis-golgi marker with wild-type or mutant proteins carrying p.P594L, p.A959T or p.V972GfsX39 mutation (Figure 3.8). The mutant proteins localised to the cell periphery and cytoplasm as was observed on single labelling described in section 3.3.3. However, we observed some co-localisation of the mutant proteins with p.T940I or p.D942fsXC71 mutation with the cis-golgi marker as shown in Figure 3.9 (arrows). This indicated that some of the mutant protein was retained in the cis-golgi apparatus Additionally, a small proportion of cells showed peripheral localisation of these two mutant proteins indicating delayed recruitment of the mutant protein to the cell membrane (Figure 3.9, second and fourth row). The cells single-labelled for both the proteins, were used as positive controls.

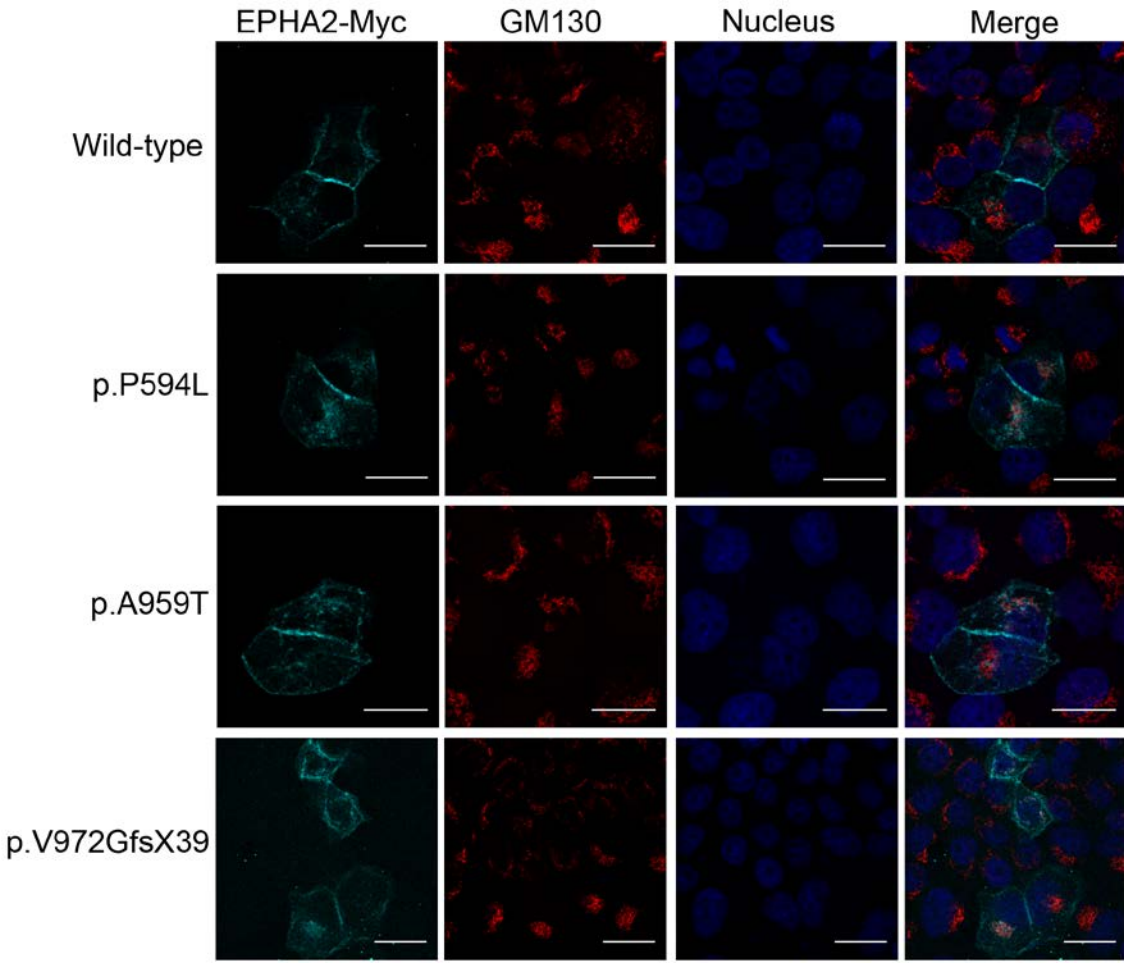

Figure 3.8: Co-localisation of wild-type and mutant EPHA2 proteins with cis-golgi marker in MDCK cells

Ectopically expressed EPHA2-Myc (cyan) in MDCK cells was detected using a mouse anti-Myc antibody and anti-mouse IgG conjugated with Cy5; cis-golgi apparatus (red) was detected using a rabbit anti-GM130 cis golgi marker and an anti-rabbit IgG conjugated with Alexa Flour 555. Nucleus (blue) was labelled with DAPI. EPHA2-Myc with p.P594L (second row), p.A959T (third row) or p.V972GfsX39 (fourth row) mutation show peripheral and cytoplasmic localisation similar to the wild-type protein (first row). No co-localisation with the cis-golgi marker was observed in cells expressing these mutant proteins (Merge). The figure presents representative images from two independent experiments. Scale-bar, 20 µm

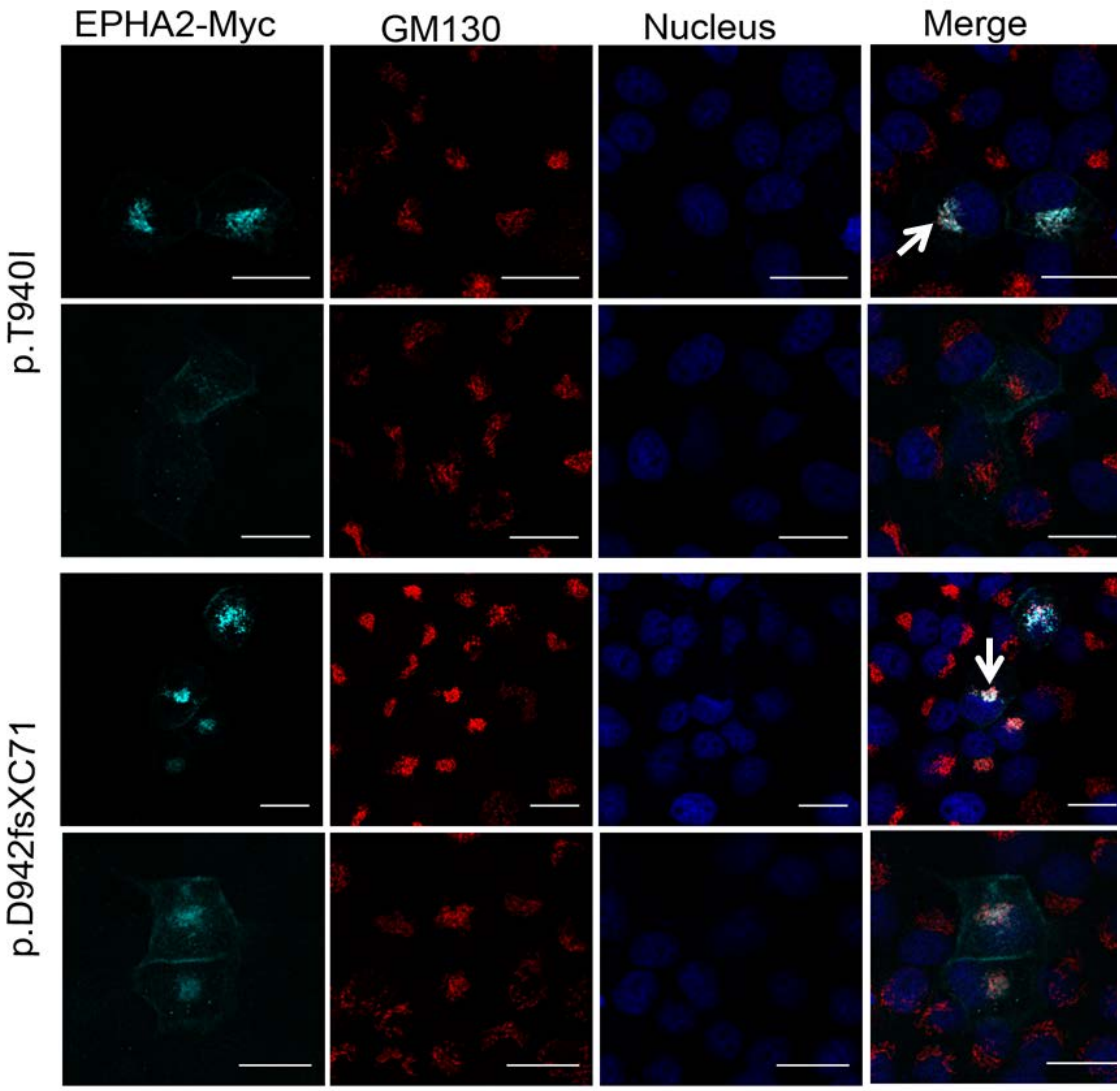

Figure 3.9: Co-localisation of mutant EPHA2 protein and cis-golgi marker in MDCK cells

Ectopically expressed EPHA2-Myc (cyan) was detected using a mouse anti-Myc antibody and an anti-mouse IgG conjugated with Cy5; cis-golgi apparatus (red) was detected using a rabbit anti-GM130 cis-golgi marker and an anti-rabbit IgG conjugated with Alexa Flour 555. Nucleus (blue) was labelled with DAPI. EPHA2-Myc carrying p.T940I and p.D942fsXC71 mutation mis-localise in the perinuclear space and show some co-localisation (white) with the cis-golgi marker as shown in the merged image in the first and third row (arrow). Second and the fourth row show a few cells expressing these mutant proteins with peripheral and cytoplasmic localisation. The figure illustrates representative images from two independent experiments. Scale-bar, 20 µm

The positive control cells showed perinuclear localisation of GM130 and peripheral and predominantly perinuclear localisation of mutant EPHA2 with p.T940I (Figure 3.10, first and second row). The cells labelled by swapping the secondary antibodies used for detection of the two proteins demonstrated that the secondary antibodies did not exhibit any cross-reactivity (Figure 3.10, third and fourth row). Cells labelled with only the secondary antibodies also showed minimal background (Figure 3.10, fifth row).

We observed similar results for wild-type and all the mutant EPHA2 proteins in Caco2 cells as illustrated in Figure 3.11 and Figure 3.12. The co-localisation, of mutant EPHA2 protein with cis-golgi apparatus, detected in cells expressing mutant protein carrying p.A959T or p.V972GfsX39 mutation may again be due to overexpression of the ectopically expressed protein; although this was not observed for wild-type or other mutant proteins. The positive controls showed expected labelling and the negative controls showed minimal background as illustrated in are Figure 3.13. Overall, our results show that p.T940I and p.D942fsXC71 mutations in the EPHA2 protein have a more severe effect on protein localisation in epithelial cells compared to the other mutations analysed in the present study.

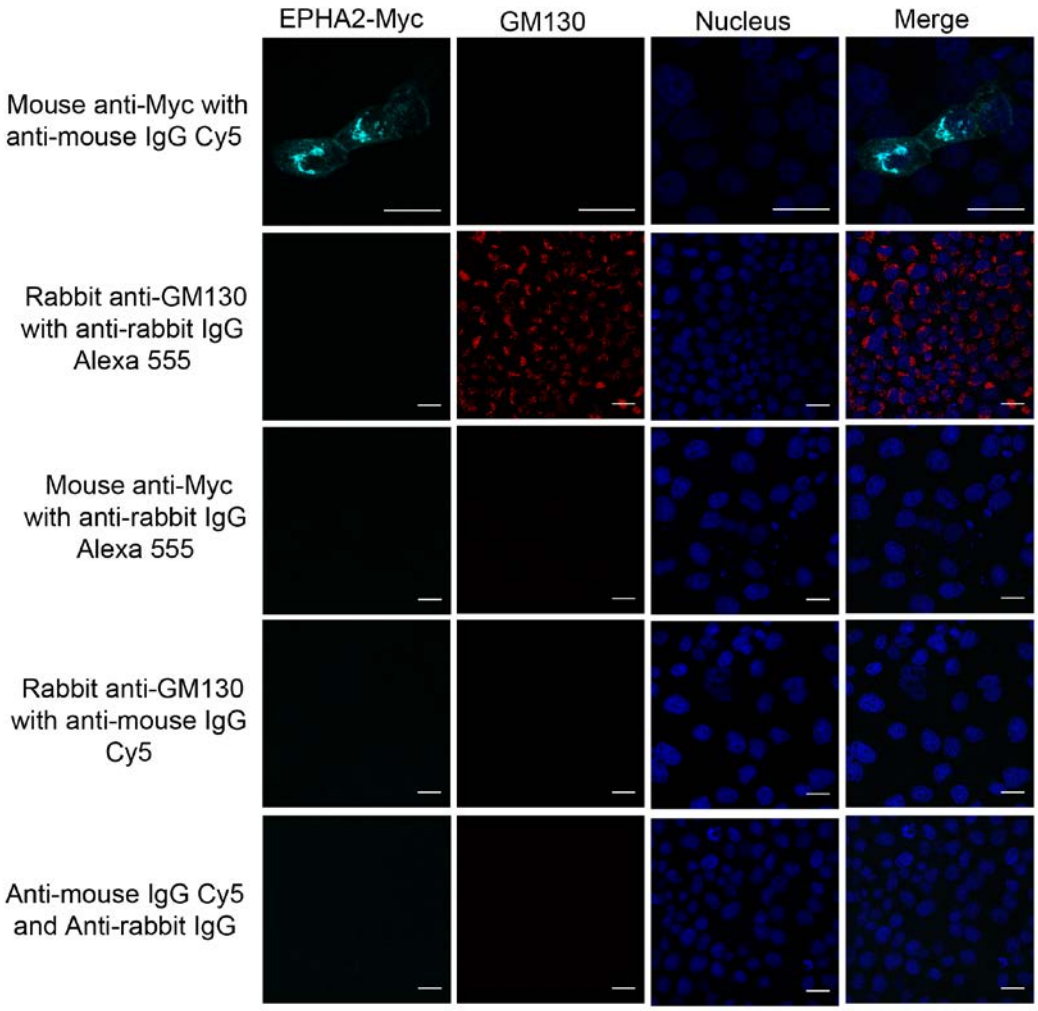

Figure 3.10: Positive and negative controls for co-localisation of EPHA2-Myc protein with cis-golgi marker in MDCK cells

MDCK cells ectopically expressing EPHA2 protein with p.T940I mutation (cyan) were labelled with mouse anti-Myc antibody detected using an anti-mouse IgG conjugated with Cy5 (positive control, first row) or anti-rabbit IgG conjugated with Alexa Flour 555 (control for cross-reactivity of the secondary antibody, third row). The cis-golgi apparatus (red) was detected using a rabbit anti-GM130 and an anti-rabbit IgG conjugated with Alexa Flour 555 (positive control, second row) or anti-mouse IgG conjugated with Cy5 (control for cross-reactivity of the secondary antibody, fourth row). Mock transfected cells labelled only with both the secondary antibodies were used as negative control. Nucleus (blue) was labelled with DAPI. The figure shows representative images of controls from two independent experiments. Scale-bar, 20 µm

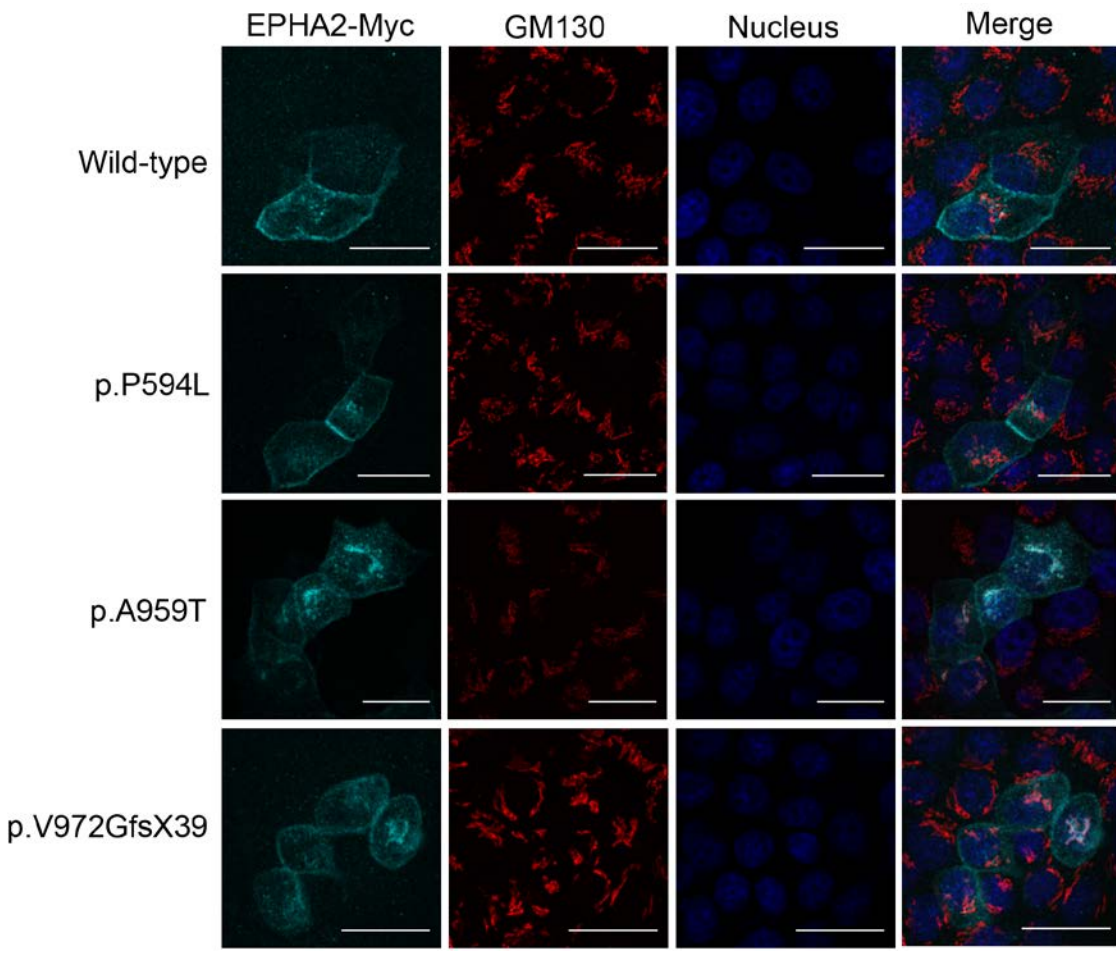

Figure 3.11: Co-localisation of wild-type and mutant EPHA2 protein with cis-golgi marker in Caco2 cells

Transiently transfected Caco2 cells were labelled with a mouse anti-Myc antibody and an anti-mouse Cy5 to detect EPHA2-Myc (cyan); and with a rabbit anti-GM130 cis-golgi marker and an anti-rabbit IgG conjugated with Alexa Flour 555 to detect the cis-golgi apparatus (red). Nucleus (blue) was labelled with DAPI. EPHA2-Myc carrying p.P594L (second row), p.A959T (third row) or p.V972GfsX39 (fourth row) mutation show peripheral and cytoplasmic localisation comparable to the wild-type EPHA2-Myc protein (first row). The cells expressing mutant EPHA2-Myc carrying p.A959T and p.V972GfsX39 mutation demonstrate perinuclear localisation along with presence of the protein in the cell periphery. These cells show some co-localisation with the cis-golgi marker (white in the merged images) suggesting that this is the normal route of post-translational processing of EPHA2 protein. The figure shows representative images from two independent experiments. Scale-bar, 20 µm

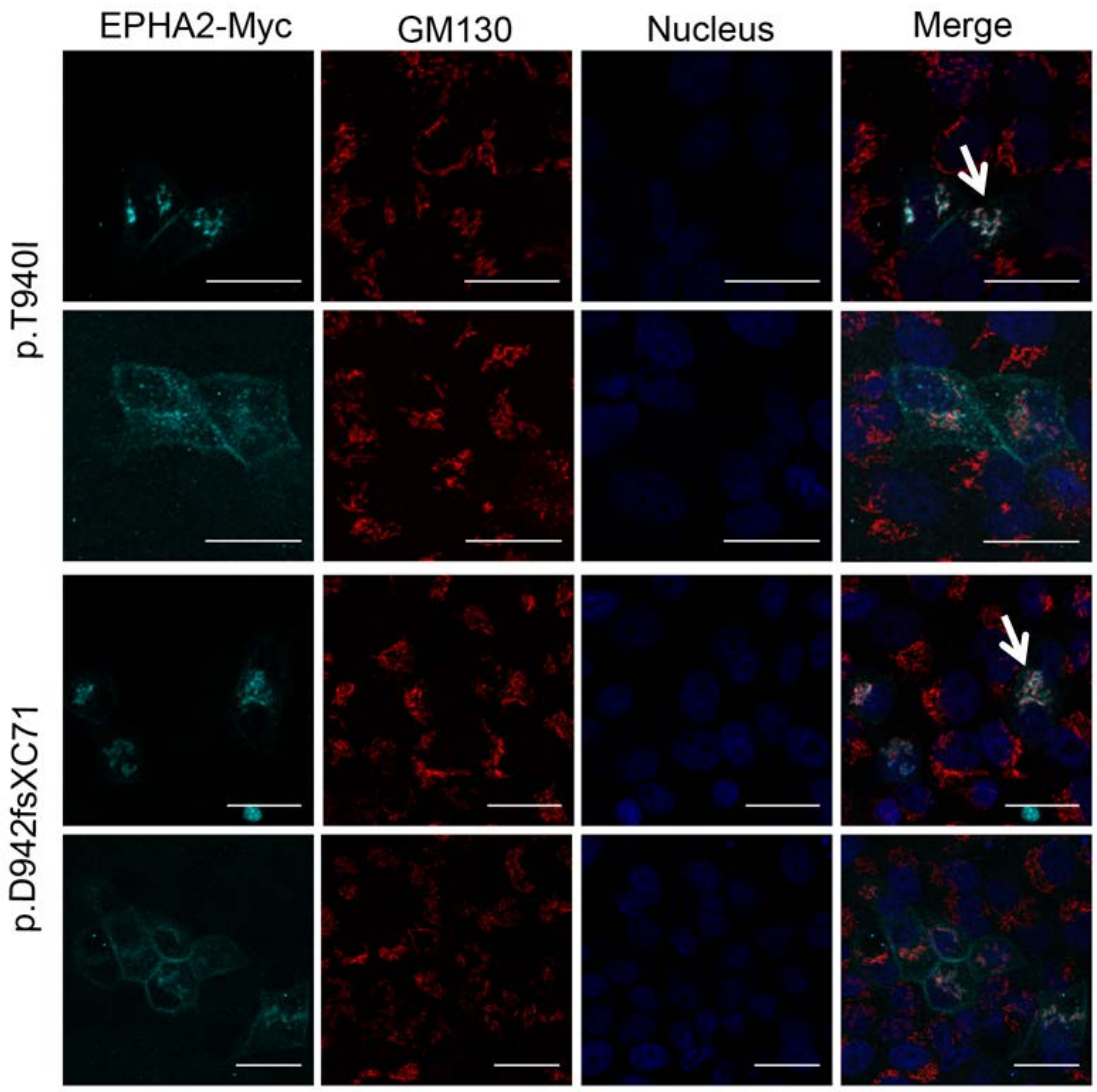

Figure 3.12: Co-localisation of mutant EPHA2 proteins with cis-golgi marker in CaCo2 cells

Ectopically expressed EPHA2-Myc (cyan) was detected using a mouse anti-Myc antibody and an anti-mouse IgG conjugated with Cy5; cis-golgi apparatus (red) was detected using a rabbit anti-GM130 cis-golgi marker and an anti-rabbit Alexa Flour 555. Nucleus (blue) was labelled with DAPI. Mutant EPHA2-Myc proteins with p.T940I and p.D942fsXC71 mutation predominantly mis-localise in the perinuclear region and show some co-localisation with the cis-golgi marker. Merged image in the first and third rows illustrates the co-localisation in white marked by arrows. A few cells expressing these mutant proteins also exhibited peripheral and cytoplasmic localisation shown in the second and the fourth rows. The figure shows representative images from two independent experiments. Scale-bar, 20 µm

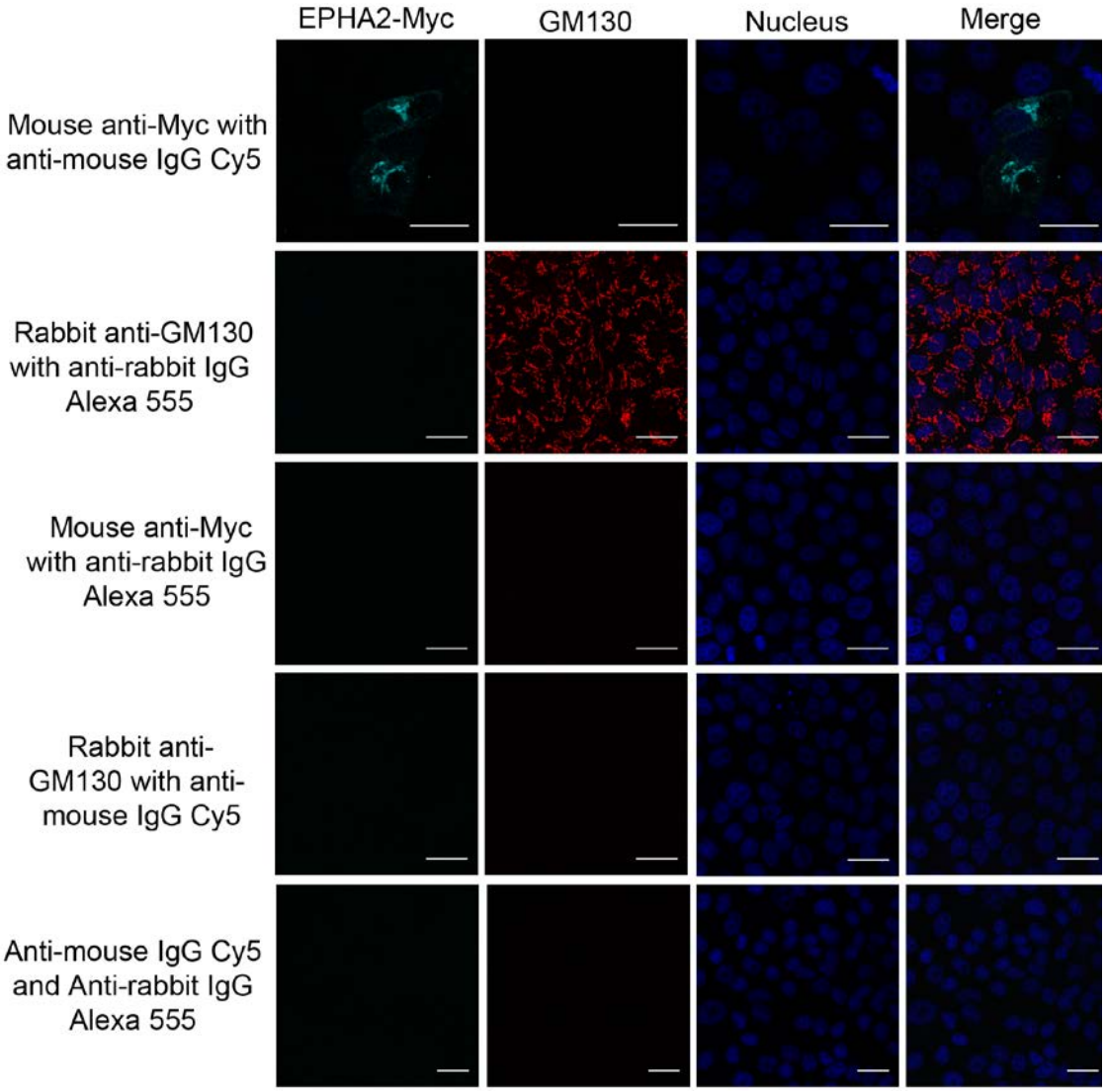

Figure 3.13: Positive and negative controls for co-localisation of EPHA2-Myc protein with cis-golgi marker in Caco2 cells

Caco2 cells ectopically expressing EPHA2 protein with p.T940I mutation (cyan) were labelled with mouse anti-Myc antibody detected using an anti-mouse IgG conjugated with Cy5 (positive control, first row) or anti-rabbit IgG conjugated with Alexa Flour 555 (control for cross-reactivity of the secondary antibody, third row). The cis-golgi apparatus (red) was detected using a rabbit anti-GM130 and an anti-rabbit IgG conjugated with Alexa Flour 555 (positive control, second row) or anti-mouse IgG conjugated with Cy5 (control for cross-reactivity of the secondary antibody, fourth row). Mock transfected cells labelled only with both the secondary antibodies used as negative control. Nucleus (blue) was labelled with DAPI. The figure shows representative images of controls from two independent experiments. Scale-bar, 20 µm

3.4.Discussion

In this study, the effect of five congenital cataract causing mutations in *EPHA2* on subcellular localisation of the resultant mutant proteins was analysed in MDCK and Caco2 epithelial cells. These included mutant proteins carrying p.P594L (c.1751C>T) mutation in the juxtamembrane domain, p.T940I (c.2918C>T), p.D942fsXC71 (c.2826-9G>A) and p.A959T (c.2875G>A) mutations in the SAM domain and p.V972GfsXC39 (c.2915_2916delTG) mutation in the PDZ domain of EPHA2.

Previously reported functional analysis of p.T940I, p.D942fsXC71 and p.V972GfsXC39 mutation in HEK293A and αTN4 cells revealed that these mutations rendered the mutant protein insoluble and resulted in protein aggregation in the cytoplasm (215). The mutant proteins were reported to have a reduced half-life and degradation through the proteosomal pathway.

Upon subcellular localisation analysis, we found that the EPHA2 proteins carrying p.T940I or p.D942fsXC71 mutation mis-localised to the perinuclear space and co-localised with GM130, a cis-golgi marker both in MDCK and Caco2 epithelial cells. Some mutant protein was also found in the cell membrane, however it may be incapable of triggering cellular signalling due to the presence of the mutation. These results are consistent with previous findings (215). Membrane proteins such as EPHA2 are partially translated in the cytoplasm and undergo co-translational transport on the rough endoplasmic reticulum (RER) and then transported to the golgi apparatus for further processing (303). The proteins are folded and glycosylated in the ER and then transported to the golgi apparatus for further

glycosylation. The golgi apparatus comprises of cisternae which are organized in the cis, medial and trans fashion providing a distinct polarity to the organelle (303). The cis-cisternae proximal to the ER receive the folded glycosylated protein from the ER whereas the mis-folded proteins are retained in the ER. The proteins are modified by a series of enzymes as they pass through the medial and trans-golgi network and are finally transported to their final destination in the cell through packaging in the secretary vesicles, which in the case of EPHA2 is the cell membrane. Therefore co-localisation of these two mutant proteins with the cis-golgi marker suggests altered folding or glycosylation of the proteins.

The SAM domain of EPHA2 protein has five helical loops in its secondary structure (305). The mutations, p.T940I and p.D942fsXC71, are located in or in proximity to the helical loop 4 in the protein (Figure 3.14). The frameshift due to p.D942fsXC71 mutation alters residues not only in helix 4 but in helix 5 as well; including residues predicted to be critical for the intramolecular interactions (305). The p.T940I mutation alters a neutral polar amino acid residue threonine preceding the helical loop 4 to a highly hydrophobic amino acid residue isoleucine, which may again have implication on the protein structure. These mutations perhaps, affect mutant protein folding and post-translational modifications leading to its retention in the perinuclear region of the ER/Golgi network. This is consistent with the previously reported reduced solubility of both these mutant proteins perhaps due to altered protein conformation (215). However, neither of these mutant proteins showed complete co-localisation with the cis-golgi marker suggesting that they could be either retained in the ER or in mid/trans-golgi network during transport to the cell membrane. Performing co-localisation studies with markers for ER, mid/trans-golgi may help in

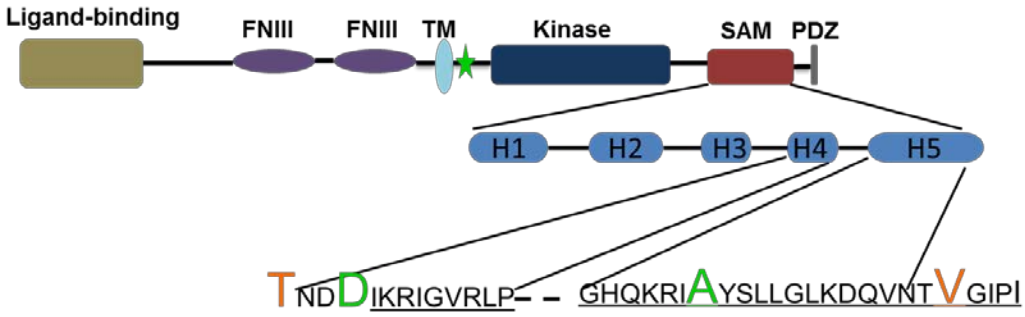

Figure 3.14: Structural domains of EPHA2 and location of the mutations analysed in the study

Schematic representation of the ligand binding (brown), fibronectin (purple), transmembrane segment (sky blue), kinase (dark blue), SAM (red) and the PDZ domain (grey) of the EPHA2 protein. The position of mutations identified in our genetic study, namely p.P594L (green star), p.D942fsXC71 and p.A959T is highlighted in green. The two previously reported mutations p.T940I and p.V972GfsXC39 are highlighted in orange. p.P594L mutant protein affects a residue in the juxtamembrane region of the protein, however does not affect protein localisation. The mutant proteins mis-localising to the perinuclear region carry p.T940I and p.D942fsXC71 mutation which affects the helix 4 in the SAM domain. Mutant protein with p.A959T alters a residue in helix 5 in the SAM domain and with p.V972GfsXC39 affects residues in the PDZ domain of EPHA2 but show no effect on protein localisation.

further deciphering the fate of these two mutant proteins. Whether the aggregated localisation reflects degradation of the misfolded protein by the proteosomal pathway as has been reported previously, needs further investigation (215). Further, the other mutant EPHA2 proteins with p.P594L, p.A959T or p.V972GfsXC39 mutation localised to the cell periphery or cytoplasm similar to the wild-type protein. In addition to cell periphery, the wild-type and mutant EPHA2 proteins were found in the perinuclear space in transfected cells. This may be explained by over-expression of the ectopically expressed protein which perhaps also leads to the co-localisation observed with the cis-golgi marker. The localisation of these mutants in the perinuclear region is different from the EPHA2 proteins with p.T940I and p. D942fsXC71 mutations as the latter two mutants show minimal protein in the cell periphery, which may lead to insufficient signalling. Even though these three mutant proteins do not affect protein localisation these mutants may still have functional effects. For example, the mutant p.A959T alters a residue downstream of an isoleucine, at position 958, predicted to be important for intramolecular interactions (305). Therefore this mutation could potentially disrupt such interactions. As mentioned in Chapter 2, section 2.4, the p.P594L mutant may alter phosphorylation states of tyrosine residues and affect protein activation and signalling. EPHA2 is activated by interaction with its Ephrin ligand which leads to oligomerisation and cell signalling (225). It is possible that after reaching the cell periphery these mutant proteins have impaired ability to form signalling clusters or interact with other downstream signalling molecules, thus disrupting cell signalling. For instance, p.V972GfsXC39 mutation alters residues in the PDZ domain of EPHA2. PDZ domains of proteins are key regulators of their interactions

with other molecules (306). A previous report has demonstrated that addition of 15 amino acids to the C-terminal of EPHB2 leads to loss of interaction with a ras-binding protein Afadin (AF6) known to play a role in cellular junctions (307). The functional effect of p.V972GfsXC39 mutation has been examined previously (215), whereas the possible effects of p.P594L and p.A959T mutation are a matter for future investigation.

All the investigations in the present work were performed on transiently transfected cells. Similar analysis may also be conducted in other relevant cell lines such as human lens cell lines (HLE-B3) or mouse lens epithelial cell lines such as 17EM15 and 21EM15. Additional studies examining the effect of these mutants on cell-junctions in cells, transiently or stably expressing the mutant EPHA2 proteins, may assist in deciphering the mechanism of cataract development.

3.5. Conclusion

In the present study, only mutant proteins with p.T940I and p.D942fsXC71 mutation were predominantly present in perinuclear region which may affect role of EPHA2 in cellular junctions resulting in cataract. The mutant EPHA2 proteins carrying p.P594L, p.A959T and p.V972GfsXC39 mutation localised similar to the wild-type protein and may disrupt signalling through EPHA2. The results from this study are different from what has been previously reported and demonstrate the importance of utilizing a functionally relevant cell culture system for localisation analysis.

4. Effect of age and gender on *Epha2* mediated age-related cataract

4.1 Introduction

Age-related cataract (ARC) is a multifactorial disease; interplay of well-established environmental risk factors such as age, female gender, smoking, ultraviolet light exposure and diabetes with genetic factors contribute to cataract development. These environmental risk factors and genetic factors have been explained in more detail in Chapter 1, section 1.3.2.2 and section 1.3.2.3, respectively.

Recently association of SNPs in the *EPHA2* gene with ARC was reported. As mentioned in Chapter 2, section 2.1, mutations in the gene were initially identified through linkage analysis as a cause of congenital cataract. This chromosomal locus was previously reported to be associated with age-related cortical cataract (189). Therefore role of *EPHA2* in age-related cataract was examined through candidate gene association studies. SNPs in *EPHA2* were found to be associated with age-related cortical cataract in an Italian (68), American, British and an Australian cohort (191). Association of SNPs in the gene with ARC has not only been reported in Caucasian but in Asian populations such as Han Chinese (190) and Indian (192). The SNPs associated in the different populations are listed in Table 4.1. *EPHA2* is the only gene which has been reproducibly implicated in ARC in multiple populations.

Table 4.1: SNPs in the *EPHA2* gene associated with ARC in different populations.

Population	Cataract Phenotype	Associated SNPs	Location in the gene	Reference
Italian	Cortical	rs7543472, rs11260867, rs3754334	Downstream and Exon 17	(68)
American	Cortical	rs3768293, rs6603867, rs6678616	Intron3-4 and Exon 3,	(191)
British	Cortical	rs3754334	Exon 17	(191)
Australian	Cortical	rs7548209	Downstream	(191)
Chinese	Cortical	rs477558, rs7548209	Upstream and Downstream	(190)
Indian	Cortical and posterior subcapsular	rs7543472, rs11260867	Downstream	(192)

Additionally, studies in *Epha2*$^{-/-}$ mice have suggested a role of Eph signalling in maintaining lens cell homeostasis (191, 212, 213). *Epha2*$^{-/-}$ mice (Strain: B6;129P2-Epha2$^{Gt(KST085)Byg}$), developed by secretary gene trap method, on FVB/NJ background were reported to develop progressive age-related cortical cataract from 5 months of age while *Epha2*$^{+/-}$ mice did not develop cataract until 14 months of age (191). Additionally, compared to *Epha2*$^{+/+}$ lenses, the lenses of *Epha2*$^{-/-}$ mouse were found to have upregulated expression of Heat Shock Protein 25 (HSP25) suggesting increased stress in the lens due to lack of functional Epha2. The same study found another *Epha2*$^{-/-}$ mouse strain, Epha2$^{Gt(ROSABetageo)CN3Yiw}$, generated using gene trapping by an insertion in intron 1 on C57BL/6J background, developed progressive cataract with similar morphology; however, the age at which these mice develop cataract was not mentioned in the report (191). These studies provide substantial evidence for the importance of Epha2 signalling in maintaining lens clarity.

As the name suggests, increasing age increases the risk of all phenotypes of ARC and female gender is associated with higher risk of mainly cortical cataract in multiple population-based studies (117, 145-147). Interestingly, both age and gender also affect EPHA2 expression and/or signalling. Epha2 expression reduces with age in mouse lens (191) and female hormone estrogen negatively regulates EPHA2 signalling *in vitro* in cultured mammary epithelial cells (270). Therefore we wanted to investigate if interaction between these environmental factors and *EPHA2* gene could be the underlying cause of cataract development in humans. In this study we used a knockout mouse model which served as a tool for studying the role of environmental factors in *Epha2* mediated ARC development.

4.2 Materials and Methods

4.2.1 Epha2$^{Gt(KST085)Byg}$ or KST085 strain

The KST085 line of *Epha2*$^{-/-}$ mice on C57BL/6J background was received from Mutant Mouse Regional Resources Centers, U.S.A. The KST085 strain was generated via secretory trap method by insertion of β-galactosidase and neomycin phosphotransferase (β-geo) reporter gene cassette between Exon 5 and Exon 6 of mouse *Epha2* gene as illustrated in Figure 4.1 (308, 309). The inserted bicistronic vector carried the *human placental alkaline phosphatase* (*PLAP*) gene following an internal ribosome entry site (IRES) after the β-geo cassette. This vector insertion leads to independent translation of the partial Epha2 protein fused to β-geo and the PLAP protein. The fusion protein is expected to be inserted in the lumen in endoplasmic reticulum retaining its β-galactosidase activity (310). Lack of ability of the truncated Epha2 fusion protein to reach the cell membrane renders it functionally inactive.

4.2.2 Animal maintenance

Ethics approval for the project was obtained from the Animal Welfare Committee, Flinders University, Adelaide. All procedures using mice were performed in accordance with the Australian code of practice for the care and use of animals for scientific purposes (311).

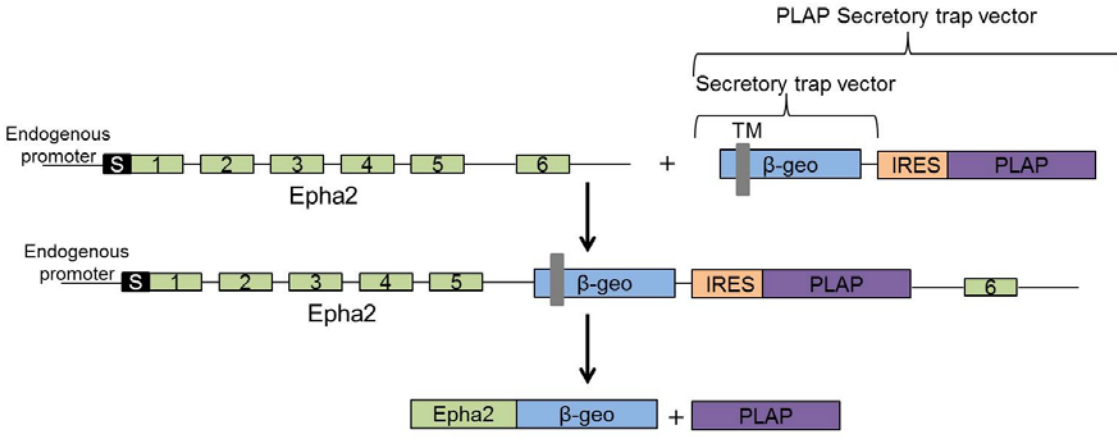

Figure 4.1: Strategy for generation of KST085 mouse strain

pGT1tm carrying *β-geo* (fusion between *β-galactosidase* and *neomycin phosphotransferase*) and *human placental alkaline phosphatase* (*PLAP*) following an internal ribosome entry site (IRES) was inserted in intron 5 of the *Epha2* gene. This leads to independent translation of a partial Epha2 fusion protein and the PLAP protein. Adapted from Leighton et al., 2001, Nature, 410. (301).

The mice were housed in a Physical containment level 2 (PC2) room in the Flinders Animal Facility, School of Medicine. The mice had unrestricted access to water and feed, were exposed to a 12 hour light-dark cycle and an ambient temperature of 24ºC. The mice were monitored weekly for their general well-being.

4.2.3 Animal Breeding

Litters from *Epha2*$^{+/-}$ × *Epha2*$^{+/-}$, *Epha2*$^{+/-}$ × *Epha2*$^{+/+}$, *Epha2*$^{+/+}$ × *Epha2*$^{+/+}$ and *Epha2*$^{-/-}$ × *Epha2*$^{+/+}$ breeder pairs were used for the study. All the breeder pairs bred normally except pair *Epha2*$^{-/-}$ × *Epha2*$^{+/-}$ which only bred using a female *Epha2*$^{-/-}$ mice. The *Epha2*$^{-/-}$ × *Epha2*$^{-/-}$ pairs did not breed successfully. Occasionally mice were also found to have Peter's anomaly (1.7%) or anophthalmos (0.34%) and were not used for any experiments. The breeder pairs producing offspring with anophthalmos were not used for further breeding or experiments. All the other mice developed normally without any abnormalities.

4.2.4 DNA extraction from mouse tissue for genotyping

Ear-notches or tail-tips from 2-3 weeks old mice were obtained and stored at -20°C till used for extractions. For DNA extraction, the tissues were incubated in 500 µl of lysis buffer (0.1 M Tris-HCl pH 8.3, 0.2 M NaCl, 0.005 M EDTA, 0.2% SDS, 100 µg/ml Proteinase K) at 55°C overnight. The following day, lysates were centrifuged at 18000 × g for 10 minutes. The supernatant was incubated with equal volume of isopropanol for 1 minute and then centrifuged at 18000 × g for 10 minutes. DNA pellets obtained were washed twice with chilled 70% ethanol to remove residual salts and left for drying at room

temperature. Dried DNA pellets were resuspended in 50 µl of Milli-Q water and used for genotyping.

4.2.5 *Bfsp2* and *Epha2* genotyping

The KST085 mice were generated on a B6;129P mixed genetic background. The 129 mice carry a deletion mutation in the *Beaded filament structural protein 2* (*Bfsp2*) gene leading to disruption of the encoded CP49 protein that results in cataract (312, 313). Therefore to determine if the KST085 strain used in this study carried this mutation, *Bfsp2* genotyping was performed as previously reported (312). PCR-based genotyping was performed for the two genes as illustrated in Figure 4.2 a) and b). *Bfsp2* was genotyped using primers CP49fwd, CP49Rev and CP49MutR. The expected sizes of the PCR product from the wild-type and mutant allele were 905 bp and 386 bp, respectively. See Appendix 2.5 for sequences of the primers. Likewise, *Epha2* genotyping was performed using primers M30828F, M30828WTR and M30828MutR. The expected PCR products of 200 bp in size corresponding to wild-type allele and 400 bp in size corresponding to mutant allele, were used to distinguish between $Epha2^{+/+}$, $Epha2^{+/-}$, and $Epha2^{-/-}$ mice. Sequences of the primers are listed in Appendix 2.6.

Forty nanograms (determined spectrophotometrically as described previously in Chapter 2, section 2.2.3) or 2 µl of extracted DNA was amplified by PCR. The PCR was set-up as previously described in Chapter 2, section 2.2.3 in a total 10 µl volume. The Hot Star Taq *Plus* polymerase enzyme was activated at 95°C for 5 minutes. Denaturation was performed at 95°C for 30 seconds, followed by annealing for 30 seconds at 61°C for *Epha2* and 68°C

for *Bfsp2* genotyping and extension at 72°C for 30 seconds for 35 cycles. A post-extension at 72°C for 1 minute was followed by incubation at 4°C for 5 minutes. PCR products of *Epha2* and *Bfsp2* genotyping were, respectively, analysed on 1.4% and 1% agarose gels prepared in TBE.

4.2.6 Slit-lamp examinations

Mice were mildly sedated by isofluorane inhalation in an anesthetic pot and then anesthetized by an intraperitoneal injection of 10% Ketamine (Lyppard Australia Pty. Ltd., SA, Australia) at 75 mg/kg body weight and 100 µl of 10% Medetomidine (Troy Laboratories Pty. Ltd., NSW, Australia) followed by induction of mydriasis with 1% tropicamide (Bausch & Lomb Pty. Ltd., NSW, Australia). Their eyes were examined on a photo-slit lamp biomicroscope (Topcon Medical Systems Inc., NJ, U.S.A.) and lenses were clinically graded. Cortical cataract was graded using the Lens Opacities Classification System (LOCS) III (314). All mice were examined within 5-10 minutes of drug administration. Examination was performed by an observer blinded to the genotype, gender and age of mice.

The observations were recorded by digital photography at 40 × magnification using EZ Capture software (Topcon Medical Systems Inc., NJ, U.S.A.) with flash set to maximum level. Three images were documented for each eye, photo-slit lamp settings for which are listed below.

1. Diffused illumination: Maximum slit width with slit height 5 was set for the first image. The diffusion filter was on with light angle set at 35º.

2. Cross-section illumination of the lens: Slit width of 2 mm and slit height 2 was used for the second image. For this image the diffusion filter was off and the light angle set at 45º
3. Retroillumination: For this, the slit width was set to 3 or 5 mm and slit height 5. Again the diffusion filter was off with camera perpendicular to the eye.

After examination the mice were revived with an intraperitoneal injection of 100 µl of 10% Atipamizole (Troy Laboratories Pty. Ltd., NSW, Australia). The mice were monitored for revival after administration of the drug and for general well-being at least 24 hours after examination.

4.2.7 Tissue collection

Mice were euthanized by isofluorane inhalation and tissues dissected under a dissecting microscope. To dissect the lens, an incision was made in the sclera with a scalpel blade and the cornea was dissected with the help of a toothed forceps and vannas dissecting scissors. The lens was then removed using the forcep and snap frozen in liquid nitrogen. The lenses were stored at -80°C till further use for protein extraction

For histological and immunofluorescence analysis, whole eyes were removed using a splinter forcep and a general laboratory dissecting scissor. The orbital tissue covering the optic nerve was dissected by vannas dissecting scissors The enucleated eyes were pierced at the back with a 25G needle and fixed in 10% Neutral Buffered Formalin (NBF; see Appendix 3.17). After fixation for 24-72 hours at room temperature, the eyes were washed thrice with 1× PBS and stored in 70% ethanol at 4°C till paraffin embedded.

4.2.8 Tissue embedding and sectioning

For embedding, whole eyes were first transferred to histology cassettes (ProSci Tech Pty Ltd, QLD, Australia). They were then dehydrated in 80% ethanol (1 hour), 90% ethanol (1 hour) and 100% ethanol (1 × 2 hours and 1 × 1 hour); followed by incubation in chloroform overnight. The following day cassettes with eyes were transferred to molten wax (Paraplast tissue embedding medium, Tyco healthcare Group, Mansfield, MA, USA) for 30 minutes at 64°C. Then they were left in molten wax under vacuum at pressure 90 kPa (2 × 1 hour) followed by embedding in wax blocks. 7 µm thick serial tissue sections were cut on a microtome (Leica RM2/35; Leica Microsystems, Gladesville, NSW, Australia) and collected on Superfrost Plus (Menzel-Glaser, Thermo Fisher Scientific Australia Pty Ltd, VIC, Australia) slides. The sections were dehydrated at 37°C overnight and then stored at room temperature. The tissue sections were used for experiments within 12 months of sectioning.

4.2.9 Histological analysis

For histological analysis, tissue sections were stained with haematoxylin (See Appendix 3.18) and eosin (See Appendix 3.19) to stain the nuclei and cytoplasm, respectively. The sections were dewaxed in xylene (2 × 2 minutes) and hydrated in 100% ethanol (2 × 2 minutes), 90% ethanol (1 × 2 minutes) and 70% ethanol (1 × 2 minutes). They were then rinsed in deionized water (dH_2O; 1 × 2 minutes) before staining with haematoxylin (1 × 10 minutes). After a rinse in dH_2O to remove excess stain, the sections were dipped in lithium

carbonate to remove non-specific staining. They were then rinsed in dH_2O (1 × 1 minute) and stained with eosin (1 × 2 minutes). After removal of excess stain by rinsing in dH_2O, they were dehydrated in 100% ethanol (3 × 1 minute). The sections were cleared to minimize light refraction while imaging by treatment with xylene (2 × 1 minute) and mounted using DePex mounting medium (BDH laboratory Supplies, Poole, UK). The slides were imaged using 40 × objectives on an Olympus Brightfield BX50 upright microscope (Olympus Australia Pty. Ltd., VIC, Australia) equipped with QImaging RTV 5 megapixel Digital Camera (QImaging, BC, Canada). The QCapture software (QImaging, BC, Canada) was used for capturing images.

4.2.10 Immunolabelling

Tissue sections were incubated at 65°C for 10-40 minutes to enhance tissue adherence to the slide. They were then dewaxed in Xylene (2 × 2 minutes) and hydrated in 100% ethanol (2 × 5 minutes), 90% ethanol (2 × 2 minutes) and 70% ethanol (1 × 2 minutes). The sections were then incubated in PBS before performing antigen retrieval. Antigens were retrieved by heat-induced epitope retrieval. The epitopes for N-cadherin and beta (β) -catenin were retrieved using 0.01M citrate buffer with 0.05% Tween 20, pH 6 (See Appendix 3.20) and those for Epha2 and β-galactosidase were retrieved using the Target Retrieval Solution, pH 9 (Dako Australia Pty Ltd, NSW, Australia). The citrate buffer retrieval solution was heated in a microwave (Panasonic Australia, SA, Australia; Power output: 1100W) at high setting for 1 minute and 30 seconds, to heat the buffer to at least 65°C. The sections were then immersed in the buffer and heated in the microwave for 10 minutes at medium-low settings. For alkaline solution based antigen retrieval, the target

retrieval solution was heated in the microwave at high setting for 4 minutes to heat the buffer to at least 95°C. The sections were then immersed in the buffer and heated in the microwave for 15 minutes at medium-low settings. After performing antigen retrieval, the sections were left at room temperature to cool down before labelling.

For labelling, the sections were blocked for 30 minutes in blocking buffer consisting of 3% goat or donkey serum (Sigma-Aldrich Pty Ltd, NSW, Australia) prepared in wash buffer (0.1% BSA in PBS). The choice of serum used in the blocking buffer was dependent on the host animal used to generate the secondary antibody. The sections were labelled using mouse anti-β-catenin (1:200, BD Transduction Laboratories, CA, U.S.A.) or mouse anti-N-cadherin (1:200, Life Technologies Australia Pty Ltd, VIC, Australia) or goat anti-mEpha2 (1:40, R&D Systems, Inc, MN, USA) or rabbit anti-β-galactosidase (1:250, Novus Biologicals, CO, USA) primary antibody diluted in the appropriate blocking buffer at 4ºC overnight. Equivalent amount of mouse, goat or rabbit IgG diluted in blocking buffer was used as a negative control. The sections were washed thrice for 5 minutes each in wash buffer. This was followed by hybridization with the anti-mouse or anti-goat IgG conjugated with Alexa Flour 488 (1:1000, Life Technologies Australia Pty Ltd, VIC, Australia) or anti-rabbit IgG conjugated with Alexa Flour 594 (1:1000, Life Technologies Australia Pty Ltd, VIC, Australia) secondary antibody diluted in wash buffer. After hybridization, the sections were washed thrice for 5 minutes each in wash buffer and mounted in Prolong AntiFade with DAPI (Life Technologies Australia Pty Ltd, VIC, Australia). The labelled sections were imaged using a 63 × objective on a Leica TCS SP5 Spectral Confocal Microscope (Leica Microsystems Pty Ltd, NSW, Australia) equipped with Leica Application Suite (Leica Microsystems Pty Ltd, NSW, Australia) software for

image capture. DAPI was excited using 405 laser, Alexa Flour 488 was excited with the argon laser and Alexa Flour 594 was excited using DPSS 561 laser line. The emission spectrum for DAPI, Alexa Flour 488 and Alexa Flour 594 was set to 408-488 nm, 492-561 nm and 565-645 nm, respectively. Adobe Photoshop was used to enhance the brightness and contrast of the images used to prepare the figures presented in this thesis.

4.2.11 Protein extraction and Western blotting

Mouse lenses were homogenised using a tissue grinder pestle in 50 µl of RIPA buffer (Refer to Chapter 3, Section 3.2.7 for buffer recipe). The homogenate was left on ice for 30 minutes to ensure complete extraction of proteins followed by centrifugation at 18000 × g for 10 minutes at 4ºC to pellet the cell debris. The supernatant was transferred to fresh eppendorf tubes and protein concentration estimated by BCA Protein assay (Thermo Fischer Scientific, VIC, Australia) using BSA standards according to manufacturer's protocol. Forty micrograms of total soluble lens protein was size separated on 4-15% Mini-PROTEAN® TGX Stain-Free™ precast gels (BioRad Laboratories Pty Ltd, NSW, Australia) by SDS- PAGE.

For Western blotting, the proteins were transferred on to PVDF-LF membrane as described in Chapter 3, Section 3.2.8. The membrane was blocked in 5% skim milk made in TBST for 1 hour. To detect Epha2, the blot was first developed after hybridisation with only rabbit anti-goat IgG conjugated with biotin (1:500, Dako Australia Pty Ltd, NSW, Australia) for 1 hour and Streptavidin (SA) conjugated with HRP (1:1000, Dako Australia Pty Ltd, NSW, Australia) for 20 minutes. Following this, it developed after hybridisation

with the goat anti-mEpha2 (1:1000, R&D Systems, Inc, MN, USA) primary antibody for 1 hour followed by the rabbit anti-goat IgG conjugated with biotin (1 hour, 1:500) and SA-HRP (20 minute, 1:1000). To examine β-galactosidase expression, the membrane was hybridised with a rabbit anti-β-galactosidase (1:500, Novus Biologicals, CO, USA) primary antibody and HRP-conjugated goat anti-rabbit IgG (1:20,000, Rocklands Immunochemicals Inc, PA, USA) secondary antibody for 1 hour each. The blots were washed thrice for 5 minutes each with TBST between hybridisations. Blots were developed using Amersham™ ECL™ Prime western blotting reagent (GE Healthcare Australia Pty Ltd, NSW, Australia). The signal was imaged using ImageQuant LAS 4000 Imager (GE Healthcare Australia Pty Ltd, NSW, Australia)

4.2.12 Statistical analysis

All statistical analysis was performed using IBM Statistical Package for the Social Science (SPSS) Statistics 19. The normality of distribution of cataract grades was analysed by Shapiro-Wilk statistical test. As the data was not normally distributed, non-parametric tests were used for all the analysis.

The effect of age on cataract grades in mice of different age-groups was analysed using Mann-Whitney *U* test. The effect of *Epha2* genotype at each age was analysed using Kruskal-Wallis statistical test and significant differences were further assessed using Mann-Whitney *U* test. The effect of age on cataract progression in mice of each genotype was analysed using Friedman test and any significant difference was further assessed by Wilcoxon Signed Ranks test. The effect of gender on cataract progression was analysed at each age using Mann-Whitney *U* test.

4.3 Results

4.3.1 *Bfsp2* and *Epha2* genotyping

Bfsp2 genotyping was performed, because as mentioned in section 4.2.5, the KST085 mice are generated on a B6;129P strain background and may carry a mutation in the *Bfsp2* gene found in the 129 strain. The mutation leads to deletion of the splice site in intron 1 of the gene leading to complete deletion of exon 2 from the mutated transcript (312). *Bfsp2* genotyping was performed in the first and second generation of KST085 breeders. Figure 4.2a) illustrates a schematic of the wild-type and mutant *Bfsp2* gDNA with the position of primers used for genotyping and expected sizes of PCR products. A representative agarose gel with PCR products obtained from gDNA of KST085 breeders and 129 strain is also shown. $CP49^{+/+}$ mice exhibited a 905 bp product corresponding to the wild-type allele and $CP49^{-/-}$ mice showed presence of a 386 bp PCR product corresponding to the mutant allele. All KST085 breeders were found to carry the wild-type allele for *Bfsp2* gene. Hence *Bfsp2* genotyping was not performed in the successive generations.

Epha2 genotyping was performed for all litters except for the ones obtained by breeding of $Epha2^{+/+} \times Epha2^{+/+}$ or $Epha2^{-/-} \times Epha2^{+/+}$ mice. Figure 4.2b) shows wild-type and mutant *Epha2* alleles with the position of primers used for genotyping and the expected sizes of PCR products. The figure also illustrates an image of representative genotyping results of a KST085 litter. The $Epha2^{+/+}$ mice exhibited a product 200 bp in size corresponding to the wild-type allele; $Epha2^{+/-}$ mice showed a 400 bp product

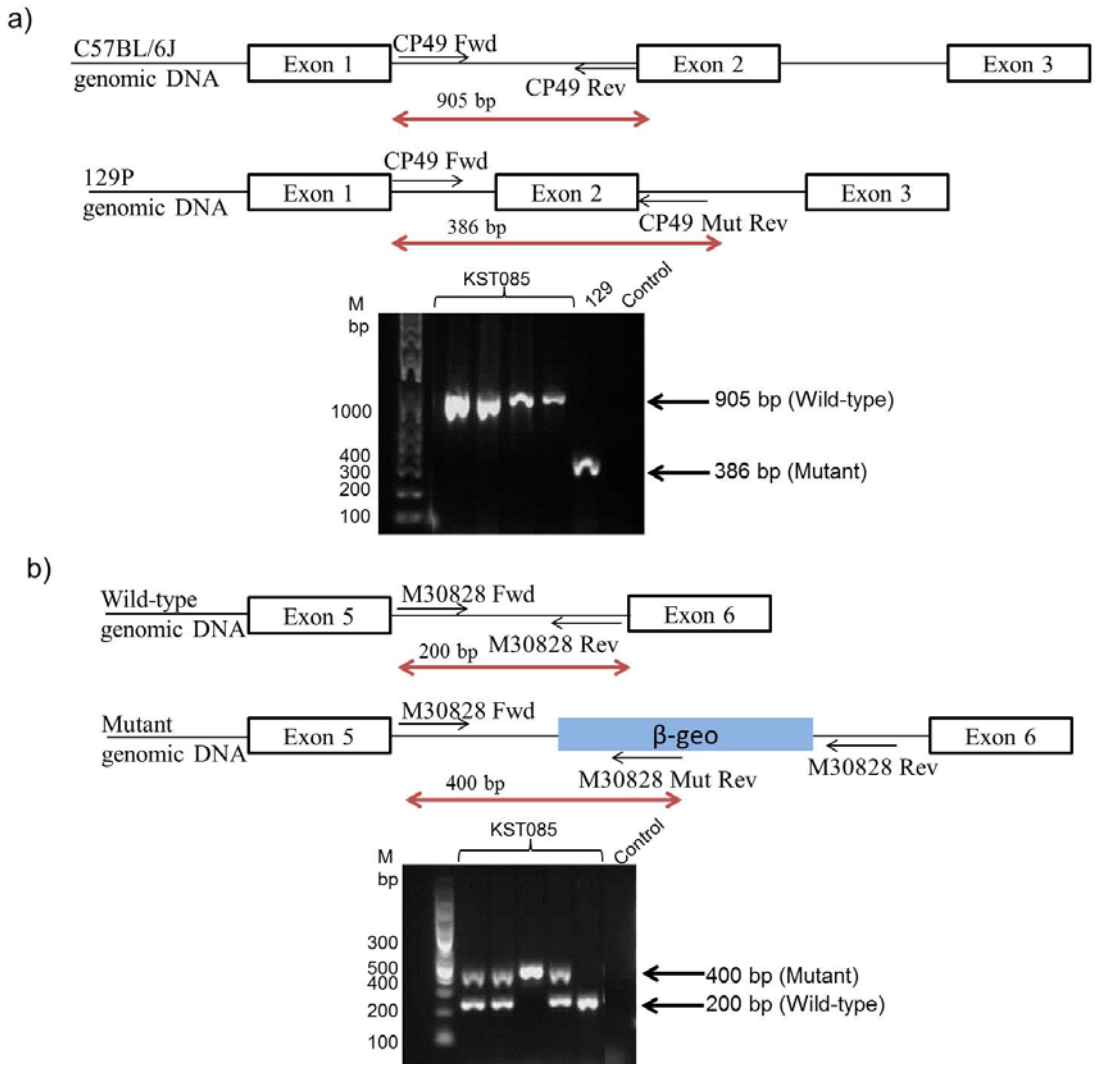

Figure 4.2: *Bfsp2* and *Epha2* genotyping

a) Depicts a schematic of *Bfsp2* gDNA in wild-type, C57BL/6J, and mutant, 129, mice. The black arrows indicate the position of primers used for genotyping. The red double arrow represents the expected PCR product sizes from each gDNA. The 129 mice carry a deletion in Intron 1 and start of exon 2 which leads to deletion of Exon 2 in the transcript. A representative agarose gel shows the wild-type allele amplified from the gDNA of KST085 breeders used for this study. Mutant allele amplified from gDNA of 129 mice served as positive control. b) illustrates schematic of gDNA, primer positions and PCR product sizes for *Epha2* genotyping as described above. A representative agarose gel shows wild-type allele amplified from gDNA of *Epha2*$^{+/+}$ mice, both wild-type and mutant alleles from gDNA of *Epha2*$^{+/-}$ and mutant allele from gDNA of *Epha2*$^{-/-}$ mice. PCRs with no template were used as negative controls. Product sizes and DNA molecular size markers (M) are as indicated in base pairs (bp).

corresponding to the mutant allele along with a 200 bp sized product consistent with the wild-type allele; *Epha2*$^{-/-}$ mice exhibited only a product 400 bp in size corresponding to the mutant allele.

4.3.2 Effect of age on cataract development and progression

The KST085 mice on FVB/NJ background were previously reported to develop progressive cortical cataract from 5 months of age, while the *Epha2*$^{+/-}$ mice did not develop cataract until 14 months of age (191). Therefore we wanted to investigate, whether *Epha2*$^{+/-}$ mice older than 14 months develop cataract. For this study, *Epha2*$^{+/+}$ and *Epha2*$^{+/-}$ mice were examined for cataract development. However, our preliminary results showed that *Epha2*$^{+/-}$ mice developed cataract at an earlier age than 14 months, which precluded the need for examination until 14 months of age.

4.3.2.1 Cataract development in mice of different ages

Groups of 2, 4, 6, 8, 10 and 12 months old *Epha2*$^{+/+}$ and *Epha2*$^{+/-}$ mice were examined for cataract development. *Epha2*$^{+/+}$ mice of each age presented with mild anterior cortical cataract (grade 0-2). Two, four and six months old *Epha2*$^{+/-}$ mice exhibited only mild anterior cortical cataract but 8 months old *Epha2*$^{+/-}$ mice presented with severe anterior cortical cataract (grade 4-5). Severe anterior cortical cataract was observed in 10 and 12 months old *Epha2*$^{+/-}$ mice as well. The phenotype of cataract in *Epha2*$^{+/+}$ and *Epha2*$^{+/-}$ mice at each age is presented in Figure 4.3. Five to eleven mice were examined in each group; variation in the number of mice examined in each group was due to the availability

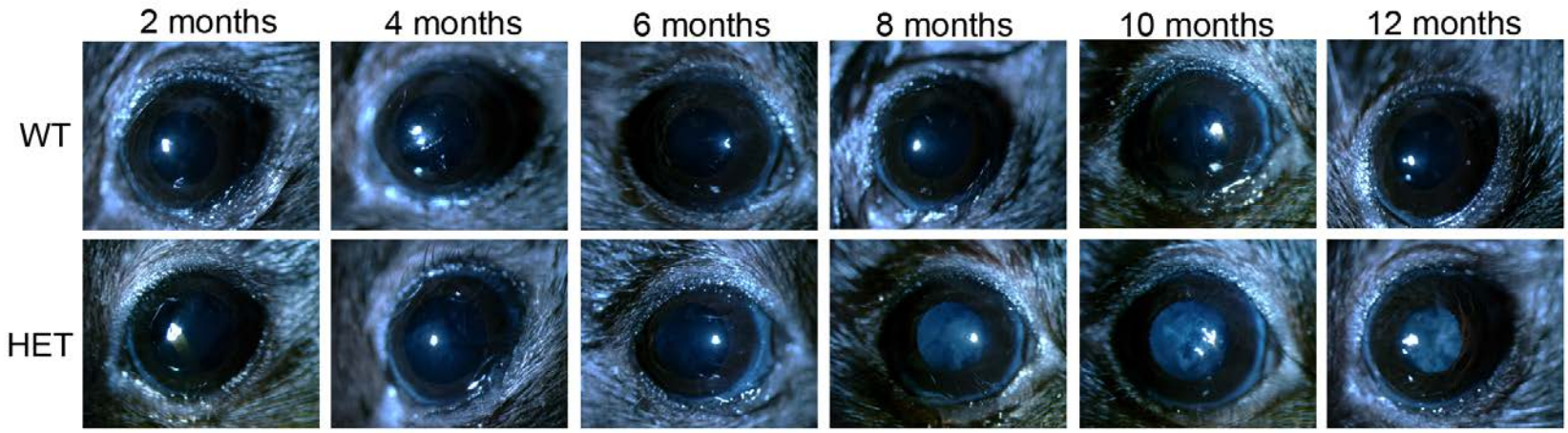

Figure 4.3: Anterior cortical cataract development in *Epha2*$^{+/+}$ and *Epha2*$^{+/-}$ mice of different ages

Representative images of cataract phenotype in 2, 4, 6, 8, 10 and 12 months old *Epha2*$^{+/+}$ (WT; top row) and *Epha2*$^{+/-}$ (HET; bottom row) mice. The age of mice is indicated above each column. Two, four and six months old *Epha2*$^{+/+}$ and *Epha2*$^{+/-}$ mice showed mild anterior cortical cataract. Eight, ten and twelve months old *Epha2*$^{+/-}$ mice developed severe cataract while *Epha2*$^{+/+}$ mice had relatively clear lenses till 12 months of age.

of mice at the required age. The average cataract grade (ACG), calculated as an average of the anterior cortical cataract grade of both the eyes for each mouse, was used for statistical analysis. Both the genotypes developed similar grades of cataract at 2 months (Mean ACG in *Epha2*$^{+/+}$mice = 0.7 ± 0.58; *Epha2*$^{+/-}$ mice =0.6 ± 0.77; p = 0.474 , Figure 4.4a), 4 months (Mean ACG in *Epha2*$^{+/+}$ mice = 1.3 ± 0.5; *Epha2*$^{+/-}$ mice = 1.4 ± 0.45; p = 0.96, Figure 4.4b) and 6 months (Mean ACG in *Epha2*$^{+/+}$ mice = 1.6 ± 0.7; *Epha2*$^{+/-}$ mice = 1.9 ± 0.9; p = 0.439, Figure 4.4c) of age. Hence, no significant difference was observed between the two genotypes at these ages. Eight months old *Epha2*$^{+/-}$ mice developed a mean ACG of 4.3 ± 0.37 which was significantly higher than mean ACG of 0.43± 0.39 in the *Epha2*$^{+/+}$ mice (p =0.001) (Figure 4.4d).

A similar statistically significant difference between the two genotypes was observed in 10 months (p = 0.001) and 12 months old (p = 0.004) mice (Figure 4.4e and f). The *Epha2*$^{+/+}$ mice developed low grades of cataract ranging between 0-2 however these grades varied between ages. For example, 4, 6 and 10 months old *Epha2*$^{+/+}$ mice developed higher grades of cataract as compared to 2, 8 and 12 months old *Epha2*$^{+/+}$ mice. As this experiment was performed over a period of more than a year, this difference may be due to observational variation in grading lower grades (0-2) of cataract over time.

Consistent with previous report (191), the *Epha2* knockout mice developed only anterior cortical cataract. However, this study demonstrated that 8 months old *Epha2*$^{+/-}$ mice of the KST085 strain on C57BL/6J background develop severe cataract, which was different from what had been previously reported in this strain (191). The results of this study prompted us to determine cataract progression in *Epha2*$^{+/+}$, *Epha2*$^{+/-}$ and *Epha2*$^{-/-}$ mice over time

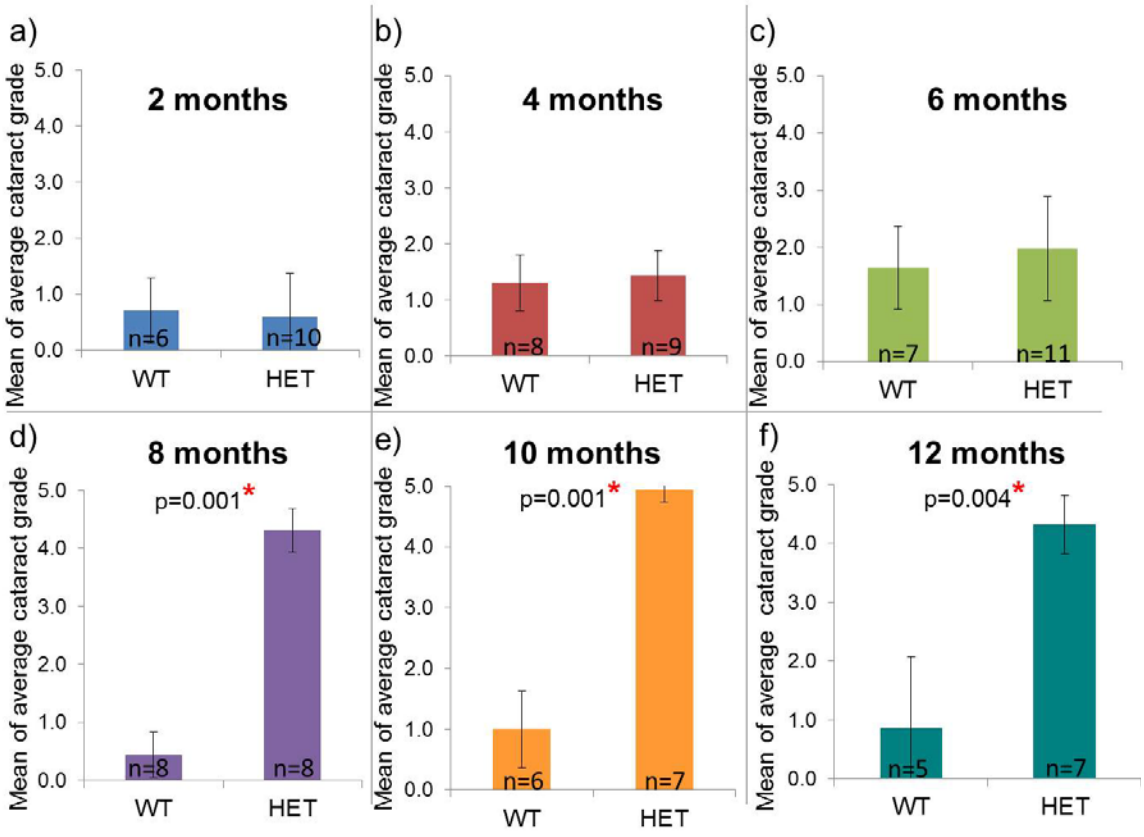

Figure 4.4: Comparison of cataract severity in *Epha2*$^{+/+}$ and *Epha2*$^{+/-}$ mice of different ages

Two, four, six, eight, ten and twelve months old *Epha2*$^{+/+}$ (WT) and *Epha2*$^{+/-}$ (HET) mice were examined for cataract development. Mean ACG at these ages are plotted in the graph and error bars depict the standard deviation in each group. The number of mice examined in each group is indicated at the bottom of each bar. Comparison of data at each age by Mann-Whitney *U* test showed a significant difference between 8, 10 and 12 months old *Epha2*$^{+/+}$ and *Epha2*$^{+/-}$ mice.

4.3.2.2 Cataract development and progression in mice over time

Epha2$^{+/+}$ (*n* = 18), *Epha2*$^{+/-}$ (*n* = 25) and *Epha2*$^{-/-}$ (*n* = 19) mice were monitored for development and progression to severe anterior cortical cataract (grade 4-5). Majority of the *Epha2*$^{+/+}$ and *Epha2*$^{+/-}$ mice were monitored bimonthly from 4 months until 8 months of age and a subset of these mice (*Epha2*$^{+/+}$ *n*=3; *Epha2*$^{+/-}$ *n*=9) were monitored bimonthly from 2 months until 8 months of age. This was based on the results described in section 4.3.2.1, which revealed that *Epha2*$^{+/+}$ and *Epha2*$^{+/-}$ mice developed similar grades of cataract up to 4 months of age. All *Epha2*$^{-/-}$ mice were monitored monthly from 2 months until 4 months of age.

Figure 4.5 illustrates the phenotype of cataract in the three genotypes of mice at different ages over time. Figure 4.6 graphically shows the mean ACG at each age. For the purpose of statistical analysis the data for *Epha2*$^{-/-}$ mice at 4 months were used at 6 and 8 months of age. This was based on the assumption that cataract severity in *Epha2*$^{-/-}$ mice will not reduce from what it was at 4 months of age. Similarly the data for *Epha2*$^{+/+}$ (*n* = 15) and *Epha2*$^{+/-}$ (*n* = 16) mice at 4 months of age were used at 2 months of age assuming that their cataract severity at 2 months would not be worse than that at 4 months of age. Cataract progression was compared using either ACG or the cataract grade of the severe eye. ACG was calculated as mentioned in section 4.3.2.1. Comparison of the ACG data in mice by Kruskal-Wallis statistical test revealed a significant difference between the three genotypes at each age. Table 4.2 lists the *p* values obtained at each age. This difference was further evaluated by Mann-Whitney *U* test to determine the difference between individual genotypes.

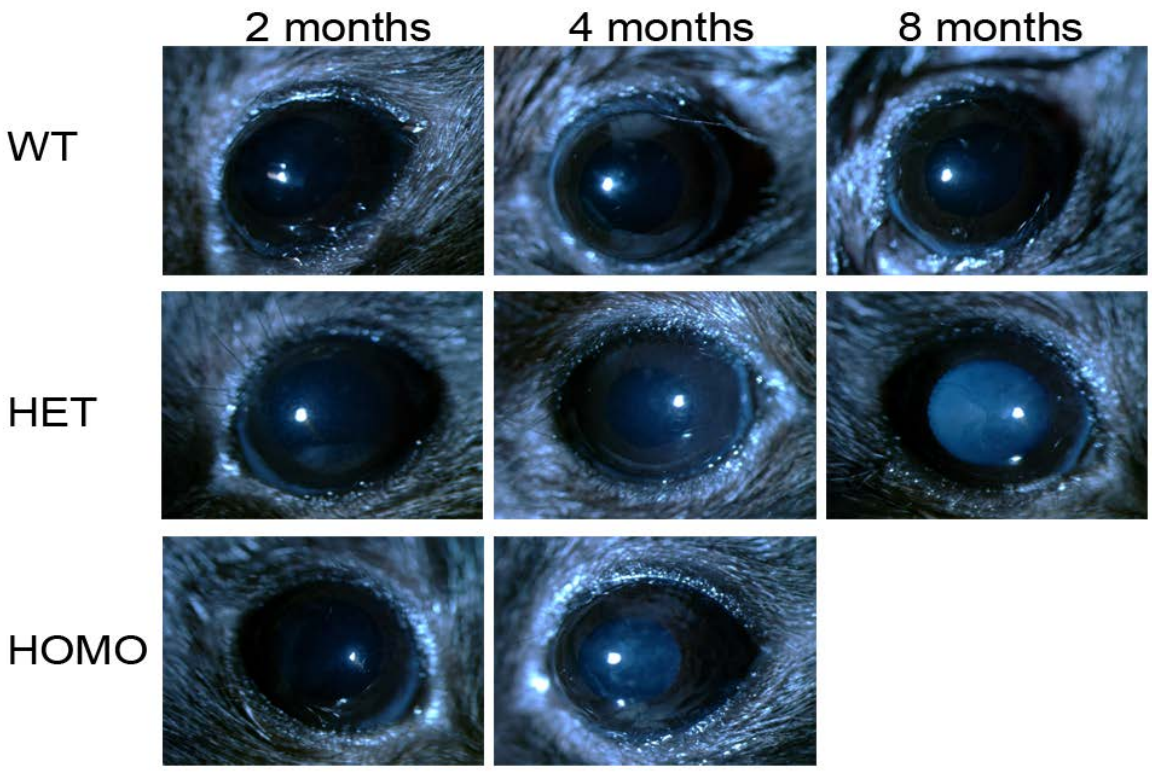

Figure 4.5: Anterior cortical cataract progression in *Epha2*$^{+/+}$, *Epha2*$^{+/-}$ and *Epha2*$^{-/-}$ mice over time

Representative images of *Epha2*$^{+/+}$ (WT; first row) and *Epha2*$^{+/-}$ (HET; second row) mice at 2, 4 and 8 months of age and *Epha2*$^{-/-}$ (HOMO; third row) mice at 2 and 4 months of age, are shown. The age of mice is indicated above each column. *Epha2*$^{-/-}$ mice progressively develop severe anterior cortical cataract by 4 months of age while *Epha2*$^{+/-}$ mice develop severe cataract by 8 months of age. *Epha2*$^{+/+}$ mice which continue to have relatively clear lenses until 8 months of age.

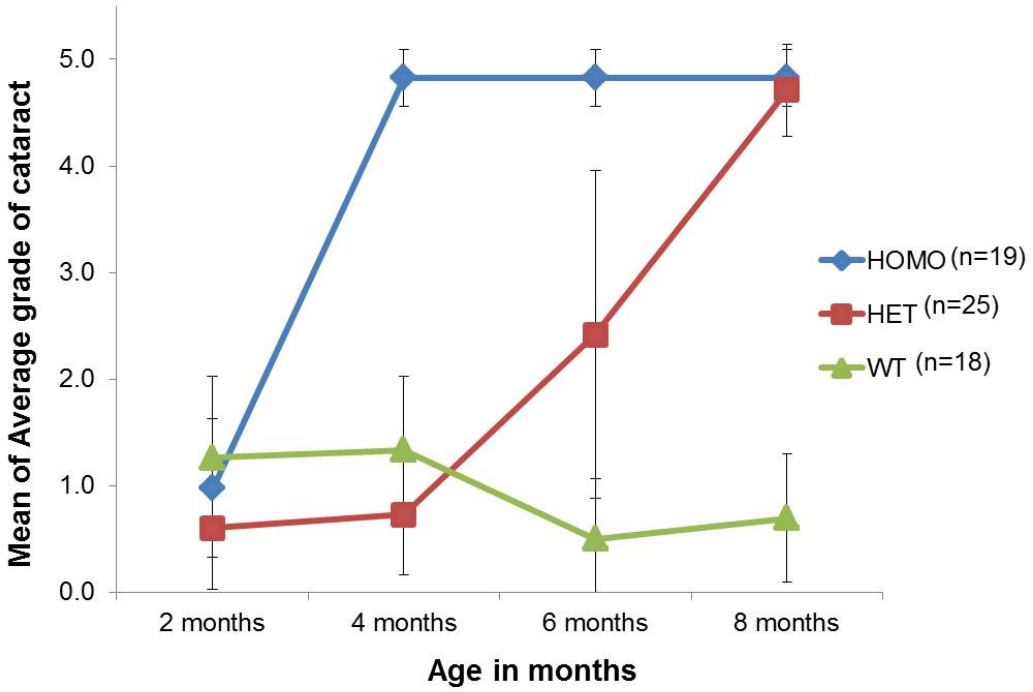

Figure 4.6: Comparison of cataract severity in *Epha2*$^{+/+}$, *Epha2*$^{+/-}$ and *Epha2*$^{-/-}$ mice over time

Epha2$^{+/+}$ and *Epha2*$^{+/-}$ mice were monitored bimonthly for cataract progression from 2 until 8 months of age. *Epha2*$^{-/-}$ mice were monitored monthly for cataract progression from 2 until 4 months of age. Mean ACG at 2, 4, 6 and 8 months are plotted in the graph. The error bars represent standard deviation. Comparison of the data by Kruskal-Wallis test revealed a significant effect of *Epha2* genotype at each age with *p* values of 0.009, 3.3×10^{-10}, 1.2×10^{-10} and 9.1×10^{-10} at 2, 4, 6, and 8 months, respectively. Comparing the data by Friedman test revealed a significant effect of age on cataract progression in *Epha2*$^{+/+}$, *Epha2*$^{+/-}$ and *Epha2*$^{-/-}$ mice with *p* values of 0.006, $3.3 \times 10^{-13}$and 2.5×10^{-12}, respectively.

Table 4.2: Comparison of cataract development between genotypes at each examined age; *Epha2*$^{+/+}$ (*n* = 18), *Epha2*$^{+/-}$ (*n* = 25) and *Epha2*$^{-/-}$ (*n* = 19)

Age	*p* values*; **WT vs HET vs HOMO**	*p* values** for multiple comparisons		
		WT vs HET	**WT vs HOMO**	**HET vs HOMO**
2 months	0.009	0.002	0.047	0.456
4 months	3.3×10^{-10}	0.003	1.03×10^{-7}	1.08×10^{-8}
6 months	1.2×10^{-10}	1.4×10^{-4}	9.4×10^{-8}	2.3×10^{-8}
8 months	9.1×10^{-10}	1.6×10^{-8}	1×10^{-7}	0.329

* From Kruskal-Wallis test; ** From Mann-Whitney *U* test; *Epha2*$^{+/+}$ (WT), *Epha2*$^{+/-}$ (HET), *Epha2*$^{-/-}$ (HOMO)

Table 4.3: Comparison of cataract development in *Epha2*$^{+/+}$, *Epha2*$^{+/-}$ and *Epha2*$^{-/-}$ mice over time; *Epha2*$^{+/+}$ (*n* = 18), *Epha2*$^{+/-}$ (*n* = 25) and *Epha2*$^{-/-}$ (*n* = 19)

Genotype	*p* values *; **2 vs 4 vs 6 vs 8 months**	*p* values ** for multiple comparisons		
		2 months vs 4 months	**4 months vs 6 months**	**6 months vs 8 months**
Epha2$^{+/+}$	0.006	N/A	0.002	0.2
Epha2$^{+/-}$	3.3×10^{-13}	N/A	2.5×10^{-4}	1.2×10^{-5}
Epha2$^{-/-}$	2.5×10^{-12}	1.2×10^{-4}	N/A	N/A

* From Friedman Test; ** From Wilcoxon Signed Ranks Test

As three comparisons were performed, an adjusted alpha (α) level of ≤0.016 (0.05/3) was used. Mice of all the three genotypes developed similar cataract grades by 2 months of age (Mean ACG in *Epha2*$^{+/+}$ mice = 1.26 ± 0.76; in *Epha2*$^{+/-}$ mice = 0.6 ± 0.57; and in *Epha2*$^{-/-}$ mice=0.97 ± 0.65). Therefore a statistically significant difference between the three genotypes observed by Kruskal-Wallis test and between *Epha2*$^{+/+}$ and *Epha2*$^{+/-}$ mice as determined by Mann-Whitney *U* test at 2 months of age may be due to observational variation.

By 4 months of age the *Epha2*$^{-/-}$ mice developed severe anterior cortical cataract with mean ACG of 4.8 ± 0.26 while both *Epha2*$^{+/+}$ and *Epha2*$^{+/-}$ mice presented with mild anterior cortical cataract with mean ACG of 1.3 ± 0.7 and 0.73 ± 0.56, respectively. Further, monitoring of these mice revealed that the *Epha2*$^{+/-}$ mice progressively developed anterior cortical cataract and presented with severe cataract by 8 months of age with mean ACG of 2.4 ± 1.5 at 6 months and 4.7 ± 0.43 at 8 months of age. The *Epha2*$^{+/+}$ mice still presented with mild cortical cataract with mean ACG of 0.5 ± 0.56 and 0.69 ± 0.6 respectively at 6 months and 8 months of age. A high standard deviation in the *Epha2*$^{+/-}$ mice at this age also demonstrates a large variation in grades of cataract observed at this age.

Next, the data was compared using Friedman test to analyse the change in cataract grade in each genotype over time. Table 4.3 lists the *p* values for each comparison. We found a significant effect of age in each genotype. Wilcoxon Signed Ranks test was performed to determine the difference between two successive ages. We found a statistically significant difference between cataract grades of *Epha2*$^{+/-}$ mice at 6 months of age as compared to their grades at 4 months and 8 months of age. As expected, the cataract grades of *Epha2*$^{-/-}$ mice at 2 months were significantly different from their cataract grades at 4 months of age.

A statistically significant difference observed in *Epha2*$^{+/+}$ mice with age may be due to observational bias in grading lower grades of cataract. The mean ACG in *Epha2*$^{+/+}$ mice at 4 months is higher than at 6 or 8 months of age; further supporting that the cataract observed in these mice is not age-related. As the data of *Epha2*$^{+/+}$ and *Epha2*$^{+/-}$ mice at 4 months was used at 2 months of age and of *Epha2*$^{-/-}$ mice at 4 months was used at 6 and 8 months of age, the comparison between these ages in the respective genotypes was not applicable. Overall, these results demonstrated that age of the mouse affects *Epha2* mediated cataract development and progression.

Similar results were obtained on performing this test using cataract grade of the severe eye. The results from this analysis are shown in Appendix 4.1and 4.2.

4.3.3 Effect of gender on cataract development and progression

The data from *Epha2*$^{+/+}$, *Epha2*$^{+/-}$ and *Epha2*$^{-/-}$ mice monitored for cataract progression were also used to determine gender-related differences in cataract progression. Figure 4.7 shows graphical representation of the mean ACG in the three genotypes. Either ACG or cataract grade in the severe eye was analysed using the test. The *p* values for each genotype are listed in Table 4.4, Table 4.5 and Table 4.6.

We found that both male (n = 9) and female (n = 9) *Epha2*$^{+/+}$ mice developed only mild anterior cortical cataract with ACG ranging from 0-2 until 8 months of age. There was no difference in cataract progression between *Epha2*$^{+/+}$ male and female mice. Unlike *Epha2*$^{+/+}$mice, analysis of ACG data of *Epha2*$^{+/-}$ mice (males; n = 13, females; n = 12)

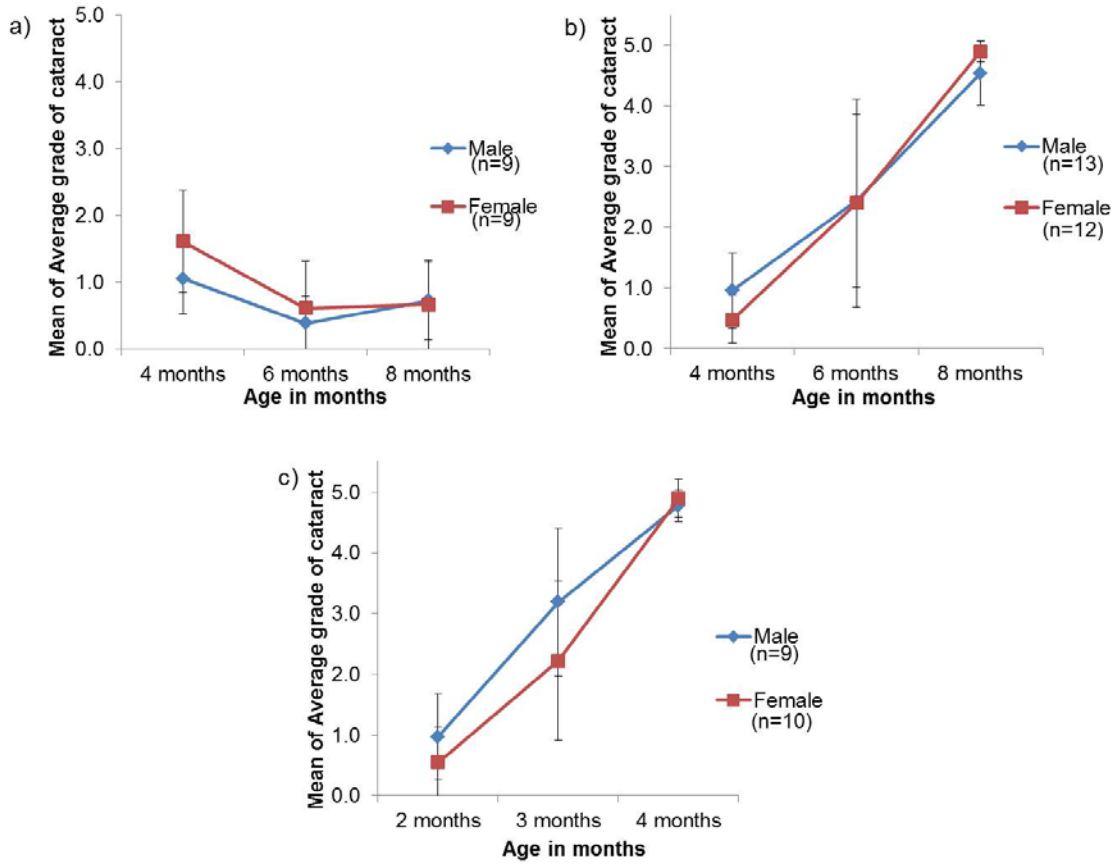

Figure 4.7: Comparison of progression of cataract between genders in *Epha2*$^{+/+}$, *Epha2*$^{+/-}$ and *Epha2*$^{-/-}$ mice.

Epha2$^{+/+}$ *and Epha2*$^{+/-}$ mice were monitored bimonthly for cataract progression from 4 to 8 months of age. *Epha2*$^{-/-}$ mice were monitored monthly from 2 to 4 months of age. The graphs show ACG in a) *Epha2*$^{+/+}$, b) *Epha2*$^{+/-}$ and c) *Epha2*$^{-/-}$ male and female mice at different ages. Mann-Whitney *U* test on the data at these ages showed no difference between the two genders in *Epha2*$^{+/+}$ and *Epha2*$^{-/-}$ mice at any age. A significant difference with a *p* value of 0.041 was observed between *Epha2*$^{+/-}$ males and females mice at 4 months of age. There was no difference between the two genders at 6 months and 8 months of age. Error bars represent standard deviation.

Table 4.4: Comparison of cataract development in *Epha2*$^{+/+}$ male and female mice. *p* values determined by Mann-Whitney *U* test are indicated; Males (*n* = 9) and Females (*n* = 9)

Data analysed	4 months	6 months	8 months
ACG	0.108	0.680	0.787
Cataract grade of severe eye	0.085	0.489	0.796

Table 4.5: Comparison of cataract development in *Epha2*$^{+/-}$ male and female mice. *p* values determined by Mann-Whitney *U* test are indicated; Males (*n* = 13) and Females (*n* = 12)

Data analysed	4 months	6 months	8 months
ACG	0.041	0.585	0.105
Cataract grade of severe eye	0.034	0.526	0.009

Table 4.6: Comparison of cataract development in *Epha2*$^{-/-}$ male and female mice. *p* values determined by Mann-Whitney *U* test are indicated; Males (*n* = 9) and Females (*n* = 10)

Data analysed	2 months	3 months	4 months
ACG	0.074	0.173	0.129
Cataract grade of severe eye	0.939	0.211	0.105

revealed a significant difference between the two genders at 4 months of age (Mean ACG in males = 0.96 ± 0.6 and in females = 0.47 ± 0.4) with a *p* value of 0.041. There was a lot of variation in the cataract grades in *Epha2*$^{+/-}$ mice at 6 months of age which was also evident from their standard deviations (1.4 and 1.7 in males and females, respectively). The females developed higher grades of cataract at 8 months of age (4.9 ± 0.17) as compared to the males (4.5 ± 0.5). However, there was no significant difference between the two genders at 6 months or 8 months of age. The results obtained by statistical analysis of cataract grade of the severe eye were slightly different and are shown in Figure 4.8. A significant difference between the two genders was noted in *Epha2*$^{+/-}$ mice both at 4 months ($p = 0.034$) and 8 months of age ($p = 0.009$).

The analysis on *Epha2*$^{-/-}$ mice (males; $n = 9$, females; $n = 10$) revealed no significant difference between the two genders at any age. However, similar to the trend in *Epha2*$^{+/-}$ mice, *Epha2*$^{-/-}$ female mice presented with lower grade of cataract compared to males at 2 months of age (Mean ACG in males = 0.97 ± 0.7 and in females = 0.5 ± 0.6) but developed higher grades of cataract by 4 months of age (Mean ACG in males = 4.7 ± 0.26 and in females = 4.9 ± 0.3).

Overall, these results indicate that there is a small effect of gender on cataract development and progression. This effect of gender was only observed in *Epha2*$^{+/-}$ mice indicating that lack of *Epha2* and gender together might have an effect on cataract development and progression.

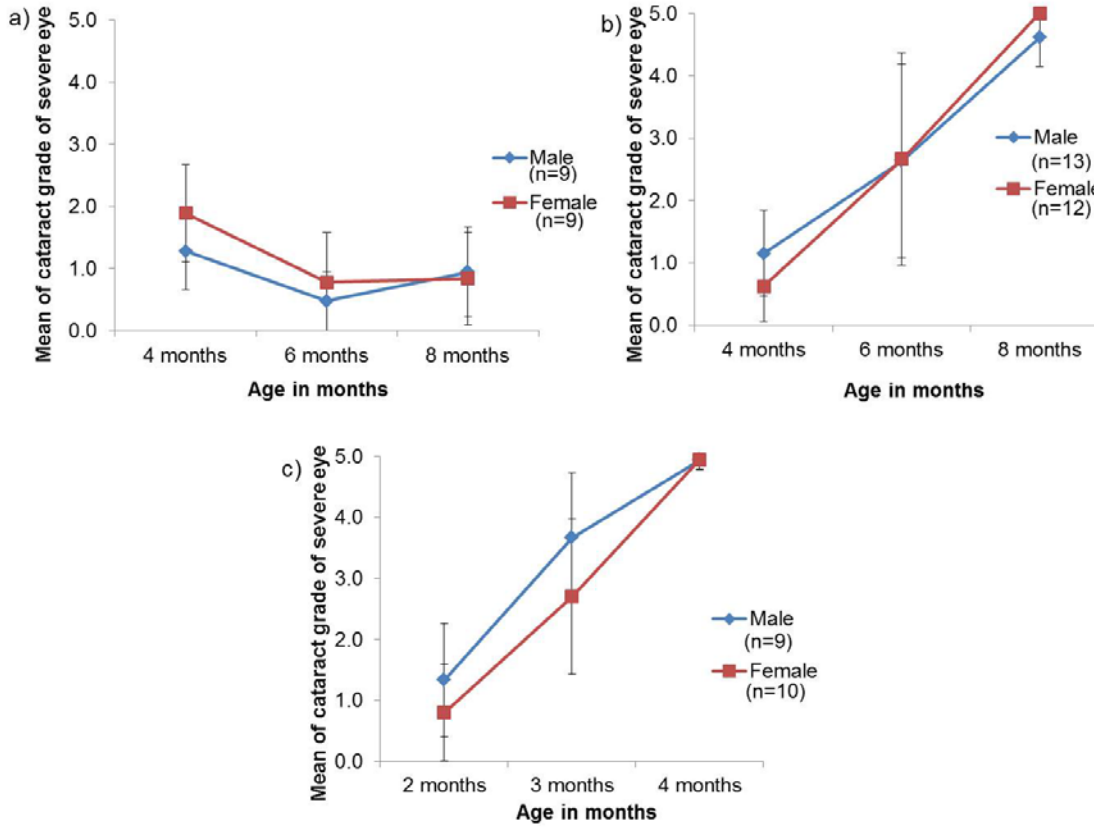

Figure 4.8: Comparison of progression of cataract in the severe eye between genders in *Epha2*$^{+/+}$, *Epha2*$^{+/-}$ and *Epha2*$^{-/-}$ mice

Epha2$^{+/+}$ *and Epha2*$^{+/-}$ mice were monitored bimonthly for cataract progression from 4 until 8 months of age. *Epha2*$^{-/-}$ mice were monitored monthly from 2 until 4 months of age. The graphs show mean cataract grade of severe eye in a) *Epha2*$^{+/+}$, b) *Epha2*$^{+/-}$ and c) *Epha2*$^{-/-}$ male and female mice at different ages. Mann-Whitney *U* test on the data at these ages showed no difference between the two genders in *Epha2*$^{+/+}$ and *Epha2*$^{-/-}$ mice. A significant difference with a *p* value of 0.034 and 0.009 was observed between *Epha2*$^{+/-}$ male and female mice at 4 and 8 months of age, respectively. There was no difference between the two genders in *Epha2*$^{+/-}$ mice at 6 months of age. Error bars represent standard deviation.

4.3.4 Analysis of *Epha2* knockout mouse lenses

To further understand the effect of loss of functional *Epha2* on lens architecture in the *Epha2* knockout mice, histological and immunofluorescence analysis was performed on lenses of mice of all the three *Epha2* genotypes. We observed only mild cataract in *Epha2*$^{+/+}$and *Epha2*$^{+/-}$ mice but severe cataract in *Epha2*$^{-/-}$ mice by 4 months of age and *Epha2*$^{+/-}$ mice developed severe cataract by 10 months of age. Therefore, *Epha2*$^{+/+}$, *Epha2*$^{+/-}$ and *Epha2*$^{-/-}$ mouse lenses were analysed at 4 months of age; lenses of *Epha2*$^{+/+}$ and *Epha2*$^{+/-}$ mice were also analysed at 10 months of age. Lenses of at least two mice of each genotype were analysed at each age.

4.3.4.1 Histological analysis

Figure 4.9 shows results of Haematoxylin and Eosin staining of lens sections from the three genotypes. On histological analysis of the lens, no obvious differences were observed in lenses of 4 months old *Epha2*$^{+/+}$ and *Epha2*$^{+/-}$ mice. These lenses showed normal morphology of lens epithelial and fiber cells. In contrast, the lenses of 4 months old *Epha2*$^{-/-}$ mice showed gross disorganisation of fiber cell arrangement and exhibited presence of vacuoles, observed as white spaces, in the lens epithelial cells. Similar to lenses of *Epha2*$^{-/-}$ mice, disorganisation of fiber cell packing was observed in the anterior cortex in lenses of 10 months old *Epha2*$^{+/-}$ mice; whereas lenses of 10 months old *Epha2*$^{+/+}$ mice exhibited normal lens epithelial and fiber cell morphology. These observations were consistent with increased severity of cataract in *Epha2*$^{+/-}$ and *Epha2*$^{-/-}$ mice at 10 months and 4 months of

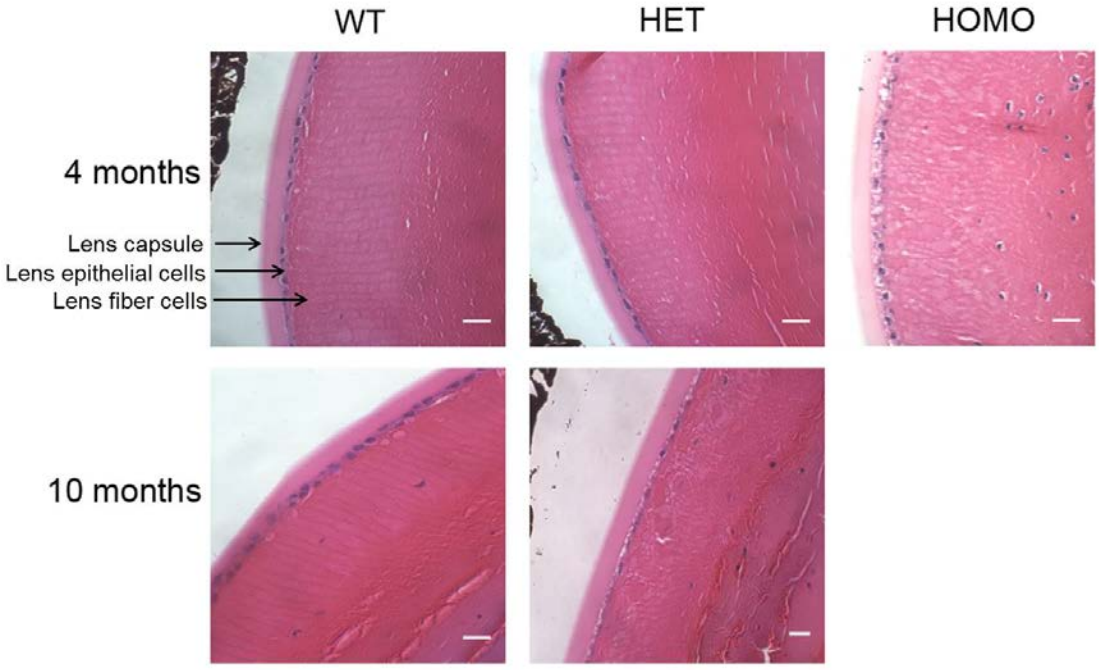

Figure 4.9: Histological analysis of *Epha2*$^{+/+}$, *Epha2*$^{+/-}$ and *Epha2*$^{-/-}$ lenses

Lens sections of 4 months old *Epha2*$^{+/+}$ (WT), *Epha2*$^{+/-}$ (HET) and *Epha2*$^{-/-}$ (HOMO) mice and 10 months old *Epha2*$^{+/+}$ and *Epha2*$^{+/-}$ mice were analysed by heamatoxylin and eosin staining. Representative images of lens sections from each genotype at 4 months and 10 months of age are shown in the figure. Blue heamatoxylin staining shows the nuclei and pink eosin staining shows the cytoplasm of lens epithelial and fiber cells. The lens capsule, lens epithelial cells and lens fiber cells are indicated by arrow in the lens section of 4 months old *Epha2*$^{+/+}$ mouse. Lenses of 4 months old *Epha2*$^{-/-}$ and 10 months old *Epha2*$^{+/-}$ mice illustrate disruption of fiber cell arrangement. Scale-bar 20 µm

age, respectively. The lenses of 4 months old *Epha2*$^{-/-}$ mice showed the presence of more nucleated fiber cells as compared to 4 months old *Epha2*$^{+/-}$ and *Epha2*$^{+/+}$ mouse lenses. As the sections used for this analysis were closer to the lens equator, the fiber cells in the region may still be undergoing enucleation. Histological analysis revealed disruption of lens architecture in cataractous lenses however, morphology of fiber cells could not be clearly defined. Therefore these lenses were further analysed by immunolabelling.

4.3.4.2 Immunofluorescence labelling

Immunofluorescence labelling in lenses from *Epha2*$^{+/+}$, *Epha2*$^{+/-}$ and *Epha2*$^{-/-}$ mice was performed to understand the effect of absence of full-length functional Epha2 on cellular junctions. N-cadherin is a cellular junction protein and β-catenin is a junction associated protein (315, 316). Localisation of both these proteins to the cell periphery is an indicator of integrity of cellular junction. Figure 4.10 illustrates results of labelling of N-cadherin in *Epha2*$^{+/+}$, *Epha2*$^{+/-}$ and *Epha2*$^{-/-}$ lenses. Lens sections labelled with mouse IgG instead of the primary antibody were used as negative controls (bottom right panel). N-cadherin was primarily expressed in the cell periphery in cortical fiber cells in 4 months and 10 months old lenses. Labelling in lenses of 4 months old *Epha2*$^{+/+}$and *Epha2*$^{+/-}$ mice showed arrangement of fiber cells in meridional rows (first and second image in the top row). However, in lenses of 4 months old *Epha2*$^{-/-}$ mice there was a distinct difference in the shape of fiber cells (third image in the top row). The newly formed cortical fiber cells were larger in size and were disorganized. The lenses of 10 months old *Epha2*$^{+/+}$ mice showed normal arrangement of fiber cells in meridional rows whereas cortical region in 10 months old *Epha2*$^{+/-}$ mouse lenses showed presence of enlarged and disarrayed fiber cells (first and

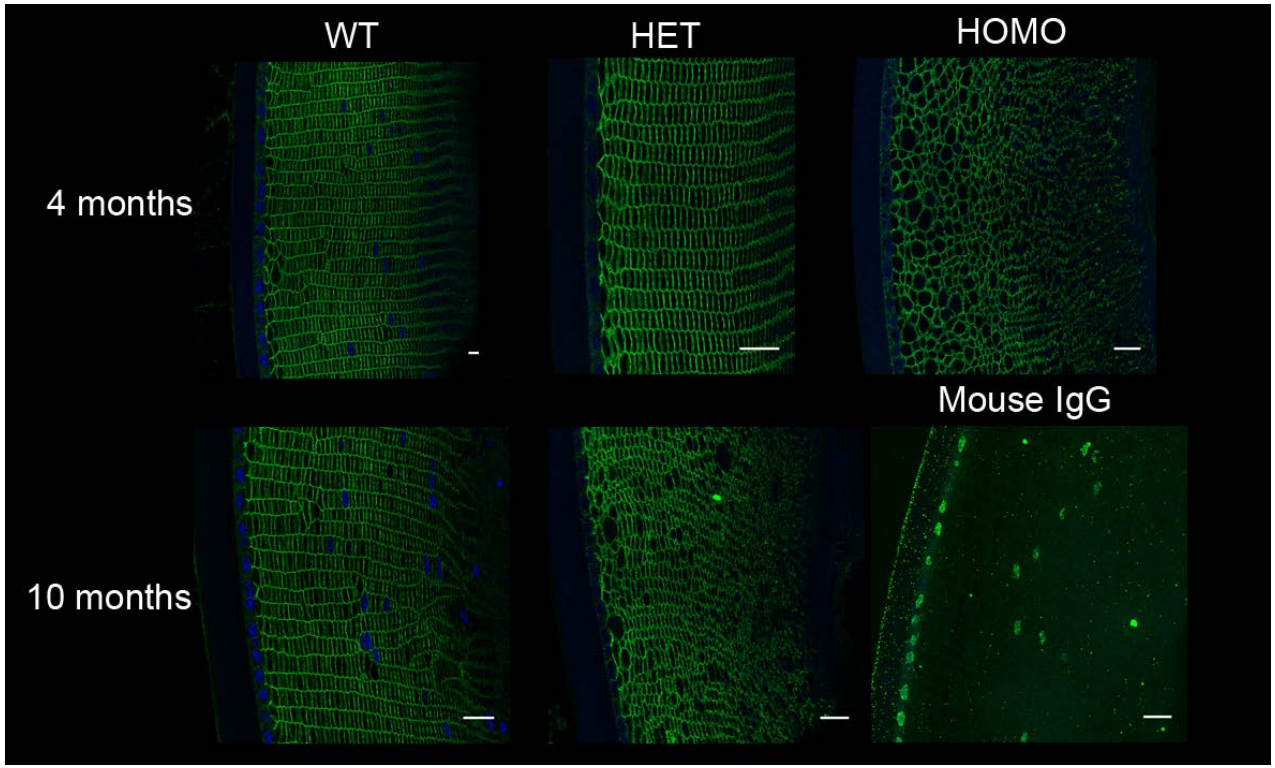

Figure 4.10: Immunofluorescence labelling of N-cadherin in lenses of *Epha2*$^{+/+}$, *Epha2*$^{+/-}$ and *Epha2*$^{-/-}$ mice

Lens sections of 4 months old *Epha2*$^{+/+}$ (WT), *Epha2*$^{+/-}$ (HET) and *Epha2*$^{-/-}$ (HOMO) and 10 months old *Epha2*$^{+/+}$and *Epha2*$^{+/-}$ were labelled with a mouse anti-N-cadherin antibody. Sections probed with mouse IgG were used as negative control. Representative images of lens section from each genotype at 4 months or 10 months are shown in the figure. N-cadherin labelling delineates the cell periphery showing presence of bigger and disorganized fiber cells at 4 months in *Epha2*$^{-/-}$ and at 10 months in *Epha2*$^{+/-}$ lenses. The lenses of *Epha2*$^{+/+}$ mice at both the ages and *Epha2*$^{+/-}$ mice at 4 months show presence of well packed fiber cells arranged in meridional rows. Green is N-cadherin hybridised to secondary antibody conjugated with Alexa Flour 488 and blue is DAPI stained nuclei. Scale-bar 20µm

second image bottom panel). The areas of disorganized fiber cells were similar to those observed in *Epha2*$^{-/-}$ lenses. Overall, there was distinct difference in lens architecture between lenses of 10 months old *Epha2*$^{+/-}$ and 4 months old *Epha2*$^{-/-}$ mice compared to the lenses of *Epha2*$^{+/+}$ mice at both the ages. β-catenin labelling also revealed similar results as shown in Figure 4.11. These results suggest that loss of functional Epha2 affects cellular morphology and fiber cell arrangement with age and hence contributes to cataract development.

4.3.5 Epha2 expression analysis in mutant lenses

Next, Epha2 localisation was analysed in lenses of *Epha2*$^{+/+}$, *Epha2*$^{+/-}$ and *Epha2*$^{-/-}$ mice. Figure 4.12 shows labelling of Epha2 in lenses of 4 months old *Epha2*$^{+/+}$, *Epha2*$^{+/-}$ and *Epha2*$^{-/-}$ mice (top row) and 10 months old lenses of *Epha2*$^{+/+}$ and *Epha2*$^{+/-}$ mice (bottom row). Epha2 was present in lens epithelial cells in lenses of *Epha2*$^{+/+}$ mice at both the ages. Similar to the localisation of N-cadherin and β-catenin, Epha2 was also observed in the cell periphery of fiber cells in lenses of 4 months and 10 months old *Epha2*$^{+/+}$ mice (first image in the top and bottom row). This localisation was consistent with previous reports (191, 212) and further emphasizes an important role of Epha2 in the lens cell junctions. However, in lenses of 4 and 10 months old *Epha2*$^{+/-}$ mice, besides its presence in cell periphery, Epha2 protein was also present as inclusions in lens epithelial and fiber cells (second image in the top and bottom row). Similar inclusions were also observed in lenses of 4 months old *Epha2*$^{-/-}$ mice (third image in the top row). Lens sections labelled with only goat IgG instead of the primary antibody were used as negative control (bottom right image). We suspected that these inclusions were due to the partial Epha2 fusion protein

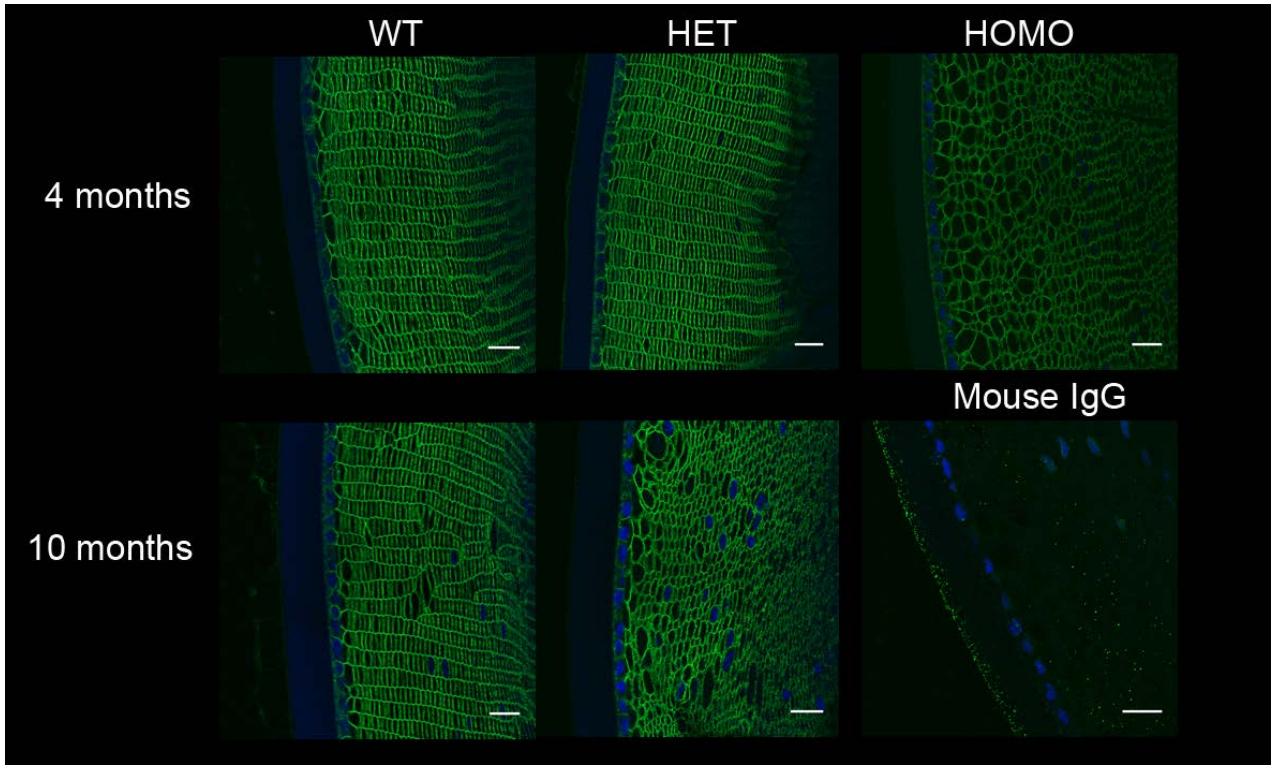

Figure 4.11: Immunofluorescence labelling of β-catenin in lenses of *Epha2*$^{+/+}$, *Epha2*$^{+/-}$ and *Epha2*$^{-/-}$ mice

Lens sections from 4 months old *Epha2*$^{+/+}$ (WT), *Epha2*$^{+/-}$ (HET) and *Epha2*$^{-/-}$ (HOMO) and 10 months old *Epha2*$^{+/+}$and *Epha2*$^{+/-}$ were labelled with mouse anti-β-catenin antibody. Lens sections probed with mouse IgG were used as negative control. The figure shows representative images of lens section from each genotype at both the ages. Similar to N-cadherin, β-catenin labelling also shows lack of fiber cell arrangement in 4 months old *Epha2*$^{-/-}$ and 10 months old *Epha2*$^{+/-}$ lenses. Lens sections of *Epha2*$^{+/+}$ mice at both the ages and of 4 months old *Epha2*$^{+/-}$ mice show normal fiber cell shape and arrangement. Green is β -catenin hybridised to Alexa Flour 488 conjugated secondary antibody and blue is DAPI stained nuclei. Scale-bar 20μm

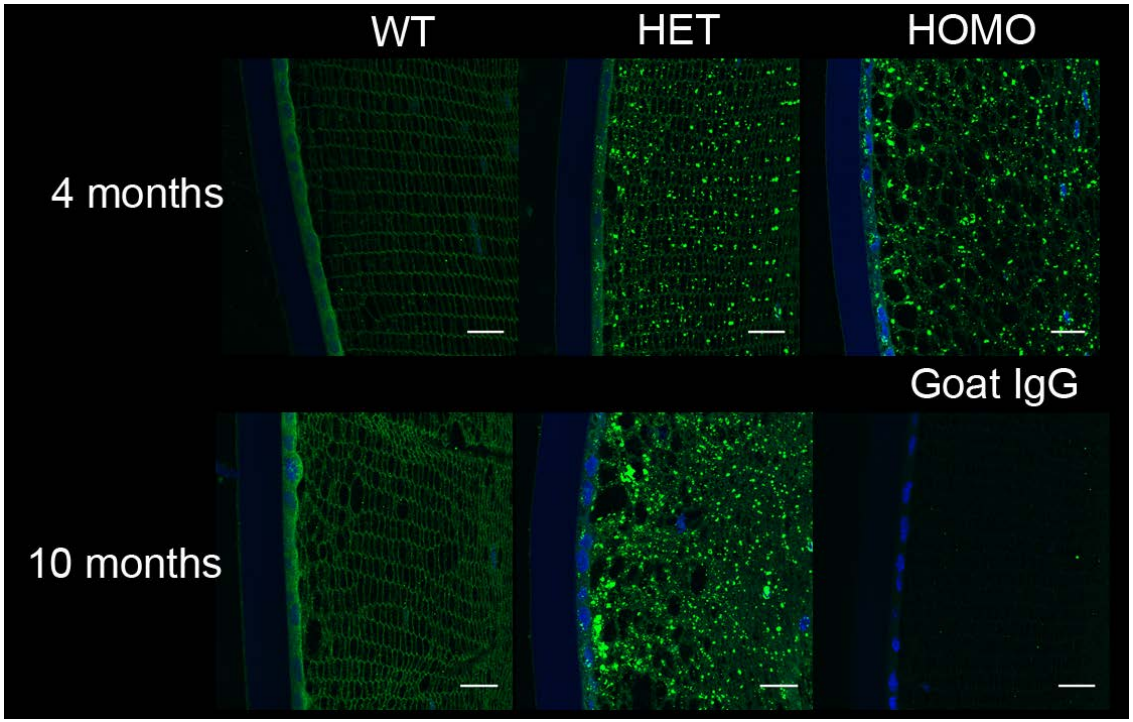

Figure 4.12: Immunofluorescence labelling of Epha2 in lenses of *Epha2*$^{+/+}$, *Epha2*$^{+/-}$ and *Epha2*$^{-/-}$ mice

Lens sections of 4 months old *Epha2*$^{+/+}$ (WT), *Epha2*$^{+/-}$ (HET) and *Epha2*$^{-/-}$ (HOMO) and 10 months old *Epha2*$^{+/+}$and *Epha2*$^{+/-}$ were labelled with anti-mEpha2 antibody. Sections hybridised with the goat IgG were used as negative control. Representative images of lens section from each genotype at each age are illustrated in the figure. The lenses of 4 months and 10 months old *Epha2*$^{+/+}$ mice show presence of Epha2 in lens epithelial cells and in the periphery of fiber cells. Lenses of 4 months old *Epha2*$^{+/-}$ mice exhibit presence of the Epha2 in both lens epithelial and lens fiber cells. These lenses also show presence of inclusions in the lens cells. Similar inclusions were observed in 4 months old *Epha2*$^{-/-}$ and 10 months old *Epha2*$^{+/-}$ mice. These inclusions may be the partial Epha2 fusion protein. Green is Epha2 detected using Alexa Flour 488 conjugated secondary antibody and blue is DAPI stained nuclei. Scale-bar 20µm

produced as a result of the knockout. To further investigate this, the lenses were also labelled for β-galactosidase reporter protein and Figure 4.13 illustrates the results of this labelling. This labelling also exhibited the presence of similar inclusions in lens epithelial and fiber cells in lenses of 4 months and 10 months old *Epha2*$^{+/-}$ mice (second image in the top and bottom row) and 4 months old *Epha2*$^{-/-}$ mice (third image in the top row). Lenses of *Epha2*$^{+/+}$ mice were not expected to have any β-galactosidase reporter protein. The labelling in *Epha2*$^{+/+}$ mouse lenses (first image in the top and bottom row) was comparable to the lenses hybridized with rabbit IgG used as controls (fourth image in the top and bottom row) and hence was considered background labelling.

To further confirm the presence of the partial Epha2 fusion protein, we examined its expression in lenses from *Epha2* knockout mice by western blotting. Lenses from three mice of each genotype at 2 months of age were used for the analysis; as the results from progression study, described in section 4.3.2.2, revealed that there was no phenotypic difference between the three genotypes at this age.

Results of the analysis are presented in Figure 4.14. On hybridization with the anti-mEpha2 antibody (Figure 4.14a) we found a faint protein band around 130 kDa in size in lenses of *Epha2*$^{+/+}$and *Epha2*$^{+/-}$ mice which was consistent with the size of the full-length Epha2 protein. Epha2 expression reduces with age in lens (191) and a faint band corresponding to the full-length protein was detected in a previous report. A protein band around 200 kDa, indicated by arrow, was differentially expressed with highest expression in lenses of *Epha2*$^{-/-}$ mice, intermediate in *Epha2*$^{+/-}$ mice and completely absent in *Epha2*$^{+/+}$ mice. This protein band perhaps corresponded to the partial Epha2 fusion protein seen as inclusions in Epha2 knockout lenses. The partial Epha2 fusion protein consists of a part of the Epha2

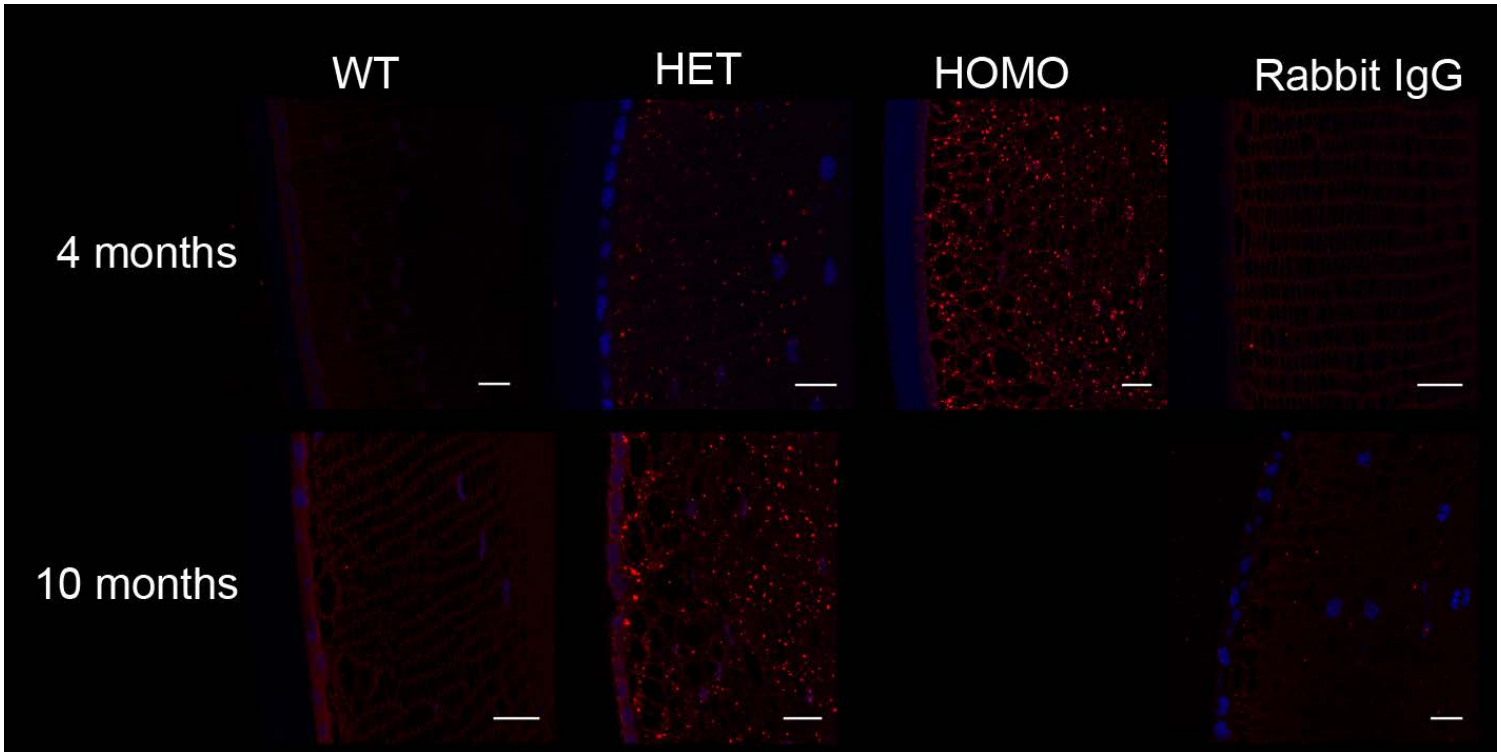

Figure 4.13: Immunofluorescence labelling of β-galactosidase in lenses of *Epha2*$^{+/+}$, *Epha2*$^{+/-}$ and *Epha2*$^{-/-}$ mice.

Lens sections of 4 months old *Epha2*$^{+/+}$ (WT), *Epha2*$^{+/-}$ (HET) and *Epha2*$^{-/-}$ (HOMO) and 10 months old *Epha2*$^{+/+}$and *Epha2*$^{+/-}$ were labelled with anti-β-galactosidase antibody. Sections probed with rabbit IgG were used as controls. Representative images of lens section from each genotype at 4 months or 10 months are illustrated in the figure. The labelling in *Epha2*$^{+/+}$ mice were comparable to the negative controls. Lenses of 4 months old *Epha2*$^{-/-}$ and *Epha2*$^{+/-}$ mice and 10 months old *Epha2*$^{+/-}$ mice demonstrate presence of inclusions which may be the Epha2 fusion protein. Red is beta-galactosidase detected using Alexa Flour 594 conjugated secondary antibody and blue is DAPI stained nuclei. Scale-bar 20 µm

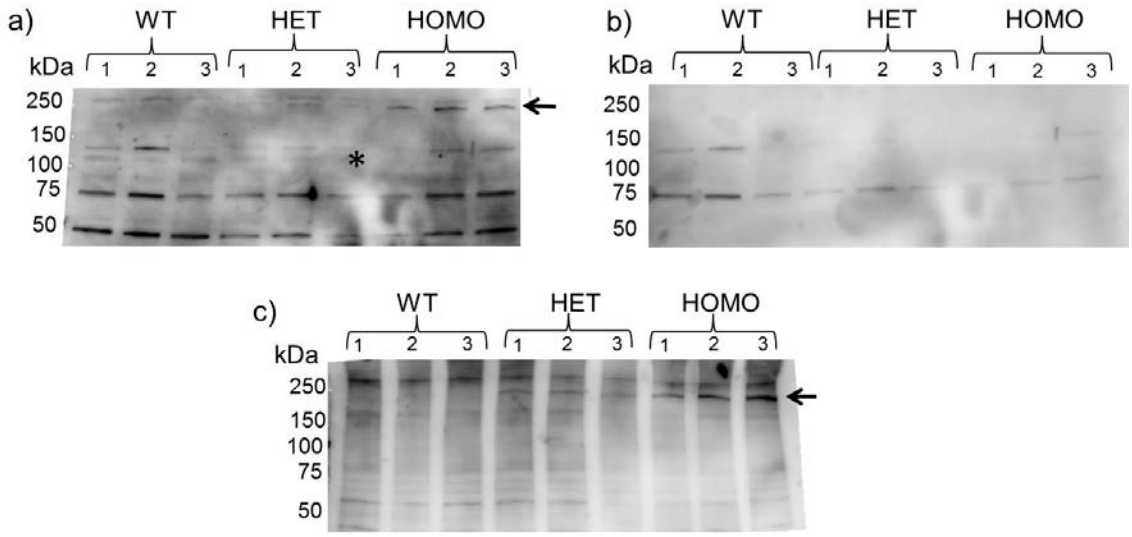

Figure 4.14: Epha2 expression analysis in lenses of *Epha2*$^{+/+}$, *Epha2*$^{+/-}$ and *Epha2*$^{-/-}$ mice

Lens homogenates of three 2 months old *Epha2*$^{+/+}$ (WT), *Epha2*$^{+/-}$ (HET) and *Epha2*$^{-/-}$ (HOMO) mice were analysed for Epha2 and fusion protein expression. Forty micrograms of lens protein was size separated by SDS-PAGE and hybridized with a) goat anti-mEpha2 primary and anti-goat biotin and SA-HRP secondary antibody; b) anti-goat biotin and SA-HRP; c) rabbit anti β-galactosidase primary and anti-rabbit HRP secondary antibody. Arrow in panel a) illustrates the partial Epha2 fusion protein around 200 kDa in size in HOMO and HET lenses. The partial Epha2 fusion protein migrated slower than its expected size of 163 kDa. The WT and HET mouse lenses show presence of the full-length Epha2 protein 130 kDa in size marked by an asterisk. A non-specific band ~ 50 kDa due to hybridisation with the primary antibody was also observed. The other bands observed on the blot were due to non-specific hybridisation of the secondary antibody and are also observed in panel b. Panel b) shows the non-specific bands of < 150 kDa and ~ 75 kDa due to hybridisation with the secondary antibody. Panel c) depicts the fusion protein, marked by an arrow, in lens proteins from *Epha2*$^{+/-}$ and *Epha2*$^{-/-}$ mice. This protein band is likely to be the same band as detected by the anti-mEpha2 antibody in panel a). 1, 2 and 3 indicate the three mice of each genotypes used for expression analysis. The molecular weight standards are as marked. kDa is kilo dalton.

ectodomain fused to the β-galactosidase reporter protein. This fusion protein was expected to be around 163 kDa in size but possibly migrated slower than its expected size perhaps due to post-translational modifications. A non-specific band of around 50 kDa due to the primary antibody was present in all the samples. In addition, we also observed non-specific bands due to the secondary antibody illustrated in the Figure 4.14b). Hybridization with the anti-β-galactosidase antibody also revealed the presence of protein band corresponding to the fusion protein at around 200 kDa. These results suggest that both anti-mEpha2 and anti-β-galactosidase antibody detected the presence of the same fusion protein band.

4.4 Discussion

The involvement of *EPHA2* in cataract development in both human and mouse provides evidence for a crucial role of Epha2 signalling in the lens. In the present study we used an *Epha2* knockout mice strain, B6;129P2-Epha2$^{Gt(KST085)By}$ (KST085) to investigate if environmental modifiers such as age and gender influence Epha2 signalling in the lens and affect cataract development and progression. These mice have been previously shown to have increased susceptibility to skin cancers (317) and increased *Epha2* expression in the kidney in *Epha2*$^{+/-}$ mice following renal ischemia-reperfusion injury (318). The KST085 strain used in the present study had been generated on a B6; 129P mixed background. As mentioned previously, the 129 strain carry a cataract causing splice site mutation in the *Bfsp2* gene (312, 313). The mice used in our study developed cataract much sooner than previously reported (191). Therefore *Bfsp2* genotyping was performed to know if mutation in *Bfsp2* was the underlying cause of the early-onset of cataract. The results showed that all mice bred for obtaining experimental animals were wild-type for *Bfsp2* and did not carry

the mutation. Additionally an examination of mice soon after administration of the anesthetic drugs also ensured that the cataract phenotype was not anesthetic induced (319). Hence the phenotype of the KST085 mice in the present study was contributed to by their *Epha2* genotype.

Upon monitoring cataract progression in *Epha2*$^{+/+}$, *Epha2*$^{+/-}$ and *Epha2*$^{-/-}$ mice, we observed a significant effect of age and *Epha2* genotype on cataract. We found that *Epha2*$^{-/-}$ and *Epha2*$^{+/-}$ mice developed progressive anterior cortical cataract presenting with severe cataract by 4 months and 8 months of age, respectively. This was further supported by histological and immunofluorescence analysis of cataractous lenses from *Epha2*$^{-/-}$ and *Epha2*$^{+/-}$ mice which revealed altered shape, size and packing of fiber cells. Similar disorganisation of cells along with disruption of meridional rows and lens fulcrum was previously reported in the *GFP+Epha2*$^{-/-}$ mice at postnatal day 21 (Strain: C57BL/6; 129S6-Epha2^{tm1Jrui} developed by vector insertion in exon 5 of *Epha2*) (213, 214). However, another study using *Epha2*$^{-/-}$ mice of the same strain but without GFP incorporated in the genome, reported that the mice did not develop cataract till 10 months of age but presented with abnormal lens suture formation due to altered cell migration (212). *Epha2* plays an important role in cell migration during development (320). Congenital cataract causing mutations in *EPHA2* affect phosphorylation of Akt, a downstream effector molecule in c-src signalling pathway, which is involved in cell migration (215, 321, 322). Consistently, lenses from homozygous knockout mice were previously reported to have reduced amounts of phosphorylated c-Src and cytoskeletal proteins such as cortactin and actin, important for cell motility (214). Overall, findings in *Epha2* knockout lenses from the present and previously reported studies suggest that lack of *Epha2* in the lens may lead to

dysregulation of lens cell migration, disrupting lens architecture and hence contribute to cataract development.

Further, on Epha2 expression analysis in the lenses from *Epha2* knockout mice, we found presence of the partial Epha2 fusion protein. The fusion protein migrated slower than its expected size. Similar slower migration of high molecular weight proteins has been previously reported (323). Immunolabelling analysis showed presence of the fusion protein in lens epithelial and fiber cells. The fusion protein was expected to be in the cytoplasm of the cells (308). However, it was difficult to determine if the protein was present in the plasma membrane or the cytoplasm in these cells. The accumulation of this protein over time may be contributing to the severity of phenotype and differences in rate of cataract progression between *Epha2*$^{+/-}$ and *Epha2*$^{-/-}$ mice.

A previous study reported that in the same KST085 strain on FVB/NJ background, the *Epha2*$^{+/-}$ mice did not develop cataract until 14 months of age while the *Epha2*$^{-/-}$ mice progressively developed cortical cataract from 5 months of age (191). In the present study, the KST085 *Epha2*$^{+/-}$ and *Epha2*$^{-/-}$ mice on C57BL/6J background developed severe anterior cortical cataract by 8 months and 4 months of age, respectively. This difference in rate of cataract progression between the KST085 mice used in the two studies may be due to the difference in genetic background of the mice used in these studies.

Similar background and/or underlying mutation related differences in phenotype have been also observed in *Ephrin-A5*$^{-/-}$ mice. Ephrin-A5 is a ligand for Epha2 (225). *Ephrin-A5*$^{-/-}$ mice on FVB/NJ background developed nuclear cataract (221) while *GFP+ Ephrin-A5*$^{-/-}$ mice on C57BL/6J background present with an anterior polar opacity in their lenses (213).

The site of *GFP* integration in the genome in these mice is also not known (213). Loss of the ligand, Ephrin-A5, leads to epithelial-mesenchymal transformation of cells with an aberrant cell growth in the anterior polar region (213). Additionally, analysis of postnatal lenses of *Ephrin-A5*$^{-/-}$ mice on FVB/NJ background revealed presence of disordered fiber cells but no effect on lens epithelial cells (324). On the other hand, *GFP+ Ephrin-A5*$^{-/-}$ mice on C57BL/6J background have normal lens fiber cells but show disrupted lens epithelial cell layer homeostasis (213). These mice also show disruption of E-cadherin and β-catenin based junctions in the lens epithelial cells (213).

Difference in phenotype in *Epha2*$^{-/-}$ mouse strains have also been found in previous reports depending on the mutation in *Epha2* resulting in the knockout (191, 212-214). As mentioned earlier, a *Epha2*$^{-/-}$ mice on C57BL/6J background (Strain: C57BL/6; 129S6-Epha2^{tm1Jrui}) have transparent lenses up to 12 months of age but present with small lenses and reduced lens refraction compared to their wild-type counterparts (212). Interestingly, *GFP* positive (*GFP+*) *Epha2*$^{-/-}$ mice of the same strain on C57BL/6J background develop nuclear cataract (213). However, the genomic position of *GFP* integration or the age of cataract development in these mice was not reported.

The *GFP+* transgenic mice, which were intercrossed with the *Epha2* and *Ephrin-A5* knockout mice to generate their *GFP+* counterparts, were not examined for presence of cataract (325). However unlikely, but differences in phenotypes in both *GFP+ Epha2*$^{-/-}$ and *GFP+ Ephrin-A5*$^{-/-}$ mice as compared to their *GFP* negative counterparts, may be attributed to insertion of an additional *GFP* gene in the mouse genome. The analysis of *Epha2* and *Ephrin-A5* knockout lenses suggests that the Eph-Ephrin signalling is crucial

for lens fiber cell organization and architecture of the lens which is important for maintaining lens transparency.

Next, we wanted to understand if gender had an effect on rate of cataract progression in each *Epha2* genotype. Interestingly, we noted different results depending on how the data were analysed. Utilising ACG facilitated equal representation of cataract grades in both the eyes and the analysis revealed a marginally significant effect of gender in *Epha2*$^{+/-}$ mice. Analysis of the cataract grade of the severe eye may perhaps be more biologically relevant as it defined the severity of the disease. This analysis in *Epha2*$^{+/-}$ mice again revealed a significant effect of gender both at 4 months and 8 months of age. Although marginally significant, differences in cataract progression between genders was only observed in *Epha2*$^{+/-}$ mice suggesting that *Epha2* genotype of the mice might have a role to play in this difference. Slower progression of cataract in the *Epha2*$^{+/-}$ mice as compared to *Epha2*$^{-/-}$ mice also helped demonstrate a small gender-related difference in cataract progression. Increasing the number of *Epha2*$^{-/-}$ mice monitored for cataract progression and a more regular examination will help determine gender-related difference in these mice. Similarly, more frequent examination of *Epha2*$^{+/-}$ mice might reduce the variation observed in this group.

A small effect of gender on cataract progression is consistent to what is observed in humans (117, 145-147). Estrogen receptors are expressed in human and mouse lens epithelium (326, 327) suggesting that the hormone has a function in the lens. In breast cancer cell lines overexpression of estrogen leads to repression of Epha2 (270, 328). However, the effect of estrogen in an aging lens is not known. Difference in levels of estrogen between the two genders is the most apparent explanation. Reduced estrogen in

post-postmenopausal years renders females more susceptible to various diseases including cataract (329-331). However, the *Epha2*$^{+/-}$ mice demonstrating these differences may be pre- or close to menopausal age. Perhaps, a synergistic effect of both lack of Epha2 and changes in estrogen levels could modulate the progression of cataract. Further investigation of the downstream effector molecules of both Epha2 and estrogen might reveal their role in cataract development.

4.5 Conclusion

Overall, results from this study clearly demonstrate a dosage effect of *Epha2* on cataract progression. This study shows a distinct effect of age and a small effect of gender on *Epha2* mediated cataract. In addition, accumulation of the fusion protein in the knockout lenses might contribute to the severity of cataract phenotype. Consistent with previous reports, we found that loss of functional Epha2 disrupts lens architecture affecting cataract development.

5. Effect of ultraviolet light on *Epha2* mediated age-related cataract

5.1.Introduction

Exposure to ultraviolet (UV) radiation has been established as a risk factor for development of age-related cataract (ARC) (117, 118, 125). UV radiation reaching the earth comprises of UV-A (400-315 nm), UV-B (315-280 nm) and UV-C (280-100 nm). Out of these three, only UV-A and UV-B penetrate through the atmosphere and reach the earth. In the eye, the cornea absorbs all UV radiation below 295 nm and radiation up to 400 nm is absorbed by the lens (332). With thinning of the ozone layer, atmospheric protection from UV radiation is being lost, causing more UV radiation to reach the earth (333). This in turn leads to increased daily exposure, especially in populations living at higher altitudes or involved in outdoor occupations, which increases susceptibility to UV-induced cataract (334, 335). Exposure to UV-B specifically is associated with an increased risk of development of cortical cataract in humans (115, 125). However, it is difficult to estimate the minimum UV-B exposure sufficient to cause cataract mostly due to the difficulty in quantifying the regular UV-B exposure for an individual. Therefore studies in animal models have been employed for investigating the doses of UV radiation sufficient to cause cataract and possible mechanisms of damage to the crystalline lens (196, 198, 336, 337).

The amount of UV radiation transmitted to the lens is different in animal models than in humans due to the differences in corneal thickness and general anatomy of the eye between species (338). Nevertheless, similar to humans, UV-B is found to be more cataractogenic than UV-A in animal models (339).

Various studies in animal models have demonstrated damage in the ocular lens due to UV-B light exposure (332, 336). Unlike UV-A exposed lenses, bovine lenses exposed to repeated low-dose UV-B demonstrate altered light transmittance (340). Similarly, albino mice exposed to a chronic dose of UV-B developed posterior cataract while UV-A exposure was weakly cataractogenic (195). Additionally, increasing doses of UV-B lead to an exponential increase in the forward scattering of light by exposed rat lenses (341). Age-dependent modulation in sensitivity to UV-induced cataract has been also reported in rats (342). Apoptosis or necrosis is thought to be the main cause of UV radiation mediated damage in rodent lenses (198, 343). Oxidative stress, metabolic imbalance and post-translational modification of lens proteins are some of the known effects of UV exposure on rodent lens that eventually contribute to cataract development (197). Alterations in the human lens in response to UV exposure still need to be determined. However, a vast majority of the studies in rodents have demonstrated damage to the lens caused by a single above-threshold dose of UV-B (198, 199, 344, 345); threshold dose is the minimum dose adequate to cause cataract. Only a few studies have investigated effects of repeated below-threshold doses of UV-B exposure on the lens (346), which is comparable to the UV exposure in humans.

In addition to environmental modifiers such as UV-B exposure, the development of ARC in humans is also influenced by genetic factors. As described in Chapter 4, genetic variation in the *EPHA2* gene is associated with age-related cataract in humans (65, 68, 191). Epha2 is important for UV-induced apoptosis and is up-regulated upon UV exposure in cultured cells (269). However, whether or not UV exposure of the lens leads to an

increased risk of *Epha2* mediated cataract development is unknown. In the present study this association was explored in the *Epha2* knockout mice.

Results in Chapter 4 describe effect of age and gender on cataract development in *Epha2* knockout mouse. The present study examined susceptibility of *Epha2* knockout mice on C57BL/6J background to cataract development on exposure to multiple below-threshold doses of UV-B. We found that the severity of cataract was associated with the dose of UV-B administered but was unaffected by the *Epha2* genotype of the mouse.

5.2.Materials and Methods

5.2.1. Animals

Ethics approval for the project was obtained from the Animal Welfare Committee, Flinders University, Adelaide. *Epha2*$^{+/+}$ and *Epha2*$^{+/-}$ mice from the B6;129P2-Epha2$^{Gt(KST085)Byg}$ (KST085) strain were used for this study. Animal breeding, maintenance and genotyping were performed as described in Chapter 4, sections 4.2.1- 4.2.5.

5.2.2. UV-B treatment of mice

A UV-B exposure station designed and built by the Department of Biomedical Engineering, Flinders Medical Centre, Adelaide, Australia, was used for this study. The exposure station comprised of a trolley with two shelves (Figure 5.1a). Two 20 W UV-B broadband (290-315 nm) fluorescent lamps (Philips TL 20 W/12 RS SLV) mounted below

the top shelf of the trolley were used as a source of UV-B. The dose of UV-B exposure was monitored using a UVX digital Radiometer attached to the UVX series sensor (UVP Inc, CA, USA; Figure 5.1b). The output recorded by the radiometer was logged using the 0 to 2.5 V Tiny Talk data logger (Gemini data Loggers Ltd, West Sussex, U.K.) and was used to determine the treatment duration. The recording from the logger, with a maximum reading of 2 V, was used to determine the output UV-B radiation from the lamps. A timer was used to control exposure times and hence the final dose of UV-B administered. For example, if the recording from the data logger was 0.0027 V with the radiometer set to record a maximum of 20 mW/cm^2; the treatment duration for a final dose of 0.05 J/cm^2 was calculated as follows:

A reading of 2 V in the data logger is equivalent to 20 mW/cm^2

Therefore, 1 V = 10 mW/cm^2

0.0027 V = 0.027 mW/cm^2 or 0.027×10^{-3} J/cm^2 per second

So, a UV-B dose of 0.027×10^{-3} J/cm^2 is administered in 1 second

Therefore a dose of 0.05 J/cm^2 will be administered in:

$(0.05 \times 1)/ (0.027 \times 10^{-3})$ = 1851.8 seconds = 30 minutes 52 seconds

A polycarbonate animal holder with a capacity to hold twelve mice in separate slots was used to expose mice to UV-B (Figure 5.1c). A mesh was placed on top of the animal holder, with minimum UV-B attenuation, to restrain the mice in the slots. The same mesh was also placed on top of the UVX sensor, to ensure accurate estimation of the UV-B dose administered.

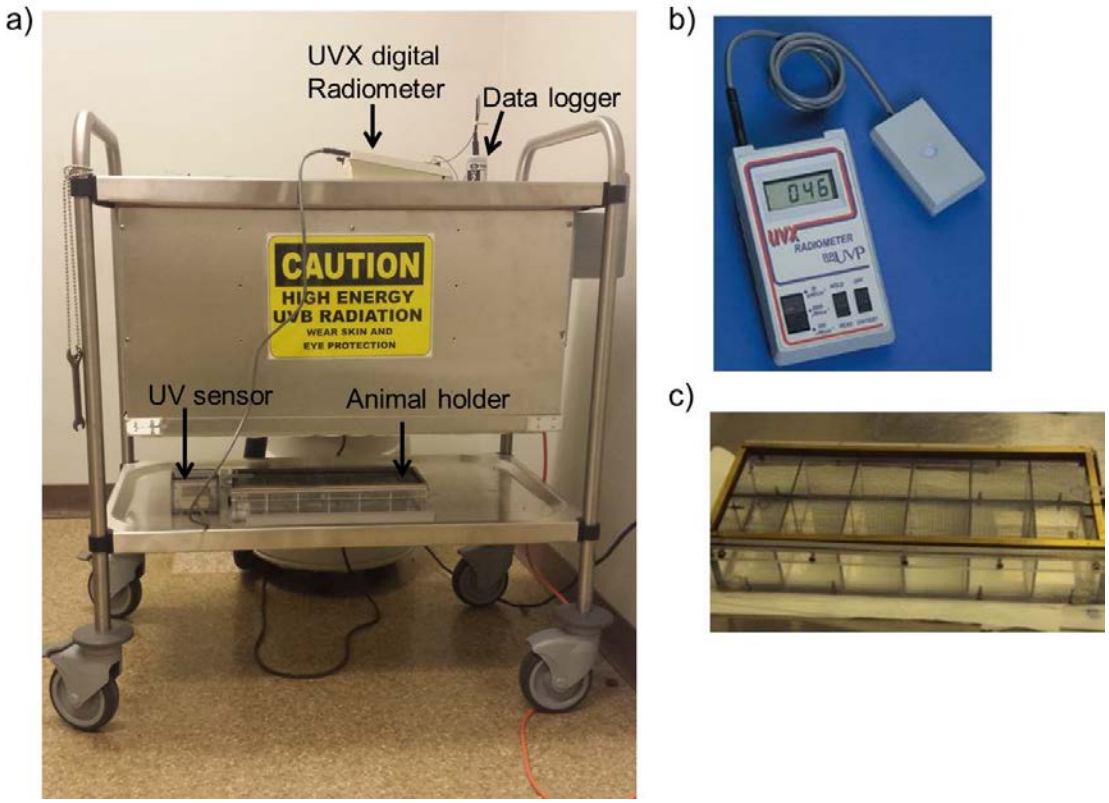

Figure 5.1: Set-up used for UV-B treatment of mice

The figure illustrates a) UV-B exposure station with the UVX radiometer, data logger, UVX sensor and the animal holder indicated by arrows; b) UVX radiometer and sensor used to record UV-B dose of each treatment; c) Animal holders used to restrain mice for the duration of UV-B treatment. Each mouse was held in a separate slot and a metal mesh on the top was used to restrain the mice.

The Maximum Tolerable dose or $MTD_{2.3:16}$, which determines the threshold dose of UV-B for avoidance of cataract, is 2.9 kJ/m^2 for C57BL/6J mice (347, 348); UV-B doses lower than this $MTD_{2.3:16}$ were used for the present study. Three weeks old *Epha2*$^{+/+}$ mice were treated with UV-B dose of 0.1 J/cm^2, every alternate day, three times a week for two weeks. With the exception of this treatment regimen, all the subsequent treatments were performed after installation of a 0.25 mm thick PTFE (Teflon) layer to cover the UV-B lamps. This teflon layer attenuated 48% of the total power of the UV-B radiation.

Five week old, *Epha2*$^{+/+}$ and *Epha2*$^{+/-}$ mice were exposed to 0.05 J/cm^2, 0.025 J/cm^2 or 0.0125 J/cm^2 dose of UV-B seven times, every third or fourth day. The UV-B treated mice were monitored weekly for their well-being and observations were recorded on a clinical record sheet.

5.2.3. Slit-lamp examinations

Clinical cataract grading in untreated and UV-B treated mice were conducted 24-48 hours after the last treatment that is at 9 weeks of age. This was followed by a subsequent examination at 13-16 weeks of age. As the UV-B dose of 0.1 J/cm^2 was administered to 3 week old mice, their after treatment and follow-up examinations were conducted at 6 weeks and then at 10-12 weeks of age, respectively.

For examinations, mice were anesthetized and revived after examination as described in Chapter 4, section 4.2.6. Anterior polar and cortical cataracts were graded separately in all the treated and untreated mice. Cortical cataract was clinically graded as described in Chapter 4, section 4.2.6. Due to unavailability of a standard clinical grading system for

anterior polar cataract, we developed a grading system based on the size of the anterior polar opacity as a measure of cataract severity. Depending on the severity, anterior polar cataract was assigned a grade between 0-3, with 0 representing no anterior polar cataract and 3 indicating severe anterior polar cataract. Figure 5.2 illustrates examples of each of the grades of anterior polar cataract. The lenses were graded by an observer blinded to the UV-B treatment doses and genotypes of mice. Cataract was either clinically examined or graded through photographs. The observations were recorded by digital photography as described in Chapter 4, section 4.2.6.

5.2.4. Histological analysis

After their last examination, the UV-B treated and untreated mice were euthanized by isofluorane inhalation. Whole eyes were enucleated and fixed in 10% NBF as described in Chapter 4 section 4.2.7. The eyes were paraffin embedded, sectioned and used for histological analysis as described in sections 4.2.8 and 4.2.9.

The slides were imaged using 20× objectives on an Olympus Brightfield BX50 Upright microscope equipped with QImaging RTV 5 megapixel Digital Camera (QImaging, BC, Canada) and QCapture software (QImaging, BC, Canada) for capturing images.

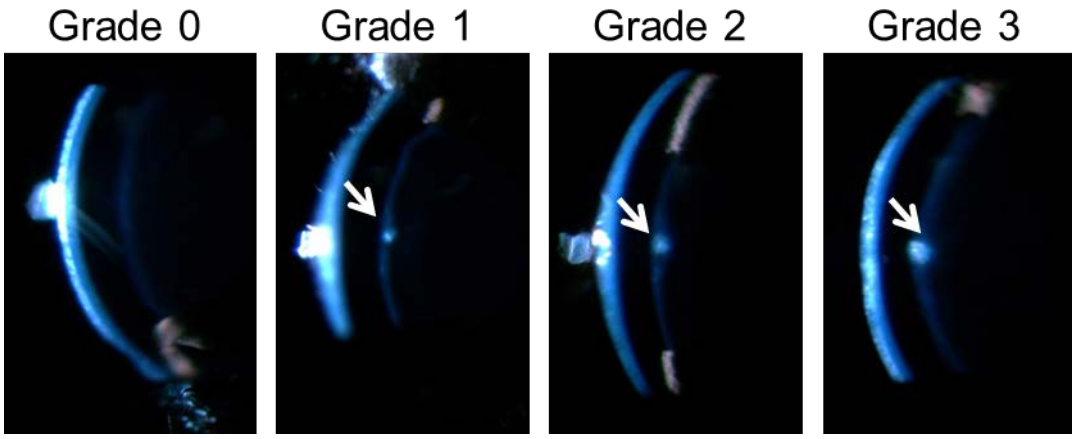

Figure 5.2: Grading system for anterior polar cataract

The figure shows representative images of cross-section illumination of the lens. Each image shows a cross-section of the cornea (bright arc) on the anterior side, followed by the anterior chamber (dark region) and then the lens. Anterior polar cataract in the lens is indicated by arrows. The cataract grade assigned to each image is indicated above the image. This grading system was used to grade anterior polar cataract in UV-B treated mice.

5.2.5. Statistical analysis

All statistical analysis was performed using IBM Statistical Package for the Social Science (SPSS) Statistics 19. The average anterior cortical and anterior polar cataract grade of both the eyes was used for analysis. The normality of distribution was estimated by Shapiro-Wilk statistical test. As the data was not normally distributed, non-parametric tests were used for all the comparisons.

The effect of different UV-B doses on cataract development in *Epha2*$^{+/+}$ and *Epha2*$^{+/-}$ mice was analysed using the Kruskal-Wallis statistical test, with individual comparisons performed using Mann-Whitney *U* test. The difference in cataract development within a group (for example *Epha2*$^{+/+}$ mice treated with UV-B dose of 0.05 J/cm^2) at the two time points was analysed using Wilcoxon Signed Ranks test. The difference between cataract development in UV-B treated *Epha2*$^{+/+}$ and *Epha2*$^{+/-}$ mice was analysed using Mann-Whitney *U* test at each time-point.

5.3. Results

We examined the effect of UV-B exposure on *Epha2* mediated cataract using the *Epha2* knockout mouse as a model. Three or five weeks old mice received repeated whole body exposure of different doses of UV-B. The repeated below-threshold exposures were administered to reproduce a regular repeated exposure in humans.

The results described in Chapter 4, section 4.3.2.2 reveal an age-dependent progression in anterior cortical cataract in *Epha2*$^{-/-}$ and *Epha2*$^{+/-}$ mice, with development of severe cataract by 4 months and 8 months of age, respectively. The slower progression to severe cataract in *Epha2*$^{+/-}$ mice, as compared to the *Epha2*$^{-/-}$ mice, made it easier to eliminate the effect of age on cataract and evaluate only the effect of UV-B exposure on cataract progression. Therefore we investigated susceptibility to UV-B induced cataract only in *Epha2*$^{+/-}$ mice; *Epha2*$^{+/+}$ mice were used as controls.

Three week old *Epha2*$^{+/+}$ (n = 6) mice received UV-B dose of 0.1 J/cm^2 seven times, twice a week every 3-4 days. Severe epithelial erosion as observed on examination of these mice at 24-48 hours after completion of their treatment. As a result it was not possible to grade their lenses for cataract. The data from these mice were not included in the analysis. Thereafter, to attenuate the radiation intensity a teflon sheet was used and older (five week old) mice were used for UV-B treatments. UV-B doses lower than 0.1 J/cm^2 were administered to examine the effect on ocular lens.

The *Epha2*$^{+/+}$ and *Epha2*$^{+/-}$ mice were treated thrice a week every alternate day seven times. Cataract was graded in lenses of all UV-B exposed mice at 24-48 hours after the last exposure, followed by an examination at least a month after their last exposure. To avoid gender bias equal numbers of male and female mice were used in each treatment group, except in the group of *Epha2*$^{+/+}$ mice treated with the UV-B dose of 0.025 J/cm^2 (6 males and 2 females). However, as there was no difference between genders in *Epha2*$^{+/+}$ mice, it is unlikely that the skewness towards males in this treatment group would have affected the results.

5.3.1. Effect of different doses of UV-B on cataract development

Mice were exposed to one of the three different doses of UV-B - 0.05 J/cm^2, 0.025 J/cm^2 and 0.0125 J/cm^2. At least 8 mice of each genotype were included in each treatment group. These mice developed either anterior polar or mild anterior cortical cataract. Figure 5.3 and Figure 5.4 illustrate the effect of UV-B dose on anterior polar and cortical cataract respectively at 9 weeks and 13-16 weeks of age. Figure 5.4 also depicts the mild epithelial erosion in the cornea in the UV-B treated mice. The exposure to different doses of UV-B resulted in differences in cataract development. *Epha2*$^{+/+}$ and *Epha2*$^{+/-}$ mice exposed to the UV-B dose of 0.05 J/cm^2 developed anterior polar cataract with mild anterior cortical cataract. Similarly, mice exposed to 0.025 J/cm^2 dose developed either anterior polar with mild anterior cortical cataract or only mild anterior cortical cataract. However, *Epha2*$^{+/+}$ and *Epha2*$^{+/-}$ mice exposed to the lowest dose of 0.0125 J/cm^2 developed only mild anterior cortical cataract apart from one *Epha2*$^{+/+}$ mice that developed grade 1-2 anterior polar cataract. The cornea of mice exposed to both the 0.05 J/cm^2 and 0.025 J/cm^2 doses showed slight punctate epithelial erosion 24-48 hours after the last exposure but this did not interfere with their cataract grading. Moreover, the cornea of treated mice healed by their follow-up eye examination. Eyes exposed to UV-B dose of 0.0125 J/cm^2 did not develop any corneal abnormality.

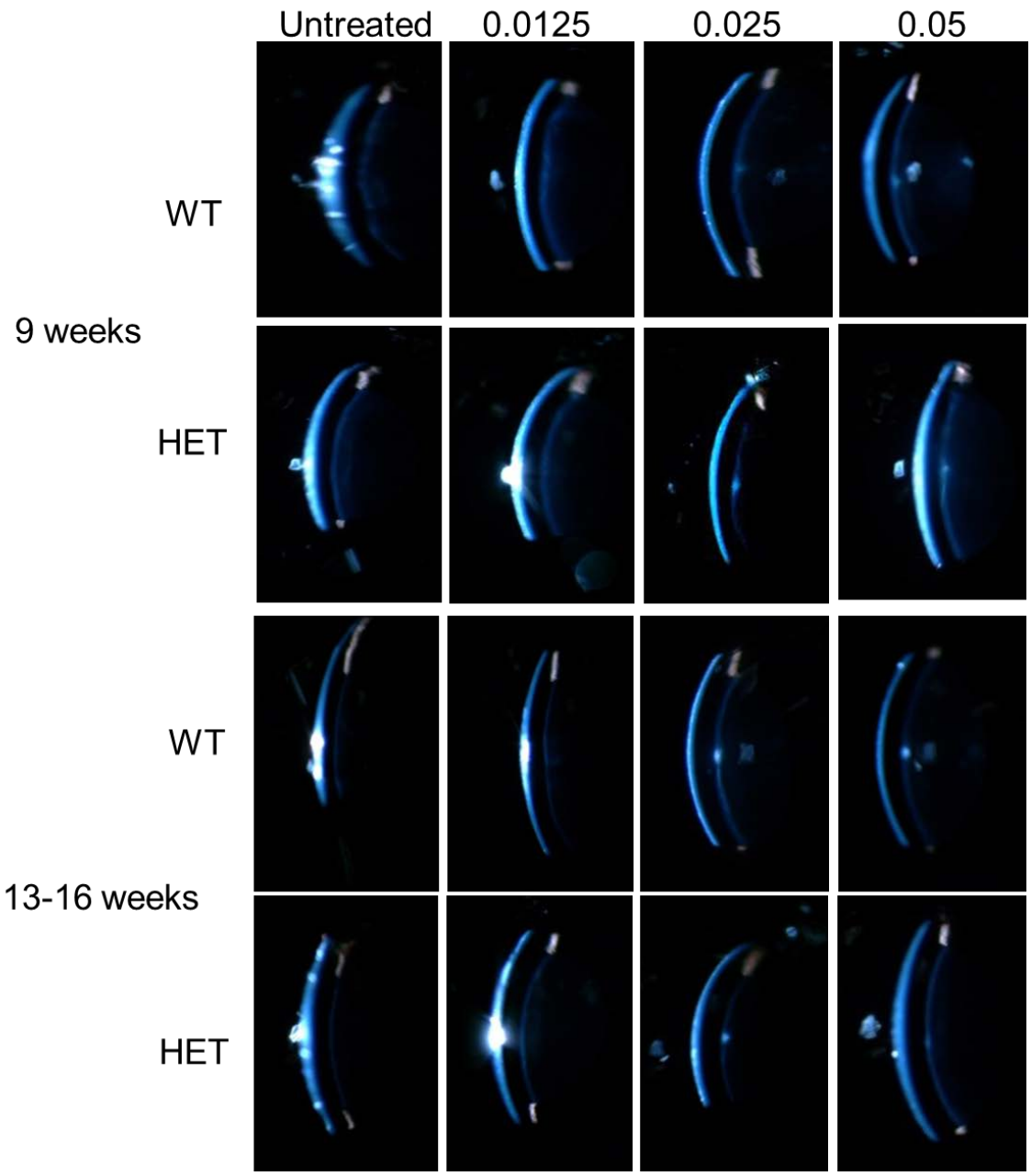

Figure 5.3: Anterior polar cataract in UV-B treated *Epha2*$^{+/+}$ and *Epha2*$^{+/-}$ mice

Representative images of anterior polar cataract in untreated and UV-B treated *Epha2*$^{+/+}$ (WT) and *Epha2*$^{+/-}$ (HET) mice are shown. The UV-B dose administered is indicated on the top of each column. Anterior polar cataract was observed both at 9 weeks and 13-16 weeks of age in *Epha2*$^{+/+}$ mice (shown in the first and third row) and *Epha2*$^{+/-}$ mice (shown in the second and fourth row). Most of the untreated mice and ones treated with the UV-B dose of 0.0125 J/cm^2 did not develop anterior polar cataract. Mice of both the genotypes exposed to UV-B dose of 0.05 J/cm^2 or 0.025 J/cm^2 developed anterior polar cataract.

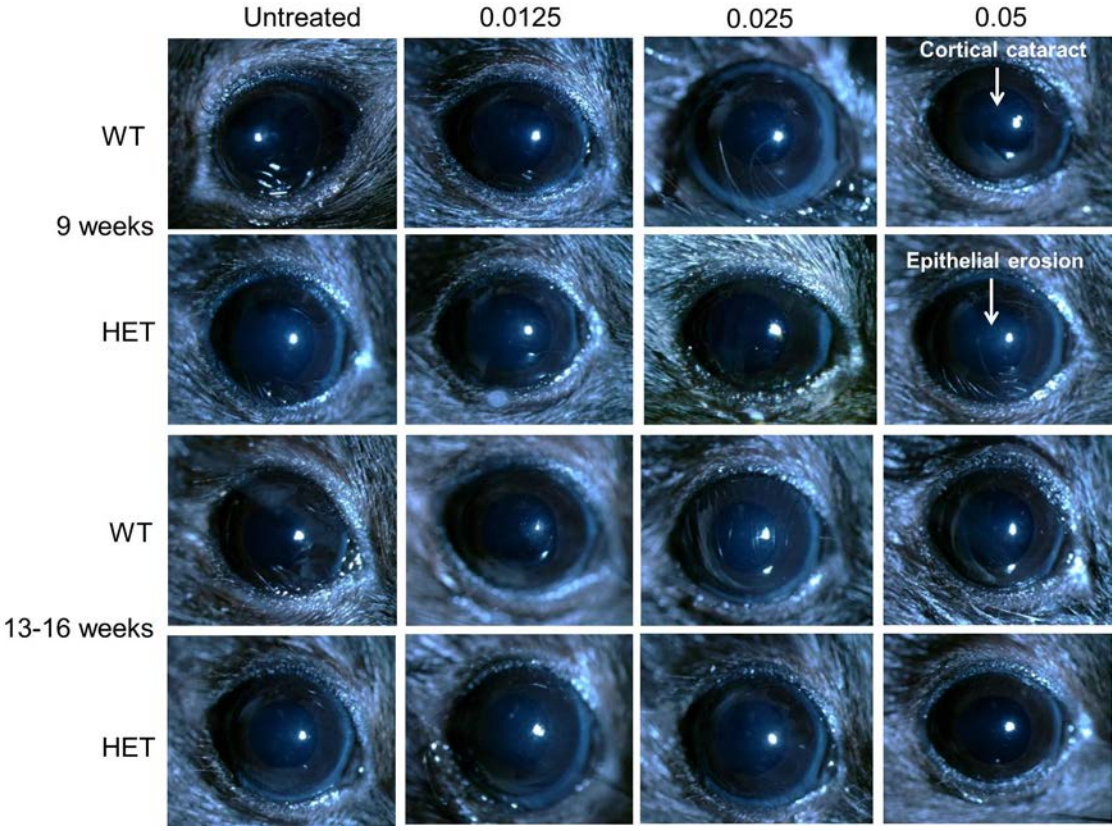

Figure 5.4: Anterior cortical cataract in UV-B treated *Epha2*$^{+/+}$ and *Epha2*$^{+/-}$ mice

Representative images of anterior cortical cataract developed in untreated and UV-B treated *Epha2*$^{+/+}$ (WT) and *Epha2*$^{+/-}$ (HET) mice. All the treated and untreated mice developed mild anterior cortical cataract, which may be anaesthetic induced. There was no difference in grades of anterior cortical cataract between the untreated and UV-B treated mice. Mice treated with UV-B dose of 0.05 J/cm^2 and 0.025 J/cm^2 showed mild corneal epithelial erosion at their first examination. The cornea healed and was normal by the follow-up examination.

The average anterior cortical cataract grade in each mouse and the mean of average grade of anterior cortical cataract in both *Epha2*$^{+/+}$ and *Epha2*$^{+/-}$ mice are listed in Table 5.1. Figure 5.5 graphically illustrate the spread of grades of anterior cortical cataract developed in the UV-B treated and untreated groups of mice of both the genotypes. On comparison of anterior cortical cataract grades by Kruskal-Wallis statistical test no significant difference was observed between the treated and untreated *Epha2*$^{+/+}$ (p = 0.693 at 9 weeks and 0.902 at 13-16 weeks of age) and *Epha2*$^{+/-}$ (p = 1 at 9 weeks and 0.681 at 13-16 weeks of age) mice. This suggests that cortical cataract in these mice was not altered by the UV-B treatment and was perhaps anesthetic induced. Hence this data was not analysed to compare cataract grades between the two time-points or between genotypes.

The average anterior polar cataract grades of each mouse and the mean of average grade of anterior polar cataract are listed in Table 5.2. The observed variation in sensitivity to UV-B within groups indicated by the high standard deviations has been reported in previous studies (349). Additionally, the treatment doses ranged from 0.0112-0.0137 J/cm^2 for an expected dose of 0.0125 J/cm^2; 0.022-0.0268 J/cm^2 for 0.025 J/cm^2 and 0.045-0.055 J/cm^2 for 0.05 J/cm^2. This variability in the administered doses may account for the variation observed in cataract grades. Figure 5.6 depicts the spread of grades of anterior polar cataract. Upon analysis by Kruskal-Wallis statistical test we found a significant difference between different treatment groups in *Epha2*$^{+/+}$ mice at 9 weeks (p = 0.026) and 13-16 weeks of age (p = 0.001). Further, multiple comparisons for comparing untreated mice with each of the three groups of UV-B treated mice, Mann-Whitney U test was performed. An adjusted α level of ≤0.016 (0.05/3) was set for the difference to be statistically significant.

Table 5.1: Average grade of anterior cortical cataract in untreated and UV-B treated mice

Genotype	Dose of UV-B	Number of mice	Average cortical cataract grade of each mouse at 9 weeks	Mean ±SD at 9 weeks	Average cortical cataract grade of each mouse at 13-16 weeks	Mean ±SD at 13-16 weeks
Epha2 $^{+/+}$	0	9	1.5, 2, 1.5, 1, 2, 2, 1.5, 2.5, 1.5	1.7 ± 0.4	2, 1, 1.25, 2.25, 2, 2, 1.5, 2, 1.5	1.7±0.4
	0.0125	8	1, 2, 1.5, 0.5, 1.5, 2, 1.5, 2	1.6 ± 0.64	2, 1.25, 2.25, 1.75, 2, 2, 2.25, 1.5	1.8 ± 0.35
	0.025	8	2.25, 2.5, 2, 2, 1.5, 2.25, 1.5, 1.25	1.9 ± 0.4	2, 2, 2.25, 2, 2.25, 0, 1.25, 2	1.7 ± 0.76
	0.05	8	2, 2, 2, 2, 2, 2, 1.75, 1.5	1.7 ± 0.4	2, 2, 1.5, 1.5, 2.5, 2.25, 1.5, 1	1.7 ± 0.5
Epha2 $^{+/-}$	0	8	2, 1.5, 2.5, 1.25, 2.25, 1.5, 2, 2	1.8 ± 0.4	0.75, 1.5, 1, 2.25, 1.25, 2.5, 1.75, 1.5	1.5 ± 0.6
	0.0125	8	1.5, 1.75, 1.75, 2, 2.25, 2, 2, 2	1.9 ± 0.23	2, 1.5, 2, 2.25, 1.75, 1.5, 1.5, 1.25	1.7 ± 0.34
	0.025	8	2, 2, 1, 1.75, 2, 2, 2, 2	1.8 ± 0.35	1.75, 1.75, 1.5, 1.75, 2, 1.5, 1.5, 1	1.5 ± 0.3
	0.05	8	2, 1.5, 2, 2, 1.75, 1.5, 2.5, 2	1.9 ± 0.32	2, 2, 1.5, 1.5, 1.5, 1.75, 2, 2	1.7 ± 0.24

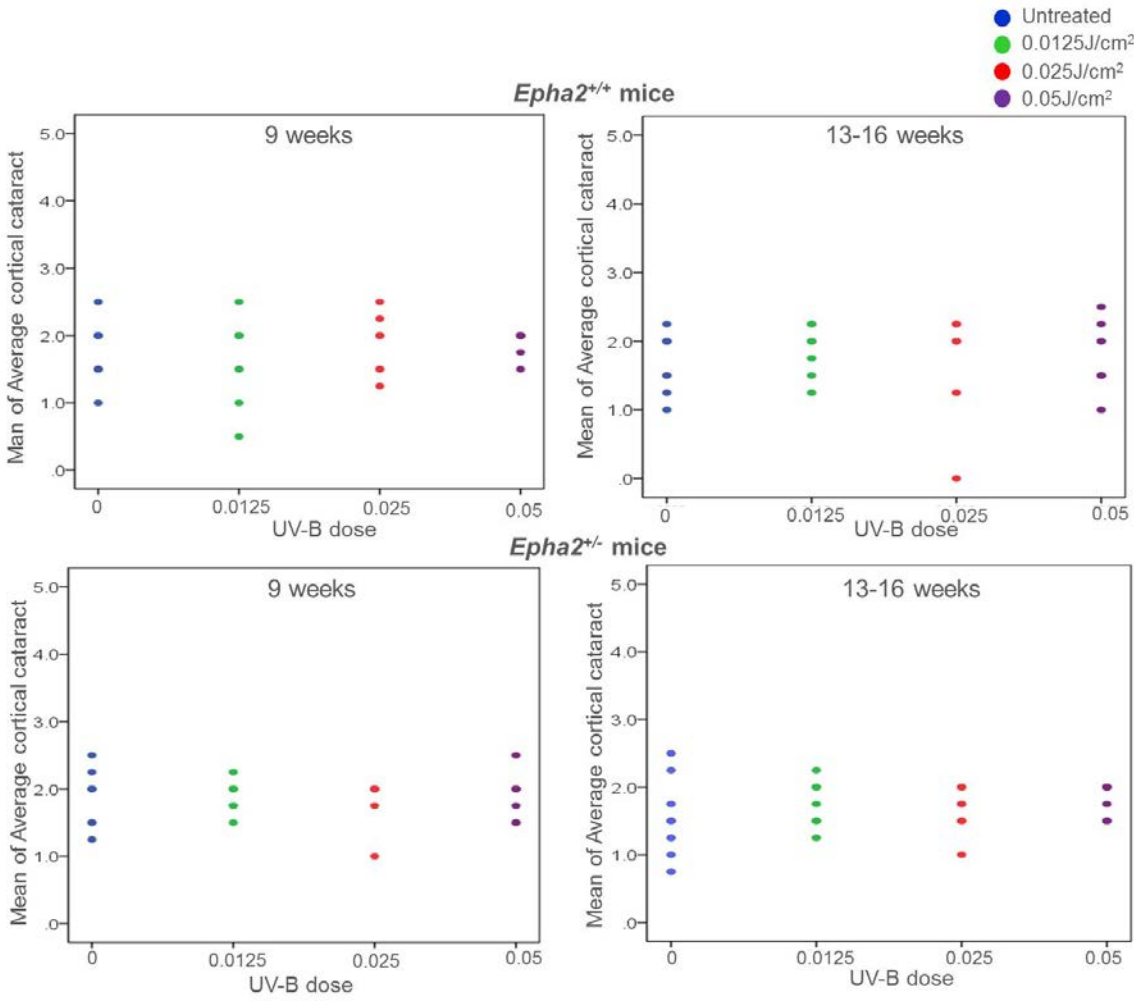

Figure 5.5: Distribution of anterior cortical cataract grades in untreated and UV-B exposed *Epha2*$^{+/+}$ and *Epha2*$^{+/-}$ mice

Scatter plots show the distribution of grades of anterior cortical cataract in untreated and UV-B treated *Epha2*$^{+/+}$ and *Epha2*$^{+/-}$ mice. The untreated and UV-B treated *Epha2*$^{+/+}$ (top row) and *Epha2*$^{+/-}$ (bottom row) mice developed mild anterior cortical cataract. The mice developed comparable grades of cortical cataract at both, 9 (top left and bottom left panel) weeks and 13-16 weeks (top right and bottom right panel) of age. Some points on the graphs also represent cataract grades of multiple animals.

Table 5.2: Average anterior polar cataract grade in untreated and UV-B treated mice

Genotype	Dose of UV-B	Number of mice	Average anterior polar cataract grade of each mouse at 9 weeks	Mean ±SD at 9 weeks	Average anterior polar cataract grade of each mouse at 13-16 weeks	Mean ±SD at 13-16 weeks
Epha2 $^{+/+}$	0	9	0	0	0	0
	0.0125	8	0,0,0,0,1,0,0,0	0.1 ± 0.35	0,0,0,0,2,0,0,0	0.25 ± 0.7
	0.025	8	0.75, 1.75, 2, 0, 0, 0, 0, 0	0.5 ± 0.8	1.5, 2.5, 2.25, 0.25, 0,0,0,0	0.8 ± 1.1
	0.05	8	0,0,2.5, 2.5, 0, 0.5, 0.5, 1.25	0.9 ± 1.1	2.5, 2, 2, 2, 0, 2, 1.75, 2	1.7 ± 0.7
Epha2 $^{+/-}$	0	8	0	0	0,0,0,0,0,1,0,0	0.1 ± 0.35
	0.0125	8	0	0	0	0
	0.025	8	0, 0.75, 1.5, 1.5, 0.75, 1, 0, 0	0.68 ± 0.63	0,0.5, 0.75, 1.25, 1.75, 0,0,0	0.5 ± 0.67
	0.05	8	0.75, 1.25, 1, 2, 1.75, 1.25, 2, 2	1.5 ± 0.5	1.5, 1.5, 1.75, 2, 1.75, 2, 1.25, 0	1.5 ± 0.6

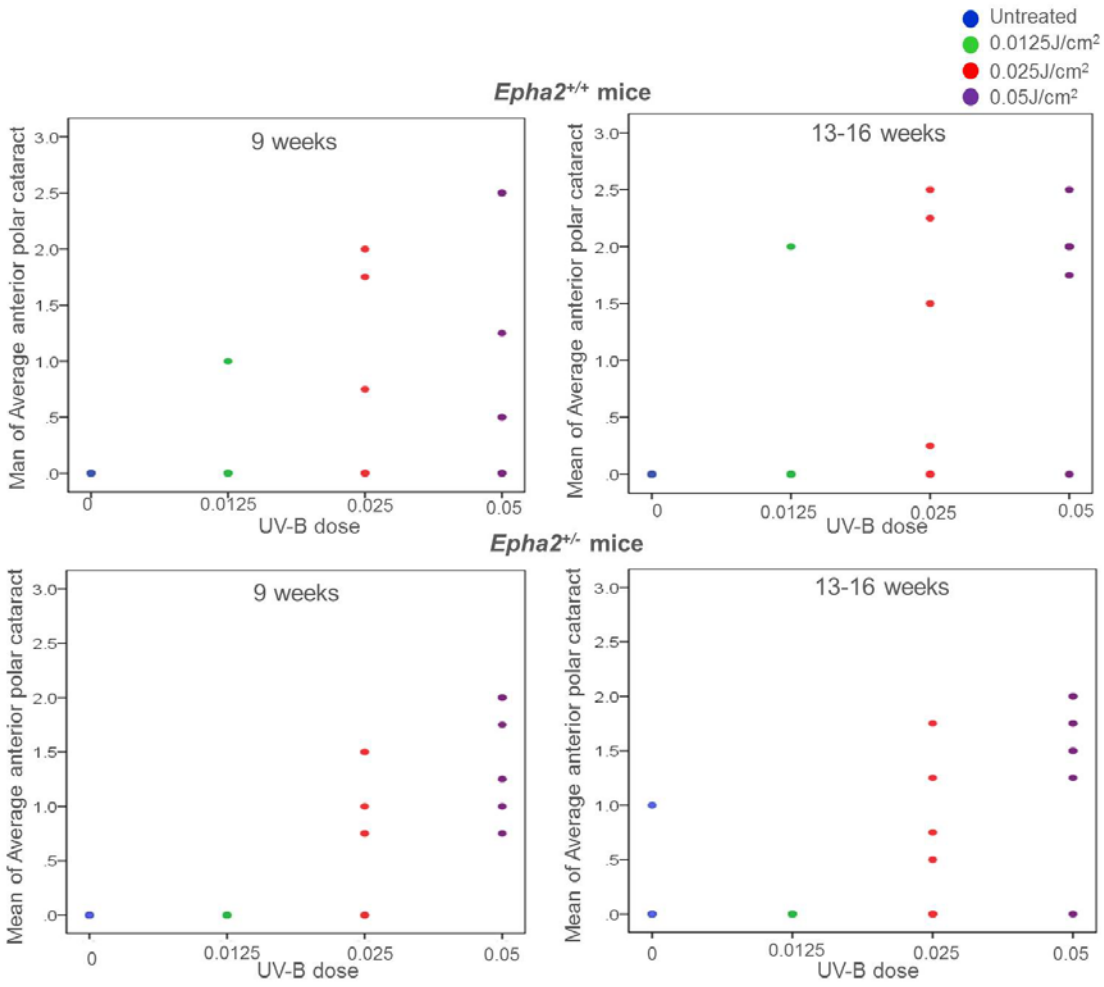

Figure 5.6: Distribution of anterior polar cataract grades in untreated and UV-B exposed *Epha2*$^{+/+}$ and *Epha2*$^{+/-}$ mice

Scatter plots show the distribution of grades of anterior polar cataract in untreated and UV-B treated *Epha2*$^{+/+}$ (top row) and *Epha2*$^{+/-}$ (bottom row) mice. The UV-B treated mice developed anterior polar cataract as a result of the exposure. The graphs indicate the grades of anterior polar cataract at the two time-points, at 9 weeks (top left and bottom left panel) and 13-16 weeks (top right and bottom right panel) of age. UV-B treated *Epha2*$^{+/+}$ mice developed higher grades of anterior polar cataract on their follow-up examinations while untreated mice presented with no anterior polar cataract at both the time-points. UV-B treated *Epha2*$^{+/-}$ mice developed similar grades of anterior polar cataract on their follow-up examinations. One untreated *Epha2*$^{+/-}$ mice also developed anterior polar cataract at 13-16 weeks of age. Some points on the graph also represent cataract grades of multiple animals.

The results revealed significant differences in the grade of anterior polar cataract between the untreated *Epha2*$^{+/+}$ mice and the group treated with UV-B dose of 0.05 J/cm^2 at both the time-points. There was no difference between the untreated and the group treated with the UV-B dose of 0.025 J/cm^2 at the two time-points; perhaps due to variation in the anterior polar cataract grades of the mice treated with 0.025 J/cm^2 UV-B dose. There was no difference between untreated and mice treated with the UV-B dose of 0.0125 J/cm^2 as majority of mice in this treatment group did not develop any anterior polar cataract. Table 5.3 lists the *p* values obtained from these comparisons. Similarly in *Epha2*$^{+/-}$mice a significant difference was observed between treatment groups at 9 weeks (*p* value = 3.2×10^{-5}) and 13-16 weeks (*p* value = 4.5×10^{-4}) of age. A significant difference was observed between untreated and groups treated with 0.025 J/cm^2 and 0.05 J/cm^2 dose of UV-B at both the time-points. Table 5.3 lists the *p* values obtained from comparisons between different treatment groups.

Table 5.3: Comparison of anterior polar cataract between different treatment groups in *Epha2*$^{+/+}$ and *Epha2*$^{+/-}$ mice. *p* values form Mann-Whitney *U* test are indicated; *n* = 8 per group

Comparisons	***Epha2*** $^{+/+}$ **mice**		***Epha2*** $^{+/-}$ **mice**	
	9 weeks	13-16 weeks	9 weeks	13-16 weeks
0 vs 0.0125	0.289	0.289	1	0.317
0 vs 0.025	0.05	0.02	0.01	0.0125
0 vs 0.05	0.007	0.001	3.1×10^{-4}	0.002

5.3.2. Effect of genotype and time for repair on cataract in UV-B exposed mice

We further analysed the data to determine if *Epha2* genotype of the treated mice had an effect on susceptibility to cataract development on UV-B exposure. The data in *Epha2*$^{+/+}$ and *Epha2*$^{+/-}$ mice at both the time-points was compared by Mann-Whitney *U* test. Table 5.4 lists the *p* values from these comparisons and the results of the analysis are graphically depicted in Figure 5.7. In all the UV-B treated groups, *Epha2*$^{+/+}$ and *Epha2*$^{+/-}$ mice developed similar grades of anterior polar cataract at both the time-points and no significant difference was observed between the two genotypes. These results suggest that the *Epha2*$^{+/-}$ mice do not have increased susceptibility to UV-B induced cataract.

Next, to determine the effect of time of repair in the UV-B treated mice, Wilcoxon Signed Ranks Test was used to compare the grades of anterior polar cataract in *Epha2*$^{+/+}$and *Epha2*$^{+/-}$ mice. Table 5.5 lists the *p* values obtained from these comparisons. Over 60% of *Epha2*$^{+/+}$ mice exposed to the 0.05 J/cm^2 dose developed anterior polar cataract 24-48 hours after the last exposure, whereas close to 90% of these mice were found have these opacities at their follow-up examination. This was because two *Epha2*$^{+/+}$ mice which did not develop anterior polar opacities at their first examination, presented with these opacities at their second examination. Therefore *Epha2*$^{+/+}$ mice had higher grades of anterior polar cataract at the subsequent examination (Mean 1.7 ± 0.7) compared to when first examined (Mean 0.9 ± 1.1). In the group of *Epha2*$^{+/-}$ mice treated with the UV-B dose of 0.05 J/cm^2, all the mice developed anterior polar cataract. However, one *Epha2*$^{+/-}$ mice recovered the damage caused due to UV-B exposure and was found to have no anterior

Table 5.4: Comparison of anterior polar cataract between the two genotypes. *p* values of Mann-Whitney *U* test are indicated; *n* = 8 per group

Dose of UV-B (J/cm^2)	9 weeks	13-16 weeks
0.0125	0.317	0.317
0.025	0.612	0.736
0.05	0.168	0.069

Table 5.5: Comparison of anterior polar cataract grade at the two time-points. *p* values from Wilcoxon Signed Ranks test are indicated; *n* = 8 per group

Genotype	Dose of UV-B (J/cm^2)		
	0.0125	**0.025**	**0.05**
Epha2$^{+/+}$	0.317	0.063	0.063
Epha2$^{+/-}$	1	0.414	0.829

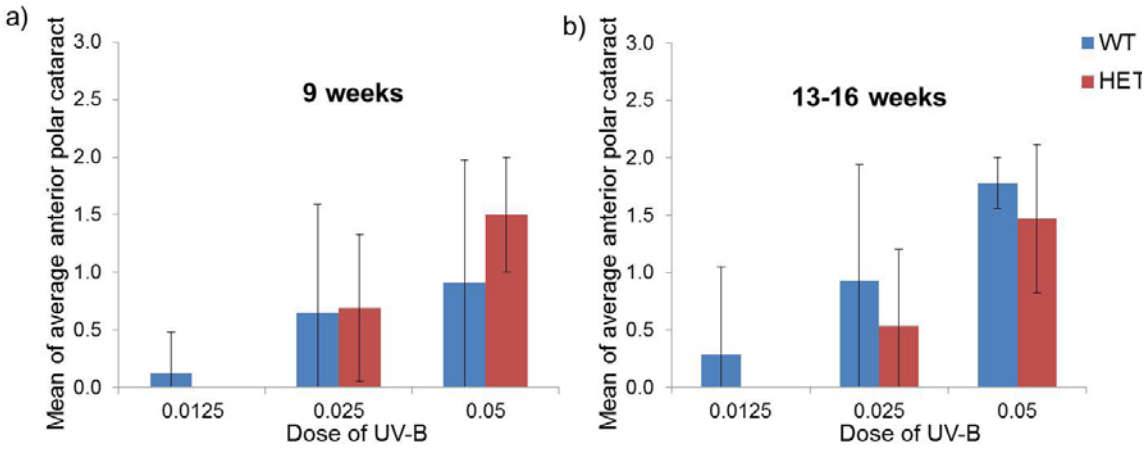

Figure 5.7: Comparison of anterior polar cataract in UV-B treated *Epha2*$^{+/+}$ and *Epha2*$^{+/-}$ mice.

Anterior polar cataract grades in UV-B exposed *Epha2*$^{+/+}$ and *Epha2*$^{+/-}$ mice at a) 9 weeks and b) 13-16 weeks of age. The UV-B doses are indicated on the x-axis and the grades of anterior polar cataract are indicated on the y-axis. Both the *Epha2*$^{+/+}$ and *Epha2*$^{+/-}$ mice developed comparable grades of anterior polar cataract at both the time-points.

polar cataract by the follow-up examination. However, these differences between the two time points, in both the *Epha2*$^{+/+}$ and *Epha2*$^{+/-}$ mice, were not statistically significant. Further, in *Epha2*$^{+/+}$ mice exposed to 0.025 J/cm^2 dose, only close to 40% mice developed anterior polar opacities while 50% of these mice presented with anterior polar cataract on their second examination. Over 60% of *Epha2*$^{+/-}$ mice treated with this UV-B dose developed anterior polar cataract; 50% of them presented with these opacities by the follow-up examination. However, again these differences were not statistically significant. Nevertheless, these observations suggest that even multiple treatments with this below-threshold dose of UV-B can lead to permanent damage in the lens.

Lastly, in groups of *Epha2*$^{+/+}$ and *Epha2*$^{+/-}$ mice exposed to 0.0125 J/cm^2 dose only one *Epha2*$^{+/+}$ mouse developed anterior polar cataract and presented with similar grade of anterior polar cataract at the follow-up examination; thus indicating that this dose does not cause any damage to the lens.

5.3.3. Histological analysis

Histological analysis was performed on two lenses each from untreated mice and *Epha2*$^{+/+}$ and *Epha2*$^{+/-}$ mice treated with UV-B dose of 0.025 J/cm^2 and 0.05 J/cm^2. The *Epha2*$^{+/+}$ and *Epha2*$^{+/-}$ mice treated with the lowest dose of 0.0125 J/cm^2 did not show any difference as compared to the untreated mice and therefore were not included in the analysis. After their second examination, the lenses of untreated and treated mice were examined by haematoxylin and eosin staining. Figure 5.8 illustrates the results of this analysis. We found that the untreated and lenses from mice treated with UV-B dose of

0.025 J/cm^2 showed normal morphology of lens epithelial and lens fiber cells (first and second column). These lenses perhaps show presence of vacuoles (white spaces) at the epithelial-fiber interface which are not observed in untreated lenses. The lenses of *Epha2*$^{+/+}$ and *Epha2*$^{+/-}$ mice treated with UV-B dose of 0.05 J/cm^2 exhibited epithelial cell hyperplasia (third column). This growth of epithelial cells invaginates into the anterior fiber cells and disrupts their arrangement. Lack of presence of vacuoles in lenses treated with 0.05 J/cm^2 dose of UV-B is perhaps due to a more localised lesion in these lenses. The equatorial and posterior regions of the lens appeared normal in all the treated and untreated lenses.

Overall these results show that repeated exposure to even below-threshold dose of UV-B leads to cataract. The phenotype of cataract is dependent on the dose of UV-B and perhaps on the time given to the ocular lens to repair damage between two exposures. However, the *Epha2* genotype of the mouse did not have any effect of the nature of damage to the lens.

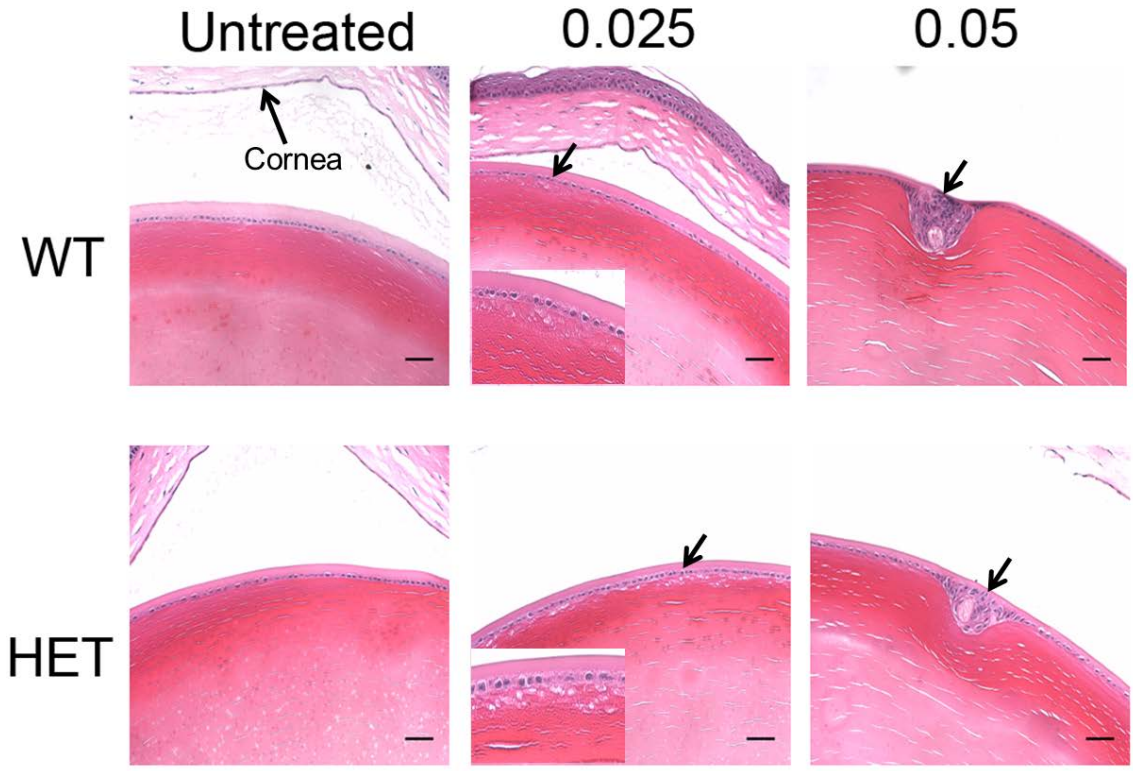

Figure 5.8: Histological analysis of untreated and UV-B treated lenses

Lenses of untreated and UV-B exposed *Epha2*$^{+/+}$ (WT) and *Epha2*$^{+/-}$ (HET) mice were analysed by heamatoxylin and eosin staining. Representative images of the pupillary region of the lens section of each genotype are shown. The dose of UV-B is indicated above each column. Blue heamatoxylin staining shows the nuclei and pink eosin staining shows the cytoplasm of lens epithelial and fiber cells. Cornea of the untreated and UV treated eyes, visible in some sections, is indicated. Lenses of mice treated with UV-B dose of 0.025 J/cm^2 perhaps show some disruption of the epithelial-fiber cell interphase as indicated by the arrow. An inset of the region is also shown in the image. Lenses of *Epha2*$^{+/+}$ and *Epha2*$^{+/-}$ mice treated with the UV-B dose of 0.05 J/cm^2 show aberrant lens epithelial cell growth (indicated by arrows) which disrupts the arrangement of the underlying fiber cells. Scale-bar 50 µm

5.4.Discussion

A complex interaction of environmental stress factors and genetic factors influence the development of ARC. *Epha2* knockout mouse was used as a model to determine an interaction between UV and *Epha2* and its effect on cataract development. *Epha2*$^{+/+}$ and *Epha2*$^{+/-}$ mice were exposed to three different below-threshold doses of UV-B and examined for cataract 24-48 hours after and at least a month after the last exposure. The effect of different UV-B doses, time of repair and *Epha2* genotype was examined on cataract development.

The results described in Chapter 4, section 4.3.2 demonstrated that the *Epha2* knockout mice were susceptible to anterior cortical cataract. The mice used in the present study for treatment, examinations and histological analysis were up to 4 months of age. The untreated *Epha2*$^{+/+}$ and *Epha2*$^{+/-}$ mice were found to have comparable grades of anterior cortical cataract by 4 months of age as described in Chapter 4, section 4.3.2.1. Therefore any difference in cortical cataract, if observed in this study, was attributed to exposure to UV-B. However, we did not observe any difference in anterior cortical cataract development between untreated and UV-B treated *Epha2*$^{+/+}$ and *Epha2*$^{+/-}$ mice. Instead, we observed dose-dependent differences in anterior polar cataract development due to repeated below-threshold dose of UV-B in both the genotypes. The difference in damage to the lens in response to different UV-B doses observed in the histological analysis further supported the dose-dependent difference observed in anterior polar cataract grades. We observed epithelial hyperplasia in lenses treated with the 0.05 J/cm^2 dose. This is consistent with previous studies which have reported that aberrant cell divisions causes multi-layering

under the capsule by the mitotically quiescent lens epithelial cells in response to UV exposure (199, 339). Additionally, we noted a possible disruption of the epithelial-fiber cell interphase in lenses treated with 0.025 J/cm^2 dose. Swelling of the fiber cells or accumulation of cellular debris in the region has been reported to contribute to the anterior cortical opacity observed at 24-48 hours after last exposure (196, 339). UV exposure to a single above-threshold dose in rats has been found to activate repair mechanism in the lens which removes the damaged cells by apoptosis leading to disappearance of the cortical cataract by subsequent examination (196, 199). However, we did not observe any alterations in grades of anterior cortical cataract on UV-B exposure suggesting that the doses and treatment regime used in the present study either do not affect cortical cataract development or activate mechanisms to repair the damage.

Exposures of above or close-to threshold dose of UV radiation, with inter-exposure time of either three days and one day, respectively, has been reported to be most damaging to rat lens (350, 351). However, few studies demonstrate the effect of multiple below-threshold UV-B exposures on lens (346). In the present study mice were exposed to below-threshold UV-B dose of 0.05 J/cm^2, 0.025 J/cm^2 and 0.0125 J/cm^2, seven times, every third or fourth day. A simple additive effect of the multiple treatments of 0.05 J/cm^2, 0.025 J/cm^2 and 0.0125 J/cm^2 dose results in a cumulative doses of 0.35 J/cm^2, 0.175 J/cm^2 and 0.0875 J/cm^2, respectively. We found that a close-to-threshold cumulative dose of 0.35 J/cm^2 and 0.175 J/cm^2 led to anterior polar cataract. These findings are consistent with the phenotype of cataract observed in previous reports (199, 339, 349, 350).

Rodent lenses exposed to UV-B dose of 0.2 J/cm^2 /2 days for a period of at least two months were reported to develop anterior polar cataract (339). This is consistent with our

findings where multiple exposures of even below-threshold doses of 0.05 J/cm^2 and 0.025 J/cm^2 are sufficient to cause permanent damage to the lens. The presence of anterior polar cataract with multiple exposures to 0.05 J/cm^2 and 0.025 J/cm^2 dose indicates permanent damage to the lens epithelium which could not be repaired. No significant effect of multiple exposures of UV-B dose of 0.0125 J/cm^2 suggests that either the dose was too low to initiate any response in the lens or the lens can rapidly repair with the damage caused by exposure to this dose.

The forward light scattering by a UV-B exposed lens is also affected by latency period after the exposure (349, 352). One week after exposure is suggested to be the optimal time to record observations related to lenticular changes which remain unchanged between 1 week to 32 weeks of latency, following a dose of 0.05 J/cm^2 in rat lens (352). This suggests that with exposure to below-threshold doses of UVR the observations do not change over a long latency period. In this work we observed changes 24-48 hours and approximately a month after exposure. Interestingly, in the group of *Epha2*$^{+/+}$ mice treated with 0.05 J/cm^2 and 0.025 J/cm^2 dose of UV-B, we found an increased number of mice with anterior polar cataract with an overall higher grade of anterior polar cataract at the follow-up examination. This suggests that lenses from these mice demonstrated a delayed response to UV-B exposure or the latency period facilitated in demonstrating the accumulated damage due to exposure to UV-B. We did not observe any significant effect of time available for repair on grades of anterior polar cataract recorded on the subsequent examination in *Epha2*$^{+/-}$ mice suggesting permanent damage to the lens caused by the UV-B doses used in the study. However, comparison of morphological, physiological and molecular

characteristics of the UV-B treated lens at the two time-points may demonstrate differences over time.

Previous studies (191, 212-214) and work in this project reported in Chapter 4 have demonstrated that *Epha2* knockout mice are susceptible to cataract development perhaps due to disruption of lens homeostasis and architecture. We further investigated if UV-B exposure alters their susceptibility to cataract development. Our results show that *Epha2*$^{+/-}$ mice did not demonstrate increased susceptibility to UV-induced cataract.

A majority of studies have been performed by UV treatment of anaesthetized animals. In addition to having more control on the dose of UV delivered to the lens, the contralateral eye of the anaesthetized animal had served as an untreated control. Nevertheless, anesthetic drugs have been shown to influence the cataract phenotype in animals (353). In the present study, we performed exposure of anaesthetized mice in an attempt to replicate the UV exposure in humans. The treatment regime used in the present study is perhaps most similar to daily exposure in humans.

We did not measure the forward light scattering from the lenses of UV-B exposed mice. Therefore these results can't be directly compared to the majority of studies conducted in animal models. Additionally, dark field microscopy or scanning electron microscopy of the UV-B treated lenses may assist in evaluating damage to the lens due to the different doses of UV-B. Testing other treatment regimens by altering the inter-exposure days or extending the exposures might lead to a better understanding of the effect of *Epha2* genotype on cataractogenesis due to UV-B treatment. Other treatment regimens and UV-B

doses may lead to a different phenotype in both *Epha2*$^{+/+}$ and *Epha2*$^{+/-}$ mice and provides grounds for further investigations.

5.5. Conclusion

In conclusion, to the best of our knowledge this is the first study to demonstrate effect of repeated exposure to below-threshold UV-B radiation on cataract development in *Epha2* knockout mice. Our results demonstrate an dose-dependent effect of UV-B on anterior polar cataract and suggest that *Epha2*$^{+/-}$ mice do not exhibit increased susceptibility to UV-induced cataract.

6. Discussion

6.1 Brief overview

At the commencement of this project in 2011, *EPHA2* was, and still remains, the most recently identified gene in both congenital and age-related cataract (65, 66, 68, 190, 191). Since 2011, multiple reports have examined the role of *EPHA2* in the lens and in congenital or age-related cataractogenesis (64, 69, 192, 212-215). Further studies were still needed to elucidate the commonalities between developments of both the forms of *EPHA2* mediated cataract. Therefore the present study investigated the role of *EPHA2* gene in congenital and age-related cataract. We, for the first time, determined the frequency of mutations in the gene in inherited cataracts in an Australian cohort. Further, functional effects of the causative mutations were examined in a cell culture system. Additionally, to understand its role in age-related cataract (ARC), studies were undertaken to ascertain the interaction of established environmental modifiers with *Epha2* and its effect on cataract development. The important findings from this study and other parallel studies are discussed in the following sections. Finally, potential relevance of these results to cataract in humans is discussed.

6.2 Key Findings

The genetic burden due to mutations in *EPHA2* on congenital cataract was evaluated in a South-Eastern Australian cohort of congenital cataract cases. Our findings revealed that 4.7% of inherited cataracts in this cohort were due to mutations in the *EPHA2* gene.

Firstly, these findings showed that frequency of causative mutations in *EPHA2* in this cohort was comparable to mutations in a group of crystallin genes taken together (272). We identified the underlying cataract causing mutation in four families from our cohort. This will assist in genetic counselling in these families and in better management of the disease by regular ocular examination of the individuals carrying the mutations. Genetic testing for the non-synonymous variant (c.2875G>A; p.A959T) found in both late-onset congenital and age-related cataract, may help in early detection of mutation carriers who may need regular monitoring. Of great interest was the splice mutation (c.2826-9G>A; p.D942fsXC71) as it was previously reported in an Australian family from our cohort (65). Multiple unrelated families with the same splice mutation in the cohort suggest that this mutation commonly occurs in the population and may potentially be present in other affected families. In addition to detecting the carriers, genetic testing for these mutations will also identify the non-carriers of the mutation and relieve them from future follow-up examinations. Identification of the rare variant in cataract affected individuals highlighted that the rate and severity of cataract development can be dependent on other genetic and environmental factors. Lastly, the mutations, c.1751C>T and c.2875G>A, found in this study also add novel mutations to the existing repository of congenital cataract causing mutations in humans.

The findings of this study may be valuable for establishing genetic screens for other affected families which will facilitate prenatal or early detection of an affected individual. Similar studies determining congenital cataract causing mutations in a population/cohort may further assist in streamlining the genes that should be screened in affected families at their first presentation.

Next, in an attempt to further understand the implications of identified mutations on the protein, we analysed the localisation of five mutant EPHA2 proteins in two epithelial cell lines namely, MDCK and Caco2 cells which are known to polarize and have established cell-junctions. Similar to the wild-type protein, EPHA2 with p.P594L, p.A959T or p.V972GfsXC39 mutation localised to the cell periphery. The mutant proteins carrying p.T940I or p.D942fsXC71 mutation were predominantly found in the perinuclear region and demonstrated some co-localisation with the cis-golgi marker in both the cell lines. These results are different from the previously reported subcellular localisation of mutant EPHA2 proteins (215) suggesting that localisation of these proteins is cell-type dependent.

The presence of p.P594L and p.D942fsXC71 mutation leads to nuclear cataract while p.V972GfsXC39 and p.T940I mutation lead to posterior polar cataract in humans (65, 354). Perhaps the altered residues affect epithelial cell homeostasis and/or epithelial to fiber cell transformation and cell migration resulting in the observed cataract phenotype. Further, in support of this hypothesis, Park et al. had previously reported altered cell migration of p.D942fsXC71, p.V972GfsXC39 and p.T940I mutant proteins (215).

During lens development, lens epithelial cells in the posterior of the lens elongate and give rise to the primary fiber cells which constitute the lens nucleus while epithelial cells in the bow region divide and differentiate into secondary fiber cells which elongate and extend to the poles (8). Epha2 expression has been detected throughout mouse lens development (324). In addition to the bow region, high expression of Epha2 was observed in the posterior pole of the developing lens (324) suggesting a role of the protein in these regions in the lens. Based on this expression pattern, disruption of EPHA2 function due to presence of these mutations is likely to lead to the nuclear or posterior polar cataract phenotypes.

Mutant EPHA2 with p.A959T leads to cortical or posterior subcapsular cataract in teenage years, which correlates with Epha2 expression in the cortical fiber cells in postnatal and adult mouse lenses. Although mutant EPHA2 proteins with p.P594L, p.A959T or p.V972GfsXC39 mutation do not mis-localise, they may disrupt EPHA2 signalling and affect its role in the cell. The two mutant proteins carrying p.T940I or p.D942fsXC71 mutation demonstrate severe effect on localisation and may lead to delayed recruitment of the mutant EPHA2 to the cell periphery. This can potentially affect cell migration which may in turn affect lens architecture and lead to cataract. Further investigation using animal models carrying the causative mutations in *EPHA2* may improve our understanding of the effect of these mutations on lens development.

Furthermore, to understand the involvement of *EPHA2* in ARC, we examined effect of environmental factors namely, age, gender and UV-B exposure on *EPHA2* and cataract development. For this we used an *Epha2* knockout mouse model (Strain: KST085). Jun et al. had previously reported that the *Epha2*$^{+/-}$ mice of KST085 strain on FVB/NJ background did not develop cataract up to 14 months of age while *Epha2*$^{-/-}$ mice developed cataract by 5-8 months of age (191). In the present study we used the KST085 strain on C57BL/6J background. We found that compared to relatively clear lenses of *Epha2*$^{+/+}$ mice, *Epha2*$^{-/-}$ mice developed severe cataract by 4 months of age and *Epha2*$^{+/-}$ mice demonstrated intermediate phenotype and developed severe cataract by 8 months of age. These differences between genotypes were statistically significant demonstrating a distinct dosage effect of *Epha2* copy number on ARC progression, which was a novel finding. The difference in age-of-onset of cataract as compared to the previous report is possibly attributed to differences in genetic background of the mice used in the two studies. Similar,

genetic background related differences in cataract phenotype have been reported in *Connexin 46*$^{-/-}$, *Connexin 50*$^{-/-}$ and *Ephrin-A5*$^{-/-}$ mice as well (221, 355, 356). Changes in the genetic background leading to altered susceptibility to cataract development once again suggest that cataract is a multi-genic disease. A comparative molecular analysis between the mouse strains will provide insight into the genetic modifiers leading to variations in severity of the phenotype. Similarly, the individuals carrying the rare variant, c.2875G>A; p.A959T, found in our genetic study may be susceptible to cataract development in the presence of other genetic and/or environmental factors.

Interestingly, despite expression of *Epha2* in a variety of epithelial cells, the *Epha2* knockout mice present only with cataract without any other systemic abnormality. Loss of Epha2 function in other organs is perhaps compensated by other Eph receptors (289). However, this loss of function is not compensated for in the lens hence resulting in cataract. Consistently, no other systemic abnormality has been reported in congenital cataract patients with causative mutations in *EPHA2* yet, indicating a similar compensatory mechanism in humans. However, ARC phenotype, observed in *Epha2* knockout mice, as opposed to autosomal dominant congenital cataract due to mutations in *EPHA2*, observed in humans, likely reflects the differences in mouse and human lens development. It also suggests that complete absence of functional Epha2, in *Epha2* knockout mouse, may lead to age-related phenotype which is susceptible to genetic and environmental modifiers. In contrast, mutant *EPHA2,* present in human congenital cataract cases, may lead to disrupted EPHA2 signalling during lens development resulting in accelerated cataract development.

The molecular analysis of cataractous lenses correlates with the observed cataract phenotype and is consistent with previous reports (191, 213). The histological and

immunofluorescence analysis of cataractous lenses suggests that lack of full-length Epha2 in the lens affects its role at cellular junctions resulting in abnormal fiber cell shape and defects in fiber cell packaging. Cooper et al. reported similar disruption of fiber cell packing in *Ephrin-A5*$^{-/-}$ mice (221) suggesting an important role of Eph-Ephrin signalling in maintenance of lens architecture. Cheng et al. reported lack of phosphorylated Src (a non-receptor tyrosine kinase) and cortactin (an actin-binding protein) in lenses of *Epha2*$^{-/-}$ mice (214). These downstream effector molecules play an important role in regulating cell migration and maintaining cellular morphology (357, 358). The disruption of lens architecture observed in the *Epha2* knockout mice also correlates with possible effect of congenital cataract causing mutations on cellular junctions due to mis-localisation of the mutant proteins found in this study. Park et al. found lack of activation of Akt, a downstream molecule in the EPHA2 signalling pathway, and altered cell migration due to the mutant EPHA2 proteins (215). This again supports the hypothesis that EPHA2 signalling may act through Src-Akt signalling pathway in the lens and affect processes critical for lens homeostasis such as integrity of lens cell-junctions, morphology and migration.

An intriguing observation was that only newly formed cortical cells exhibited this disruption while the central fiber cells did not show presence of the protein. This is consistent with previous report (191, 212, 324) and potentially reflects a function of Epha2 only in the cortical fiber cells in adult lens. Spatial switch in gene expression of other genes involved in ocular development has been previously reported (359). Whether altered regulation of *Epha2* in response to age is responsible for the observed cataract phenotype and progression needs further investigation.

A partial Epha2 fusion protein generated as a result of the knockout was detected in lenses of *Epha2* knockout mice and localised as inclusion in the lens cells. This has not been reported previously and is a novel finding. The presence of this fusion protein may increase light scattering in the lenses of *Epha2* knockout mice and be a contributing factor to the severity of cataract phenotype. Analysis of properties of the partial Epha2 fusion protein such as solubility and half-life may indicate if accumulation of this protein in lenses from *Epha2* knockout mice over time contributes to ARC phenotype.

Furthermore, our findings demonstrate that gender of mice altered ARC progression only in *Epha2*$^{+/-}$ mice. We noted that male *Epha2*$^{+/-}$ mice had higher grades of cataract compared to age-matched female mice up to 6 months of age. However, on their examination at 8 months, the female mice developed higher grades of cataract than the male mice. This observation suggests a potential role of gender on *Epha2* mediated cataract progression. Epidemiological studies in humans suggest an increased risk of cortical cataract development in post-menopausal females and a potential protective effect of estrogen hormones against cataract (74, 139, 148, 151). However, gender-related differences in *Epha2*$^{+/-}$ mice were observed both in pre- and around menopausal ages. Thus changes in the levels of estrogen may be the underlying molecular basis of this gender-related difference in cataract progression in *Epha2* knockout mice. Estrogen acts through the c-Src signalling pathway (360), and lack of functional Epha2 in these mice might affect the downstream signalling. However, in the human scenario post-menopausal females have an increased risk of cataract development; possibly due to reduced levels of estrogen affecting this signalling pathway in addition to loss of protection of lens from oxidative stress due to environmental insults (361, 362).

In addition to the effect of inevitable risk factors such as age and gender, we examined the effect of preventable environmental stress from UV-B exposure on cataract development in *Epha2* knockout mice. To the best of our knowledge this is the first study to analyse the effect of repeated below-threshold dose of UV-B exposure on cataract development in the *Epha2* knockout mice. Our findings suggest that multiple exposures of even below-threshold UV-B doses of 0.025 J/cm^2 and 0.05 J/cm^2 were cataractogenic in both *Epha2*$^{+/+}$ and *Epha2*$^{+/-}$ mice. We demonstrated UV-B dose dependent severity of anterior polar cataract phenotypes. Previous work in rodents has demonstrated repair in mouse lens after UV-B exposure (344). However, we did not observe such an effect with the doses and the treatment regimen used in this study. On the contrary, we noted increase in cataract severity in *Epha2*$^{+/+}$ mice on their follow-up examination conducted at least a month after their last exposure. Perhaps the response of the lens to multiple exposures of below-threshold dose of UV-B is different from a single above-threshold dose used in other studies and detailed investigation is needed to understand the difference in response.

A few studies analysing effect of UV-B exposure on genetically susceptible mouse models have either demonstrated no effect or increased susceptibility to cataract development (204, 363). Our findings reveal that the *Epha2*$^{+/-}$ mice do not have increased susceptibility to UV-B induced cataract. UV-B exposure of *Epha2*$^{-/-}$ mice and long-term monitoring of cataract progression in the UV-B treated *Epha2*$^{+/-}$ mice may further provide insight to the effect of UV-B exposures on development of anterior cortical cataract in these mice.

The UV-B exposure in humans is difficult to quantify due to difference in times of exposure and atmospheric conditions which alter the UV radiation reaching the earth. West et al. determined the human UV-B exposure in Maryland Sun-Year (MSY) which was a

measure of the ultraviolet energy that falls on a horizontal surface in Maryland in 1 year (364). This was equivalent to a daily 0.208 J/cm^2 dose of UV-B exposure per day and exposure to 0.01 MSY was found to be associated with a 10% increased risk of development of cataract. The present study certainly is the most similar to UV-B exposure in humans. UV exposure in humans is associated with an increased risk of cortical cataract development. However, UV-B exposure in the *Epha2*$^{+/+}$ and *Epha2*$^{+/-}$ mice leads to anterior polar cataract. The histological analysis of UV-B treated mice lenses revealed that epithelial hyperplasia may be the underlying cause of anterior polar cataract in mice exposed to the UV-B dose of 0.05 J/cm^2 whereas some disruption of epithelial fiber cell interphase was observed in the lenses of mice treated with the 0.025 J/cm^2 dose. The cataract observed in *Epha2* knockout mice was over a small period of UV-B exposure whereas UV-induced cataract in humans is due to accumulated damage to the lens over a life-time. The UV-induced damage in the epithelial cells may get transmitted to the newly differentiated fiber cells in the cortex and perhaps explain the cortical cataract phenotype observed in humans.

We performed detailed characterization of the *Epha2* knockout mouse (KST085) strain on C57BL/6J background enabling us to document cataract progression and changes in lens architecture over time. With the help of these findings and due to the progressive ARC cataract in these mice, the KST085 strain on C57BL/6J background may prove to be a model for testing novel therapies for ARC.

6.3 Overall conclusions

The findings from the present study reveal that *Epha2* mediated cataract is susceptible to both, environmental modifiers such as age and gender and genetic modifiers such as variances in the genetic background of different mouse strains. A combination of environmental factors determines the development and progression of *EPHA2* mediated congenital and age-related cataract in humans, as observed in the cataract phenotype of the rare variant found in the genetic study. These results again demonstrate that cataract is a multi-factorial disease with arbitrary boundaries set for categorizing congenital and age-related cataract. An underlying genetic alteration susceptible to a combination of gene-environment interactions determines the age-of-onset of cataract.

7. Appendices

Appendix 1

1.1: List of genes, mutations in which lead to isolated inherited congenital cataract. Autosomal Dominant (AD); Autosomal recessive (AR)

POSITION	GENE	INHERITANCE	EFFECT ON PROTEIN	REFERENCE
Crystallins				
21q22.3	Alpha Crystallin A *(CRYAA)*	AD/AR	Missense	(365)
11q22.3-23.1	Alpha Crystallin B *(CRYAB)*	AD/AR	Missense/Frameshift	(366)
17q11.2-12	Beta Crystallin A1 *(CRYBA1)*	AD	Missense	(367)
22q12.1	Beta Crystallin A4 *(CRYBA4)*	AD	Missense	(368)
22q11.2-12.2	Beta Crystallin B1 *(CRYBB1)*	AD/AR	Missense/Frameshift	(369)
22q11.2-12.2	Beta Crystallin B2 *(CRYBB2)*	AD	Missense	(370)
22q11.2-12.2	Beta Crystallin B3 *(CRYBB3)*	AR	Missense	(371)
2q33-35	Gamma Crystallin C *(CRYGC)*	AD	Missense/Frameshift	(372)
2q33-35	Gamma Crystallin D *(CRYGD)*	AD	Missense/Frameshift	(372)
3q27	Gamma Crystallin S *(CRYGS)*	AD	Missense	(373)
2q33-q35	Gamma Crystallin B *(CRYGB)*	AD	Frameshift	(374)

Membrane Proteins				
13q11	Gap junction alpha-3 *(GJA3)*	AD	Missense/Frameshift	(375)
1q21.1	Gap junction alpha-8 *(GJA8)*	AR	Missense/Frameshift	(376)
12q13	Major intrinsic protein *(MIP)*	AD	Missense/Frameshift	(377)
19q	Lens intrinsic membrane protein *(LIM2)*	AR	Missense	(378)
1p36	Ephrin type A receptor-2 *(EPHA2)*	AD/AR	Missense/Frameshift	(68)
Membrane associated proteins				
16p13.3	Transmembrane protein 114 *(TMEM114)*	AD	Missense	(379)
20q11.22	Charged multivesicular body protein 4b *(CHMP4B)*	AD	Missense	(380)
Cytoskeletal proteins				
20p12.1-	Filensin *(BFSP1)*	AD	Missense	(381)
3q21-25	Phakinin *(BFSP2)*	AD	Missense/Frameshift	(382)
10p13	Vimentin *(VIM)*	AD	Missense	(383)
Transcription factors				
16q21-22.1	Heat shock factor protein 4 *(HSF4)*	AD/AR	Missense/Frameshift	(384)
Cytoplasmic protein				
3p21.31	FYVE and coiled-coil domain containing protein *(FYCO1)*	AD	Missense	(385)
9p13	Galactose-1 phosphate uridyltransferase *(GALT)*	AD	Missense	(175)
9q22.33	Tudor Domain containing protein 7 *(TDRD7)*	AD	Missense	(386)

Appendix 2: Primer sequences

2.1 Primer sequences for PCR amplification of coding regions of *EPHA2* for in-house sequencing

Exon	Forward Primer (5'-3')	Reverse Primer (5'-3')
1	GGCCCCTTTAAAGACATTCC	CGACACCAGGTAGGTTCCAA
2	CTGGAGGGATCCTCACCTTT	GTGAGAAGCTGGACCCTGAG
3	F1- GGAGAGCACGAACTGGAAAG F2- GATGAGATCACCGTCAGCAG	R1- AGGCCAGGTAGAAGCCTTTG R2- AGCAGGGATGAGCTTACCAA
4-5	GGGGTGGAAGCAGATTGAA	GTCCTCCTTAAGCCCCACCT
6	GGCTCCACGTCCACTTGT	TCAGATGGCTGGGTGGTT
7	ATTCCGAGCCTCAGTTTCCT	TCCTTTCCCAAGATGTCTCAA
8	CTCTGGAGCCTTCCCAAGT	TGAGGAAATGGAGGTTCCTG
9	ACTGGGCCGCATTCTGAG	CAGTGCCCTGGGAACACC
10-11	TGACCTTCTCCTCTGACTCCA	GTGGGCACAGTCACAGACAG
12-13	ACCTTCCCCCATATCTGTGC	AGGTGTGCAGGTGAGAGGAC
14	CTTGGCTGCAATGGTCCT	AGAGCAAAACTCCGTCTCCA

15	TTCTGGGATGTTCCTGTTCC	GTGGCCACTCTACCGAAGTG
16	TCATCCAGGTTAGGGAGCAG	GTTCTGCCCTTCTCTTCCAA
17	CCAGAGCTCTCTTGCCCTAC	GCAGGGGGAGGAAAGAACTA

2.2 Primer sequences for PCR amplification of coding regions and 3'UTR of *EPHA2* used at AGRF

Exon	Forward Primer (5'-3')	Reverse Primer (5'-3')
1	AGGGCATGAATGAACAGGAG	CTGAAACCGCTTATTCTCCG
2	TGTCTGAGAGTTGGGGTTCC	GCCAGAGATCCCTCTGACTG
3	F1- TAGTGCCCTACTCTGCCACC F2- ACTACGGCACCAACTTCCAG	R1- GGCACCGATATCCTGGAAG R2- AACCTGGGAATGCAGAACC
4	CTTCTTGCAGGAGCCAGTG	GAGGAGTCAGTGCTGTGCTG
5	CAGCACAGCACTGACTCCTC	TCTCTAAACACACCCGAGCC
6	CTGTGGAGGATGTGGCTCC	GCCATGTCTTCTCTCGTACAAATC
7	GCTAGCTTGGGGTGGTCTC	CACACCACTGTCGTGAATCC

8	GGAACTCCCTTGTCATCAGC	CGAAGGCATTCCCATTAGAG
9	AGACCTCACTGACCTCCCTG	CGAGTGACACAGGATGGATG
10	TCCTCTGACTCCAGAGCACC	AAGTCCACTCGCTGCTTCTC
11	CACATATGAGGACCCCAACC	GACAGAGCCCCTGCTAAGTG
12	TCAATACCTGTGCCCTCCTC	CTGAACTCGCCATCCTTCTC
13	TTCCTTCGGGTAAGGATGTG	AGGTGTTCTGCCTCCTGAAG
14	ACCACCAGTGTAAGTTGGGG	TAAACTGTCCTCTGCCCAGC
15	AGGCCCTTCCTGTCTGTTTC	GTGGCCACTCTACCGAAGTG
16	TGAACCCTACTTGACTGGGC	TCTTCCAAGGAGCCTCTTCC
17	CTCTTGCCCTACAGGTCCC	TGCTAAGTGCTCAGCTGTGTG
3’UTR	TAGTTCTTCCTCCCCCTGC ACTGGGTGAGACCCAAAGC CCCATCTCTCATCCTTTTGG	ACCTCAACACAACCAAGCATC TCCCAAGACTGAAAGCCAAG TTGCTGTTCTCCTACCTCCC

2.3 Sequence for primers used for Taqman Assay

Forward Primer (5'-3')	Reverse Primer (5'-3')
CCCACCCCTTCTCCTTCCA	TGAACTTCAACACAGCCTGGTT

2.4 Sequences of primers used for PCR-based mutagenesis

Mutation	PCR round and primer	Name	Primer Sequence (5'-3')
c.1751C>T; (p.P594L)	Forward primer for PCR 1	Eph Exon10mut Fwd	CCGTGACCCTGGACGCAATG
	Reverse Primer for PCR 1	Eph 1751 Rev	GTGGGGATCCACGTATGTCTTCAGGAGCTTCAG
	Forward Primer for PCR 2	Eph1751 Fwd	CTGAAGCTCCTGAAGACATACGTGGATCCCCAC
	Reverse primer for PCR 2	Eph Exon10mut Rev	CATGAGCTGGTAGATGGCGGAGG
c.2819C>T; (T940I)	Forward primer for PCR 1	Eph Mut Fwd	TCAAGACCCTGGCTGACTTTGACC
	Reverse Primer for PCR 1	Eph2819 Rev	CTTGATATCGTCGTTGATCATCTGCACCACCTTC
	Forward primer for PCR 2	Eph2819 Fwd	GAAGGTGGTGCAGATGATCAACGACGATATCAAGAG

	Reverse primer for PCR 2	Eph BglII Rev	GGGAGAGGGGCGGAATTCCAGATCTGTTAATTAAACTC
c.2826-9G>A; (D942fsXC71),	Forward primer for PCR 1	Eph Mut Fwd	As above
	Reverse Primer for PCR 1	Eph2826 mod Rev	CTTGATGTCGCTGTGGGTCGTTGGTCATCTGCACCACCTTCT
	Forward primer for PCR 2	Eph2826 mod Fwd	GATGACCAACGACCCACAGAGACATCAAGAGGATTGGGGT
	Reverse primer for PCR 2	Eph BglII Myc Rev	CACACACACACAAGATCTTACAGATCCTCTTCTGAGATGAG TTTTTGTTCGAAATAAATAAAGTCCCCAGTGGCCCAGCAT
c.2875G>A; (p.A959T)	Forward primer for PCR 1	Eph Mut Fwd	As above
	Reverse Primer for PCR 1	Eph2875 Rev	CAGCAGGCTGTAGGTGATGCGC
	Forward primer for PCR 2	Eph2875 Fwd	CGCATCACCTACAGCCTGCTGG
	Reverse primer for PCR 2	Eph BglII Rev	As above
c.2915-2916delTG; (V972GfsXC39)	Forward primer for PCR 1	Eph Mut Fwd	As above
	Reverse Primer for PCR 1	Eph2915 Rev	GGATCCCCAGTGTTCACCTGGTCCTTGAGTCCCAG
	Forward primer for PCR 2	Eph2915 Fwd	GACCAGGTGAACACTGGGGATCCCCATCTGAGC
	Reverse primer for PCR 2	Eph BglII Myc Rev	As above

2.5 Primer sequences for *CP49* genotyping

Primer name	Sequence (5'-3')
CP49 Fwd (Forward Primer)	TGGGGTTGGGCTAGAAATCTCAGA
CP49 WT Rev (Wild-type Reverse Primer)	TACTCAAAAGGCAGTAGTCCCTGC
CP49 Mut Rev (Mutant Reverse Primer)	AGCCCCTACGACCTGATTTTTGAG

2.6 Primer sequences for *Epha2* genotyping

Primer name	Sequence (5'-3')
M30828F (Forward Primer)	CACCTCACTCAGTATAGTGCTCCA
M30828 WT R(Wild-type Reverse Primer)	CGTCTTCCCAGTCATACTCTACTT
M30828 Mut R (Mutant Reverse Primer)	CCATACAGTCCTCTTCACATCCAT

Appendix 3: Buffers recipes

3.1 TBE

Constituents	Weight
Tris	54 g
Boric Acid	27.5 g
0.5 M EDTA	20 ml

The volume was made up to 1 L using dH_2O. The solution was autoclaved before use.

3.2 LB Agar

Constituents	Weight
Bacto-tryptone	5 g
Bacto-yeast extract	2.5 g
NaCl	5 g
Bacto agar	5 g

Dissolved in 350 ml Milli-Q water made up to 500 ml using Milli-Q water. The solution was autoclaved before use.

3.3 LB Medium

Constituents	Weight
Bacto-tryptone	5 g
Bacto-yeast extract	2.5 g
NaCl	5 g

Dissolved in 350 ml Milli-Q water made up to 500 ml using Milli-Q water. The solution was autoclaved before use.

3.4 Solution P1

Constituents	Volume
50 mM Tris HCl pH 8.0	5 ml of 1 M stock
10 mM EDTA pH 8.0	2 ml of 0.5 M stock

Volume was adjusted to 100 ml using Milli-Q water. The solution was autoclaved before use.

3.5 Solution P2

Constituents	Volume
200 mM NaOH	5 ml of 4M stock
1% SDS	10 ml of 10% stock

Volume was adjusted to 100 ml using Milli-Q water.

3.6 Solution P3

Constituents	Weight/Volume
3M/5M Potassium Acetate	29.44 g
Glacial acetic acid	30 ml

pH was adjusted to 5.5 using KOH and the final volume made up to 100 ml using Milli-Q water. The solution was autoclaved before use.

3.7 Phosphate Buffered Saline; pH 7.4 (10×)

Constituents	Final concentration	Weight
NaH_2PO_4	19 mM	2.28 g
Na_2HPO_4	81.3 mM	11.5 g
NaCl	1.3 M	75.97 g

The solution was made up to a final volume of 1 litre using Milli-Q water.

3.8 Separating gel buffer (4×)

Constituents	Weight
Tris	18.2 g
SDS	0.4 g

Constituents were dissolved in 60 ml Milli-Q water. The pH was adjusted to 8.8 and the final volume was made up to 100 ml.

3.9 Stacking gel buffer (4×)

Constituents	Weight
Tris	6.05 g
SDS	0.4 g

Constituents were dissolved in 40 ml Milli-Q water. pH adjusted to 6.8 and the final volume made up to 100 ml.

3.10 Separating gel

Constituents	8% gel
29:1 Acrylamide (40%)	1.5 ml
Separating gel buffer (4X)	1.875 ml
Milli-Q water	4.31 ml
APS (20%)	12.5 µl
Temed	10 µl

3.11 Stacking gel

Constituents	4% gel
29:1 Acrylamide (40%)	0.25 ml
Separating gel buffer (4X)	0.625 ml
Milli-Q water	1.6 ml

APS (20%)	6.25 µl
Temed	2.5 µl

3.12 Gel loading buffer (4×)

Constituents	Volume/Weight
0.25 M Tris-HCl pH 6.8	2.5 ml of 1M Tris-HCl (pH 6.8) stock
8% SDS	800 mg
40% glycerol	4 ml of 10% glycerol stock
20% β-mercaptoethanol	2 ml of 100% β-mercaptoethanol
10% Bromophenol blue	1 ml Bromophenol blue

The final volume was adjusted to 10 ml using Milli-Q water.

3.13 Gel running buffer (10×)

Constituents	Weight
0.25 M Tris	30.275 g
1.92 M Glycine	144.13 g
1 % SDS	10 g

pH was adjusted to 8.3 with HCl and the final volume was made up to 1 litre using Milli-Q water.

3.14 Towbin Western Transfer Buffer (10×)

Constituents	Weight	Final concentration
Tris base	30.275 g	25 mM
Glycine	144.13 g	192 mM

The volume was adjusted to 1 litre using Milli-Q water.

3.15 Western Transfer Buffer (1x)

Constituents	Volume
Western Transfer Buffer (10X)	50 ml
Methanol	75 ml

The volume was made up to 500 ml using Milli-Q water. The buffer was prepared fresh before use.

3.16 Western Blotting Buffer (10X TBST)

Constituents	Weight	Final concentration (1X)
Tris base	60.5 g	50 mM
NaCl	87.6 g	150 mM

Constituents were dissolved in 800ml Milli-Q water. pH was adjusted to 7.4 with HCl. One milli-litre tween 20 was added and volume adjusted to 1 litre.

3.17 Neutral Buffered Formalin

Component	Volume or weight
Formalin (40%w/v)	50 ml
$NaH_2PO_4.H_2O$	2 g
Na_2HPO_4	3.25 g
dH_2O	450 ml

3.18 Haematoxylin solution (Modified Harris)

Component	Volume or weight
Haematoxylin	5 g
Glycerol	300 ml
Aluminium potassium sulphate	50 g
Glacial Acetic acid	20 ml

Sodium iodate	1 g
dH_2O	700 ml

Haematoxylin was dissolved in a small amount of 95% ethanol (approximately 95%). Potassium alum was dissolved in 250 ml water over gentle heat. It was allowed to cool before adding the remaining water and haematoxylin to it. Sodium iodate, acetic acid and glycerol were added to the solution in the fume hood. The solution was filtered through Whatman No.1 paper and stored in dark to preserve.

3.19 Eosin (Stock Solution)

Component	Volume or weight
5% Aqueous Eosin	20 ml
95% Ethanol	360 ml
Na_2HPO_4	3.25 g
Glacial acetic acid	2 ml
1% Phloxin B	5 ml

3.20 Citrate buffer

Component	Volume or weight
Trisodium citrate (dehydrate)	2.94 g
Milli-Q water	900 ml

The pH was adjusted to 6 with 1 N HCl. Five-hundred microliter of Tween 20 was added and the volume was made up to a litre.

Appendix 4: Statistical analysis

Table 4.1: Comparison of cataract grade of the severe eye between genotypes at each age. *Epha2*$^{+/+}$ (*n* = 18), *Epha2*$^{+/-}$ (*n* = 25) and *Epha2*$^{-/-}$ (*n* = 19)

Age	*p** value; **WT vs HET vs HOMO**	*p*** value from multiple comparisons		
		WT vs HET	**WT vs HOMO**	**HET vs HOMO**
2 months	0.003	0.003	0.122	0.202
4 months	2.6×10^{-10}	0.006	4.1×10^{-8}	5.2×10^{-9}
6 months	1.2×10^{-10}	1.2×10^{-4}	3.8×10^{-8}	2.5×10^{-8}
8 months	4.8×10^{-11}	6.1×10^{-9}	3.9×10^{-8}	0.204

* From Kruskal-Wallis test; ** From Mann-Whitney *U* test; *Epha2*$^{+/+}$ (WT), *Epha2*$^{+/-}$ (HET), *Epha2*$^{-/-}$ (HOMO)

Table 4.2: Comparison of cataract grade of the severe eye in *Epha2*$^{+/+}$, *Epha2*$^{+/-}$, *Epha2*$^{-/-}$ mice over time. *Epha2*$^{+/+}$ (*n* = 18), *Epha2*$^{+/-}$ (*n* = 25) and *Epha2*$^{-/-}$ (*n* = 19)

Genotype	*p** value; **2 months vs 4 months vs 6 months vs 8 months**	*p*** value from multiple comparisons		
		2 months vs 4 months	**4 months vs 6 months**	**6 months vs 8 months**
Epha2$^{+/+}$	0.005	N/A	0.002	0.131
Epha2$^{+/-}$	7.8×10^{-13}	N/A	2×10^{-4}	5.6×10^{-5}
Epha2$^{-/-}$	2.5×10^{-12}	1.2×10^{-4}	N/A	N/A

* From Friedman Test; ** From Wilcoxon Signed Ranks Test

8. References

1. Scanlon VC, Sanders T. The senses. Essentials of Anatomy and Physiology. 6th ed: F.A. Davis Company; 2010.
2. Kolb H. Gross Anatomy of the Eye. In: Kolb H, Fernandez E, Nelson R, editors. The Organization of the Retina and Visual System 2005.
3. Forrester JV, Dick Andrew D., McMenamin Paul G. , Lee WR. Anatomy of the eye and orbit. The Eye Basic Sciences in Practice. 2nd ed: Saunders; 2002.
4. Wormstone IM, Wride MA. The ocular lens: a classic model for development, physiology and disease. Philos Trans R Soc Lond B Biol Sci 2011;366(1568):1190-1192.
5. Michael R, Bron AJ. The ageing lens and cataract: a model of normal and pathological ageing. Philos Trans R Soc Lond B Biol Sci 2011;366(1568):1278-1292.
6. Horwitz J. Alpha-crystallin. Exp Eye Res 2003;76(2):145-153.
7. Bassnett S, Shi Y, Vrensen GF. Biological glass: structural determinants of eye lens transparency. Philos Trans R Soc Lond B Biol Sci 2011;366(1568):1250-1264.
8. McAvoy JW, Chamberlain CG, de Iongh RU, Hales AM, Lovicu FJ. Lens development. Eye (Lond) 1999;13 (Pt 3b):425-437.
9. Gilbert SF. Induction and Competence. Developmental Biology 2000 [cited; 6th:[Available from: http://www.ncbi.nlm.nih.gov/books/NBK9993/
10. Gilbert SF. Development of the Vertebrate Eye. Developmental Biology 2000 [cited; 6th:[Available from: http://www.ncbi.nlm.nih.gov/books/NBK10024/
11. Francis PJ, Berry V, Moore AT, Bhattacharya S. Lens biology: development and human cataractogenesis. Trends Genet 1999;15(5):191-196.
12. Bassnett S, Beebe DC. Coincident loss of mitochondria and nuclei during lens fiber cell differentiation. Dev Dyn 1992;194(2):85-93.
13. Zhou M, Leiberman J, Xu J, Lavker RM. A hierarchy of proliferative cells exists in mouse lens epithelium: implications for lens maintenance. Invest Ophthalmol Vis Sci 2006;47(7):2997-3003.
14. Martinez G, de Iongh RU. The lens epithelium in ocular health and disease. Int J Biochem Cell Biol 2010;42(12):1945-1963.
15. Sparrow JM, Bron AJ, Brown NA, Ayliffe W, Hill AR. The Oxford Clinical Cataract Classification and Grading System. Int Ophthalmol 1986;9(4):207-225.
16. Dubbelman M, Van der Heijde GL, Weeber HA, Vrensen GF. Changes in the internal structure of the human crystalline lens with age and accommodation. Vision Res 2003;43(22):2363-2375.
17. Chamberlain CG, McAvoy JW. Evidence that fibroblast growth factor promotes lens fibre differentiation. Curr Eye Res 1987;6(9):1165-1169.
18. McAvoy JW, Chamberlain CG. Fibroblast growth factor (FGF) induces different responses in lens epithelial cells depending on its concentration. Development 1989;107(2):221-228.
19. Liu H, Mohamed O, Dufort D, Wallace VA. Characterization of Wnt signaling components and activation of the Wnt canonical pathway in the murine retina. Dev Dyn 2003;227(3):323-334.

20. Stump RJ, Ang S, Chen Y, von Bahr T, Lovicu FJ, Pinson K, de Iongh RU, Yamaguchi TP, Sassoon DA, McAvoy JW. A role for Wnt/beta-catenin signaling in lens epithelial differentiation. Dev Biol 2003;259(1):48-61.
21. Choi J, Park SY, Joo CK. Hepatocyte growth factor induces proliferation of lens epithelial cells through activation of ERK1/2 and JNK/SAPK. Invest Ophthalmol Vis Sci 2004;45(8):2696-2704.
22. Ireland ME, Mrock LK. Expression and activation of the epidermal growth factor receptor in differentiating cells of the developing and post-hatching chicken lens. Exp Eye Res 2004;79(3):305-312.
23. Kok A, Lovicu FJ, Chamberlain CG, McAvoy JW. Influence of platelet-derived growth factor on lens epithelial cell proliferation and differentiation. Growth Factors 2002;20(1):27-34.
24. Maddala R, Reddy VN, Epstein DL, Rao V. Growth factor induced activation of Rho and Rac GTPases and actin cytoskeletal reorganization in human lens epithelial cells. Mol Vis 2003;9:329-336.
25. Reddan JR, Wilson-Dziedzic D. Insulin growth factor and epidermal growth factor trigger mitosis in lenses cultured in a serum-free medium. Invest Ophthalmol Vis Sci 1983;24(4):409-416.
26. Shirke S, Faber SC, Hallem E, Makarenkova HP, Robinson ML, Overbeek PA, Lang RA. Misexpression of IGF-I in the mouse lens expands the transitional zone and perturbs lens polarization. Mech Dev 2001;101(1-2):167-174.
27. Chandrasekher G, Sailaja D. Differential activation of phosphatidylinositol 3-kinase signaling during proliferation and differentiation of lens epithelial cells. Invest Ophthalmol Vis Sci 2003;44(10):4400-4411.
28. Ebong S, Chepelinsky AB, Robinson ML, Zhao H, Yu CR, Egwuagu CE. Characterization of the roles of STAT1 and STAT3 signal transduction pathways in mammalian lens development. Mol Vis 2004;10:122-131.
29. Potts JD, Kornacker S, Beebe DC. Activation of the Jak-STAT-signaling pathway in embryonic lens cells. Dev Biol 1998;204(1):277-292.
30. de Iongh RU, Lovicu FJ, Overbeek PA, Schneider MD, Joya J, Hardeman ED, McAvoy JW. Requirement for TGFbeta receptor signaling during terminal lens fiber differentiation. Development 2001;128(20):3995-4010.
31. Hung FC, Zhao S, Chen Q, Overbeek PA. Retinal ablation and altered lens differentiation induced by ocular overexpression of BMP7. Vision Res 2002;42(4):427-438.
32. Zinn KM. Changes in corneal ultrastructure resulting from early lens removal in the developing chick embryo. Invest Ophthalmol Vis Sci 1970;9:165-182.
33. Ashery-Padan R, Marquardt T, Zhou X, Gruss P. Pax6 activity in the lens primordium is required for lens formation and for correct placement of a single retina in the eye. Genes Dev 2000;14(21):2701-2711.
34. Coulombre AJ, Coulombre JL. LENS DEVELOPMENT. I. ROLE OF THE LENS IN EYE GROWTH. J Exp Zool 1964;156:39-47.
35. Wride MA. Lens fibre cell differentiation and organelle loss: many paths lead to clarity. Philos Trans R Soc Lond B Biol Sci 2011;366(1568):1219-1233.

36. Shestopalov VI, Bassnett S. Expression of autofluorescent proteins reveals a novel protein permeable pathway between cells in the lens core. J Cell Sci 2000;113 (Pt 11):1913-1921.
37. Shi Y, Barton K, De Maria A, Petrash JM, Shiels A, Bassnett S. The stratified syncytium of the vertebrate lens. J Cell Sci 2009;122(Pt 10):1607-1615.
38. Giblin FJ. Glutathione: a vital lens antioxidant. J Ocul Pharmacol Ther 2000;16(2):121-135.
39. Jahngen-Hodge J, Cyr D, Laxman E, Taylor A. Ubiquitin and ubiquitin conjugates in human lens. Exp Eye Res 1992;55(6):897-902.
40. Lou MF. Redox regulation in the lens. Prog Retin Eye Res 2003;22(5):657-682.
41. Spector A. Oxidative stress-induced cataract: mechanism of action. FASEB J 1995;9(12):1173-1182.
42. Pascolini D, Mariotti SP. Global estimates of visual impairment: 2010. Br J Ophthalmol 2011.
43. Santana A, Waiswo M. The genetic and molecular basis of congenital cataract. Arq Bras Oftalmol 2011;74(2):136-142.
44. Lambert SR, Drack AV. Infantile cataracts. Surv Ophthalmol 1996;40(6):427-458.
45. Hejtmancik JF. Congenital cataracts and their molecular genetics. Semin Cell Dev Biol 2008;19(2):134-149.
46. Churchill A, Graw J. Clinical and experimental advances in congenital and paediatric cataracts. Philos Trans R Soc Lond B Biol Sci 2011;366(1568):1234-1249.
47. Mickler C, Boden J, Trivedi RH, Wilson ME. Pediatric cataract. Pediatr Ann 2011;40(2):83-87.
48. Tatham A, Odedra N, Tayebjee S, Anwar S, Woodruff G. The incidence of glaucoma following paediatric cataract surgery: a 20-year retrospective study. Eye (Lond) 2010;24(8):1366-1375.
49. Chak M, Rahi JS. Incidence of and factors associated with glaucoma after surgery for congenital cataract: findings from the British Congenital Cataract Study. Ophthalmology 2008;115(6):1013-1018 e1012.
50. Wirth MG, Russell-Eggitt IM, Craig JE, Elder JE, Mackey DA. Aetiology of congenital and paediatric cataract in an Australian population. Br J Ophthalmol 2002;86(7):782-786.
51. Merin S, Crawford JS. The etiology of congenital cataracts. A survey of 386 cases. Can J Ophthalmol 1971;6(3):178-182.
52. Eshaghian J, Streeten BW. Human posterior subcapsular cataract. An ultrastructural study of the posteriorly migrating cells. Arch Ophthalmol 1980;98(1):134-143.
53. Wright KW, Spiegel PH. Lens Abnormalities. Pediatric Ophthalmology and Strabismus. 2nd ed. New York: Springer Science & Business Media; 2003.
54. Sia DI, Muecke J, Hammerton M, Ngy M, Kong A, Morse A, Holmes M, Piseth H, Hamilton C, Selva D. A survey of visual impairment and blindness in children attending four schools for the blind in Cambodia. Ophthalmic Epidemiol 2010;17(4):225-233.
55. Titiyal JS, Pal N, Murthy GV, Gupta SK, Tandon R, Vajpayee RB, Gilbert CE. Causes and temporal trends of blindness and severe visual impairment in children in schools for the blind in North India. Br J Ophthalmol 2003;87(8):941-945.

56. Bermejo E, Martinez-Frias ML. Congenital eye malformations: clinical-epidemiological analysis of 1,124,654 consecutive births in Spain. Am J Med Genet 1998;75(5):497-504.
57. Reddy MA, Francis PJ, Berry V, Bhattacharya SS, Moore AT. Molecular genetic basis of inherited cataract and associated phenotypes. Surv Ophthalmol 2004;49(3):300-315.
58. Shiels A, Bennett TM, Hejtmancik JF. Cat-Map: putting cataract on the map. Mol Vis 2010;16:2007-2015.
59. Millonig G, Muckenthaler MU, Mueller S. Hyperferritinaemia-cataract syndrome: worldwide mutations and phenotype of an increasingly diagnosed genetic disorder. Hum Genomics 2010;4(4):250-262.
60. Burdon KP, McKay JD, Sale MM, Russell-Eggitt IM, Mackey DA, Wirth MG, Elder JE, Nicoll A, Clarke MP, FitzGerald LM, Stankovich JM, Shaw MA, Sharma S, Gajovic S, Gruss P, *et al*. Mutations in a novel gene, NHS, cause the pleiotropic effects of Nance-Horan syndrome, including severe congenital cataract, dental anomalies, and mental retardation. Am J Hum Genet 2003;73(5):1120-1130.
61. Kondo Y, Saitsu H, Miyamoto T, Lee BJ, Nishiyama K, Nakashima M, Tsurusaki Y, Doi H, Miyake N, Kim JH, Yu YS, Matsumoto N. Pathogenic mutations in two families with congenital cataract identified with whole-exome sequencing. Mol Vis 2013;19:384-389.
62. Reis LM, Tyler RC, Muheisen S, Raggio V, Salviati L, Han DP, Costakos D, Yonath H, Hall S, Power P, Semina EV. Whole exome sequencing in dominant cataract identifies a new causative factor, CRYBA2, and a variety of novel alleles in known genes. Hum Genet 2013;132(7):761-770.
63. Jia X, Zhang F, Bai J, Gao L, Zhang X, Sun H, Sun D, Guan R, Sun W, Xu L, Yue Z, Yu Y, Fu S. Combinational analysis of linkage and exome sequencing identifies the causative mutation in a Chinese family with congenital cataract. BMC Med Genet 2013;14:107.
64. Aldahmesh MA, Khan AO, Mohamed JY, Hijazi H, Al-Owain M, Alswaid A, Alkuraya FS. Genomic analysis of pediatric cataract in Saudi Arabia reveals novel candidate disease genes. Genet Med 2012;14(12):955-962.
65. Zhang T, Hua R, Xiao W, Burdon KP, Bhattacharya SS, Craig JE, Shang D, Zhao X, Mackey DA, Moore AT, Luo Y, Zhang J, Zhang X. Mutations of the EPHA2 receptor tyrosine kinase gene cause autosomal dominant congenital cataract. Hum Mutat 2009;30(5):E603-611.
66. Kaul H, Riazuddin SA, Shahid M, Kousar S, Butt NH, Zafar AU, Khan SN, Husnain T, Akram J, Hejtmancik JF, Riazuddin S. Autosomal recessive congenital cataract linked to EPHA2 in a consanguineous Pakistani family. Mol Vis 2010;16:511-517.
67. Shentu XC, Zhao SJ, Zhang L, Miao Q. A novel p.R890C mutation in EPHA2 gene associated with progressive childhood posterior cataract in a Chinese family. Int J Ophthalmol 2013;6(1):34-38.
68. Shiels A, Bennett TM, Knopf HL, Maraini G, Li A, Jiao X, Hejtmancik JF. The EPHA2 gene is associated with cataracts linked to chromosome 1p. Mol Vis 2008;14:2042-2055.

69. Reis LM, Tyler RC, Semina EV. Identification of a novel C-terminal extension mutation in EPHA2 in a family affected with congenital cataract. Mol Vis 2014;20:836-842.
70. Graw J. Cataract mutations as a tool for developmental geneticists. Ophthalmic Res 1996;28 Suppl 1:8-18.
71. Pang M, Su JT, Feng S, Tang ZW, Gu F, Zhang M, Ma X, Yan YB. Effects of congenital cataract mutation R116H on alphaA-crystallin structure, function and stability. Biochim Biophys Acta 2010;1804(4):948-956.
72. Xi JH, Bai F, Gross J, Townsend RR, Menko AS, Andley UP. Mechanism of small heat shock protein function in vivo: a knock-in mouse model demonstrates that the R49C mutation in alpha A-crystallin enhances protein insolubility and cell death. J Biol Chem 2008;283(9):5801-5814.
73. Shiels A, Hejtmancik JF. Genetic origins of cataract. Arch Ophthalmol 2007;125(2):165-173.
74. Abraham AG, Condon NG, West Gower E. The new epidemiology of cataract. Ophthalmol Clin North Am 2006;19(4):415-425.
75. Congdon N, Vingerling JR, Klein BE, West S, Friedman DS, Kempen J, O'Colmain B, Wu SY, Taylor HR. Prevalence of cataract and pseudophakia/aphakia among adults in the United States. Arch Ophthalmol 2004;122(4):487-494.
76. Murthy GV, Gupta SK, Maraini G, Camparini M, Price GM, Dherani M, John N, Chakravarthy U, Fletcher AE. Prevalence of lens opacities in North India: the INDEYE feasibility study. Invest Ophthalmol Vis Sci 2007;48(1):88-95.
77. McGavin DD. The global initiative for the elimination of avoidable blindness - vision 2020: the right to sight. Community Eye Health 1999;12(30):32.
78. Ashwin PT, Shah S, Wolffsohn JS. Advances in cataract surgery. Clin Exp Optom 2009;92(4):333-342.
79. Van Den Berg TJ, Van Rijn LJ, Michael R, Heine C, Coeckelbergh T, Nischler C, Wilhelm H, Grabner G, Emesz M, Barraquer RI, Coppens JE, Franssen L. Straylight effects with aging and lens extraction. Am J Ophthalmol 2007;144(3):358-363.
80. Weeber HA, Eckert G, Pechhold W, van der Heijde RG. Stiffness gradient in the crystalline lens. Graefes Arch Clin Exp Ophthalmol 2007;245(9):1357-1366.
81. Borchman D, Delamere NA, McCauley LA, Paterson CA. Studies on the distribution of cholesterol, phospholipid, and protein in the human and bovine lens. Lens Eye Toxic Res 1989;6(4):703-724.
82. Borchman D, Lamba OP, Yappert MC. Structural characterization of lipid membranes from clear and cataractous human lenses. Exp Eye Res 1993;57(2):199-208.
83. Truscott RJ. Presbyopia. Emerging from a blur towards an understanding of the molecular basis for this most common eye condition. Exp Eye Res 2009;88(2):241-247.
84. Truscott RJ. Age-related nuclear cataract-oxidation is the key. Exp Eye Res 2005;80(5):709-725.
85. Harding JJ. Free and protein-bound glutathione in normal and cataractous human lenses. Biochem J 1970;117(5):957-960.

86. Harrington V, Srivastava OP, Kirk M. Proteomic analysis of water insoluble proteins from normal and cataractous human lenses. Mol Vis 2007;13:1680-1694.
87. Harrington V, McCall S, Huynh S, Srivastava K, Srivastava OP. Crystallins in water soluble-high molecular weight protein fractions and water insoluble protein fractions in aging and cataractous human lenses. Mol Vis 2004;10:476-489.
88. Sweeney MH, Truscott RJ. An impediment to glutathione diffusion in older normal human lenses: a possible precondition for nuclear cataract. Exp Eye Res 1998;67(5):587-595.
89. Vrensen GF, de Wolf A. Calcium distribution in the human eye lens. Ophthalmic Res 1996;28 Suppl 2:78-85.
90. Varma SD, Chand D, Sharma YR, Kuck JF, Jr., Richards RD. Oxidative stress on lens and cataract formation: role of light and oxygen. Curr Eye Res 1984;3(1):35-57.
91. Ren Q, Riquelme MA, Xu J, Yan X, Nicholson BJ, Gu S, Jiang JX. Cataract-causing mutation of human connexin 46 impairs gap junction, but increases hemichannel function and cell death. PLoS One 2013;8(9):e74732.
92. Mathew MC, Ervin AM, Tao J, Davis RM. Antioxidant vitamin supplementation for preventing and slowing the progression of age-related cataract. Cochrane Database Syst Rev 2012;6:CD004567.
93. Randazzo J, Zhang P, Makita J, Blessing K, Kador PF. Orally active multi-functional antioxidants delay cataract formation in streptozotocin (type 1) diabetic and gamma-irradiated rats. PLoS One 2011;6(4):e18980.
94. Rautiainen S, Lindblad BE, Morgenstern R, Wolk A. Total Antioxidant Capacity of the Diet and Risk of Age-Related Cataract: A Population-Based Prospective Cohort of Women. JAMA Ophthalmol 2013.
95. Leske MC, Chylack LT, Jr., He Q, Wu SY, Schoenfeld E, Friend J, Wolfe J. Antioxidant vitamins and nuclear opacities: the longitudinal study of cataract. Ophthalmology 1998;105(5):831-836.
96. Tan AG, Mitchell P, Flood VM, Burlutsky G, Rochtchina E, Cumming RG, Wang JJ. Antioxidant nutrient intake and the long-term incidence of age-related cataract: the Blue Mountains Eye Study. Am J Clin Nutr 2008;87(6):1899-1905.
97. Yoshida M, Takashima Y, Inoue M, Iwasaki M, Otani T, Sasaki S, Tsugane S. Prospective study showing that dietary vitamin C reduced the risk of age-related cataracts in a middle-aged Japanese population. Eur J Nutr 2007;46(2):118-124.
98. Ravindran RD, Vashist P, Gupta SK, Young IS, Maraini G, Camparini M, Jayanthi R, John N, Fitzpatrick KE, Chakravarthy U, Ravilla TD, Fletcher AE. Inverse association of vitamin C with cataract in older people in India. Ophthalmology 2011;118(10):1958-1965 e1952.
99. Rautiainen S, Lindblad BE, Morgenstern R, Wolk A. Vitamin C supplements and the risk of age-related cataract: a population-based prospective cohort study in women. Am J Clin Nutr 2010;91(2):487-493.
100. Zheng Selin J, Rautiainen S, Lindblad BE, Morgenstern R, Wolk A. High-dose supplements of vitamins C and E, low-dose multivitamins, and the risk of age-related cataract: a population-based prospective cohort study of men. Am J Epidemiol 2013;177(6):548-555.

101. Christen WG, Glynn RJ, Sesso HD, Kurth T, MacFadyen J, Bubes V, Buring JE, Manson JE, Gaziano JM. Age-related cataract in a randomized trial of vitamins E and C in men. Arch Ophthalmol 2010;128(11):1397-1405.
102. Ayala MN, Soderberg PG. Vitamin E can protect against ultraviolet radiation-induced cataract in albino rats. Ophthalmic Res 2004;36(5):264-269.
103. Rooban BN, Sasikala V, Sahasranamam V, Abraham A. Vitex negundo modulates selenite-induced opacification and cataractogensis in rat pups. Biol Trace Elem Res 2010;138(1-3):282-292.
104. Vibin M, Siva Priya SG, B NR, Sasikala V, Sahasranamam V, Abraham A. Broccoli regulates protein alterations and cataractogenesis in selenite models. Curr Eye Res 2010;35(2):99-107.
105. Chethan S, Dharmesh SM, Malleshi NG. Inhibition of aldose reductase from cataracted eye lenses by finger millet (Eleusine coracana) polyphenols. Bioorg Med Chem 2008;16(23):10085-10090.
106. Ajani EO, Salako AA, Sharlie PD, Akinleye WA, Adeoye AO, Salau BA, Adebawo OO. Chemopreventive and remediation effect of Hydrocotyl bonariensis Comm. Ex Lam (Apiaceae) leave extract in galactose-induced cataract. J Ethnopharmacol 2009;123(1):134-142.
107. Suryanarayana P, Saraswat M, Mrudula T, Krishna TP, Krishnaswamy K, Reddy GB. Curcumin and turmeric delay streptozotocin-induced diabetic cataract in rats. Invest Ophthalmol Vis Sci 2005;46(6):2092-2099.
108. Suryanarayana P, Krishnaswamy K, Reddy GB. Effect of curcumin on galactose-induced cataractogenesis in rats. Mol Vis 2003;9:223-230.
109. Kumar PA, Suryanarayana P, Reddy PY, Reddy GB. Modulation of alpha-crystallin chaperone activity in diabetic rat lens by curcumin. Mol Vis 2005;11:561-568.
110. Grama CN, Suryanarayana P, Patil MA, Raghu G, Balakrishna N, Kumar MN, Reddy GB. Efficacy of biodegradable curcumin nanoparticles in delaying cataract in diabetic rat model. PLoS One 2013;8(10):e78217.
111. Sasaki K, Sasaki H, Jonasson F, Kojima M, Cheng HM. Racial differences of lens transparency properties with aging and prevalence of age-related cataract applying a WHO classification system. Ophthalmic Res 2004;36(6):332-340.
112. Leske MC, Wu SY, Nemesure B, Hennis A. Causes of visual loss and their risk factors: an incidence summary from the Barbados Eye Studies. Rev Panam Salud Publica 2010;27(4):259-267.
113. Zhang JS, Xu L, Wang YX, You QS, Wang JD, Jonas JB. Five-year incidence of age-related cataract and cataract surgery in the adult population of greater Beijing: the Beijing Eye Study. Ophthalmology 2011;118(4):711-718.
114. Rosman M, Zheng Y, Lamoureux E, Saw SM, Aung T, Tay WT, Wang JJ, Mitchell P, Tai ES, Wong TY. Review of key findings from the Singapore Malay Eye Study (SiMES-1). Singapore Med J 2012;53(2):82-87.
115. West SK, Duncan DD, Munoz B, Rubin GS, Fried LP, Bandeen-Roche K, Schein OD. Sunlight exposure and risk of lens opacities in a population-based study: the Salisbury Eye Evaluation project. JAMA 1998;280(8):714-718.
116. Vashist P, Talwar B, Gogoi M, Maraini G, Camparini M, Ravindran RD, Murthy GV, Fitzpatrick KE, John N, Chakravarthy U, Ravilla TD, Fletcher AE. Prevalence

of cataract in an older population in India: the India study of age-related eye disease. Ophthalmology 2011;118(2):272-278 e271-272.
117. West SK, Valmadrid CT. Epidemiology of risk factors for age-related cataract. Surv Ophthalmol 1995;39(4):323-334.
118. Abraham AG, Cox C, West S. The differential effect of ultraviolet light exposure on cataract rate across regions of the lens. Invest Ophthalmol Vis Sci 2010;51(8):3919-3923.
119. Truscott RJ, Wood AM, Carver JA, Sheil MM, Stutchbury GM, Zhu J, Kilby GW. A new UV-filter compound in human lenses. FEBS Lett 1994;348(2):173-176.
120. Taylor LM, Aquilina JA, Willis RH, Jamie JF, Truscott RJ. Identification of a new human lens UV filter compound. FEBS Lett 2001;509(1):6-10.
121. Van Heyningen R. Fluorescent glucoside in the human lens. Nature 1971;230(5293):393-394.
122. Wood AM, Truscott RJ. Ultraviolet filter compounds in human lenses: 3-hydroxykynurenine glucoside formation. Vision Res 1994;34(11):1369-1374.
123. Taylor LM, Andrew Aquilina J, Jamie JF, Truscott RJ. UV filter instability: consequences for the human lens. Exp Eye Res 2002;75(2):165-175.
124. Bova LM, Sweeney MH, Jamie JF, Truscott RJ. Major changes in human ocular UV protection with age. Invest Ophthalmol Vis Sci 2001;42(1):200-205.
125. McCarty CA, Nanjan MB, Taylor HR. Attributable risk estimates for cataract to prioritize medical and public health action. Invest Ophthalmol Vis Sci 2000;41(12):3720-3725.
126. Raman R, Pal SS, Adams JS, Rani PK, Vaitheeswaran K, Sharma T. Prevalence and risk factors for cataract in diabetes: Sankara Nethralaya Diabetic Retinopathy Epidemiology and Molecular Genetics Study, report no. 17. Invest Ophthalmol Vis Sci 2010;51(12):6253-6261.
127. Richter GM, Choudhury F, Torres M, Azen SP, Varma R. Risk factors for incident cortical, nuclear, posterior subcapsular, and mixed lens opacities: the Los Angeles Latino eye study. Ophthalmology 2012;119(10):2040-2047.
128. Kuang TM, Tsai SY, Liu CJ, Ko YC, Lee SM, Chou P. Seven-year incidence of age-related cataracts among an elderly Chinese population in Shihpai, Taiwan: The Shihpai Eye Study. Invest Ophthalmol Vis Sci 2013;54(9):6409-6415.
129. Klein BE, Klein R, Moss SE. Prevalence of cataracts in a population-based study of persons with diabetes mellitus. Ophthalmology 1985;92(9):1191-1196.
130. Sankeshi V, Kumar PA, Naik RR, Sridhar G, Kumar MP, Gopal VV, Raju TN. Inhibition of aldose reductase by Aegle marmelos and its protective role in diabetic cataract. J Ethnopharmacol 2013;149(1):215-221.
131. Zhang P, Xing K, Randazzo J, Blessing K, Lou MF, Kador PF. Osmotic stress, not aldose reductase activity, directly induces growth factors and MAPK signaling changes during sugar cataract formation. Exp Eye Res 2012;101:36-43.
132. Franke S, Dawczynski J, Strobel J, Niwa T, Stahl P, Stein G. Increased levels of advanced glycation end products in human cataractous lenses. J Cataract Refract Surg 2003;29(5):998-1004.
133. Bras ID, Colitz CM, Kusewitt DF, Chandler H, Lu P, Gemensky-Metzler AJ, Wilkie DA. Evaluation of advanced glycation end-products in diabetic and

inherited canine cataracts. Graefes Arch Clin Exp Ophthalmol 2007;245(2):249-257.
134. Obrosova IG, Stevens MJ. Effect of dietary taurine supplementation on GSH and NAD(P)-redox status, lipid peroxidation, and energy metabolism in diabetic precataractous lens. Invest Ophthalmol Vis Sci 1999;40(3):680-688.
135. Lin HJ, Huang YC, Lin JM, Liao WL, Wu JY, Chen CH, Chou YC, Chen LA, Lin CJ, Tsai FJ. Novel susceptibility genes associated with diabetic cataract in a Taiwanese population. Ophthalmic Genet 2013;34(1-2):35-42.
136. Tan JS, Wang JJ, Younan C, Cumming RG, Rochtchina E, Mitchell P. Smoking and the long-term incidence of cataract: the Blue Mountains Eye Study. Ophthalmic Epidemiol 2008;15(3):155-161.
137. Wu R, Wang JJ, Mitchell P, Lamoureux EL, Zheng Y, Rochtchina E, Tan AG, Wong TY. Smoking, socioeconomic factors, and age-related cataract: The Singapore Malay Eye study. Arch Ophthalmol 2010;128(8):1029-1035.
138. Ye J, He J, Wang C, Wu H, Shi X, Zhang H, Xie J, Lee SY. Smoking and risk of age-related cataract: a meta-analysis. Invest Ophthalmol Vis Sci 2012;53(7):3885-3895.
139. West S. Epidemiology of cataract: accomplishments over 25 years and future directions. Ophthalmic Epidemiol 2007;14(4):173-178.
140. Kalariya NM, Nair B, Kalariya DK, Wills NK, van Kuijk FJ. Cadmium-induced induction of cell death in human lens epithelial cells: implications to smoking associated cataractogenesis. Toxicol Lett 2010;198(1):56-62.
141. Lindblad BE, Hakansson N, Wolk A. Smoking Cessation and the Risk of Cataract: A Prospective Cohort Study of Cataract Extraction Among Men. JAMA Ophthalmol 2014.
142. Lindblad BE, Hakansson N, Svensson H, Philipson B, Wolk A. Intensity of smoking and smoking cessation in relation to risk of cataract extraction: a prospective study of women. Am J Epidemiol 2005;162(1):73-79.
143. Koo E, Chang JR, Agron E, Clemons TE, Sperduto RD, Ferris FL, 3rd, Chew EY. Ten-year incidence rates of age-related cataract in the Age-Related Eye Disease Study (AREDS): AREDS report no. 33. Ophthalmic Epidemiol 2013;20(2):71-81.
144. Duan XR, Liang YB, Wang NL, Wong TY, Sun LP, Yang XH, Tao QS, Yuan RZ, Friedman DS. Prevalence and associations of cataract in a rural Chinese adult population: the Handan Eye Study. Graefes Arch Clin Exp Ophthalmol 2013;251(1):203-212.
145. Kanthan GL, Wang JJ, Rochtchina E, Tan AG, Lee A, Chia EM, Mitchell P. Ten-year incidence of age-related cataract and cataract surgery in an older Australian population. The Blue Mountains Eye Study. Ophthalmology 2008;115(5):808-814 e801.
146. Klein BE, Klein R, Lee KE, Gangnon RE. Incidence of age-related cataract over a 15-year interval the Beaver Dam Eye Study. Ophthalmology 2008;115(3):477-482.
147. Chang JR, Koo E, Agron E, Hallak J, Clemons T, Azar D, Sperduto RD, Ferris FL, 3rd, Chew EY. Risk factors associated with incident cataracts and cataract surgery in the Age-related Eye Disease Study (AREDS): AREDS report number 32. Ophthalmology 2011;118(11):2113-2119.

148. Lindblad BE, Hakansson N, Philipson B, Wolk A. Hormone replacement therapy in relation to risk of cataract extraction: a prospective study of women. Ophthalmology 2010;117(3):424-430.
149. Freeman EE, Munoz B, Schein OD, West SK. Incidence and progression of lens opacities: effect of hormone replacement therapy and reproductive factors. Epidemiology 2004;15(4):451-457.
150. Kanthan GL, Wang JJ, Burlutsky G, Rochtchina E, Cumming RG, Mitchell P. Exogenous oestrogen exposure, female reproductive factors and the long-term incidence of cataract: the Blue Mountains Eye Study. Acta Ophthalmol 2010;88(7):773-778.
151. Lai K, Cui J, Ni S, Zhang Y, He J, Yao K. The effects of postmenopausal hormone use on cataract: a meta-analysis. PLoS One 2013;8(10):e78647.
152. Kanthan GL, Mitchell P, Rochtchina E, Cumming RG, Wang JJ. Myopia and the long-term incidence of cataract and cataract surgery: the Blue Mountains Eye Study. Clin Experiment Ophthalmol 2013.
153. Pan CW, Boey PY, Cheng CY, Saw SM, Tay WT, Wang JJ, Tan AG, Mitchell P, Wong TY. Myopia, axial length, and age-related cataract: the Singapore Malay eye study. Invest Ophthalmol Vis Sci 2013;54(7):4498-4502.
154. Pan CW, Cheng CY, Saw SM, Wang JJ, Wong TY. Myopia and age-related cataract: a systematic review and meta-analysis. Am J Ophthalmol 2013;156(5):1021-1033 e1021.
155. Zhu XJ, Zhou P, Zhang KK, Yang J, Luo Y, Lu Y. Epigenetic Regulation of alphaA-crystallin in High Myopia-Induced Dark Nuclear Cataract. PLoS One 2013;8(12):e81900.
156. Kanthan GL, Mitchell P, Burlutsky G, Rochtchina E, Wang JJ. Pseudoexfoliation syndrome and the long-term incidence of cataract and cataract surgery: the blue mountains eye study. Am J Ophthalmol 2013;155(1):83-88 e81.
157. Kaimbo Wa Kaimbo D. Pseudoexfoliation syndrome in Congolese patients. J Fr Ophtalmol 2012;35(1):40-45.
158. Rouhiainen H, Terasvirta M. Presence of pseudoexfoliation on clear and opacified crystalline lenses in an aged population. Ophthalmologica 1992;204(2):67-70.
159. Puska P, Tarkkanen A. Exfoliation syndrome as a risk factor for cataract development: five-year follow-up of lens opacities in exfoliation syndrome. J Cataract Refract Surg 2001;27(12):1992-1998.
160. Chandrasekaran S, Cumming RG, Rochtchina E, Mitchell P. Associations between elevated intraocular pressure and glaucoma, use of glaucoma medications, and 5-year incident cataract: the Blue Mountains Eye Study. Ophthalmology 2006;113(3):417-424.
161. Klein BE, Klein R, Lee KE, Danforth LG. Drug use and five-year incidence of age-related cataracts: The Beaver Dam Eye Study. Ophthalmology 2001;108(9):1670-1674.
162. Wang JJ, Rochtchina E, Tan AG, Cumming RG, Leeder SR, Mitchell P. Use of inhaled and oral corticosteroids and the long-term risk of cataract. Ophthalmology 2009;116(4):652-657.

163. Klein BE, Klein R, Lee KE, Meuer SM. Socioeconomic and lifestyle factors and the 10-year incidence of age-related cataracts. Am J Ophthalmol 2003;136(3):506-512.
164. Kanthan GL, Mitchell P, Burlutsky G, Wang JJ. Alcohol consumption and the long-term incidence of cataract and cataract surgery: the Blue Mountains Eye Study. Am J Ophthalmol 2010;150(3):434-440 e431.
165. Lu M, Taylor A, Chylack LT, Jr., Rogers G, Hankinson SE, Willett WC, Jacques PF. Dietary fat intake and early age-related lens opacities. Am J Clin Nutr 2005;81(4):773-779.
166. Theodoropoulou S, Samoli E, Theodossiadis PG, Papathanassiou M, Lagiou A, Lagiou P, Tzonou A. Diet and cataract: a case-control study. Int Ophthalmol 2014;34(1):59-68.
167. Hammond CJ, Duncan DD, Snieder H, de Lange M, West SK, Spector TD, Gilbert CE. The heritability of age-related cortical cataract: the twin eye study. Invest Ophthalmol Vis Sci 2001;42(3):601-605.
168. Congdon N, Broman KW, Lai H, Munoz B, Bowie H, Gilbert D, Wojciechowski R, West SK. Cortical, but not posterior subcapsular, cataract shows significant familial aggregation in an older population after adjustment for possible shared environmental factors. Ophthalmology 2005;112(1):73-77.
169. Congdon N, Broman KW, Lai H, Munoz B, Bowie H, Gilber D, Wojciechowski R, Alston C, West SK. Nuclear cataract shows significant familial aggregation in an older population after adjustment for possible shared environmental factors. Invest Ophthalmol Vis Sci 2004;45(7):2182-2186.
170. Zhou Z, Wang B, Hu S, Zhang C, Ma X, Qi Y. Genetic variations in GJA3, GJA8, LIM2, and age-related cataract in the Chinese population: a mutation screening study. Mol Vis 2011;17:621-626.
171. Shi Y, Shi X, Jin Y, Miao A, Bu L, He J, Jiang H, Lu Y, Kong X, Hu L. Mutation screening of HSF4 in 150 age-related cataract patients. Mol Vis 2008;14:1850-1855.
172. Zuercher J, Neidhardt J, Magyar I, Labs S, Moore AT, Tanner FC, Waseem N, Schorderet DF, Munier FL, Bhattacharya S, Berger W, Kloeckener-Gruissem B. Alterations of the 5'untranslated region of SLC16A12 lead to age-related cataract. Invest Ophthalmol Vis Sci 2010;51(7):3354-3361.
173. Bhagyalaxmi SG, Srinivas P, Barton KA, Kumar KR, Vidyavathi M, Petrash JM, Bhanuprakash Reddy G, Padma T. A novel mutation (F71L) in alphaA-crystallin with defective chaperone-like function associated with age-related cataract. Biochim Biophys Acta 2009;1792(10):974-981.
174. Zhou P, Luo Y, Liu X, Fan L, Lu Y. Down-regulation and CpG island hypermethylation of CRYAA in age-related nuclear cataract. FASEB J 2012;26(12):4897-4902.
175. Karas N, Gobec L, Pfeifer V, Mlinar B, Battelino T, Lukac-Bajalo J. Mutations in galactose-1-phosphate uridyltransferase gene in patients with idiopathic presenile cataract. J Inherit Metab Dis 2003;26(7):699-704.
176. Zhang Y, Zhang L, Sun D, Li Z, Wang L, Liu P. Genetic polymorphisms of superoxide dismutases, catalase, and glutathione peroxidase in age-related cataract. Mol Vis 2011;17:2325-2332.

177. Mamata M, Sridhar G, Reddy KR, Nagaraju T, Padma T. Is the variant c.422+90G --> A in intron 4 of indoleamine 2, 3 -dioxygenase (IDO) gene related to age related cataracts? Mol Vis 2011;17:1203-1208.
178. Zetterberg M, Tasa G, Prince JA, Palmer M, Juronen E, Veromann S, Teesalu P, Karlsson JO, Blennow K, Zetterberg H. Methylenetetrahydrofolate reductase genetic polymorphisms in patients with cataract. Am J Ophthalmol 2005;140(5):932-934.
179. Guven M, Unal M, Sarici A, Ozaydin A, Batar B, Devranoglu K. Glutathione-S-transferase M1 and T1 genetic polymorphisms and the risk of cataract development: a study in the Turkish population. Curr Eye Res 2007;32(5):447-454.
180. Juronen E, Tasa G, Veromann S, Parts L, Tiidla A, Pulges R, Panov A, Soovere L, Koka K, Mikelsaar AV. Polymorphic glutathione S-transferases as genetic risk factors for senile cortical cataract in Estonians. Invest Ophthalmol Vis Sci 2000;41(8):2262-2267.
181. Jiang Z, Liang K, Zhang Q, Tao L. Glutathione S-transferases polymorphisms confer susceptibility to senile cortical cataract in the Han Chinese population. Mol Vis 2012;18:1247-1252.
182. Meyer D, Parkin DP, Seifart HI, Maritz JS, Engelbrecht AH, Werely CJ, van Helden PD. NAT2 slow acetylator function as a risk indicator for age-related cataract formation. Pharmacogenetics 2003;13(5):285-289.
183. Tamer L, Yilmaz A, Yildirim H, Ayaz L, Ates NA, Karakas S, Oz O, Yildirim O, Atik U. N-acetyltransferase 2 phenotype may be associated with susceptibility to age-related cataract. Curr Eye Res 2005;30(10):835-839.
184. Padma G, Mamata M, Reddy KR, Padma T. Polymorphisms in two DNA repair genes (XPD and XRCC1)--association with age related cataracts. Mol Vis 2011;17:127-133.
185. Luo YF, Wang BB, Zhou Z, Ding XC, Hu SS, Zhou GK, Ma X, Qi YH. Polymorphisms of the DNA repair genes XPD and XRCC1 and the risk of age-related cataract development in Han Chinese. Curr Eye Res 2011;36(7):632-636.
186. Chandra A, Raza ST, Abbas S, Singh L, Rizvi S, Ahmed F, Eba A, Mahdi F. Polymorphism of GST and FTO Genes in Risk Prediction of Cataract among a North Indian Population. Ophthalmic Genet 2014.
187. Lim LS, Tai ES, Aung T, Tay WT, Saw SM, Seielstad M, Wong TY. Relation of age-related cataract with obesity and obesity genes in an Asian population. Am J Epidemiol 2009;169(10):1267-1274.
188. Peng CH, Liu JH, Woung LC, Lin TJ, Chiou SH, Tseng PC, Du WY, Cheng CK, Hu CC, Chien KH, Chen SJ. MicroRNAs and cataracts: correlation among let-7 expression, age and the severity of lens opacity. Br J Ophthalmol 2012;96(5):747-751.
189. Iyengar SK, Klein BE, Klein R, Jun G, Schick JH, Millard C, Liptak R, Russo K, Lee KE, Elston RC. Identification of a major locus for age-related cortical cataract on chromosome 6p12-q12 in the Beaver Dam Eye Study. Proc Natl Acad Sci U S A 2004;101(40):14485-14490.
190. Tan W, Hou S, Jiang Z, Hu Z, Yang P, Ye J. Association of EPHA2 polymorphisms and age-related cortical cataract in a Han Chinese population. Mol Vis 2011;17:1553-1558.

191. Jun G, Guo H, Klein BE, Klein R, Wang JJ, Mitchell P, Miao H, Lee KE, Joshi T, Buck M, Chugha P, Bardenstein D, Klein AP, Bailey-Wilson JE, Gong X, *et al.* EPHA2 is associated with age-related cortical cataract in mice and humans. PLoS Genet 2009;5(7):e1000584.
192. Sundaresan P, Ravindran RD, Vashist P, Shanker A, Nitsch D, Talwar B, Maraini G, Camparini M, Nonyane BA, Smeeth L, Chakravarthy U, Hejtmancik JF, Fletcher AE. EPHA2 Polymorphisms and Age-Related Cataract in India. PLoS One 2012;7(3):e33001.
193. Giavini E, Prati M. Morphogenesis of diabetes-induced congenital cataract in the rat. Acta Anat (Basel) 1990;137(2):132-136.
194. Sasaki K, Kuriyama H, Yeh LI, Fukuda M. Studies on diabetic cataract in rats induced by streptozotocin. I. Photodocumentation of lens opacification. Ophthalmic Res 1983;15(4):185-190.
195. Jose JG. Posterior cataract induction by UV-B radiation in albino mice. Exp Eye Res 1986;42(1):11-20.
196. Michael R, Vrensen GF, van Marle J, Lofgren S, Soderberg PG. Repair in the rat lens after threshold ultraviolet radiation injury. Invest Ophthalmol Vis Sci 2000;41(1):204-212.
197. Michael R, Brismar H. Lens growth and protein density in the rat lens after in vivo exposure to ultraviolet radiation. Invest Ophthalmol Vis Sci 2001;42(2):402-408.
198. Galichanin K, Svedlund J, Soderberg P. Kinetics of GADD45alpha, TP53 and CASP3 gene expression in the rat lens in vivo in response to exposure to double threshold dose of UV-B radiation. Exp Eye Res 2012;97(1):19-23.
199. Galichanin K, Lofgren S, Bergmanson J, Soderberg P. Evolution of damage in the lens after in vivo close to threshold exposure to UV-B radiation: cytomorphological study of apoptosis. Exp Eye Res 2010;91(3):369-377.
200. Xiong H, Cheng HM. Aqueous/vitreous tonicity in "sugar' cataracts. Ophthalmic Res 1989;21(4):292-296.
201. Suryanarayana P, Patil MA, Reddy GB. Insulin resistance mediated biochemical alterations in eye lens of neonatal streptozotocin-induced diabetic rat. Indian J Exp Biol 2011;49(10):749-755.
202. Kuck JF, Kuwabara T, Kuck KD. The Emory mouse cataract: an animal model for human senile cataract. Curr Eye Res 1981;1(11):643-649.
203. Shang F, Nowell T, Jr., Gong X, Smith DE, Dallal GE, Khu P, Taylor A. Sex-linked differences in cataract progression in Emory mice. Exp Eye Res 2002;75(1):109-111.
204. Congdon NT, West ST, Duncan DT, Fisher DT, Vitale ST, Rieger KT, Urist JT, Hazelwood DT, Sanchez AT, Pham T, Cole L, McNaughton C. The effect of pantethine and ultraviolet-B radiation on the development of lenticular opacity in the emory mouse. Curr Eye Res 2000;20(1):17-24.
205. Hosokawa M, Takeshita S, Higuchi K, Shimizu K, Irino M, Toda K, Honma A, Matsumura A, Yasuhira K, Takeda T. Cataract and other ophthalmic lesions in senescence accelerated mouse (SAM). Morphology and incidence of senescence associated ophthalmic changes in mice. Exp Eye Res 1984;38(2):105-114.

206. Hosokawa M, Ashida Y, Tsuboyama T, Chen WH, Takeda T. Cataract in senescence accelerated mouse (SAM). 2. Development of a new strain of mouse with late-appearing cataract. Exp Eye Res 1988;47(4):629-640.
207. Wolf N, Penn P, Pendergrass W, Van Remmen H, Bartke A, Rabinovitch P, Martin GM. Age-related cataract progression in five mouse models for anti-oxidant protection or hormonal influence. Exp Eye Res 2005;81(3):276-285.
208. Dubrovsky YV, Samsa WE, Kondratov RV. Deficiency of circadian protein CLOCK reduces lifespan and increases age-related cataract development in mice. Aging 2010;2(12):936-944.
209. Worgul BV, Smilenov L, Brenner DJ, Junk A, Zhou W, Hall EJ. Atm heterozygous mice are more sensitive to radiation-induced cataracts than are their wild-type counterparts. Proc Natl Acad Sci U S A 2002;99(15):9836-9839.
210. Puk O, Ahmad N, Wagner S, Hrabe de Angelis M, Graw J. First mutation in the betaA2-crystallin encoding gene is associated with small lenses and age-related cataracts. Invest Ophthalmol Vis Sci 2011;52(5):2571-2576.
211. Fan X, Liu X, Hao S, Wang B, Robinson ML, Monnier VM. The LEGSKO mouse: a mouse model of age-related nuclear cataract based on genetic suppression of lens glutathione synthesis. PLoS One 2012;7(11):e50832.
212. Shi Y, De Maria A, Bennett T, Shiels A, Bassnett S. A Role for Epha2 in Cell Migration and Refractive Organization of the Ocular Lens. Invest Ophthalmol Vis Sci 2011.
213. Cheng C, Gong X. Diverse Roles of Eph/ephrin Signaling in the Mouse Lens. PLoS One 2011;6(11):e28147.
214. Cheng C, Ansari MM, Cooper JA, Gong X. EphA2 and Src regulate equatorial cell morphogenesis during lens development. Development 2013;140(20):4237-4245.
215. Park JE, Son AI, Hua R, Wang L, Zhang X, Zhou R. Human Cataract Mutations in EPHA2 SAM Domain Alter Receptor Stability and Function. PLoS One 2012;7(5):e36564.
216. Pasquale EB. Eph receptors and ephrins in cancer: bidirectional signalling and beyond. Nat Rev Cancer 2010;10(3):165-180.
217. Pitulescu ME, Adams RH. Eph/ephrin molecules--a hub for signaling and endocytosis. Genes Dev 2010;24(22):2480-2492.
218. Himanen JP, Chumley MJ, Lackmann M, Li C, Barton WA, Jeffrey PD, Vearing C, Geleick D, Feldheim DA, Boyd AW, Henkemeyer M, Nikolov DB. Repelling class discrimination: ephrin-A5 binds to and activates EphB2 receptor signaling. Nat Neurosci 2004;7(5):501-509.
219. Smith A, Robinson V, Patel K, Wilkinson DG. The EphA4 and EphB1 receptor tyrosine kinases and ephrin-B2 ligand regulate targeted migration of branchial neural crest cells. Curr Biol 1997;7(8):561-570.
220. Himanen JP, Yermekbayeva L, Janes PW, Walker JR, Xu K, Atapattu L, Rajashankar KR, Mensinga A, Lackmann M, Nikolov DB, Dhe-Paganon S. Architecture of Eph receptor clusters. Proc Natl Acad Sci U S A 2010;107(24):10860-10865.
221. Cooper MA, Son AI, Komlos D, Sun Y, Kleiman NJ, Zhou R. Loss of ephrin-A5 function disrupts lens fiber cell packing and leads to cataract. Proc Natl Acad Sci U S A 2008;105(43):16620-16625.

222. Yin Y, Yamashita Y, Noda H, Okafuji T, Go MJ, Tanaka H. EphA receptor tyrosine kinases interact with co-expressed ephrin-A ligands in cis. Neurosci Res 2004;48(3):285-296.
223. Larsen AB, Stockhausen MT, Poulsen HS. Cell adhesion and EGFR activation regulate EphA2 expression in cancer. Cell Signal 2010;22(4):636-644.
224. Leroy C, Fialin C, Sirvent A, Simon V, Urbach S, Poncet J, Robert B, Jouin P, Roche S. Quantitative phosphoproteomics reveals a cluster of tyrosine kinases that mediates SRC invasive activity in advanced colon carcinoma cells. Cancer Res 2009;69(6):2279-2286.
225. Pasquale EB. Eph receptor signalling casts a wide net on cell behaviour. Nat Rev Mol Cell Biol 2005;6(6):462-475.
226. Iida H, Honda M, Kawai HF, Yamashita T, Shirota Y, Wang BC, Miao H, Kaneko S. Ephrin-A1 expression contributes to the malignant characteristics of {alpha}-fetoprotein producing hepatocellular carcinoma. Gut 2005;54(6):843-851.
227. Nakada M, Drake KL, Nakada S, Niska JA, Berens ME. Ephrin-B3 ligand promotes glioma invasion through activation of Rac1. Cancer Res 2006;66(17):8492-8500.
228. Tanaka M, Kamata R, Sakai R. Phosphorylation of ephrin-B1 via the interaction with claudin following cell-cell contact formation. EMBO J 2005;24(21):3700-3711.
229. Lee HS, Nishanian TG, Mood K, Bong YS, Daar IO. EphrinB1 controls cell-cell junctions through the Par polarity complex. Nat Cell Biol 2008;10(8):979-986.
230. Bong YS, Lee HS, Carim-Todd L, Mood K, Nishanian TG, Tessarollo L, Daar IO. ephrinB1 signals from the cell surface to the nucleus by recruitment of STAT3. Proc Natl Acad Sci U S A 2007;104(44):17305-17310.
231. Jorgensen C, Sherman A, Chen GI, Pasculescu A, Poliakov A, Hsiung M, Larsen B, Wilkinson DG, Linding R, Pawson T. Cell-specific information processing in segregating populations of Eph receptor ephrin-expressing cells. Science 2009;326(5959):1502-1509.
232. Kadison SR, Makinen T, Klein R, Henkemeyer M, Kaprielian Z. EphB receptors and ephrin-B3 regulate axon guidance at the ventral midline of the embryonic mouse spinal cord. J Neurosci 2006;26(35):8909-8914.
233. Du J, Fu C, Sretavan DW. Eph/ephrin signaling as a potential therapeutic target after central nervous system injury. Curr Pharm Des 2007;13(24):2507-2518.
234. Konstantinova I, Nikolova G, Ohara-Imaizumi M, Meda P, Kucera T, Zarbalis K, Wurst W, Nagamatsu S, Lammert E. EphA-Ephrin-A-mediated beta cell communication regulates insulin secretion from pancreatic islets. Cell 2007;129(2):359-370.
235. Luo H, Yu G, Tremblay J, Wu J. EphB6-null mutation results in compromised T cell function. J Clin Invest 2004;114(12):1762-1773.
236. Munoz JJ, Alonso CL, Sacedon R, Crompton T, Vicente A, Jimenez E, Varas A, Zapata AG. Expression and function of the Eph A receptors and their ligands ephrins A in the rat thymus. J Immunol 2002;169(1):177-184.
237. Compagni A, Logan M, Klein R, Adams RH. Control of skeletal patterning by ephrinB1-EphB interactions. Dev Cell 2003;5(2):217-230.

238. Parri M, Buricchi F, Giannoni E, Grimaldi G, Mello T, Raugei G, Ramponi G, Chiarugi P. EphrinA1 activates a Src/focal adhesion kinase-mediated motility response leading to rho-dependent actino/myosin contractility. J Biol Chem 2007;282(27):19619-19628.
239. Shamah SM, Lin MZ, Goldberg JL, Estrach S, Sahin M, Hu L, Bazalakova M, Neve RL, Corfas G, Debant A, Greenberg ME. EphA receptors regulate growth cone dynamics through the novel guanine nucleotide exchange factor ephexin. Cell 2001;105(2):233-244.
240. Andres AC, Reid HH, Zurcher G, Blaschke RJ, Albrecht D, Ziemiecki A. Expression of two novel eph-related receptor protein tyrosine kinases in mammary gland development and carcinogenesis. Oncogene 1994;9(5):1461-1467.
241. Miao H, Wang B. Eph/ephrin signaling in epithelial development and homeostasis. Int J Biochem Cell Biol 2009;41(4):762-770.
242. Lickliter JD, Smith FM, Olsson JE, Mackwell KL, Boyd AW. Embryonic stem cells express multiple Eph-subfamily receptor tyrosine kinases. Proc Natl Acad Sci U S A 1996;93(1):145-150.
243. Connor RJ, Menzel P, Pasquale EB. Expression and tyrosine phosphorylation of Eph receptors suggest multiple mechanisms in patterning of the visual system. Dev Biol 1998;193(1):21-35.
244. Studer M, Gavalas A, Marshall H, Ariza-McNaughton L, Rijli FM, Chambon P, Krumlauf R. Genetic interactions between Hoxa1 and Hoxb1 reveal new roles in regulation of early hindbrain patterning. Development 1998;125(6):1025-1036.
245. Magal E, Holash JA, Toso RJ, Chang D, Lindberg RA, Pasquale EB. B61, a ligand for the Eck receptor protein-tyrosine kinase, exhibits neurotrophic activity in cultures of rat spinal cord neurons. J Neurosci Res 1996;43(6):735-744.
246. Lindberg RA, Hunter T. cDNA cloning and characterization of eck, an epithelial cell receptor protein-tyrosine kinase in the eph/elk family of protein kinases. Mol Cell Biol 1990;10(12):6316-6324.
247. Kinch MS, Kilpatrick KE, Zhong C. Identification of tyrosine phosphorylated adhesion proteins in human cancer cells. Hybridoma 1998;17(3):227-235.
248. Walker-Daniels J, Coffman K, Azimi M, Rhim JS, Bostwick DG, Snyder P, Kerns BJ, Waters DJ, Kinch MS. Overexpression of the EphA2 tyrosine kinase in prostate cancer. Prostate 1999;41(4):275-280.
249. Thaker PH, Deavers M, Celestino J, Thornton A, Fletcher MS, Landen CN, Kinch MS, Kiener PA, Sood AK. EphA2 expression is associated with aggressive features in ovarian carcinoma. Clin Cancer Res 2004;10(15):5145-5150.
250. Fox BP, Kandpal RP. Invasiveness of breast carcinoma cells and transcript profile: Eph receptors and ephrin ligands as molecular markers of potential diagnostic and prognostic application. Biochem Biophys Res Commun 2004;318(4):882-892.
251. Miyazaki T, Kato H, Fukuchi M, Nakajima M, Kuwano H. EphA2 overexpression correlates with poor prognosis in esophageal squamous cell carcinoma. Int J Cancer 2003;103(5):657-663.
252. Kataoka H, Igarashi H, Kanamori M, Ihara M, Wang JD, Wang YJ, Li ZY, Shimamura T, Kobayashi T, Maruyama K, Nakamura T, Arai H, Kajimura M, Hanai H, Tanaka M, *et al.* Correlation of EPHA2 overexpression with high

microvessel count in human primary colorectal cancer. Cancer Sci 2004;95(2):136-141.
253. Kinch MS, Moore MB, Harpole DH, Jr. Predictive value of the EphA2 receptor tyrosine kinase in lung cancer recurrence and survival. Clin Cancer Res 2003;9(2):613-618.
254. Wykosky J, Gibo DM, Stanton C, Debinski W. EphA2 as a novel molecular marker and target in glioblastoma multiforme. Mol Cancer Res 2005;3(10):541-551.
255. Lin YG, Han LY, Kamat AA, Merritt WM, Landen CN, Deavers MT, Fletcher MS, Urbauer DL, Kinch MS, Sood AK. EphA2 overexpression is associated with angiogenesis in ovarian cancer. Cancer 2007;109(2):332-340.
256. Hess AR, Seftor EA, Gruman LM, Kinch MS, Seftor RE, Hendrix MJ. VE-cadherin regulates EphA2 in aggressive melanoma cells through a novel signaling pathway: implications for vasculogenic mimicry. Cancer Biol Ther 2006;5(2):228-233.
257. Zelinski DP, Zantek ND, Stewart JC, Irizarry AR, Kinch MS. EphA2 overexpression causes tumorigenesis of mammary epithelial cells. Cancer Res 2001;61(5):2301-2306.
258. Hu M, Carles-Kinch KL, Zelinski DP, Kinch MS. EphA2 induction of fibronectin creates a permissive microenvironment for malignant cells. Mol Cancer Res 2004;2(10):533-540.
259. Zantek ND, Azimi M, Fedor-Chaiken M, Wang B, Brackenbury R, Kinch MS. E-cadherin regulates the function of the EphA2 receptor tyrosine kinase. Cell Growth Differ 1999;10(9):629-638.
260. Kikawa KD, Vidale DR, Van Etten RL, Kinch MS. Regulation of the EphA2 kinase by the low molecular weight tyrosine phosphatase induces transformation. J Biol Chem 2002;277(42):39274-39279.
261. Sulman EP, Tang XX, Allen C, Biegel JA, Pleasure DE, Brodeur GM, Ikegaki N. ECK, a human EPH-related gene, maps to 1p36.1, a common region of alteration in human cancers. Genomics 1997;40(2):371-374.
262. Tanaka M, Ohashi R, Nakamura R, Shinmura K, Kamo T, Sakai R, Sugimura H. Tiam1 mediates neurite outgrowth induced by ephrin-B1 and EphA2. EMBO J 2004;23(5):1075-1088.
263. Edwards CM, Mundy GR. Eph receptors and ephrin signaling pathways: a role in bone homeostasis. Int J Med Sci 2008;5(5):263-272.
264. Goichberg P, Bai Y, D'Amario D, Ferreira-Martins J, Fiorini C, Zheng H, Signore S, del Monte F, Ottolenghi S, D'Alessandro DA, Michler RE, Hosoda T, Anversa P, Kajstura J, Rota M, *et al.* The ephrin A1-EphA2 system promotes cardiac stem cell migration after infarction. Circ Res 2011;108(9):1071-1083.
265. Yang XY, Zhu WJ, Jiang H. Activation of erythropoietin-producing hepatocellular receptor A2 attenuates cell adhesion of human fallopian tube epithelial cells via focal adhesion kinase dephosphorylation. Mol Cell Biochem 2012;361(1-2):259-265.
266. Vaught D, Chen J, Brantley-Sieders DM. Regulation of mammary gland branching morphogenesis by EphA2 receptor tyrosine kinase. Mol Biol Cell 2009;20(10):2572-2581.

267. Trinidad EM, Zapata AG, Alonso-Colmenar LM. Eph-ephrin bidirectional signaling comes into the context of lymphocyte transendothelial migration. Cell Adh Migr 2010;4(3):363-367.
268. Goichberg P, Kannappan R, Cimini M, Bai Y, Sanada F, Sorrentino A, Signore S, Kajstura J, Rota M, Anversa P, Leri A. Age-associated defects in EphA2 signaling impair the migration of human cardiac progenitor cells. Circulation 2013;128(20):2211-2223.
269. Zhang G, Njauw CN, Park JM, Naruse C, Asano M, Tsao H. EphA2 is an essential mediator of UV radiation-induced apoptosis. Cancer Res 2008;68(6):1691-1696.
270. Zelinski DP, Zantek ND, Walker-Daniels J, Peters MA, Taparowsky EJ, Kinch MS. Estrogen and Myc negatively regulate expression of the EphA2 tyrosine kinase. J Cell Biochem 2002;85(4):714-720.
271. McKay JD, Patterson B, Craig JE, Russell-Eggitt IM, Wirth MG, Burdon KP, Hewitt AW, Cohn AC, Kerdraon Y, Mackey DA. The telomere of human chromosome 1p contains at least two independent autosomal dominant congenital cataract genes. Br J Ophthalmol 2005;89(7):831-834.
272. Burdon KP, Wirth MG, Mackey DA, Russell-Eggitt IM, Craig JE, Elder JE, Dickinson JL, Sale MM. Investigation of crystallin genes in familial cataract, and report of two disease associated mutations. Br J Ophthalmol 2004;88(1):79-83.
273. Devi RR, Yao W, Vijayalakshmi P, Sergeev YV, Sundaresan P, Hejtmancik JF. Crystallin gene mutations in Indian families with inherited pediatric cataract. Mol Vis 2008;14:1157-1170.
274. Sun W, Xiao X, Li S, Guo X, Zhang Q. Exome sequencing of 18 Chinese families with congenital cataracts: a new sight of the NHS gene. PLoS One 2014;9(6):e100455.
275. Attebo K, Mitchell P, Smith W. Visual acuity and the causes of visual loss in Australia. The Blue Mountains Eye Study. Ophthalmology 1996;103(3):357-364.
276. NCBI db SNP build 132. 2010 13-10-11 [cited; Available from: http://www.ncbi.nlm.nih.gov/projects/SNP/snp_summary.cgi?build_id=132
277. UCSC Genome Browser. [cited; Available from: http://genome.ucsc.edu/cgi-bin/hgGateway?hgsid=296512353
278. Chenna R, Sugawara H, Koike T, Lopez R, Gibson TJ, Higgins DG, Thompson JD. Multiple sequence alignment with the Clustal series of programs. Nucleic Acids Res 2003;31(13):3497-3500.
279. Adzhubei IA, Schmidt S, Peshkin L, Ramensky VE, Gerasimova A, Bork P, Kondrashov AS, Sunyaev SR. A method and server for predicting damaging missense mutations. Nat Methods 2010;7(4):248-249.
280. Ng PC, Henikoff S. SIFT: Predicting amino acid changes that affect protein function. Nucleic Acids Res 2003;31(13):3812-3814.
281. Exome Variant Server, NHLBI GO Exome Sequencing Project (ESP);. 23-1-12 [cited; Available from: http://evs.gs.washington.edu/EVS/
282. Gulcher J. Microsatellite markers for linkage and association studies. Cold Spring Harb Protoc 2012;2012(4):425-432.
283. Yang J, Luo J, Zhou P, Fan Q, Luo Y, Lu Y. Association of the ephreceptor tyrosinekinase-type A2 (EPHA2) gene polymorphism rs3754334 with age-related cataract risk: a meta-analysis. PLoS One 2013;8(8):e71003.

284. Binns KL, Taylor PP, Sicheri F, Pawson T, Holland SJ. Phosphorylation of tyrosine residues in the kinase domain and juxtamembrane region regulates the biological and catalytic activities of Eph receptors. Mol Cell Biol 2000;20(13):4791-4805.
285. Heibeck TH, Ding SJ, Opresko LK, Zhao R, Schepmoes AA, Yang F, Tolmachev AV, Monroe ME, Camp DG, 2nd, Smith RD, Wiley HS, Qian WJ. An extensive survey of tyrosine phosphorylation revealing new sites in human mammary epithelial cells. J Proteome Res 2009;8(8):3852-3861.
286. Fang WB, Brantley-Sieders DM, Hwang Y, Ham AJ, Chen J. Identification and functional analysis of phosphorylated tyrosine residues within EphA2 receptor tyrosine kinase. J Biol Chem 2008;283(23):16017-16026.
287. Vanhoof G, Goossens F, De Meester I, Hendriks D, Scharpe S. Proline motifs in peptides and their biological processing. FASEB J 1995;9(9):736-744.
288. Rosenberg NA, Pritchard JK, Weber JL, Cann HM, Kidd KK, Zhivotovsky LA, Feldman MW. Genetic structure of human populations. Science 2002;298(5602):2381-2385.
289. Pasquale EB. Eph-ephrin bidirectional signaling in physiology and disease. Cell 2008;133(1):38-52.
290. Rosenberg IM, Goke M, Kanai M, Reinecker HC, Podolsky DK. Epithelial cell kinase-B61: an autocrine loop modulating intestinal epithelial migration and barrier function. Am J Physiol 1997;273(4 Pt 1):G824-832.
291. Tessier-Lavigne M. Eph receptor tyrosine kinases, axon repulsion, and the development of topographic maps. Cell 1995;82(3):345-348.
292. Mori T, Wanaka A, Taguchi A, Matsumoto K, Tohyama M. Differential expressions of the eph family of receptor tyrosine kinase genes (sek, elk, eck) in the developing nervous system of the mouse. Brain Res Mol Brain Res 1995;29(2):325-335.
293. Sefton M, Araujo M, Nieto MA. Novel expression gradients of Eph-like receptor tyrosine kinases in the developing chick retina. Dev Biol 1997;188(2):363-368.
294. Miyoshi J, Takai Y. Molecular perspective on tight-junction assembly and epithelial polarity. Adv Drug Deliv Rev 2005;57(6):815-855.
295. Tanaka M, Kamata R, Sakai R. EphA2 phosphorylates the cytoplasmic tail of Claudin-4 and mediates paracellular permeability. J Biol Chem 2005;280(51):42375-42382.
296. Orsulic S, Kemler R. Expression of Eph receptors and ephrins is differentially regulated by E-cadherin. J Cell Sci 2000;113 (Pt 10):1793-1802.
297. Fang WB, Ireton RC, Zhuang G, Takahashi T, Reynolds A, Chen J. Overexpression of EPHA2 receptor destabilizes adherens junctions via a RhoA-dependent mechanism. J Cell Sci 2008;121(Pt 3):358-368.
298. Wakayama Y, Miura K, Sabe H, Mochizuki N. EphrinA1-EphA2 signal induces compaction and polarization of Madin-Darby canine kidney cells by inactivating ezrin through negative regulation of RhoA. J Biol Chem 2011.
299. Dave A, Craig JE, Sharma S. The status of intercellular junctions in established lens epithelial cell lines. Mol Vis 2012;18:2937-2946.
300. Hidalgo IJ, Raub TJ, Borchardt RT. Characterization of the human colon carcinoma cell line (Caco-2) as a model system for intestinal epithelial permeability. Gastroenterology 1989;96(3):736-749.

301. Strachan T, AP R. PCR, DNA sequencing and *in vitro* mutagenesis. Human Molecular Genetics. 2nd ed. New York: Wiley-Liss; 1999.
302. Laemmli UK. Cleavage of structural proteins during the assembly of the head of bacteriophage T4. Nature 1970;227(5259):680-685.
303. Lewin B. Protein Trafficking. In: Carlson G, editor. Genes VIII: Pearson Prentice Hall; 2004. p. 787-791.
304. Minogue PJ, Liu X, Ebihara L, Beyer EC, Berthoud VM. An aberrant sequence in a connexin46 mutant underlies congenital cataracts. J Biol Chem 2005;280(49):40788-40795.
305. Smalla M, Schmieder P, Kelly M, Ter Laak A, Krause G, Ball L, Wahl M, Bork P, Oschkinat H. Solution structure of the receptor tyrosine kinase EphB2 SAM domain and identification of two distinct homotypic interaction sites. Protein Sci 1999;8(10):1954-1961.
306. Harris BZ, Lim WA. Mechanism and role of PDZ domains in signaling complex assembly. J Cell Sci 2001;114(Pt 18):3219-3231.
307. Hock B, Bohme B, Karn T, Yamamoto T, Kaibuchi K, Holtrich U, Holland S, Pawson T, Rubsamen-Waigmann H, Strebhardt K. PDZ-domain-mediated interaction of the Eph-related receptor tyrosine kinase EphB3 and the ras-binding protein AF6 depends on the kinase activity of the receptor. Proc Natl Acad Sci U S A 1998;95(17):9779-9784.
308. Leighton PA, Mitchell KJ, Goodrich LV, Lu X, Pinson K, Scherz P, Skarnes WC, Tessier-Lavigne M. Defining brain wiring patterns and mechanisms through gene trapping in mice. Nature 2001;410(6825):174-179.
309. Mitchell KJ, Pinson KI, Kelly OG, Brennan J, Zupicich J, Scherz P, Leighton PA, Goodrich LV, Lu X, Avery BJ, Tate P, Dill K, Pangilinan E, Wakenight P, Tessier-Lavigne M, *et al*. Functional analysis of secreted and transmembrane proteins critical to mouse development. Nat Genet 2001;28(3):241-249.
310. Skarnes WC, Moss JE, Hurtley SM, Beddington RS. Capturing genes encoding membrane and secreted proteins important for mouse development. Proc Natl Acad Sci U S A 1995;92(14):6592-6596.
311. Australian code of practice for the care and use of animals for scientific purposes. 2004 [cited 2014 Sept 17]; 8th:[Available from: https://www.nhmrc.gov.au/guidelines/publications/ea28
312. Alizadeh A, Clark J, Seeberger T, Hess J, Blankenship T, FitzGerald PG. Characterization of a mutation in the lens-specific CP49 in the 129 strain of mouse. Invest Ophthalmol Vis Sci 2004;45(3):884-891.
313. Sandilands A, Wang X, Hutcheson AM, James J, Prescott AR, Wegener A, Pekny M, Gong X, Quinlan RA. Bfsp2 mutation found in mouse 129 strains causes the loss of CP49' and induces vimentin-dependent changes in the lens fibre cell cytoskeleton. Exp Eye Res 2004;78(4):875-889.
314. Chylack LT, Jr., Wolfe JK, Singer DM, Leske MC, Bullimore MA, Bailey IL, Friend J, McCarthy D, Wu SY. The Lens Opacities Classification System III. The Longitudinal Study of Cataract Study Group. Arch Ophthalmol 1993;111(6):831-836.
315. Yap AS, Brieher WM, Gumbiner BM. Molecular and functional analysis of cadherin-based adherens junctions. Annu Rev Cell Dev Biol 1997;13:119-146.

316. Bagchi M, Katar M, Lewis J, Maisel H. Associated proteins of lens adherens junction. J Cell Biochem 2002;86(4):700-703.
317. Guo H, Miao H, Gerber L, Singh J, Denning MF, Gilliam AC, Wang B. Disruption of EphA2 receptor tyrosine kinase leads to increased susceptibility to carcinogenesis in mouse skin. Cancer Res 2006;66(14):7050-7058.
318. Du X, Baldwin C, Hooker E, Glorion P, Lemay S. Basal and Src kinase-mediated activation of the EphA2 promoter requires a cAMP-responsive element but is CREB-independent. J Cell Biochem 2011;112(5):1268-1276.
319. Ridder W, 3rd, Nusinowitz S, Heckenlively JR. Causes of cataract development in anesthetized mice. Exp Eye Res 2002;75(3):365-370.
320. Klein R. Eph/ephrin signalling during development. Development 2012;139(22):4105-4109.
321. Lang Y, Chen D, Li D, Zhu M, Xu T, Zhang T, Qian W, Luo Y. Luteolin inhibited hydrogen peroxide-induced vascular smooth muscle cells proliferation and migration by suppressing the Src and Akt signalling pathways. J Pharm Pharmacol 2012;64(4):597-603.
322. Cheng JQ, Lindsley CW, Cheng GZ, Yang H, Nicosia SV. The Akt/PKB pathway: molecular target for cancer drug discovery. Oncogene 2005;24(50):7482-7492.
323. Sharma S, Ang SL, Shaw M, Mackey DA, Gecz J, McAvoy JW, Craig JE. Nance-Horan syndrome protein, NHS, associates with epithelial cell junctions. Hum Mol Genet 2006;15(12):1972-1983.
324. Son AI, Cooper MA, Sheleg M, Sun Y, Kleiman NJ, Zhou R. Further analysis of the lens of ephrin-A5-/- mice: development of postnatal defects. Mol Vis 2013;19:254-266.
325. Okabe M, Ikawa M, Kominami K, Nakanishi T, Nishimune Y. 'Green mice' as a source of ubiquitous green cells. FEBS Lett 1997;407(3):313-319.
326. Ogueta SB, Schwartz SD, Yamashita CK, Farber DB. Estrogen receptor in the human eye: influence of gender and age on gene expression. Invest Ophthalmol Vis Sci 1999;40(9):1906-1911.
327. Kirker MR, Gallagher KM, Witt-Enderby PA, Davis VL. High affinity nuclear and nongenomic estradiol binding sites in the human and mouse lens. Exp Eye Res 2013;112:1-9.
328. Lu M, Miller KD, Gokmen-Polar Y, Jeng MH, Kinch MS. EphA2 overexpression decreases estrogen dependence and tamoxifen sensitivity. Cancer Res 2003;63(12):3425-3429.
329. Harris RA, Tedjasaputra V, Zhao J, Richardson RS. Premenopausal women exhibit an inherent protection of endothelial function following a high-fat meal. Reprod Sci 2012;19(2):221-228.
330. Corina M, Vulpoi C, Branisteanu D. Relationship between bone mineral density, weight, and estrogen levels in pre and postmenopausal women. Rev Med Chir Soc Med Nat Iasi 2012;116(4):946-950.
331. Ganatra DA, Johar KS, Parmar TJ, Patel AR, Rajkumar S, Arora AI, Kayastha FB, Pal AK, Gajjar DU, Vasavada AR. Estrogen mediated protection of cytoskeleton against oxidative stress. Indian J Med Res 2013;137(1):117-124.
332. Pitts DG, Cullen AP, Hacker PD. Ocular effects of ultraviolet radiation from 295 to 365 nm. Invest Ophthalmol Vis Sci 1977;16(10):932-939.

333. Young AR. The biological effects of ozone depletion. Br J Clin Pract Suppl 1997;89:10-15.
334. Katoh N, Jonasson F, Sasaki H, Kojima M, Ono M, Takahashi N, Sasaki K. Cortical lens opacification in Iceland. Risk factor analysis -- Reykjavik Eye Study. Acta Ophthalmol Scand 2001;79(2):154-159.
335. Sasaki H, Sakamoto Y, Schnider C, Fujita N, Hatsusaka N, Sliney DH, Sasaki K. UV-B exposure to the eye depending on solar altitude. Eye Contact Lens 2011;37(4):191-195.
336. Soderberg PG. Experimental cataract induced by ultraviolet radiation. Acta Ophthalmol Suppl 1990(196):1-75.
337. Michael R, Vrensen GF, van Marle J, Gan L, Soderberg PG. Apoptosis in the rat lens after in vivo threshold dose ultraviolet irradiation. Invest Ophthalmol Vis Sci 1998;39(13):2681-2687.
338. Dillon J, Zheng L, Merriam JC, Gaillard ER. The optical properties of the anterior segment of the eye: implications for cortical cataract. Exp Eye Res 1999;68(6):785-795.
339. Wegener AR. In vivo studies on the effect of UV-radiation on the eye lens in animals. Doc Ophthalmol 1994;88(3-4):221-232.
340. Stuart DD, Cullen AP, Sivak JG, Doughty MJ. Optical effects of UV-A and UV-B radiation on the cultured bovine lens. Curr Eye Res 1994;13(5):371-376.
341. Michael R, Soderberg PG, Chen E. Dose-response function for lens forward light scattering after in vivo exposure to ultraviolet radiation. Graefes Arch Clin Exp Ophthalmol 1998;236(8):625-629.
342. Dong X, Lofgren S, Ayala M, Soderberg PG. Maximum tolerable dose for avoidance of cataract induced by ultraviolet radiation-B for 18 to 60 week old rats. Exp Eye Res 2005;80(4):561-566.
343. Ayala M, Strid H, Jacobsson U, Soderberg PG. p53 expression and apoptosis in the lens after ultraviolet radiation exposure. Invest Ophthalmol Vis Sci 2007;48(9):4187-4191.
344. Michael R. Development and repair of cataract induced by ultraviolet radiation. Ophthalmic Res 2000;32 Suppl 1:ii-iii; 1-44.
345. Ayala MN, Michael R, Soderberg PG. Influence of exposure time for UV radiation-induced cataract. Invest Ophthalmol Vis Sci 2000;41(11):3539-3543.
346. Galichanin K, Lofgren S, Soderberg P. Cataract after repeated daily in vivo exposure to ultraviolet radiation. Health Phys 2014;107(6):523-529.
347. Meyer LM, Dong X, Wegener A, Soderberg P. Dose dependent cataractogenesis and Maximum Tolerable Dose (MTD(2.3:16)) for UVR 300 nm-induced cataract in C57BL/6J mice. Exp Eye Res 2008;86(2):282-289.
348. Soderberg PG, Lofgren S, Ayala M, Dong X, Kakar M, Mody V. Toxicity of ultraviolet radiation exposure to the lens expressed by maximum tolerable dose. Dev Ophthalmol 2002;35:70-75.
349. Meyer LM, Soderberg P, Dong X, Wegener A. UVR-B induced cataract development in C57 mice. Exp Eye Res 2005;81(4):389-394.
350. Ayala MN, Michael R, Soderberg PG. In vivo cataract after repeated exposure to ultraviolet radiation. Exp Eye Res 2000;70(4):451-456.

351. Dong X, Lofgren S, Ayala M, Soderberg PG. Maximum tolerable dose for avoidance of cataract after repeated exposure to ultraviolet radiation in rats. Exp Eye Res 2007;84(1):200-208.
352. Michael R, Soderberg PG, Chen E. Long-term development of lens opacities after exposure to ultraviolet radiation at 300 nm. Ophthalmic Res 1996;28(4):209-218.
353. Zhang F, Lofgren S, Soderberg PG. Interaction of anaesthetic drugs and UV-B irradiation in the anterior segment of the rat eye. Acta Ophthalmol Scand 2007;85(7):745-752.
354. Dave A, Laurie K, Staffieri SE, Taranath D, Mackey DA, Mitchell P, Wang JJ, Craig JE, Burdon KP, Sharma S. Mutations in the EPHA2 gene are a major contributor to inherited cataracts in South-Eastern Australia. PLoS One 2013;8(8):e72518.
355. Gong X, Agopian K, Kumar NM, Gilula NB. Genetic factors influence cataract formation in alpha 3 connexin knockout mice. Dev Genet 1999;24(1-2):27-32.
356. Gerido DA, Sellitto C, Li L, White TW. Genetic background influences cataractogenesis, but not lens growth deficiency, in Cx50-knockout mice. Invest Ophthalmol Vis Sci 2003;44(6):2669-2674.
357. Yeatman TJ. A renaissance for SRC. Nat Rev Cancer 2004;4(6):470-480.
358. Knoll B, Drescher U. Src family kinases are involved in EphA receptor-mediated retinal axon guidance. J Neurosci 2004;24(28):6248-6257.
359. Kechad A, Jolicoeur C, Tufford A, Mattar P, Chow RW, Harris WA, Cayouette M. Numb is required for the production of terminal asymmetric cell divisions in the developing mouse retina. J Neurosci 2012;32(48):17197-17210.
360. Li Y, Wang JP, Santen RJ, Kim TH, Park H, Fan P, Yue W. Estrogen stimulation of cell migration involves multiple signaling pathway interactions. Endocrinology 2010;151(11):5146-5156.
361. Wang X, Simpkins JW, Dykens JA, Cammarata PR. Oxidative damage to human lens epithelial cells in culture: estrogen protection of mitochondrial potential, ATP, and cell viability. Invest Ophthalmol Vis Sci 2003;44(5):2067-2075.
362. Bigsby RM, Cardenas H, Caperell-Grant A, Grubbs CJ. Protective effects of estrogen in a rat model of age-related cataracts. Proc Natl Acad Sci U S A 1999;96(16):9328-9332.
363. Forker C, Wegener A, Graw J. Effects of UV-B radiation on a hereditary suture cataract in mice. Exp Eye Res 1997;64(3):405-411.
364. West SK, Longstreth JD, Munoz BE, Pitcher HM, Duncan DD. Model of risk of cortical cataract in the US population with exposure to increased ultraviolet radiation due to stratospheric ozone depletion. Am J Epidemiol 2005;162(11):1080-1088.
365. Litt M, Kramer P, LaMorticella DM, Murphey W, Lovrien EW, Weleber RG. Autosomal dominant congenital cataract associated with a missense mutation in the human alpha crystallin gene CRYAA. Hum Mol Genet 1998;7(3):471-474.
366. Liu M, Ke T, Wang Z, Yang Q, Chang W, Jiang F, Tang Z, Li H, Ren X, Wang X, Wang T, Li Q, Yang J, Liu J, Wang QK. Identification of a CRYAB mutation associated with autosomal dominant posterior polar cataract in a Chinese family. Invest Ophthalmol Vis Sci 2006;47(8):3461-3466.

367. Kannabiran C, Rogan PK, Olmos L, Basti S, Rao GN, Kaiser-Kupfer M, Hejtmancik JF. Autosomal dominant zonular cataract with sutural opacities is associated with a splice mutation in the betaA3/A1-crystallin gene. Mol Vis 1998;4:21.
368. Billingsley G, Santhiya ST, Paterson AD, Ogata K, Wodak S, Hosseini SM, Manisastry SM, Vijayalakshmi P, Gopinath PM, Graw J, Heon E. CRYBA4, a novel human cataract gene, is also involved in microphthalmia. Am J Hum Genet 2006;79(4):702-709.
369. Cohen D, Bar-Yosef U, Levy J, Gradstein L, Belfair N, Ofir R, Joshua S, Lifshitz T, Carmi R, Birk OS. Homozygous CRYBB1 deletion mutation underlies autosomal recessive congenital cataract. Invest Ophthalmol Vis Sci 2007;48(5):2208-2213.
370. Litt M, Carrero-Valenzuela R, LaMorticella DM, Schultz DW, Mitchell TN, Kramer P, Maumenee IH. Autosomal dominant cerulean cataract is associated with a chain termination mutation in the human beta-crystallin gene CRYBB2. Hum Mol Genet 1997;6(5):665-668.
371. Riazuddin SA, Yasmeen A, Yao W, Sergeev YV, Zhang Q, Zulfiqar F, Riaz A, Riazuddin S, Hejtmancik JF. Mutations in betaB3-crystallin associated with autosomal recessive cataract in two Pakistani families. Invest Ophthalmol Vis Sci 2005;46(6):2100-2106.
372. Heon E, Priston M, Schorderet DF, Billingsley GD, Girard PO, Lubsen N, Munier FL. The gamma-crystallins and human cataracts: a puzzle made clearer. Am J Hum Genet 1999;65(5):1261-1267.
373. Sun H, Ma Z, Li Y, Liu B, Li Z, Ding X, Gao Y, Ma W, Tang X, Li X, Shen Y. Gamma-S crystallin gene (CRYGS) mutation causes dominant progressive cortical cataract in humans. J Med Genet 2005;42(9):706-710.
374. AlFadhli S, Abdelmoaty S, Al-Hajeri A, Behbehani A, Alkuraya F. Novel crystallin gamma B mutations in a Kuwaiti family with autosomal dominant congenital cataracts reveal genetic and clinical heterogeneity. Mol Vis 2012;18:2931-2936.
375. Mackay D, Ionides A, Kibar Z, Rouleau G, Berry V, Moore A, Shiels A, Bhattacharya S. Connexin46 mutations in autosomal dominant congenital cataract. Am J Hum Genet 1999;64(5):1357-1364.
376. Shiels A, Mackay D, Ionides A, Berry V, Moore A, Bhattacharya S. A missense mutation in the human connexin50 gene (GJA8) underlies autosomal dominant "zonular pulverulent" cataract, on chromosome 1q. Am J Hum Genet 1998;62(3):526-532.
377. Berry V, Francis P, Kaushal S, Moore A, Bhattacharya S. Missense mutations in MIP underlie autosomal dominant 'polymorphic' and lamellar cataracts linked to 12q. Nat Genet 2000;25(1):15-17.
378. Pras E, Levy-Nissenbaum E, Bakhan T, Lahat H, Assia E, Geffen-Carmi N, Frydman M, Goldman B. A missense mutation in the LIM2 gene is associated with autosomal recessive presenile cataract in an inbred Iraqi Jewish family. Am J Hum Genet 2002;70(5):1363-1367.
379. Jamieson RV, Farrar N, Stewart K, Perveen R, Mihelec M, Carette M, Grigg JR, McAvoy JW, Lovicu FJ, Tam PP, Scambler P, Lloyd IC, Donnai D, Black GC. Characterization of a familial t(16;22) balanced translocation associated with

congenital cataract leads to identification of a novel gene, TMEM114, expressed in the lens and disrupted by the translocation. Hum Mutat 2007;28(10):968-977.
380. Shiels A, Bennett TM, Knopf HL, Yamada K, Yoshiura K, Niikawa N, Shim S, Hanson PI. CHMP4B, a novel gene for autosomal dominant cataracts linked to chromosome 20q. Am J Hum Genet 2007;81(3):596-606.
381. Ramachandran RD, Perumalsamy V, Hejtmancik JF. Autosomal recessive juvenile onset cataract associated with mutation in BFSP1. Hum Genet 2007;121(3-4):475-482.
382. Jakobs PM, Hess JF, FitzGerald PG, Kramer P, Weleber RG, Litt M. Autosomal-dominant congenital cataract associated with a deletion mutation in the human beaded filament protein gene BFSP2. Am J Hum Genet 2000;66(4):1432-1436.
383. Muller M, Bhattacharya SS, Moore T, Prescott Q, Wedig T, Herrmann H, Magin TM. Dominant cataract formation in association with a vimentin assembly disrupting mutation. Hum Mol Genet 2009;18(6):1052-1057.
384. Bu L, Jin Y, Shi Y, Chu R, Ban A, Eiberg H, Andres L, Jiang H, Zheng G, Qian M, Cui B, Xia Y, Liu J, Hu L, Zhao G, *et al.* Mutant DNA-binding domain of HSF4 is associated with autosomal dominant lamellar and Marner cataract. Nat Genet 2002;31(3):276-278.
385. Chen J, Ma Z, Jiao X, Fariss R, Kantorow WL, Kantorow M, Pras E, Frydman M, Riazuddin S, Riazuddin SA, Hejtmancik JF. Mutations in FYCO1 cause autosomal-recessive congenital cataracts. Am J Hum Genet 2011;88(6):827-838.
386. Lachke SA, Alkuraya FS, Kneeland SC, Ohn T, Aboukhalil A, Howell GR, Saadi I, Cavallesco R, Yue Y, Tsai AC, Nair KS, Cosma MI, Smith RS, Hodges E, Alfadhli SM, *et al.* Mutations in the RNA granule component TDRD7 cause cataract and glaucoma. Science 2011;331(6024):1571-1576.